



Functional characterization of the TRRAP pseudokinase and its chaperone TTT during transcriptional regulation in colorectal cancer

Dylane Detilleux

► To cite this version:

Dylane Detilleux. Functional characterization of the TRRAP pseudokinase and its chaperone TTT during transcriptional regulation in colorectal cancer. Agricultural sciences. Université Montpellier, 2018. English. NNT : 2018MONTT092 . tel-02056668

HAL Id: tel-02056668

<https://theses.hal.science/tel-02056668>

Submitted on 4 Mar 2019

HAL is a multi-disciplinary open access archive for the deposit and dissemination of scientific research documents, whether they are published or not. The documents may come from teaching and research institutions in France or abroad, or from public or private research centers.

L'archive ouverte pluridisciplinaire **HAL**, est destinée au dépôt et à la diffusion de documents scientifiques de niveau recherche, publiés ou non, émanant des établissements d'enseignement et de recherche français ou étrangers, des laboratoires publics ou privés.

THÈSE POUR OBTENIR LE GRADE DE DOCTEUR DE L'UNIVERSITÉ DE MONTPELLIER

En Biochimie et Biologie moléculaire

École doctorale CBS2 n°168 – Sciences Chimiques et Biologiques pour la Santé

Unité de recherche UMR 5237 – Centre de Recherche en Biologie cellulaire de Montpellier

**Functional characterization of the TRRAP pseudokinase
and its chaperone TTT during transcriptional regulation
in colorectal cancer.**

**Présentée par Dylane DETILLEUX
Le 30 Novembre 2018**

**Sous la direction de Dominique HELMLINGER
Et Bérengère PRADET-BALADE**

Devant le jury composé de

Dominique HELMLINGER, CRCE, CRBM

Bérengère PRADET-BALADE, CRCE, CRBM

László TORA, DRCE1, IGBMC

Martin EILERS, Professeur, Université de Würzburg

Anne-Marie MARTINEZ, Professeur, IGH

Didier TROUCHE, DR1, LBCMCP

Directeur

Co-Directeur

Rapporteur

Rapporteur

Présidente

Examineur



UNIVERSITÉ
DE MONTPELLIER

ACKNOWLEDGEMENTS

First and foremost, I would like to thank Dr Lázló TORA, Professor Martin EILERS, Professor Anne-Marie MARTINEZ and Dr Didier TROUCHE for accepting to be a member of the jury and for taking the time to read and evaluate my thesis work.

Je tiens ensuite à exprimer toute ma reconnaissance à mon chef Dom HELMLINGER. Je n'aurais pu espérer meilleur directeur de thèse. Merci de m'avoir transmis la passion dès mon arrivée au sein de l'équipe, parmi la team *S. pombe*. Merci pour ton encadrement, ton soutien, ton aide, ton écoute et ta disponibilité au cours de ces 4 années de thèse. Merci aussi pour ton dynamisme communicatif, et surtout merci pour cette confiance que tu m'as accordée. Merci d'avoir cru en moi et mes capacités, et de m'avoir menée ici aujourd'hui.

Merci à Bérengère pour m'avoir accompagnée lors de mes débuts avec les cellules humaines. Merci de m'avoir laissé l'autonomie nécessaire tout en apportant tes inputs sur le projet, et merci aussi pour tes relectures.

Je remercie bien évidemment les membres de mon équipe, pour leur soutien, leur gentillesse, mais aussi la bonne ambiance qu'ils ont apportée au cours de ces 4 années de montagnes russes. Sans oublier leur tolérance à mon superbe caractère...

Je tiens tout particulièrement à remercier Céline, la Wonder-woman de l'équipe, non seulement elle gère le labo à merveille (et attention faut que ça file droit) mais en plus elle assure en tant que maman. En fait Céline c'est un peu notre maman au labo. Merci à toi pour ton écoute, tes conseils et ton relativisme qui m'ont bien souvent été très précieux, merci aussi pour ces bons gâteaux (le brookie c'est une tuerie !), ces instants carrés de chocolat et ces parties de badminton.

Merci aux mecs de l'équipe, Alberto et Damien, mais aussi Thomas, sans qui je n'aurais pas autant ri. Merci à Damien, le breton au bon caractère et pas si alcoolique que ça, pour ces fous rires, parfois (souvent) à ton insu j'avoue, spéciale dédicace à tes moments de solitudes où on n'a pas toujours compris tes références. Merci à Alberto, de m'avoir écoutée et rassurée plusieurs fois. J'aurai chaque année une petite pensée pour toi, être nés le même jour fallait le faire !

Ces moments post-repas au café vont quand même sacrément me manquer.

Merci à Peggy, de m'avoir soutenue pour ne pas craquer dans ces derniers mois, merci pour ta patate et tes cours d'autodérision. Merci aussi pour ces petits moments commérage, thés et mode.

Je remercie bien évidemment Fanny et nos inoubliables moments canapé (dis comme ça c'est un peu suspect), merci d'avoir été là au cours de toutes ces années, en tant que confidente-thérapeute-psychologue-psychiatre mais surtout en tant qu'amie. Merci pour ton écoute (même quand je monopolisais la parole), pour tes conseils, pour tous ces délires et ces moments hors labo aussi. Merci à Laurie, pour tes petits messages de soutien, pour tous ces restos partagés et surtout ton écoute sur les trajets du retour. Encore félicitations à toi Docteur.

Je remercie aussi Céline Gongora et Didier Trouche pour leurs encouragements et le suivi sur mon travail, lors de mes comités de thèse.

Merci aux personnes de l'institut que je n'ai pas citées mais que je remercie pour leur aide apportée, ou tout simplement leur bonne humeur.

Sans oublier ma famille là depuis le tout début de cette folle aventure. Merci de m'avoir aussi bien entourée, encouragée et soutenue, et d'être autant fiers de moi. Merci surtout de m'avoir supportée moi et mon sale caractère, et de continuer à nous supporter (c'est ça la famille, pas le choix !).

Merci à Marthe qui fait quasi-partie de la famille.

Merci à Paul d'avoir été présent et de s'être toujours plié en quatre pour me faire plaisir (fût une époque je pense que tu devais connaître les rayons de chez Carrefour par cœur). Spéciale dédicace à toi et Yo, mes supers chauffeurs avant que je n'aie le permis. Merci à mes grands-parents, mes beaux-frères, mes nièces et neveux.

Merci à vous mes sœurs, je pense particulièrement à Slo et nos moments au café Jo et puis au riche et aussi au Yam's des fois, au bibal aussi non ? A Momo qui est sans doute celle qui a le mieux compris ce que j'ai enduré pendant ces 4 années. Et puis Lauré, ma grande sœur qui m'a toujours protégée et qui continue de le faire (même si j'approche des 30ans...).

Un immense merci à ma maman, de m'avoir permis d'en être là aujourd'hui, merci pour tout ton réconfort et ton soutien.

Et puis merci à TOI, merci d'avoir compris à quel point c'était important pour moi. Merci de m'avoir accompagnée lors de ces escapades nocturnes en salle de culture (non le sur-chaussure ça ne se met pas sur la tête). Merci pour ta curiosité portée sur mon travail (une immunoprécipitation c'est quoi, ben imagine un troupeau de mouton, tu attrapes un mouton et après tu regardes avec quels autres moutons il est en contact (il fallait une sacrée imagination pour réussir à comprendre...)). Merci d'avoir tenu à lire ma thèse (après avoir piqué plusieurs fois du nez tout de même, tu y es arrivé... à la fin de l'intro). Mais surtout merci d'avoir été mon punching-ball, mon défouloir. Merci d'avoir partagé mes joies et mes tristesses.

Merci d'être toi et d'avoir partagé ça avec moi.

TABLE OF CONTENTS

SUMMARY IN FRENCH / RESUME EN FRANCAIS.....	I
ABBREVIATIONS	1
LIST OF FIGURES	6
LIST OF TABLES.....	8
PREFACE	9
INTRODUCTION.....	11
I. REGULATION OF TRANSCRIPTION INITIATION	11
1. Basal transcription.....	11
1.1. Core promoters	11
1.1.1. Core promoter feature: from a textbook description to a more and more challenged view.	11
1.1.2. Core promoter classes: variation in the transcription initiation pattern.....	13
1.2. Basal transcription machinery	14
1.2.1. RNA polymerases	14
1.2.2. Canonical PIC assembly: roles of the different GTFs.....	16
a) TFIID-DNA interaction and stabilization by TFIIA and TFIIB.....	17
b) TFIIF and Pol II recruitment.....	21
c) TFIIE, TFIIH and promoter DNA opening.....	22
2. Stimulation of the basal transcription machinery	24
2.1. Cis-acting DNA elements.....	24
2.1.1. Proximal promoter.....	24
2.1.2. Enhancers	25
2.1.3. Silencers	25
2.1.4. Insulators.....	25
2.1.5. Locus control regions	25
2.2. DNA-binding transcription regulators	26
2.3. Co-activators	27
2.3.1. Mediator co-activator complex.....	27
2.3.2. Chromatin-remodeling complexes	29
2.3.3. Histone-modifying enzymes	30
3. The SAGA coactivator complex.....	33
3.1. SAGA composition	33
3.1.1. Histone acetyltransferase module	35
3.1.2. Histone deubiquitinase module	35
3.1.3. Core structural module	35
3.1.4. TBP binding module	36
3.1.5. Splicing module.....	36
3.1.6. Transcription factor binding module	36
3.2. SAGA, a paradigm to illustrate the redundancy and the diversity in form and function of a coactivator...	38

3.2.1.	PCAF and ATAC complex.....	38
3.2.2.	DUB variants.....	40
3.2.3.	TRRAP-containing complexes.....	40
3.2.4.	SAGA and TFIID as general cofactors of RNA pol II.....	41
3.3.	SAGA recruitment to chromatin.....	42
3.3.1.	Recruitment mediated by activators.....	42
3.3.2.	Interaction with the basal transcription machinery.....	43
3.3.3.	Recruitment through chromatin-interacting domains.....	43
a)	Bromodomain.....	43
b)	SCA7.....	44
c)	Tudor.....	44
4.	<i>TIP60/NuA4, another HAT-containing complex.....</i>	<i>45</i>
4.1.	TIP60/NuA4 composition.....	45
4.2.	NuA4/TIP60 structure.....	48
4.3.	Cellular functions of TIP60.....	50
4.3.1.	The histone acetyltransferase activity of TIP60.....	50
4.3.2.	ATP-dependent histone variant deposition.....	51
II.	TTT COMPLEX, A CO-CHAPERONE OF HSP90.....	52
1.	<i>HSP90 chaperone: from conformational dynamics to co-chaperone regulation.....</i>	<i>52</i>
1.1.	Structure and function of HSP90 define a conformational cycle.....	52
1.2.	HSP90 regulation by co-chaperones.....	55
1.2.1.	TPR-containing co-chaperones.....	55
1.2.2.	Non-TPR co-chaperones.....	55
1.2.3.	Client specificity.....	56
1.2.4.	R2TP co-chaperone.....	56
2.	<i>TTT, co-chaperone dedicated to PIKKs.....</i>	<i>58</i>
2.1.	Discovery of the TTT complex as a novel HSP90 co-chaperone.....	58
2.2.	Structure and function of the PIKK family.....	60
2.2.1.	General domain organization and regulation.....	60
2.2.2.	mTOR, a PIKK responsible for cell proliferation, growth and protein synthesis.....	61
a)	mTOR function overview.....	61
b)	Structural organization of mTOR complexes.....	62
c)	Regulation of mTOR complex assembly.....	63
2.2.3.	ATR, ATM and DNAPKcs, PIKKs involved in DNA damage response.....	64
a)	Overview of ATR, ATM and DNA-PKcs function.....	64
b)	Structure and regulation of DDR-specific PIKKs.....	65
2.2.4.	SMG1 and the NMD process.....	68
2.2.5.	TRRAP and the transcription.....	69

OBJECTIVES.....72

RESULTS.....74

PART 1:	74
TRANSCRIPTIONAL REPRESSION OF INTERFERON-STIMULATED GENES BY THE TRRAP TRANSCRIPTIONAL CO-ACTIVATOR AND ITS CHAPERONE TTT	74
MATERIALS & METHODS.....	110
APPENDIX 1: CUT&RUN protocol.....	113

PART II:	124
TORC1 AND TORC2 CONVERGE TO REGULATE THE SAGA CO-ACTIVATOR IN RESPONSE TO NUTRIENT AVAILABILITY	124
DISCUSSION & PERSPECTIVES	149
1. <i>TRRAP is an evolutionarily conserved PIKK family member and requires the TTT co-chaperone to function.</i>	149
2. <i>Unexpected direct inhibitory roles for TRRAP in transcription</i>	150
3. <i>Mechanism of ISG repression by TRRAP.</i>	152
4. <i>New insights into the functional cooperation between MYC and TRRAP.</i>	156
5. <i>TRRAP governs and maintains a tumoral state, characterized by low levels of ISGs.</i>	160
6. <i>Putative roles of TRRAP over RNA polymerase II transcription.</i>	161
CONCLUSION.....	164
REFERENCES.....	166

SUMMARY IN FRENCH / RESUME EN FRANCAIS

Introduction

La régulation de l'expression des gènes est un processus essentiel à l'homéostasie cellulaire et s'effectue à plusieurs niveaux. La transcription représente l'un de ces niveaux et implique des centaines de facteurs et cofacteurs transcriptionnels. Lors de l'initiation de la transcription, plusieurs facteurs généraux vont se fixer séquentiellement au niveau de la région promotrice d'un gène afin d'y recruter l'ARN polymérase II et d'activer la transcription du gène concerné. Ce processus est hautement régulé et nécessite également l'intervention de complexes multi-protéiques appelés co-activateurs qui vont affecter la structure de la chromatine afin de la rendre accessible.

Au laboratoire nous étudions l'un de ces complexes co-activateurs de la transcription, le complexe SAGA. SAGA est composé de 18-20 sous-unités organisées en modules fonctionnels et possède deux activités enzymatiques, une activité acétyltransférase et une activité déubiquitinase des histones, portées par les sous-unités GCN5 et USP22 respectivement. Le recrutement de SAGA à la chromatine repose sur différentes de ses sous-unités et domaines qui permettent son interaction soit directe avec la chromatine par la lecture et la reconnaissance de modifications spécifiques d'histones, soit indirecte avec la machinerie basale de transcription, ou avec des facteurs de transcription. L'interaction de SAGA avec les facteurs de transcription est assurée par sa plus large sous-unité, TRRAP. TRRAP a initialement été identifié comme protéine interagissant avec les facteurs de transcription c-MYC et E2Fs. De façon intéressante, TRRAP fait aussi partie d'un autre complexe co-activateur de la transcription, TIP60 qui possède également une activité acétyltransférase mais aussi une activité de remodelage de la chromatine ATP-dépendante médiée par sa sous-unité P400.

TRRAP appartient à une famille de sérine-thréonine kinases, les PIKKs, qui interviennent dans distincts mécanismes essentiels à la cellule. Le repliement, la stabilité ainsi que l'assemblage de ces différentes kinases sont assurés par une co-chaperonne d'HSP90, le complexe Triple T ou TTT, qui doit son nom aux trois sous-unités qui le composent TELO2, TTI1 et TTI2. Contrairement aux autres PIKKs, TRRAP ne possède pas d'activité catalytique et représente donc la seule pseudo-kinase de cette famille. Outre son rôle sur la stabilité de TRRAP, aucune étude n'a analysé la conséquence d'une déplétion de TTT sur la fonction transcriptionnelle de TRRAP.

De manière surprenante, TRRAP et TTT sont surexprimés dans des tumeurs primaires de cancer colorectal comparés à leur expression dans les tissus normaux correspondants. Ainsi, TTT pourrait participer au processus de tumorigenèse en régulant un programme transcriptionnel spécifique médié par TRRAP. Pour valider cette hypothèse, mon projet de thèse s'est intéressé au rôle de TRRAP et de sa co-chaperonne TTT dans des cellules de carcinome colorectal humain. Mes objectifs pour répondre à cette problématique étaient les suivants :

1. Déterminer l'effet de la déplétion de la co-chaperonne TTT sur TRRAP la seule pseudo-kinase de la famille des PIKKs.
2. Étudier le rôle de TTT dans la transcription.
3. Identifier les cibles directes de TRRAP.

Résultats

TTT est responsable de l'assemblage de TRRAP dans SAGA.

Afin d'étudier le rôle de la co-chaperonne TTT sur son substrat TRRAP, nous avons analysé l'effet de la déplétion d'une des sous-unités la mieux caractérisée du complexe, TELO2. Puisque TELO2 est essentiel à la survie cellulaire, nous avons opté pour un système de dégron inductible, le AID (Auxin Inducible Degron). Ce système qui vient de la plante, permet une dégradation rapide, inductible et réversible d'une protéine d'intérêt à laquelle est fusionnée le dégron, suite à l'ajout d'une hormone de plante, l'auxine. La séquence du AID a été insérée au locus endogène du gène *TELO2*, à l'extrémité C-terminale de la phase ouverte de lecture, grâce à la technique du CRISPR/Cas9. Bien que TTT soit cytoplasmique, nous avons ainsi pu montrer que la délétion de TELO2 affecte majoritairement TRRAP au niveau nucléaire (**Figure 1A**). Plus précisément, nous avons démontré que TELO2 est requis à l'incorporation de TRRAP dans SAGA. En effet, nous avons observé une diminution notable de la quantité de TRRAP incorporée dans le complexe SAGA en l'absence de TELO2 (**Figure 1B**). Ces résultats suggèrent que TTT régule la stabilité de TRRAP et son incorporation dans SAGA au niveau du cytoplasme, permettant ainsi sa translocation dans le noyau.

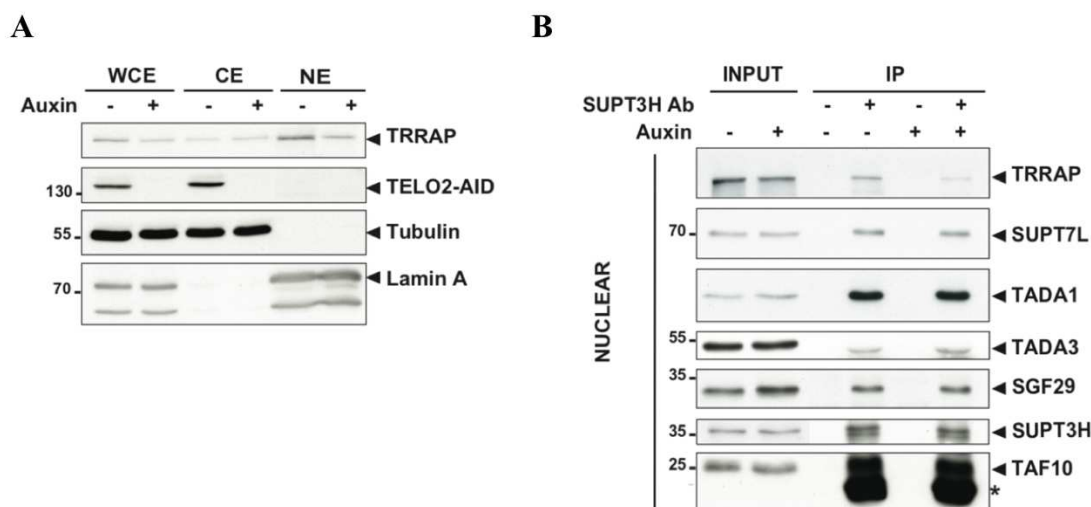


Figure 1 : TTT régule la stabilité et l'incorporation de TRRAP dans SAGA. (A) Fractionnement de cellules HCT116 exprimant la protéine endogène TELO2 fusionnée avec un AID, réalisé après un traitement à l'auxine de 48h. Les niveaux protéiques de TRRAP, TELO2 sont analysés au sein de l'extrait total (WCE), de la fraction cytoplasmique (CE) et de la fraction nucléaire (NE) par électrophorèse sur gel d'acrylamide. Les niveaux de tubuline et de lamine A servent de contrôle des fractions cytoplasmique et nucléaire, respectivement. (B) Immunoprécipitation du complexe SAGA réalisée à l'aide d'un anticorps anti-SUPT3H dans la fraction nucléaire de cellules HCT116 exprimant la protéine endogène TELO2 fusionnée avec un AID, traitées 24h avec ou sans auxine. Les niveaux protéiques de TRRAP et d'autres sous-unités de SAGA sont analysés par électrophorèse sur gel d'acrylamide au sein de l'extrait de départ (INPUT) puis après immunoprécipitation (IP). L'astérisque indique la chaîne légère des immunoglobulines.

TRRAP et sa chaperonne TTT régulent l'expression des gènes.

Puisque TTT est nécessaire à l'assemblage de TRRAP dans SAGA et que SAGA joue un rôle important dans la régulation de la transcription, nous avons voulu analyser les conséquences d'une déplétion de TELO2 sur la transcription. Nous avons pour cela réalisé une étude transcriptomique à grande échelle par séquençage des ARN messagers provenant de cellules exprimant la protéine endogène TELO2 fusionnée avec le AID, traitées ou non à l'auxine pendant 48h pour induire une déplétion totale de TELO2. Nous avons alors observé d'importants changements dans l'expression de plusieurs gènes après déplétion de TELO2 (**Figure 2**).

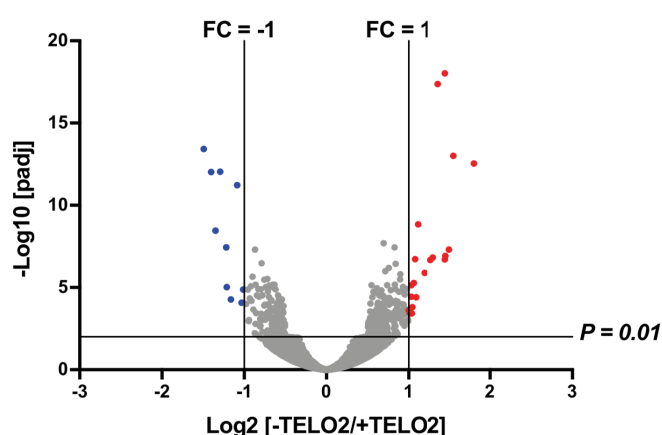


Figure 2 : La déplétion de TELO2 induit d'importants changements dans l'expression des gènes. Volcano plot montrant pour chaque gène (représenté par un point) son amplitude de variation en expression (FC) et sa significativité statistique (p value). Les amplitudes de variation d'expression pour chaque gène sont calculées comme le log2 du rapport entre leur valeur obtenue en absence de TELO2 et leur valeur en condition normale.

Puisque TTT est la co-chaperonne responsable de la stabilité, du repliement et de l'assemblage des six membres qui composent la famille des PIKKs, nos résultats de séquençage ne permettent pas de discriminer quelle PIKK est responsable des changements d'expression des gènes associés à la déplétion de TELO2. Afin de déterminer si les conséquences transcriptionnelles induites après déplétion de TTT sont corrélées à une diminution d'incorporation de TRRAP dans SAGA, nous avons reproduit la même stratégie employée pour TELO2 sur TRRAP. Ainsi TRRAP a été fusionné avec un AID en N-terminal car le domaine FATC retrouvé à l'extrémité C-terminale de l'ensemble des PIKKs est connu pour être essentiel à leurs fonctions. Selon le schéma suivi pour TELO2, nous avons réalisé un séquençage des ARN messagers de cellules où TRRAP est fusionné à un AID, après traitement ou non à l'auxine pendant 24h pour induire la dégradation totale de TRRAP.

Remarquablement, la liste de gènes différentiellement affectés après déplétion de TELO2 corrèle fortement et positivement avec celle des gènes différentiellement affectés après déplétion de TRRAP, comme indiqué par le coefficient de Spearman obtenu ($\rho=0.67$) (**Figure 3A**). De plus, on observe un clair chevauchement entre ces deux listes de gènes (**Figure 3B**).

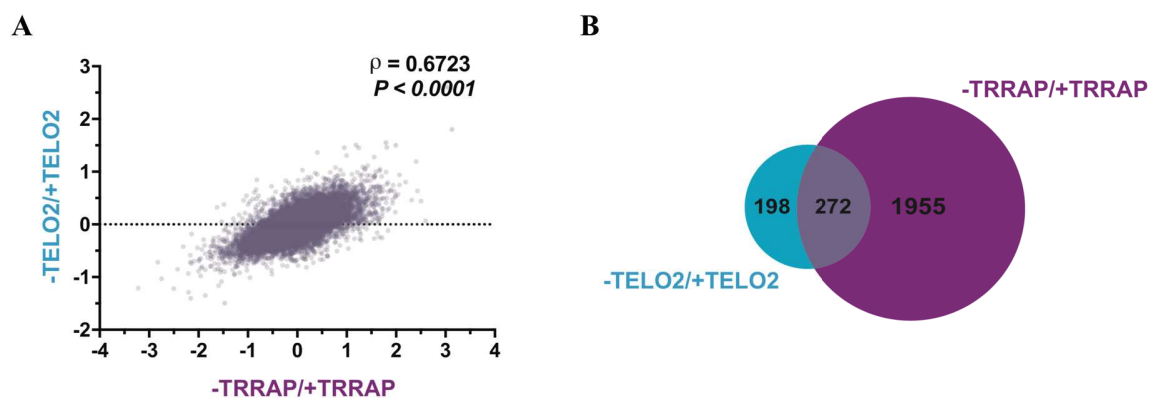


Figure 3 : Corrélation entre les conséquences transcriptionnelles induites après déplétion de TELO2 et TRRAP. (A) Représentation graphique de la corrélation entre les amplitudes de variations d’expression des gènes après déplétion de TELO2 (en ordonnée) ou déplétion de TRRAP (en abscisse). Le coefficient de Spearman (ρ) ainsi que la significativité (P) sont indiqués. (B) Diagramme de Venn montrant le chevauchement entre des gènes significativement affectés après déplétion de TELO2 (en bleu) ou de TRRAP (en violet).

En effet 272 gènes sont communs, ce qui correspond à plus de la moitié des gènes affectés par l’absence de TELO2. Ce résultat suggère que TTT régule la transcription essentiellement à travers TRRAP.

Nous avons ensuite conduit une analyse fonctionnelle sur chacune de ces listes de gènes. Nous avons fait l’observation intéressante que les trois signatures les plus significatives, enrichies après déplétion de TELO2 ou TRRAP, sont similaires. Les gènes dont l’expression est diminuée après traitement à l’auxine correspondent majoritairement à des gènes cibles des facteurs de transcription MYC et E2Fs (**Figure 4**). Puisque TRRAP est connu pour être un partenaire de ces facteurs, l’enrichissement de ces signatures après déplétion de TRRAP était prévisible. En revanche, obtenir ces mêmes signatures pour les gènes affectés après déplétion de TELO2 n’était pas attendu et renforce d’autant plus l’hypothèse que TTT joue un rôle dans la transcription principalement *via* TRRAP.

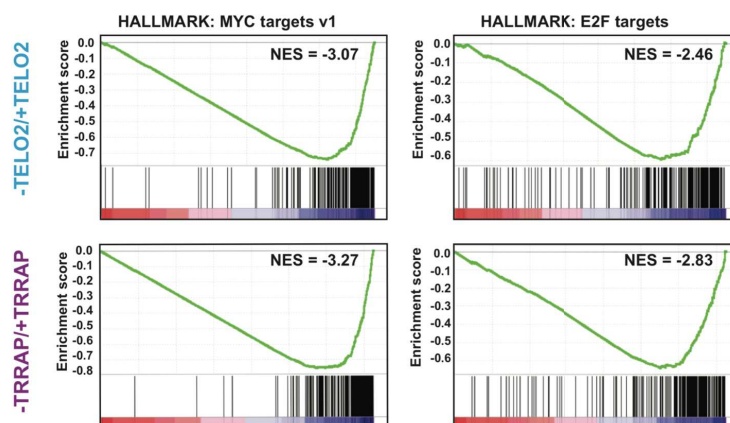


Figure 4 : TRRAP et sa chaperonne régulent un programme transcriptionnel MYC et E2F-dépendant. Analyse fonctionnelle par GSEA des gènes différentiellement exprimés après déplétion de TELO2 (panel du haut) ou de TRRAP (panel du bas), ordonnés par amplitude de variation. Le score d'enrichissement (NES) est indiqué.

Bien que TRRAP soit décrit principalement comme un co-activateur de la transcription, nous observons plusieurs gènes dont l'expression est augmentée après sa déplétion, suggérant un rôle répresseur de TRRAP sur la transcription de ces gènes. Notre analyse fonctionnelle des gènes dépendant de TRRAP montre un enrichissement de gènes induits et intervenant dans la réponse à l'interféron de type I, les ISGs (Interferon Stimulated Genes) (**Figure 5A**). Cette signature est également retrouvée après déplétion de TELO2 mais semble cependant moins prononcée. En effet, si l'on s'intéresse à la liste des ISG, on constate que 29 d'entre eux sont retrouvés significativement affectés après déplétion de TRRAP et de TELO2, avec une amplitude de variation plus marquée dans les cellules déplétées pour TRRAP (**Figure 5B**).

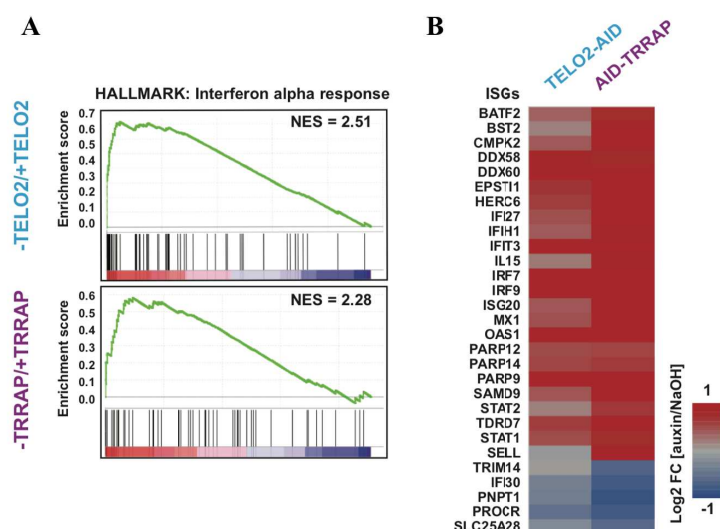


Figure 5 : TRRAP et sa chaperonne répriment l'expression des ISG. (A) Analyse fonctionnelle par GSEA des gènes différentiellement exprimés après déplétion de TELO2 (panel du haut) ou de TRRAP (panel du bas). (B) Carte thermique (heatmap) représentant l'amplitude de variation de 29 ISG communs après déplétion de TELO2 ou TRRAP ($P < 0,05$). Les valeurs positives sont représentées en rouge, et les valeurs négatives en bleu.

Les cibles directes de TRRAP dans des cellules de cancer colorectal.

Nos analyses transcriptomiques ont permis d'identifier les gènes significativement affectés positivement et négativement après la déplétion de TRRAP. Afin d'identifier parmi ces gènes les cibles directes de TRRAP, nous avons réalisé une étude pangénomique des sites de fixation de TRRAP sur la chromatine. Nous avons utilisé une technique d'immunoprécipitation de la chromatine en condition native couplée à du séquençage haut-débit, le CUT&RUN-seq. Cette technique repose sur l'utilisation de l'enzyme MNase fusionnée à la protéine A (pA-MNase) qui va cliver spécifiquement aux sites de recrutement d'une protéine d'intérêt, préalablement reconnue par un anticorps spécifique. Ainsi l'analyse du CUT&RUN de TRRAP a permis d'identifier à l'échelle du génome les gènes régulés par TRRAP. A notre surprise, notre analyse a révélé que TRRAP se fixe à plus de 9000 gènes et dans la région promotrice proximale proche du TSS (**Figure 6**).

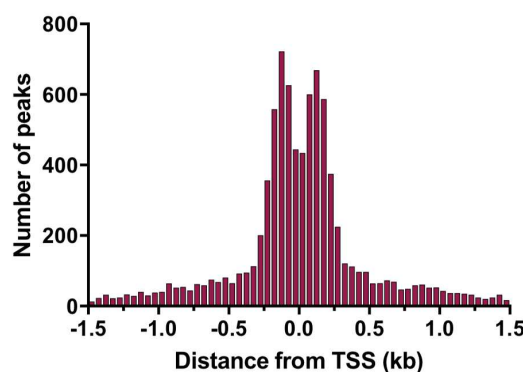


Figure 6 : Profil de fixation de TRRAP par rapport au TSS. Représentation graphique de la fréquence de distribution des sites de fixation de TRRAP entre -1 kb et 1 kb générée à partir de l'analyse du CUT&RUN-seq.

Bien que le génome humain compte entre 18000 et 22000 gènes totaux, tous ne sont pas activés en même temps dans la cellule. Récemment, une étude dans *S. cerevisiae* a montré que le co-activateur SAGA pourrait agir comme cofacteur général de la transcription par l'ARN Pol II. Ainsi, nos résultats en lien avec ces observations suggèrent que TRRAP /SAGA dans les cellules humaines pourrait jouer le même rôle.

Parmi les gènes dont l'expression est affectée après déplétion de TRRAP, plus de 60% sont liés par TRRAP. Ces gènes, qui représentent vraisemblablement les cibles directes de TRRAP, sont pour les deux tiers des gènes positivement régulés par TRRAP (960/1431), et le tiers restant des gènes réprimés par TRRAP (471/1431) (**Figure 7**). Inversement, si l'on s'intéresse aux gènes dont l'expression est diminuée après déplétion de TRRAP, 25% ne sont pas liés par TRRAP (317/1277), alors que parmi les gènes dont l'expression est induite après déplétion de TRRAP, la moitié n'est pas liée par TRRAP (479/950). Ces données sont cohérentes avec un rôle de TRRAP comme activateur de la transcription

par recrutement de TIP60 ou SAGA au promoteur des gènes cibles. De plus, nos résultats ont révélé un groupe de gènes qui semblent directement réprimés par le recrutement de TRRAP à leur promoteur.

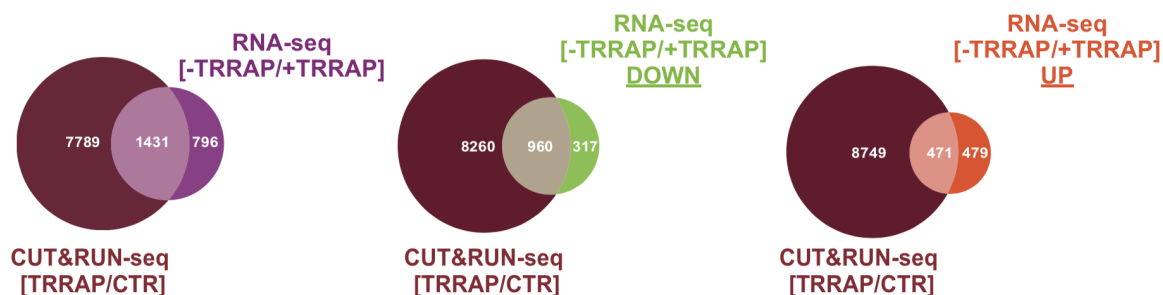


Figure 7 : Les cibles directes de TRRAP sont principalement des gènes positivement régulés par TRRAP. Diagrammes de Venn montrant le recoupement entre les gènes fixés par TRRAP (en bordeaux) et ceux dont l'expression change après déplétion de TRRAP, les gènes avec une probabilité $P < 0,01$ apparaissent en violet, ceux avec une amplitude de variation négative (DOWN, en vert) et positive (UP, en orange).

De façon intéressante, parmi les 29 ISG affectés par la déplétion de TELO2 ou de TRRAP (**Figure 5B**), environ la moitié d'entre eux sont liés par TRRAP, dont IRF9 et STAT2 qui forment le complexe ISGF3 responsable de la transcription des ISG (**Figure 8**). Ainsi, ces observations soutiennent l'hypothèse que TRRAP puisse agir comme répresseur transcriptionnel et suggèrent que les ISG affectés mais non fixés par TRRAP pourraient être régulés par IRF9/STAT2.

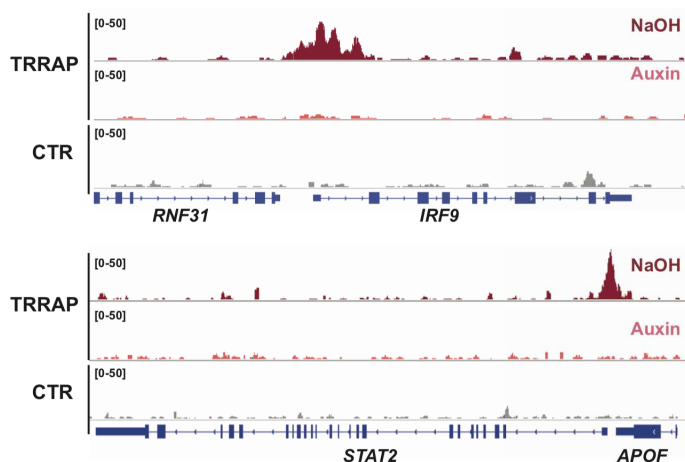


Figure 8 : TRRAP se fixe aux promoteurs d'IRF9 et STAT2, deux facteurs de transcription régulant l'expression des ISGs. Captures d'écran de la visualisation du CUT&RUN de TRRAP sur IGV (Integrative Genomics Viewer) au locus d'IRF9 (en haut) et de STAT2 (en bas). Le CUT&RUN de TRRAP a été réalisé avec un anticorps anti-HA dans des cellules 3xHA-AID-TRRAP traitées avec NaOH ou auxine pendant 12h. Le contrôle négatif (CTR) correspond au CUT&RUN réalisé dans les mêmes cellules avec un anti-IgG de lapin.

L'induction des ISG est progressive et concomitante à la dégradation de TRRAP, renforçant le rôle potentiel de TRRAP comme répresseur direct des ISG (**Figure 9**).

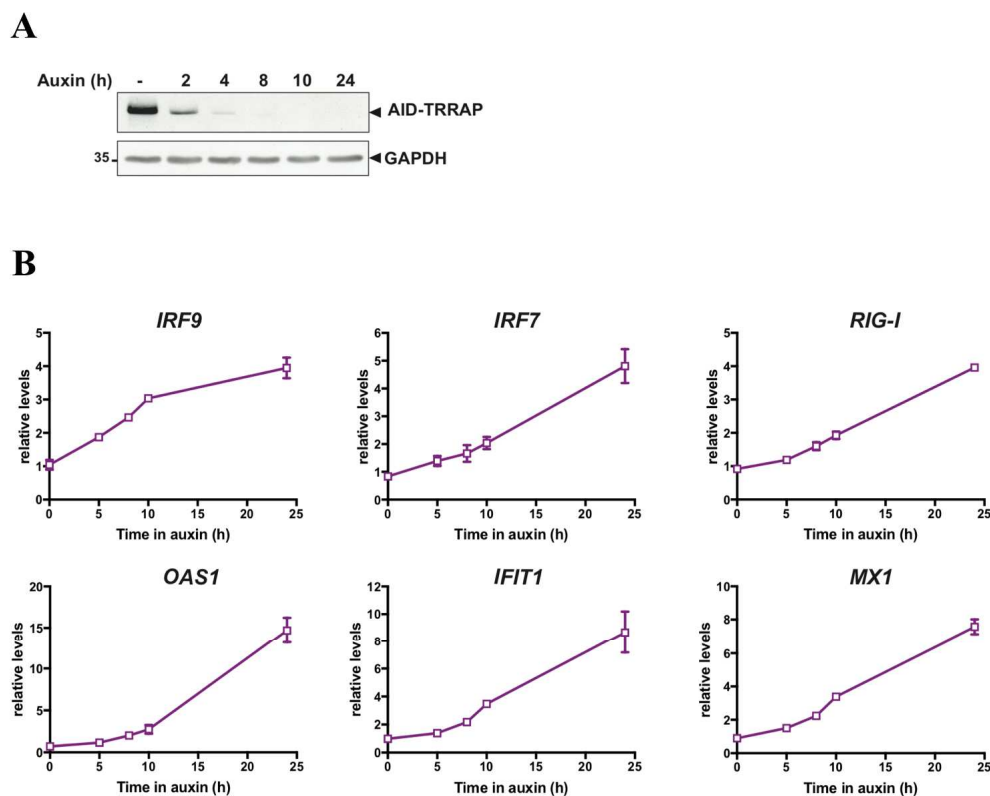


Figure 9 : Induction progressive des ISGs concomitante à la déplétion de TRRAP. (A) Cinétique de la dégradation de TRRAP par western blot au cours d'un traitement à l'auxine. (B) Expression des ARNm d'*IRF9*, *IRF7*, *RIG-I*, *OAS1*, *IFIT1* et *MX1* extraits de cellules AID-TRRAP traitées avec auxine et quantifiés par RT-qPCR au cours du temps.

De plus, en tirant profit de notre système de dégradation réversible (**Figure 10A**), nous avons observé que TRRAP se refixe rapidement au promoteur de *IRF9* (**Figure 10B**), ce qui s'accompagne d'une réversion rapide de l'expression des ISG (**Figure 10C**).

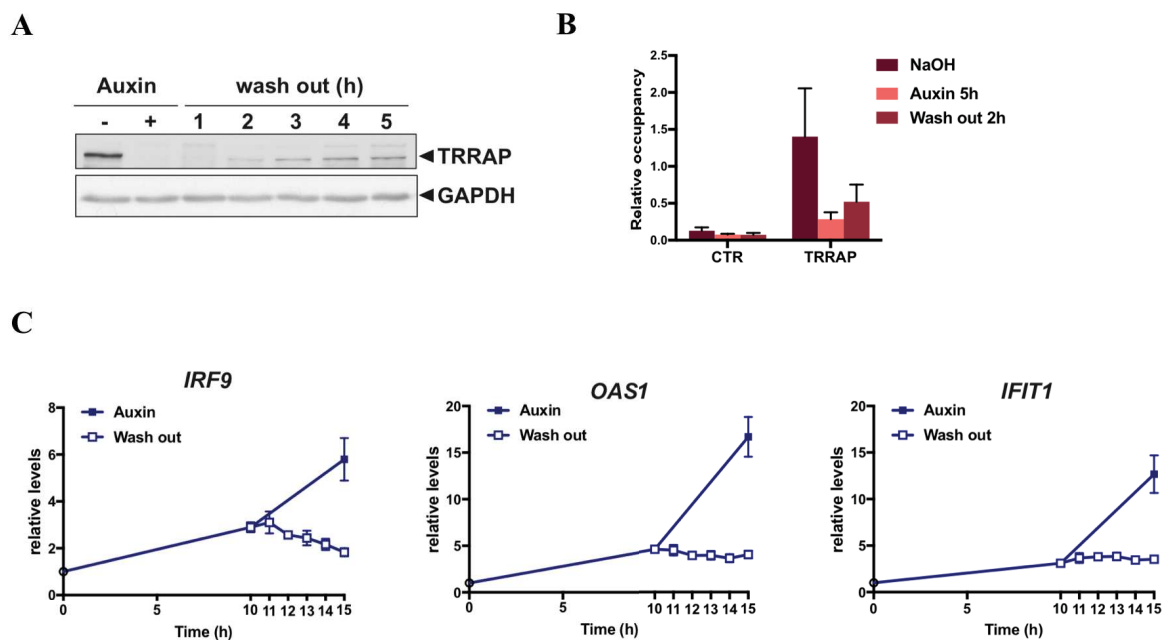


Figure 10 : La réapparition de TRRAP induit une rapide réversion de l'expression des ISG. (A) Analyse de la réapparition de TRRAP après retrait de l'auxine du milieu de culture des cellules (wash out) par western blot. Les niveaux d'expression de TRRAP dans des cellules traitées avec NaOH (- auxine) ou avec auxine (+ auxine) servent de contrôle positif et négatif de l'expression de TRRAP, respectivement. L'expression de GAPDH est utilisée comme contrôle de charge. (B) Analyse de la fixation de TRRAP par CUT&RUN puis mesure de son enrichissement au promoteur d'IRF9 par qPCR en condition basale (NaOH), puis après traitement à l'auxine pendant 5h (auxine 5h) et enfin après 2h de retrait de l'auxine (Wash out 2h). (C) Expression des ARNm d'*IRF9*, *OAS1* et *IFIT1* quantifiés par RT-qPCR aux temps indiqués. Les ARN totaux ont été extraits de cellules AID-TRRAP traitées avec auxine pendant 10h, puis soit laissées dans l'auxine 5h de plus (carrés bleus pleins), soit lavées et incubées durant 5h dans un milieu sans auxine (carrés blancs).

A partir de ces observations, nous avons voulu déterminer le complexe co-activateur responsable de la répression des ISG, et recruté par TRRAP. Nous avons donc étudié l'effet de la déplétion des activités enzymatiques des complexes SAGA et TIP60 par ARN interférence (siRNA). La diminution de la sous-unité P400 de TIP60 induit une expression d'IRF9 et OAS1 comparable à celle induite après diminution de TRRAP. En revanche, la diminution de l'activité histone acétyltransférase (HAT) de SAGA par ciblage de la sous-unité TADA3, n'a aucun effet sur l'expression d'IRF9 et OAS1. L'activité déubiquitineuse (DUB) de SAGA ciblée avec un siARN dirigé contre la sous-unité ATXN7L3, ne semble que modestement participer à l'induction d'OAS1 (**Figure 11**). Ainsi, la répression des ISG assurée par TRRAP semble impliquer l'activité de remodelage de la chromatine du complexe TIP60.

Des expériences visant à déterminer en détails le mécanisme d'action sont actuellement en cours.

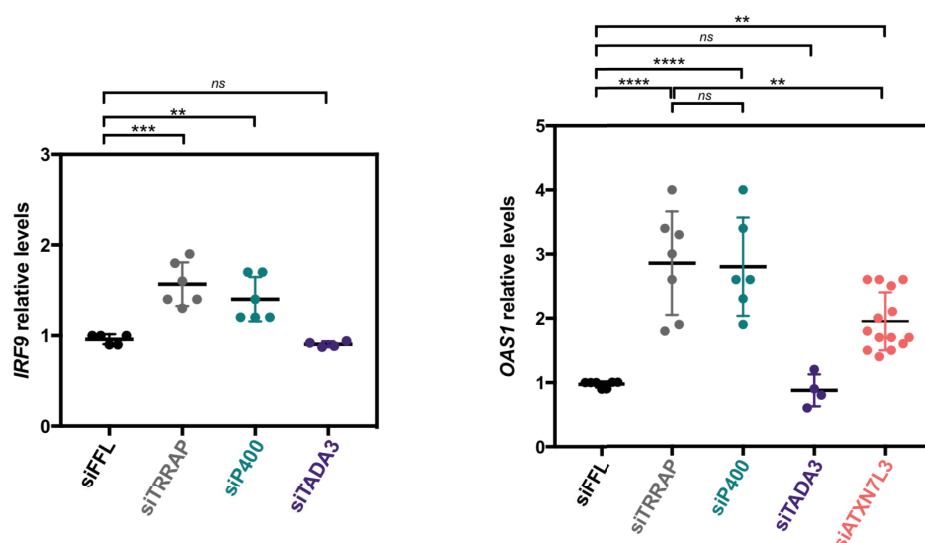


Figure 11 : Étude de l'implication de SAGA et TIP60 dans la répression des ISGs. Effet des activités régulatrices des complexes SAGA (TADA3, ATXN7L3) et TIP60 (P400) sur l'expression d'IRF9 (à gauche), et OAS1 (à droite) mesurée par RT-qPCR dans des cellules HCT116 après transfection de siRNA dirigés contre les différentes sous-unités, comme indiqués. Un siARN dirigé contre la luciférase de luciole (FFL) sert de contrôle négatif. Le siARN ciblant TRRAP sert de contrôle positif.

Conclusion

Mes travaux de thèse portant sur l'étude du cofacteur TRRAP et de sa chaperonne TTT, ont permis de montrer que l'incorporation de TRRAP dans le complexe SAGA s'effectue au niveau du cytoplasme par TTT et précède son import nucléaire. Nous avons également montré que TTT régule l'expression de nombreux gènes contrôlés par TRRAP.

Par une combinaison d'approches innovantes et complémentaires, nous avons identifié les cibles directes de TRRAP, dont la majorité correspondent à des gènes activés par TRRAP.

Mon projet de thèse a également mis en évidence un nouveau rôle de TRRAP comme répresseur transcriptionnel direct d'un groupe de gènes impliqués dans la réponse à l'interféron de type I.

ABBREVIATIONS**A**

Å	Ångström
Ab	Antibody
AID	Auxin-Inducible Degron
ASTRA	Assembly of Tel, Rvb, and Atm-like kinase
ATAC	Ada-Two-A-Containing
ATM	Ataxia-Telangiectasia Mutated
ATR	Ataxia- and Rad3-Related
ATRIP	ATR Interacting Protein

B

bHLH	basic Helix-Loop-Helix
bp	base pair
BRE	TFIIB-Recognition Element
bZIP	basic leucine Zipper

C

CAGE	Cap Analysis of Gene Expression
cDTA	comparative Dynamic Transcriptome Analysis
CE	Cytoplasmic Extract
CHD	Chromodomain Helicase DNA-binding
ChEC-seq	Chromatin Endogenous Cleavage sequencing
ChIP	Chromatin Immunoprecipitation
ChIP-seq	Chromatin Immunoprecipitation sequencing
cryo-EM	cryo-Electron Microscopy
CTD	C-Terminal Domain
CUT&RUN	Cleavage Under Targets and Release Using Nuclease
CUT&RUN-seq	Cleavage Under Targets and Release Using Nuclease sequencing

D

Da	Dalton
DBD	DNA-Binding Domain
DBTSS	Database of Transcription Start Site
DCE	Downstream Core Element
DDR	DNA Damage Response

DEG	Differentially Expressed Gene
DNA-PKcs	DNA-dependent Protein Kinase catalytic subunit
DPE	Downstream Promoter Element
DSB	Double Strand Break
dsDNA	double-stranded DNA
dsRNA	double-stranded RNA
DUB	Histone Deubiquitinase

E

EJC	Exon Junction Complex
EPD	Eukaryotic Promoter Database
ERV	Endogenous Retroviral Element
ETS	E26 Transformation-Specific

F

FAT	FRAP, ATM, TRRAP
FATC	FAT-C Terminal
FC	Fold Change
FDR	False Discovery Rate
FLAP	FATC, LBE, Activation loop, PRD
FLAP-BE	FATC, LBE, Activation loop, PRD, Binding Element
FRB	FKBP12-Rapamycin Binding

G

GNAT	Gcn5-related-N-Acetyltransferase
GSEA	Gene Set Enrichment Analysis
GTF	General Transcription Factor

H

HAT	Histone Acetyltransferase
HD	Homeodomain
HEAT	Huntingtin, Elongation factor 3, A subunit of protein phosphatase 2 and TOR1
HFD	Histone Fold Domain
HMG	High Mobility Group
HR	Homologous Recombination
HSP	Heat Shock Protein
HTH	Helix Turn Helix

I

IFN	Interferon
IgG	Immunoglobulin G
IGV	Integrative Genomics Viewer
INO80	INOsitol requiring INO80
Inr	Initiator
IR	Ionizing Radiation
ISG	Interferon-Simulated Gene
ISGF3	IFN-Stimulated Gene Factor 3
ISRE	Interferon Stimulated Response Element
ISWI	Imitation Switch

L

LCR	Locus Control Region
-----	----------------------

M

mESC	murine Embryonic Stem Cell
MNase	Micrococcal Nuclease
MRN	Mre11-Rad50-Nbs1
MSigDB	Molecular Signature Database
MTE	Motif Ten Element
mTOR	mammalian Target Of Rapamycin
MYST	MOZ Ybf2 Sas2 Tip60

N

NDR	Nucleosome-Depleted Region
NE	Nuclear Extract
NES	Normalized Enrichment Score
NHEJ	Non-Homologous End-Joining
NMD	Non-sense mediated mRNA Decay
NR	Nuclear Receptor
nt	nucleotide
NTD	N-Terminal Domain
NuA4	Nucleosome Acetyltransferase of Histone H4

P

P2A	2A Peptide
PAQosome	Particle for Arrangement of Quaternary Structure
PCAF	p300/CBP-Associated Factor
PI3K	Phosphatidylinositol 3-Kinase
PIC	Pre-Initiation Complex
PIKK	Phosphatidylinositol 3-Kinase-related protein kinase
Pol II	RNA Polymerase II
POU	Pit-Oct1/Oct2-Unc-86
PRD	PIKK Regulatory Domain
PTC	Premature Termination Codon
PTM	Post-Translational Modification

R

R2TP	RUVBL1-RUVBL2-RPAP3-P1H1D1
RNA-seq	RNA-sequencing

S

S6K1	p70-S6 Kinase
SAGA	Spt-Ada-Gcn5-Acetyltransferase
SEM	Standard Error of the Mean
sgRNA	single guide RNA
SMG1	Suppressor of Morphogenesis in Genitalia
SRCAP	SNF-2-Related CREB-Binding Protein Activator Protein
ssDNA	single-stranded DNA
STAGA	Spt3-TAFII31-Gcn5L-acetylase
SWI/SNF	Switching Defective/Sucrose Non-Fermentable

T

TAD	Topologically Associating Domain
TAF	TFIID-Associated Factor
TBP	TATA binding protein
TCGA	The Cancer Genome Atlas
TELO2	Telomere Maintenance 2
TF	Transcription Factor
TFBS	Transcription Factor Binding Site
TFTC	TBP-Free TAFII-containing Complex

TIP60	Tat Interactive Protein 60 KDa
TIR1	Transport-Inhibitor Response
TopBP1	Topoisomerase DNA II Binding Protein 1
TPR	Tetratricopeptide Repeat
TREX-2	Transcription and Export Complex 2
TRRAP	Transformation/transcription domain Associated Protein
TSS	Transcription Start Site
TTI1	Tel2-interacting protein 1
TTI2	Tel2-interacting protein 2
TTT	Triple T / TELO2-TTI1-TTI2

U

U-ISGF3	Unphosphorylated IFN-Stimulated Gene Factor 3
---------	---

W

WCE	Whole Cell Extract
WH	Winged Helix domain

Y

YFP	Yellow Fluorescent Protein
-----	----------------------------

Z

ZF	Zinc Finger
----	-------------

LIST OF FIGURES

FIGURE 1: SCHEME OF THE HUMAN CORE PROMOTER.....	12
FIGURE 2: STRUCTURE OF THE CORE MODULE OF RNA POLYMERASE II.	15
FIGURE 3: ARCHITECTURE OF THE 12-SUBUNITS POL II.....	16
FIGURE 4: STEPWISE MODEL OF POL II TRANSCRIPTION INITIATION.	17
FIGURE 5: STRUCTURE OF THE TBP-TATA ELEMENT BINDING	17
FIGURE 6: SCHEMATIC COMPOSITION OF TFIID COMPLEX	18
FIGURE 7: CRYO-EM 3D RECONSTRUCTIONS OF TFIID STATES.....	18
FIGURE 8: CRYO-EM RECONSTRUCTION OF TFIID-TFIIA AND THE SUPER CORE PROMOTER COMPLEX.	19
FIGURE 9: CURRENT MODEL OF PROMOTER BINDING BY TFIID	19
FIGURE 10: STRUCTURE OF POL II-TFIIB COMPLEX.	20
FIGURE 11: MODELS OF CLOSED AND OPEN COMPLEXES	21
FIGURE 12: DNA POSITIONING AND RETENTION BY TFIIE-TFIIF WINGED HELIX DOMAINS.....	22
FIGURE 13: STRUCTURAL TRANSITIONS ACCOMPANYING DNA MELTING.	23
FIGURE 14: SCHEMATIC REPRESENTATION OF CIS-ACTING DNA ELEMENTS.	24
FIGURE 15: DNA-BINDING DOMAIN STRUCTURES OF FOUR TRANSCRIPTION FACTORS.....	27
FIGURE 16: COMPOSITION OF THE MEDIATOR COMPLEX.	28
FIGURE 17: INTERPLAY BETWEEN MEDIATOR, THE PIC, AND THE PROMOTER ARCHITECTURE.....	29
FIGURE 18: FUNCTIONAL CLASSIFICATION OF CHROMATIN REMODELERS	30
FIGURE 19: OVERVIEW OF HISTONE MODIFICATIONS.....	31
FIGURE 20: MODULAR ORGANIZATION OF THE SAGA COMPLEX.	33
FIGURE 21: STRUCTURAL COMPARISON OF TRA1 SUBUNIT WITHIN SAGA AND NUA4 COMPLEXES.....	37
FIGURE 22: STRUCTURE OF GCN5 AND PCAF	38
FIGURE 23: NEGATIVE CORRELATION BETWEEN GCN5 AND PCAF EXPRESSION IN COLORECTAL CANCER.	39
FIGURE 24: SAGA RECRUITMENT TO CHROMATIN.....	44
FIGURE 25: MODULAR ORGANIZATION OF THE NUA4 COMPLEX.	45
FIGURE 26: ORIGIN MODEL OF HUMAN NUA4 COMPLEX.	46
FIGURE 27: MODEL OF MERGER BETWEEN NUA4 AND SWR1 COMPLEXES.	48
FIGURE 28: NUA4 STRUCTURE RESEMBLES SAGA LOBE A.	48
FIGURE 29: NUA4 AND TRA1 STRUCTURE COMPARISON.	49
FIGURE 30: OVERALL STRUCTURE OF NUA4.	49
FIGURE 31: HISTONE SUBSTRATES OF TIP60.	50
FIGURE 32: THE HSP90 DOMAIN ORGANIZATION.	53
FIGURE 33: THE HSP90 CONFORMATIONAL CYCLE.....	53
FIGURE 34: CARTOON OF THE CTD OF THE E. COLI HSP90 HOMOLOG, HIGH TEMPERATURE PROTEIN G (HPTG).	54
FIGURE 35: HSP90 REGULATION BY NON-TPR CONTAINING CO-CHAPERONE.	56
FIGURE 36: SCHEMATIC REPRESENTATION OF THE PAQOSOME CO-CHAPERONE.	57
FIGURE 37: SCHEMATIC REPRESENTATION OF THE PAQOSOME INTERACTORS.	58
FIGURE 38: SCHEMATIC REPRESENTATION OF THE GENERAL DOMAIN ORGANIZATION OF THE PIKK FAMILY.	60
FIGURE 39: OVERALL STRUCTURE OF HUMAN mTOR COMPLEXES	62
FIGURE 40: STRUCTURAL DISTINCTIONS BETWEEN mTORC1 AND mTORC2 COMPLEXES.....	63
FIGURE 41: OVERALL STRUCTURE OF DNA-PKcs AND DNA-PK.....	65
FIGURE 42: STRUCTURE OF HUMAN ATM DIMERS.	66

FIGURE 43: OVERALL STRUCTURE OF ATR-ATRIP COMPLEX.....	67
FIGURE 44: OVERALL STRUCTURE OF MEC1-Dcd2, THE YEAST HOMOLOG OF ATR-ATRIP.	67
FIGURE 45: SMG1 COMPLEX STRUCTURE.	68
FIGURE 46: TRRAP IS A PSEUDO-KINASE.	69
FIGURE 47: OVERALL STRUCTURE OF TRA1 STRUCTURALLY HOMOLOGOUS TO DNA-PKcs.	70
FIGURE 48: TYPE I INTERFERON SIGNALING.	151
FIGURE 49: TIP60 COMPLEX MAINTAINS REPRESSED ISGs.	154
FIGURE 50: TRRAP INHIBITS THE PRODUCTION OF IFN AND/OR THE JAK/STAT PATHWAY.....	155
FIGURE 51: COMMON TARGET GENES BOUND BY TRRAP AND MYC.	156
FIGURE 52: TRRAP BINDS TO ISG PROMOTER IN A MYC-INDEPENDENT MANNER.	157
FIGURE 53: TRRAP AND MYC BIND TO GENES MAINLY NOT AFFECTED AFTER TRRAP DEPLETION.....	158
FIGURE 54: TRRAP DEPLETION AFFECTS RAPIDLY THE EXPRESSION OF MIR17HG AND THE BINDING OF MYC.	159
FIGURE 55: TRRAP GOVERNS A SPECIFIC PRO-TUMORAL TRANSCRIPTIONAL PROGRAM.	160

LIST OF TABLES

TABLE 1: OVERVIEW OF DIFFERENT CLASSES OF CHROMATIN MODIFICATION.	31
TABLE 2: HAT FAMILIES.	32
TABLE 3: SAGA DOMAIN ORGANIZATION IN DIFFERENT ORGANISMS.	34
TABLE 4: NUA4 CONSERVATION FROM YEAST TO HUMAN.	47

PREFACE

The human body is made of 37 trillion cells that differentiate into approximately 200 different cell types with specific characteristics and dedicated functions. Cells are subjected to a fine regulation of the expression of their genes, whether during differentiation or to respond to signaling cues and adapt to changes in their environment. A plethora of factors and mechanisms have evolved to allow signal transduction pathways to control gene expression in time and space.

Gene expression can be regulated at many different levels, including transcription initiation, elongation, and termination, mRNA processing, export, stability, and translation. A major control of gene expression occurs during the different steps of transcription initiation.

The production of RNA from a DNA template, termed transcription, is a highly coordinated process mediated by RNA polymerases. Despite the structural complexity of these enzymes; 14, 12 and 17 subunits in RNA polymerase I, II and III respectively, RNA polymerases depend on additional components to be recruited to the transcribed loci. In eukaryotic nuclei, DNA packaging by nucleosome and higher order chromatin fibers, limits DNA accessibility and, therefore, serves as a regulatory platform for all steps of transcription. Accurate transcription at a single locus is believed to involve hundreds of transcription factors, cofactors, and chromatin regulators which are highly and tightly regulated.

During my PhD work, I focused on the regulation of co-activator complexes that have critical roles during transcription initiation by RNA polymerase II. Because regulated transcription is essential for cellular homeostasis, it is not surprising to find that dysregulation of the transcriptional machinery is associated with several human diseases. Indeed, transcription factors are often deregulated in cancer. Cancer genome studies have also revealed that mutation of cofactors is a major mechanism of tumorigenesis (Garraway and Lander, 2013). Consequently, aberrant gene expression is a hallmark of cancer. Despite the multiple genetic and epigenetic abnormalities contained in cancer cells, their growth and survival can often be reduced by the inhibition of a single oncogene, which led to the idea that many tumors show an oncogene addiction, which can be exploited to develop specific therapeutic strategies. My PhD project was especially focused on the function and regulation of Transformation/transcription domain associated protein (TRRAP), a co-activator found overexpressed in several cancers, including the colorectal cancer that constituted my working model.

The first part of the introduction will be dedicated to an overview of the transcription initiation regulation and mainly factors and co-factors involved in. I will notably focus on TRRAP-containing complexes SAGA and TIP60, which are both multiprotein complexes involved in transcription regulation. Then, the second part will aim to introduce basic concept of chaperones, which are key proteins that promote the folding, the stabilization and activation of several substrates.

INTRODUCTION

INTRODUCTION

I. Regulation of Transcription Initiation

Transcription regulation of eukaryotic genes, whether these produce protein-coding mRNAs or non-coding RNAs, is an orchestrated process involving hundreds of different actors. Transcription initiation represents an important and the first regulatory step during the production of RNAs. This regulation is achieved by the presence and activities of both *cis*-elements, such as promoter and enhancers, and factors acting in *trans*, such as transcription factors and co-factors. For example, transcription initiation by RNA polymerase II (Pol II) requires the precise assembly of many proteins, over a hundred at each core promoter, organized into large, multifunctional complexes that form a stable transcription pre-initiation complex (PIC).

1. Basal transcription

1.1. Core promoters

Transcription of class II genes initiates at a defined region of DNA, the so-called core promoter which serves as a docking site for assembly and orientation of the basal transcription machinery also referred to as PIC. The core promoter is defined as the minimal DNA fragment sufficient to direct basal levels of transcription initiation by Pol II *in vitro* (Butler and Kadonaga, 2002).

1.1.1. Core promoter feature: from a textbook description to a more and more challenged view.

The core promoter typically encompasses the transcription start site (TSS), referred to as the +1 position, and extends approximatively 40-50 base pairs (bp) upstream and downstream of the TSS. It consists of multiple short sequence elements that can be dispersed or overlapping and surrounding the TSS (Figure 1) (Maston et al., 2006; Smale and Kadonaga, 2003). Only a few sequence elements have been clearly identified so far and include:

- **Initiator element** (Inr), which consensus sequence is YYANWYY and surrounds the TSS. It is mainly bound by the TAF1 and TAF2 subunits of the general transcription factor TFIID (Chalkley and Verrijzer, 1999).
- The **TATA box**, typically located about 25–30 nt upstream of the transcription start site in metazoans, is recognized by the TATA binding protein (TBP) subunit of TFIID. Its consensus sequence is TATAWAAR.
- **Downstream Promoter Element** (DPE), which consensus sequence is RGWYV and is located at +28 to +32 relative to the TSS, is bound by the TAF6 and TAF9 subunits of TFIID and acts in conjugation with the Inr (Burke and Kadonaga, 1997; Shao et al., 2005). Indeed, the spacing between DPE and Inr motifs is invariant, which enables the cooperative binding of TFIID to the two motifs) (Burke and Kadonaga, 1997; Zhou and Chiang, 2001).

- **TFIIB-Recognition Elements (BRE)**, located immediately upstream (BRE_u) or downstream (BRE_d) of the TATA box is bound by the TFIIB basal transcription factor. BRE_u and BRE_d consensus sequences are SSRCGCC and RTDKKKK, respectively (Deng and Roberts, 2007; Lagrange et al., 1998).
- **Downstream Core Element (DCE)**, consists of three sub-elements (S) with necessary sequences: SI is CTTC, SII is CTGT, and SIII is AGC. DCE are contacted by TAF1 subunit of TFIID (Lee et al., 2005).
- and **Motif Ten Element (MTE)**, located at positions +18 to +29, MTE element functions cooperatively with a precisely positioned Inr, but its binding protein factors have not been identified yet (Lim et al., 2004).

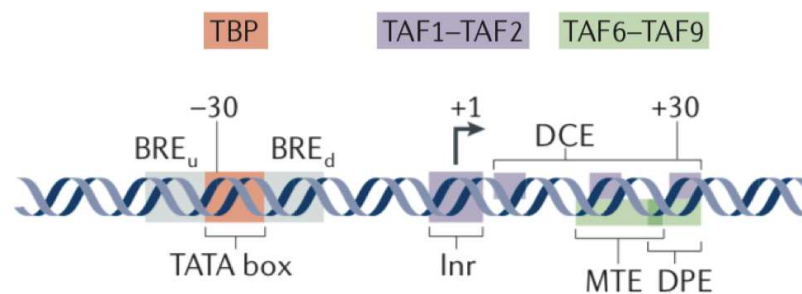


Figure 1: Scheme of the human core promoter. Major core promoter elements are depicted, including their location from the TSS (or Initiator (Inr)) and components of TFIID that bind to them. Adapted from (Sainsbury et al., 2015).

These elements define a core promoter, however there is no universal core promoter. Each of these elements are found in some but not all core promoters. For instance, the TATA-box, the first described core promoter element, was thought to be the universal promoter element. But computational analyses suggest that the prevalence of the TATA box has been overestimated in the past and that the majority of human promoters are in fact TATA-less. Therefore, the percentage of TATA-containing promoters reported in several studies has decreased significantly over time; from 78% (Bucher, 1990), to 64% (Babenko et al., 1999), to 32% (Suzuki et al., 2001), to 22% or 10% only depending on the database used (EPD (Eukaryotic Promoter Database) or DBTSS (Database of Transcription Start Sites), respectively) (Gershenson and Ioshikhes, 2005). This wide variation could be explained by the criteria used to define the TATA-box, but also the number of promoters studied or the database used (Gershenson and Ioshikhes, 2005). Thus, Yang and colleagues in 2007 addressed those issues in their study and found only ~10% of TATA-containing promoters with the canonical TATA box (TATAAWR) (Yang et al., 2007). Interestingly, analyses of *Saccharomyces cerevisiae* genomes also revealed that the canonical TATA box (TATAAWR) is present in ~20% of yeast genes (Basehoar et al., 2004). Recently Yella and Bansal reported 17% of TATA-containing promoters in *S. cerevisiae*, 14% in *D. melanogaster* and 3% only in mouse and human (Yella and Bansal, 2017).

The textbook description of the TATA-box is now challenged by these studies and establish that the TATA-box is no longer a general component of all Pol II core promoters (Müller et al., 2007).

To conclude, one level of transcription regulation lies within the core promoter element present at each gene. This significantly contributes to the complexity of eukaryotic gene expression.

1.1.2. Core promoter classes: variation in the transcription initiation pattern

Novel high-throughput-sequencing-based technologies, such as sequencing of 5' ends of mRNAs in cap analysis of gene expression (CAGE), have significantly improved the identification and annotation of TSS, providing a better understanding of promoters (Haberle and Stark, 2018). Therefore, one of the major discoveries was the existence of different types of core promoters. Although their numbers have not been settled definitely, it appears that core promoters can be divided into three main functional classes, based on several properties. These include differential usage of their TSS, sequence composition and motifs, chromatin composition and gene function, which altogether, define multiple modes of transcription initiation (Lenhard et al., 2012).

Class I: “Adult” core promoters

Core promoters included in this class, have a “focused” or “sharp” initiation pattern. This means that the initiation occurs from a single and well-defined TSS. Those core promoters are associated with highly cell-type-specific genes, they have loosely positioned nucleosomes, a high frequency of transcription binding sites and are TATA-box containing promoters.

Class II: “Ubiquitous” core promoters

Contrary to Class I, core promoters of Class II have multiple closely spaced TSSs distributed over a region of about 50–100 nt that are used with similar frequency. The initiation is called “dispersed” or “broad” in this case and occurs mainly in housekeeping genes that are expressed in many cell types. Class II promoters are TATA-less, possess less consensus binding sites and are mostly associated with a high CpG dinucleotides frequency, referred to as CpG islands. Counter-intuitively, those promoters are characterized by a more precise nucleosome positioning with a well-defined nucleosome-free region that encompasses the TSSs.

Class III: “Developmentally regulated” core promoters

Core promoters of Class III are found in genes that are regulated during development and differentiation. They harbor several large CpG islands that often extend well into the gene body. They resemble housekeeping genes core promoters since they are characterized by a “dispersed” initiation pattern and have precisely positioned and phased nucleosomes.

Whatever the class of the promoter is, their role is the same: provide a platform for the recruitment of Pol II and the formation of the PIC in order to initiate the transcription of the associated gene.

1.2. Basal transcription machinery

1.2.1. RNA polymerases

Three eukaryotic RNA polymerases (I, II, and III), were first identified by Roeder and Rutter in 1969. Few years later, α -amanitin sensitivity assays were used to resolve the specificity of each RNA polymerase. RNA Pol I is primarily involved in transcribing ribosomal RNAs (rRNAs), while RNA Pol II is dedicated to the synthesis of protein-coding genes producing messenger RNAs (mRNAs), as well as some non-coding RNAs (i.e. snoRNAs, snRNAs, pri-miRNAs), and RNA Pol III is responsible for synthesis of cellular 5S rRNA, and transfer RNAs (tRNAs). These results were consistent with the finding that RNA Pol I is localized within nucleoli, the sites for rRNA synthesis, whereas RNA Pol II and III are present in the nucleoplasm.

RNA Polymerase II is the molecular machine that transcribes protein-coding genes to produce messenger RNAs as well as various types of non-coding RNAs. RNA Pol II is a complex of 12 highly conserved subunits (Rpb1 to 12). Rpb1 is the largest subunit and contains at its C-terminus a repetitive heptapeptide motif (Tyr-Ser-Pro-Thr-Ser-Pro-Ser: Y¹S²P³T⁴S⁵T⁶S⁷) termed the C-terminal domain (CTD). Although the consensus sequence of the CTD is highly conserved among eukaryotic organisms, the repeat length varies between them. For instance, *S. pombe* has 29 repeats whereas humans include 52 repeats, suggesting that the length increases with genome complexity (Hampsey, 1998). During initiation, the CTD gets hyperphosphorylated on Ser2 and Ser5 residues and remains phosphorylated during elongation. This form of RNA Pol II is designated: RNA Pol II_O. However, after termination, dephosphorylation of the CTD is required for Pol II recycling, because only unphosphorylated Pol II, namely RNA Pol II_A, can be recruited at initiation.

Since 2000, a plethora of papers describing the structure of eukaryotic RNA Pol II have been published. The story began with the structure of RNA Pol II from the yeast *S. cerevisiae* obtained using X-ray crystallography at ~3.5 Å resolution (Cramer et al., 2000). This structure comprised 10-subunits of the RNA Pol II holoenzyme, or “core” structure of RNA Pol II, and lacked two small subunits, Rpb4 and Rpb7. One year later, the structure of Pol II at 2.8 Å (Cramer et al., 2001) and the structure of a transcribing complex at 3.3 Å resolution were obtained (Gnatt et al., 2001).

In 2003, the structure of the complete RNA Pol II was described. In order to overcome the substoichiometric amounts of Rpb4/7, which impede crystallization, Armache and colleagues, used a reconstituted 12-subunits complex with an endogenous core and recombinant Rpb4/7 (Armache et al., 2003), whereas Bushnell and colleagues used an affinity tag on Rpb4 in order to purify the complete complex devoid of core Pol II that otherwise would result in poorly ordered crystals (Bushnell and Kornberg, 2003).

The first structure of human RNA Pol II, purified from HeLa cell nuclei, at intermediate resolution was provided by the Nogales lab (Kostek et al., 2006). They found that the overall structure of human RNA Pol II was similar to the one published in yeast, as expected based on the high degree of conservation (53% of identity) between both RNA Pol II. Recently, the Cramer lab has provided the structure of transcribing mammalian RNA Pol II at high resolution (3.4 Å) from cryo-electron microscopy (cryo-

EM), which allowed to unveil multiple conformations, therefore providing a better insight into the dynamic of the complex (Bernecky et al., 2016).

Combined together, all of these studies have allowed to define 4 flexible modules of the RNA Pol II:

- The **core module** represents half of the Pol II mass and contains the Rpb3, 10, 11, 12 subunits as well as the active center formed by Rpb1 and Rpb2 with a deep cleft between them for the nucleic acid entry (Figure 2C). Rpb1 and Rpb2 are the largest subunits of Pol II and are organized into multiple domains with crucial functions for Pol II transcription initiation (Figure 2A, B). For example, Rpb2 contains a “wall” domain that blocks the DNA path leading to a 105° angle bend orienting DNA path optimally for transcription.
- The **jaw-lobe module** composed of the upper jaw made up of Rpb1, Rpb2 and Rpb9 regions.
- The **shelf module** containing the lower jaw, which consists in the assembly of domains of RPB5, RPB6 and the foot and cleft regions of Rpb1.
- The **clamp module** which comprises Rpb1, Rpb6 and Rpb2. The clamp module is connected to the cleft region through switch regions that are flexible. This flexibility allows a swinging motion of the clamp over the cleft resulting therefore in a defined and closed position of the clamp, as well as a greater opening of the cleft which may lead to the entry of promoter DNA for the initiation of transcription.

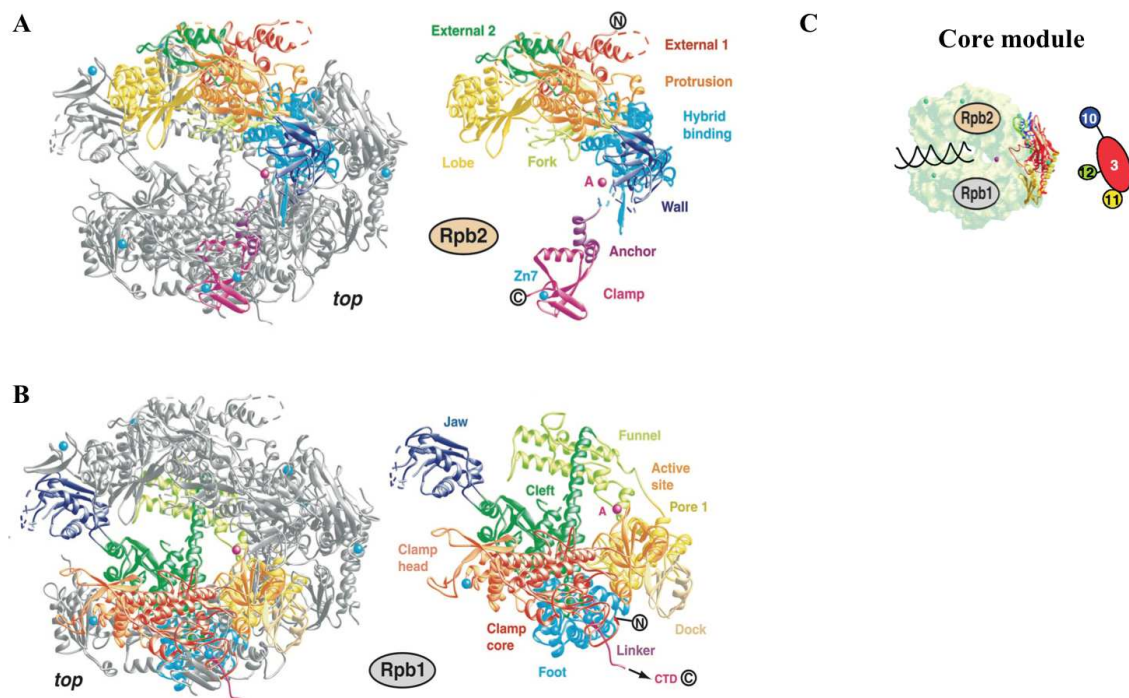


Figure 2: Structure of the core module of RNA polymerase II. Ribbon diagrams showing the location within RNA Polymerase II complex of Rpb2 (A) and Rpb1 (B) (tops views), as well as their specific domains. (C) Scheme of the core module components. Adapted from (Armache et al., 2003; Cramer et al., 2000).

Interestingly, the RNA Pol II “core” structure (10-subunits) was defective in transcription initiation, whereas the “complete structure” (12-subunits) was able to restore the initiation activity. Rpb4/7 was shown to lock the clamp in the closed conformation and to protrude from the “upstream face” of Pol II, thus extending the “dock” domain of Pol II which interacts with initiation factors (Figure 3). Therefore, the Rpb4/7 heterodimer forms the polymerase “stalk” and plays an important role in the transcribing complex assembly.

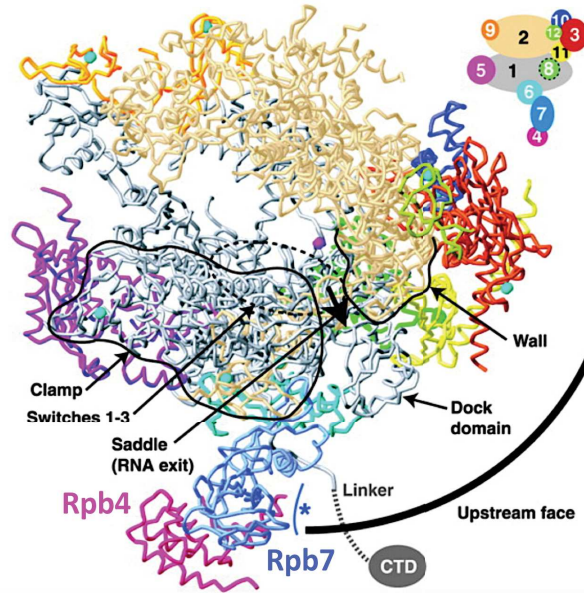


Figure 3: Architecture of the 12-subunits Pol II. Ribbon model showing the RNA Pol II upstream interaction face and the “stalk” composed of Rpb4/7. Color-coded subunit composition is shown in the upper right corner. Adapted from (Armache et al., 2003).

Despite its high complexity, RNA Polymerase II is not able to bind DNA directly and therefore requires additional proteins to bring and tether it to core promoters. These proteins are termed General Transcription Factors (GTFs) and include TFIIA, TFIIB, TFIID, TFIIIE, TFIIF and TFIH, which assemble with RNA Pol II at promoters to form the PIC.

1.2.2. Canonical PIC assembly: roles of the different GTFs

Many distinct protein complexes are involved in the activation of promoters for transcriptional initiation. Although the precise timing and ordering of their recruitment is still debated, transcription initiation results in a highly regulated reorganization of the chromatin structure within the promoter that allows the formation and stabilization of the PIC.

So far two different models of PIC assembly have been described. A sequential assembly pathway, in which GTFs assemble in a stepwise manner (Buratowski et al., 1989; Orphanides et al., 1996), and the RNA Pol II holoenzyme pathway, that bypass the recruitment of all GTFs individually. The latter has been supported by the discovery of several holoenzyme complexes containing Pol II and

a variable subset of GTFs, depending on the protocol used for the purification (Myer and Young, 1998; Ranish et al., 1999). Although pre-assembled Pol II complexes seem to exist in the cell, the stepwise pathway has been best described and studied so far. It is characterized by several steps described below (Figure 4).

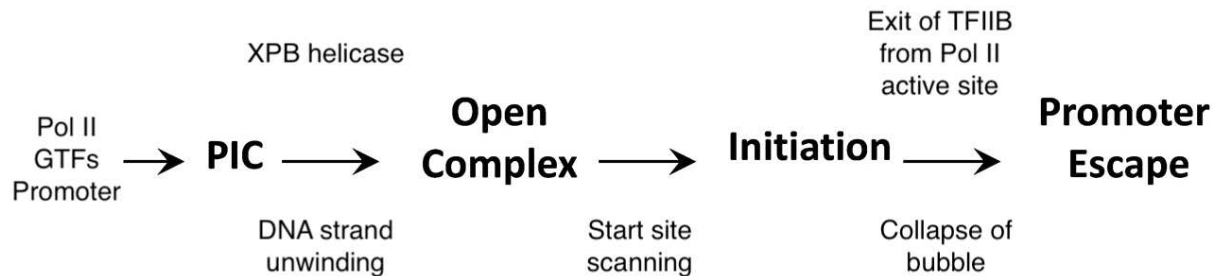


Figure 4: Stepwise model of Pol II transcription initiation. Overview of the steps that characterized the stepwise pathway of Pol II transcription initiation, starting with PIC assembly, then DNA opening. The open complex allows the TSS scanning and RNA synthesis. Soon after the beginning of transcription, TFIIB is released and Pol II undergoes promoter escape. Adapted from (Hahn and Young, 2011).

a) TFIID-DNA interaction and stabilization by TFIIA and TFIIB

The first step in the classical model of stepwise PIC assembly is the sequence-specific binding of TBP to the minor-groove of the TATA-box. The DNA is bent at an angle of about 90°, which is thought to influence the recruitment and stabilization of RNA polymerase and GTFs (Figure 5).

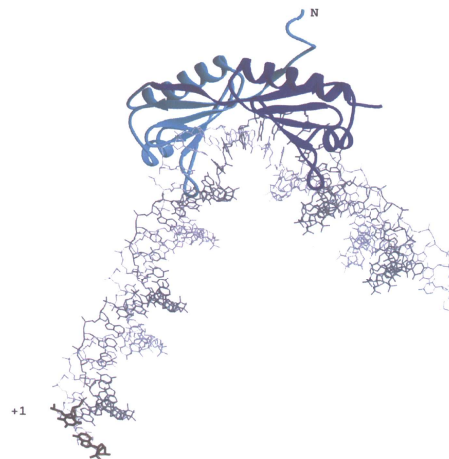


Figure 5: Structure of the TBP-TATA element binding. Ribbon representation of TBP with its amino- and carboxy- terminal parts, in light blue and dark blue, respectively. TBP binds the minor groove of the TATA element and induces a partial unwinding and bent in the DNA.

TBP interacts with 13 other proteins called TAFs (TBP-Associated Factors) to form the TFIID complex (Figure 6), which allows several interactions with DNA elements that are parts of the core promoter.

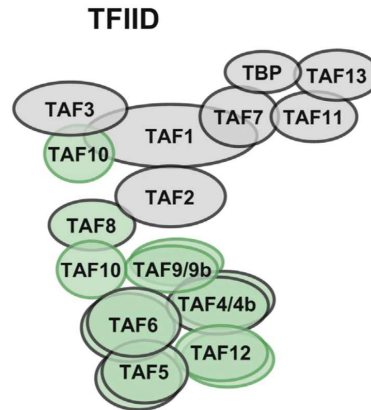


Figure 6: Schematic composition of TFIID complex. TFIID is composed of TBP subunit associated with 13 TAFs. Subunits in green are shared subunits found in other complexes. Subunits in grey are TFIID specific subunits. Adapted from (Helmlinger and Tora, 2017).

TFIID is a general transcription factor, it has a horseshoe-like structure, with a central cavity surrounded by three lobes (A, B, C). Depending on the position of lobe A, TFIID is able to rearrange and therefore adopts two major conformations, named canonical (lobe A interacts with lobe C, Figure 7 left) and rearranged (lobe A binds lobe B, Figure 7 right) (Cianfrocco et al., 2013). Lobe A can be divided in two, a more stable lobe and a highly flexible lobe, A1 and A2 respectively (Louder et al., 2016). The rearranged state appears to correspond to TFIID that binds promoter DNA, whereas the canonical conformation matches free-TFIID, and both states were shown to be modulated by TFIIA binding. In fact, Cianfrocco and colleagues showed that the presence of promoter DNA, as well as TFIIA, promote the formation of the rearranged state of TFIID. In contrast, in the absence of DNA, TFIIA maintains TFIID in the canonical state (Figure 7).

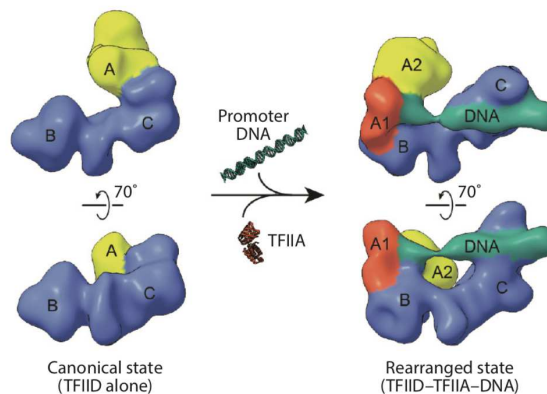


Figure 7: Cryo-EM 3D reconstructions of TFIID states. TFIID is subjected to conformational rearrangement during PIC formation. The density corresponding to the lobes B and C (in blue) does not undergo conformational changes. In contrast, the lobe A (in yellow), which is near lobe C in the canonical state (left panel), is moved near lobe B in the rearranged state, upon promoter DNA and TFIIA addition (right panel). DNA (in green) binds to the rearranged TFIID and a part of lobe A, A1 (in orange) appears after conformational changes and contains TBP and TFIIA. From (Nogales et al., 2017).

TFIIA is composed of a 12-stranded β -barrel and a 4-helix bundle motif (Figure 8). The β -barrel binds to the underside of TBP and bridges over to DNA major groove, upstream of the TATA box. In contrast, the tip of the 4-helix bundle is oriented towards lobe B of TFIID (Figure 8). This is consistent with the stabilizing role of TFIIA on TBP-DNA complex and corresponds to the second step of PIC assembly.

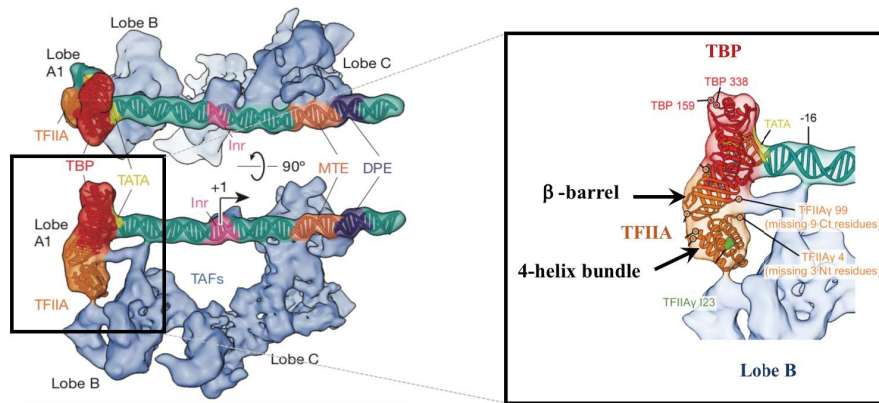


Figure 8: Cryo-EM reconstruction of TFIID-TFIIA and the super core promoter complex. Close-up view of the TBP-TFIIA-TATA binding module revealing the structural motifs of TFIIA and its specific interactions with TBP and TFIID. Adapted from (Louder et al., 2016).

The surprising degree of flexibility of TFIID may be an important determinant of PIC assembly. Moreover, TFIID modulates TBP activity through its TAF1 subunit. The N-terminus region of TAF1 contains two domains TAND1 and TAND2, which compete with the binding of TBP to DNA and to TFIIA, respectively. Indeed, the TAND1 domain mimics the structure of the TATA DNA sequence and is therefore able to bind the DNA-binding surface of TBP. The TAND2 domain binds to the convex surface of TBP, thereby competing with TFIIA. These inhibitions are relieved after the binding of TFIIA, which correlates with the conformational change in TFIID, from canonical to rearranged state (Figure 9). Therefore, the conformational rearrangement of TFIID and the binding of TFIIA are coupled and play critical roles in regulating TBP binding to DNA.

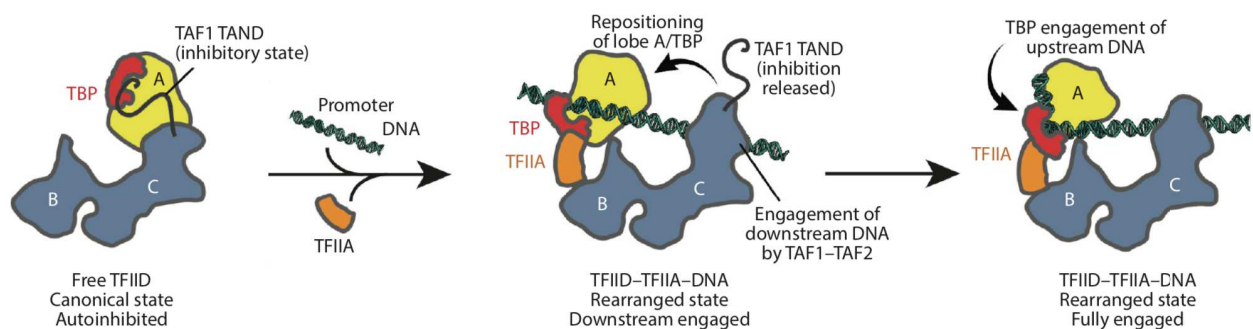


Figure 9: Current model of promoter binding by TFIID. Free TFIID (left), is in the autoinhibitory canonical state, in which TBP is blocked by the TAND1 domain of TAF1 and cannot bind to promoter DNA. Presence of TFIIA and promoter DNA release the inhibitory effect of TAF1 and drive TFIID into the rearranged state (middle). TAF1-TAF2 initiate interactions with downstream promoter region, leading to the fully engaged rearranged state (right) by placing the upstream promoter DNA in position to be engaged by TBP. Adapted from (Nogales et al., 2017)

TFIIB is the only GTF with a single polypeptide. TFIIB is absolutely required to recruit Pol II pre-bound to TFIIF and stabilize TBP interaction to the promoter, playing a central role in initiation (Deng and Roberts, 2007). The amino-terminal part of TFIIB referred to as “B-ribbon” contains a zinc-chelating motif that makes contacts with Pol II dock domain, the B-ribbon extends into the cleft of Pol II towards the active center. This extension corresponds to the B-reader and the B-linker domains (Figure 10A). The carboxy-terminal region called “B-core” bears two cyclins folds, which bind the Pol II wall and TBP-DNA, respectively (Figure 10B-C) (Kostrewa et al., 2009).

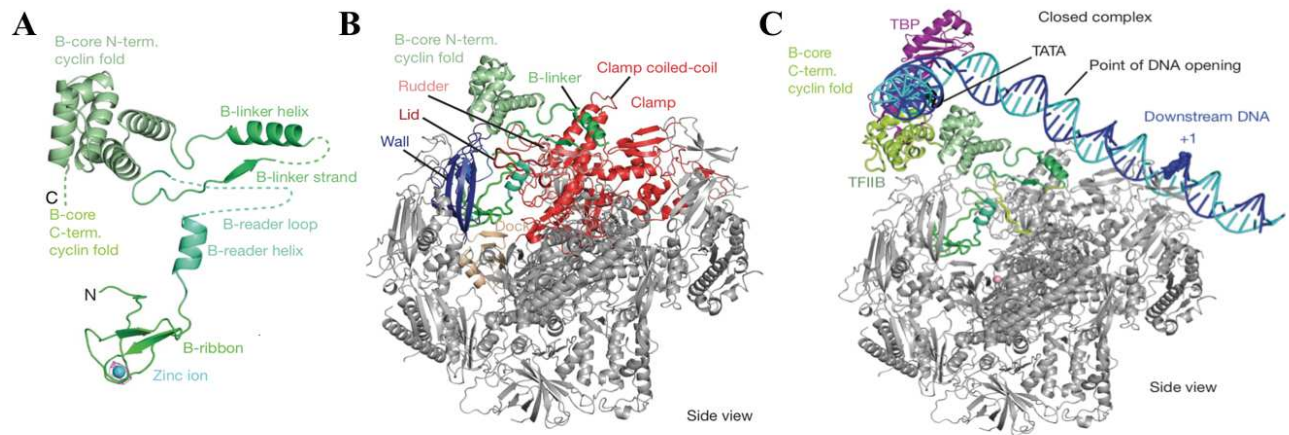


Figure 10: Structure of Pol II-TFIIB complex. (A) Ribbon representation of TFIIB structure, as observed in interaction with Pol II. (B, C) Side views of Pol II and TFIIB domain interactions, in ribbon representation. (B) Pol II domains which interact with TFIIB are highlighted. The N-term. cyclin fold domain of TFIIB interacts with the Pol II wall domain (dark blue) and (C) the C-term. cyclin fold domain of TFIIB interacts with TBP-DNA (TBP, purple; DNA template, blue and cyan). Adapted from (Kostrewa et al., 2009).

Despite its role in Pol II recruitment and stabilization of TBP to DNA, TFIIB displays additional functions, notably TSS selection and DNA opening, which is carried by the B-reader and B-linker domains, respectively. TFIIB contributes to melting of the two strands of DNA to create an open promoter confirmation, which characterizes the initiation-elongation transition (Figure 11) (Kostrewa *et al.* 2009).

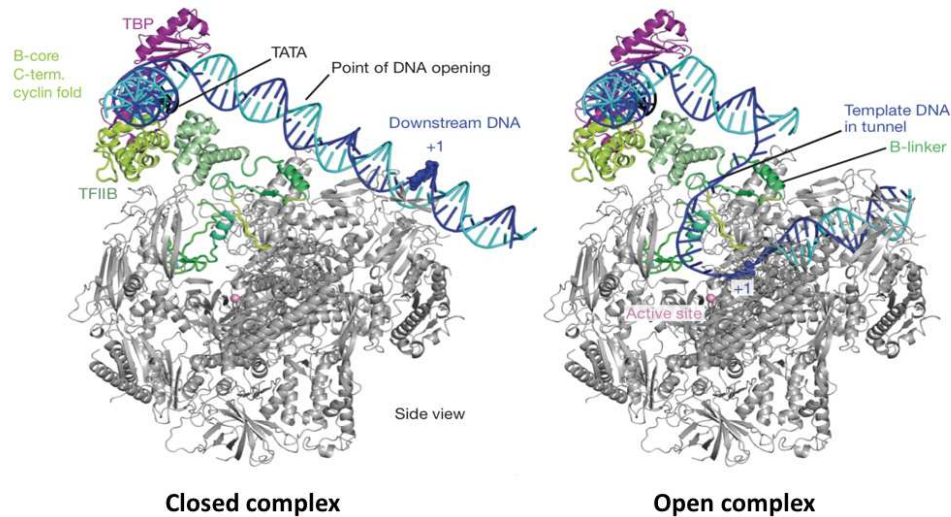


Figure 11: Models of closed and open complexes. In the closed complex (left), promoter DNA is positioned over the Pol II active center (pink sphere) with the ‘B-core’ domain that binds the Pol II wall domain. DNA is then open (right) with the help of the ‘B-linker’.

In the closed conformation, promoter DNA is positioned over the Pol II cleft by the B-core located above the wall (Figure 11, left). During the transition from a closed to an open conformation, promoter DNA is melted around 20 bp downstream the TATA-box. This leads to the formation of a bubble and provides a single-stranded template DNA, which slips into the active site of Pol II, helped by the B-linker, which interacts with the coiled-coil and the rudder (loop nearest the active center) regions of the clamp (Figure 11, right). At this moment, the DNA template is scanned by the B-reader for an Inr motif (DNA start site scanning). Then, synthesis of the RNA strand starts and TFIIB is released when the RNA reaches a length of 12-13 nucleotides. TFIIB release is accompanied by Pol II promoter escape and elongation complex formation.

b) TFIIF and Pol II recruitment

TFIIF is a heterodimer formed by two subunits TFIIF α and TFIIF β . TFIIF interacts with Pol II at separate locations through two different domains. A dimerization domain with a triple barrel fold and a β -hairpin “arm”, formed by the N-termini of both subunits, anchors the Rpb2 lobe of Pol II (Gaiser et al., 2000; He et al., 2013). The winged helix domain (WH) of TFIIF β binds the B-core of TFIIB, RNA Pol II above the protrusion domain, as well as a BRED element within upstream promoter DNA (He et al., 2013).

TFIIF is an integral component of the PIC and functions in facilitating Pol II incorporation and positioning at TSS, stabilizing TFIIB, and thus promoting transcription initiation and start site selection.

c) TFIIE, TFIIH and promoter DNA opening

TFIIE and TFIIH are recruited to form a transcriptionally competent PIC and are also involved in DNA opening. TFIIE is located between the stalk and the clamp domains of Pol II and is composed of two subunits. TFIIE α contains a WH domain at the N-terminal end (eWH) followed by a Zn ribbon domain that binds Rpb7 of the stalk domain of Pol II (Figure 12). TFIIE β consists of a tandem of two WH domains that bind the clamp domain of RNA Pol II and DNA. This triple WH structure interacts with the clamp head of RNA Pol II and encircles promoter DNA (Grünberg et al., 2012; Plaschka et al., 2016). TFIIE elongates towards TFIIF to interact with the WH domain of TFIIF β . Thus, this continuous chain of 4 consecutive WH domains allows to link the RNA Pol II clamp region with the TBP-TFIIA-TFIIIB-TFIIIF subcomplex, trapping DNA on the surface of RNA Pol II (Figure 12) (He et al., 2013).

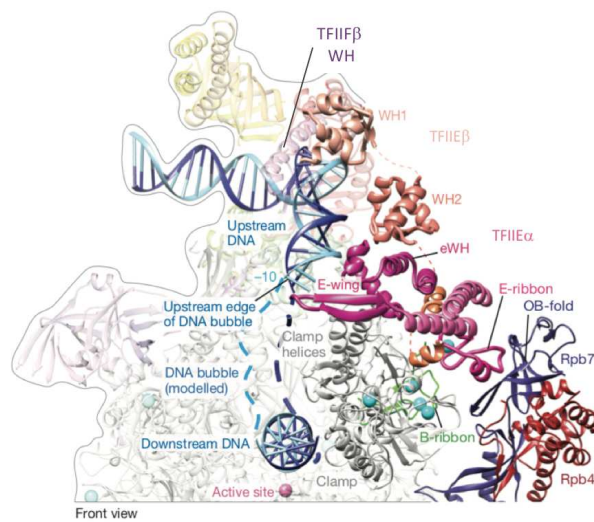


Figure 12: DNA positioning and retention by TFIIE-TFIIF winged helix domains. DNA promoter (blue and cyan) is positioned and retained over the Pol II cleft by a network of interactions involving four consecutive winged helix domains. One from TFIIF (purple) and three of TFIIE (from orange to magenta). The E-ribbon domain of TFIIE α interacts with Pol II Rpb7 (navy blue) subunit of the Pol II stalk domain. Adapted from (Plaschka et al., 2016)

Consequently, the promoter DNA is well positioned over the RNA Pol II cleft where it will be subject to melting by TFIIH. This event requires several structural transitions. First, the clamp domain of Pol II closes down to engage the open DNA bubble (Figure 13A). The separation of the two strands is facilitated by the TFIIIB linker helix and TFIIIF arm domains that align together at the promoter melting site (Figure 13B). Second, to prevent re-annealing of the melted DNA, both domains as well as the rudder of Pol II interact to maintain the upstream edge of the DNA bubble (Figure 13C).

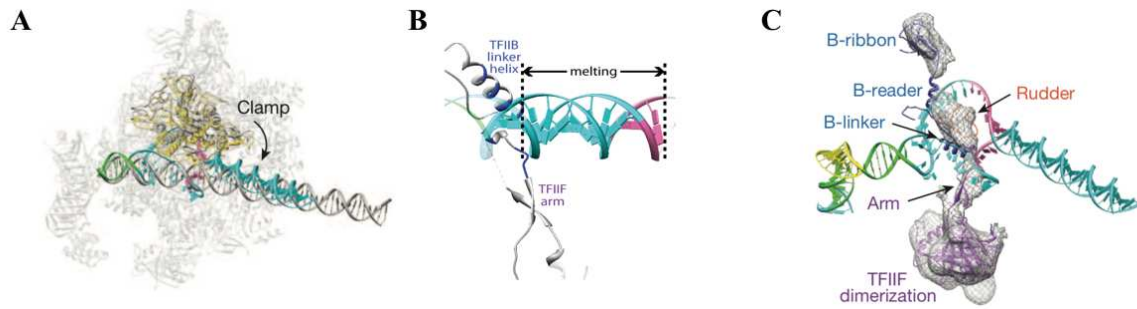


Figure 13: Structural transitions accompanying DNA melting. (A) Structures before (grey) and after (colored) promoter opening. Pol II clamp domain comes down over the open bubble. (B) The flexible TFIIB linker helix (dark blue) and the TFIIF arm (purple) align together at the melting site. The melting region of the promoter DNA, ~20bp downstream of TATA, is indicated. (C) The arm domain of TFIIF connects the rest of TFIIF and interacts with the rudder of Rpb1 (orange). Adapted from (He et al., 2013).

TFIIH is a 10-subunit factor that consists of a 6-subunit core module containing XPB, p62, p52, p34, p8 and p44 subunits; and a 3-subunit kinase module formed by CDK7-cyclin H-MAT1. These modules are bridged together by the XPD subunit. The activity of XBP during transcription initiation has been controversial. Instead of hydrolysing ATP to open DNA through a helicase activity, it was suggested that XBP acts as a translocase, walking on DNA and therefore inducing a supertwist facilitating DNA melting (He et al., 2013). Recently, Alekseev and colleagues showed that cells are able to accommodate a loss of XBP but are sensitive to an inhibition of its ATPase activity demonstrating that the XPB ATPase overcomes a transcription initiation block imposed by XBP itself (Alekseev et al., 2017). Moreover, the CDK7 kinase plays an important role in transcription initiation, because it is responsible for the phosphorylation of the RNA polymerase II CTD at Ser5.

2. Stimulation of the basal transcription machinery

PIC assembly on core promoters is sufficient to direct only low levels of transcription, referred to as basal transcription. In addition to the core promoter, others *cis*-acting DNA elements are found to regulate transcription, such as enhancers, silencers, insulators and locus control regions (LCR) (Figure 14). These more distal regulatory elements contain specific sequences, which serve as motifs of recognition for *trans*-acting DNA-binding transcription factors that greatly stimulate transcriptional activity.

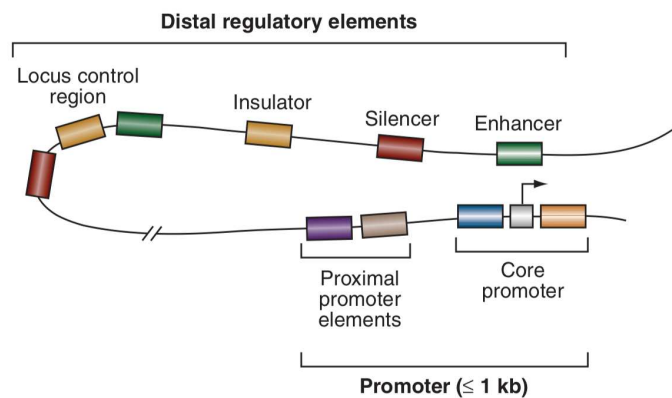


Figure 14: Schematic representation of *cis*-acting DNA elements. The regulatory region of a gene encompasses the promoter which spans less than 1kb, as well as more distal elements located up to 1Mb of the promoter and that can contact it through looping. From (Maston et al., 2006).

2.1. *Cis*-acting DNA elements

2.1.1. Proximal promoter

Proximal promoter elements correspond to regions immediately upstream of the core promoter, spanning up to hundred base pairs and altering the rate of transcription. One example is the CCAAT box which is a very frequent proximal promoter element found in 30% of eukaryotic promoters (Bucher, 1990). This motif is bound by the heterotrimeric complex NF-Y and plays a role in transcription activation (Mantovani, 1999). Another example is the CpG island associated with 60% of mammalian promoters. A high G+C nucleotide content is generally unmethylated in active genes, whereas their methylation is rather promoting gene silencing. Therefore, the proximal promoter is an important feature regulating the transcription of a gene.

2.1.2. Enhancers

Contrary to proximal promoter elements, enhancers act at a long distance, up to several kb from the core promoter and are not orientated. Enhancers contain multiple binding sites for various transcription factors. Therefore, enhancers regulate the activity of promoters through a DNA-looping model, which brings enhancers in close proximity to promoters, allowing the formation of the PIC in the appropriate spatial conformation and transcription to occur (Vilar and Saiz, 2005). Interestingly, some studies have provided evidence that Pol II and others GTFs could bind enhancers, regulating thus the timing of gene activation. Indeed, the formation of a premature PIC at distal enhancers might keep genes in a potentiated state, protected from an aberrant or unwanted activation. Therefore, enhancers function as nucleation centers that would allow a quick and efficient activation of a gene at the right time and the right place (Szutorisz et al., 2005).

2.1.3. Silencers

Like enhancers, silencers are distance- and orientation-independent elements that regulate promoters but instead of activating transcription, they negatively affect gene expression. Silencers represent binding sites for repressors factors that mediate repression either by blocking the binding of a nearby activator competing for the same site or by preventing the access or formation of the PIC on promoters.

2.1.4. Insulators

Insulators elements act as barriers to restrict the action of regulatory elements to one gene, preventing therefore the inappropriate action of enhancers or silencers on neighboring genes. Insulators are crucial organizers of the genome and partition it into domains with distinct properties. Insulators function in a distance-dependent but orientation-independent manner, through two main activities. An enhancer-blocking activity and a heterochromatin-barrier activity, which inhibit the communication between enhancers and promoters and avoid the spread of repressive chromatin marks, respectively (Brasset and Vaury, 2005). Insulators mediate their activity through *trans*-acting factors, such as the well-studied CTCF factor, which regulate the spatial organization of the genome by demarcating the boundaries of topologically associating domains (TADs) (Ghirlando and Felsenfeld, 2016).

2.1.5. Locus control regions

Locus control regions are characterized by a cluster of different *cis*-regulatory elements including those defined above, which synergize to confer proper temporal and/or spatial regulation of the expression of a cluster of nearby genes. The best example and first LCR identified in mammals is the β -globin LCR, which acts in an orientation-dependent manner and allows to temporally regulate the expression of the five globin genes during development (Tanimoto et al., 1999).

2.2. DNA-binding transcription regulators

These *cis*-regulatory regions contribute to transcriptional regulation because their information content is read and translated into regulatory activities through the recognition and binding of *trans*-acting factors, which are typically called transcription factors (TF).

A transcription factor is defined as a protein capable to bind DNA directly in a sequence-specific manner and to regulate transcription. Although, transcription factors have the ability to recognize and bind specific DNA sequences, the chromatin landscape, particularly nucleosome positioning, greatly impacts their binding (Li et al., 2007). Many transcription factor binding sites (TFBS) are indeed localized in nucleosome-depleted regions (NDR), which represent accessible DNA regions in gene promoters (Ozsolak et al., 2007). However, genome-wide analyses of TF distributions revealed that most of their putative DNA-binding sites are in fact not localized in the promoter region and are mainly unoccupied, revealing an inability for TFs to bind nucleosomal DNA, which has been shown to represent a steric barrier (Farnham, 2009; Yang et al., 2006). Therefore, in order to achieve binding in such environment, TFs rely on various strategies. For instance, most of TFBS are found clustered, so that TFs can interact in a cooperative manner allowing binding over nucleosome-wrapped sequence motifs (Adams and Workman, 1995).

Moreover, during development and cell reprogramming, a specific class of TFs was found to bind condensed chromatin, prior to gene activation and prior to the recruitment of others TFs. These factors called “pioneer transcription factors” render the chromatin competent for the subsequent binding of others TFs (Zaret and Carroll, 2011). Finally, TFs binding is also facilitated by specific histones modifications, as an example, the methylation of the lysines 4 and 79 of the histone 3 (H3K4/K79me) acts as a prerequisite for the binding of the MYC transcription factor on its binding sites (Guccione et al., 2006).

Once TFs are bound to DNA, they can mediate activation or repression of transcription. Therefore, TFs have been classified either as “activators” or “repressors”. Nevertheless, a more precise terminology is warranted since it was shown that a same TF can recruit different co-factors with opposite effects, suggesting that transcription factors act in a context-dependent manner. TFs represent 8% of all human genes and are classified in families based on the structure of their DNA-binding domain (DBD), which includes C2H2-zinc finger (ZF), homeodomain (HD), basic helix-loop-helix (bHLH), basic leucine zipper (bZIP), nuclear hormone receptor (NR), forkhead domain, E26 transformation-specific domain (ETS), high mobility group domain (HMG) or Pit-Oct1/Oct2-Unc-86 (POU) DNA-binding domain (Figure 15).

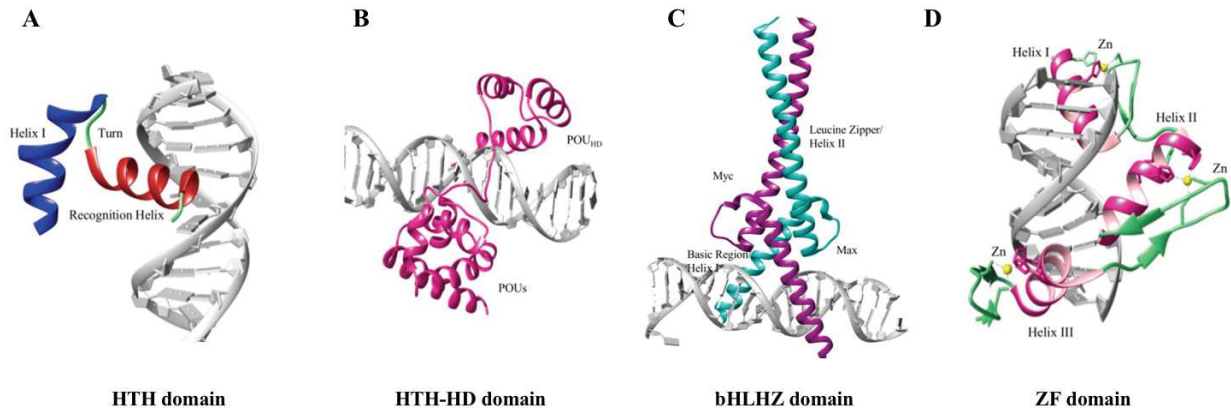


Figure 15: DNA-binding domain structures of four transcription factors. (A) HTH domain of human heat shock transcription factor 1 (HSF1). (B) POU specific domain (POUs) and POU homeodomain (POU_{HD}) of OCT4 transcription factor. (C) Basic/helix-loop-helix/leucine zipper (bHLHZ) domains of Myc-Max heterodimer. (D) Zn finger of Krüppel-like factor 4 (KLF4) transcription factor. Adapted from (Yesudhas et al., 2017).

In their study, Lambert and colleagues have analyzed 2765 putative transcription factors, including 1639 known or probable transcriptions factors and 1107 harboring a known DNA binding motif. Their analysis nicely revealed that the more represented DBD types are C2H2-ZFs (747) and Homeodomains (196) (Lambert et al., 2018).

The basic function of a TF is to activate the transcription machinery to the promoter, but TFs do not bind Pol II. Rather, TFs recruit co-regulators that control Pol II activity either directly, such as Mediator, or indirectly, such as chromatin-remodeling or -modifying complexes.

2.3. Co-activators

Co-activators are often multi-protein complexes, although monomeric co-activators exist, which regulate the rate and magnitude of transcription initiation, either by interacting directly with Pol II and/or GTFs or by locally modulating promoter chromatin architecture.

2.3.1. Mediator co-activator complex

Mediator complex has been identified more than 20 years ago in yeast and mammals as a critical transcriptional co-activator which facilitates and stabilizes PIC assembly. Mediator is a multimeric protein complex of ~1MDa comprising 30 subunits in humans that are highly conserved throughout evolution. Mediator subunits are organized in four separate modules: the head, the middle and the tail, arranged around a central scaffold formed by MED14 subunit, and transiently in contact with the fourth module, comprising the CDK8 kinase (Figure 16). The head and the middle modules form the core of the complex, which is essential to stimulate transcription initiation. In contrast, the tail and the kinase modules have more specific, regulatory functions.

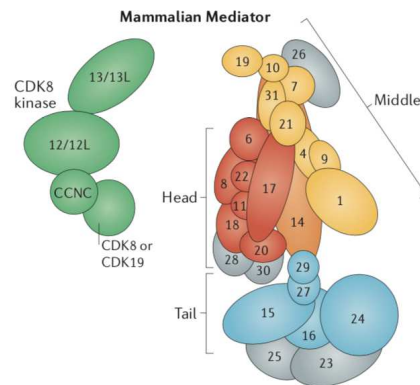


Figure 16: Composition of the Mediator complex. Schematic representation of the modular organization of the mammalian Mediator complex. Mediator comprises four distinct modules: the head module (in red), the middle module (in yellow) and the tail module (in blue). All three interact with Mediator subunit 14 (MED14) (in orange), which acts as a scaffold. The CDK8 kinase module (in green) associates transiently with the complex.

Studies of Pol II CTD in yeast have allowed the identification of Mediator (Kim et al., 1994; Thompson et al., 1993). Later it was confirmed in human that the head region of Mediator, without the CDK8-kinase module, was able to interact with Pol II CTD (Näär et al., 2002). The binding of Pol II to the Mediator complex leads to structural changes, notably in the leg/tail domain of Mediator which represents the interaction site of the CDK8 module. Therefore, the binding of Pol II and CDK8 module to Mediator is mutually exclusive. The CDK8 module acts as a switch and represents a way to regulate transcription initiation and re-initiation by ensuring appropriate timing of transcription events (Knuesel et al., 2009).

Besides Pol II, Mediator has been reported to interact physically and/or functionally with every factor of the PIC (Poss et al., 2013). Indeed, Mediator is able to form a functional bridge between transcription activators and components of the PIC (Figure 17). Therefore, by interacting and cooperating with the PIC components, Mediator assists PIC assembly. TFs cannot bind directly Pol II and Mediator is believed to serve as a bridge between TFs and RNA polymerase II.

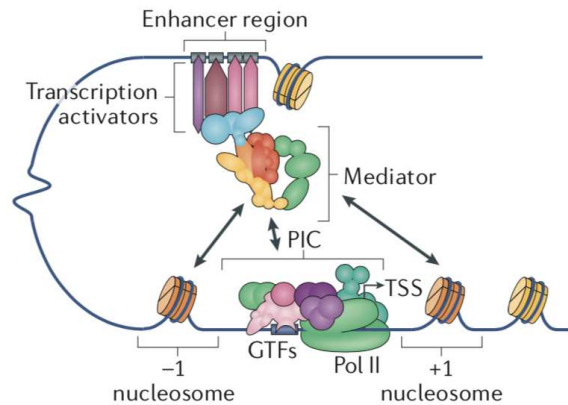


Figure 17: Interplay between Mediator, the PIC, and the promoter architecture. Mediator interacts with components of the PIC such as Pol II and some GTFs, bridging therefore transcription activators to RNA Pol II. Mediator is involved in nucleosome eviction, and therefore interacts also with the promoter architecture. These interactions are depicted by bidirectional arrows.

Mediator is recruited to enhancers via direct interactions with hundreds of different TFs. These interactions involve different subunits of Mediator specific to each TF. For instance, a knock-out model in murine embryonic stem cells (mESCs) of MED23, which is bound by the Elk-1 TF, has revealed that the transduction of the Elk-1 response was abolished in MED23 lacking cells, but not the transcription mediated by others TFs that interact with others subunits of Mediator (Stevens et al., 2002). These results suggest that TFs rely on specific subunits of Mediator to mediate their transcriptional effects. Therefore, Mediator regulates transcription by integrating signals from different TFs which in turn influence its function and its conformation (Meyer et al., 2010; Taatjes et al., 2002).

2.3.2. Chromatin-remodeling complexes

DNA is wrapped around nucleosomes, which are formed by an octamer of the H3, H4, H2A, and H2B proteins, limiting its accessibility to DNA-dependent machineries and consequently, nuclear processes such gene transcription, DNA replication, and repair. Nucleosomes and higher-order chromatin structure indeed represent a well-characterized obstacle to transcription. ATP-dependent macromolecular complexes remodel nucleosomes to make the DNA template accessible to the transcription machinery. These complexes referred to as chromatin remodelers are classified in four subfamilies: imitation switch (ISWI), chromodomain helicase DNA-binding (CHD), switching defective/sucrose non-fermentable (SWI/SNF) and inositol requiring INO80 (INO80) (Clapier et al., 2017). Chromatin remodeling is achieved through different mechanisms, including nucleosome repositioning, sliding, editing, or ejection.

Each subfamily appears to be specialized in one mechanism, for instance ISWI and CHD remodelers affect nucleosome assembly and organization, by facilitating the *de novo* assembly of nucleosomes and ensuring their regular spacing at transcribed genes. SWI/SNF regulate access to

chromatin by inducing the sliding, eviction, or ejection of nucleosomes, which expose binding sites for transcription factors. Members of the INO80 subfamily are implicated in nucleosome editing characterized by the incorporation or removal of histones variants (Figure 18). Although they display different activities, all chromatin remodelers share a common property: a conserved ATPase activity that catalyzes the disruption of DNA-histones contacts and translocates DNA.

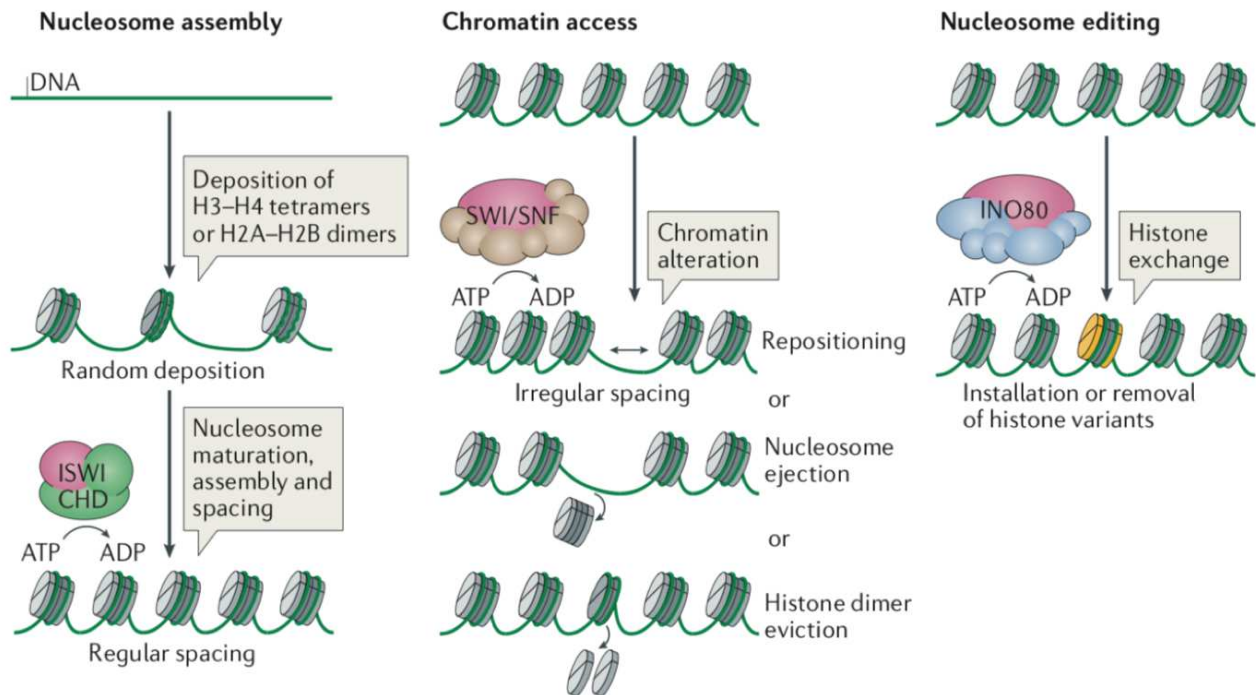


Figure 18: Functional classification of chromatin remodelers. Three major mechanisms are involved in chromatin remodeling. Nucleosome assembly (left) is characterized by the random deposition of histones, the maturation of nucleosomes and their spacing. Chromatin access (middle), which involves SWI/SNF remodelers, consists of the chromatin alteration by repositioning nucleosomes, evicting histone dimers or ejecting octamers. Nucleosome editing (right) leads to changes in nucleosome composition by exchanging canonical and variant histones (in yellow). The ATPase translocase of all remodelers is shown in pink.

2.3.3. Histone-modifying enzymes

Nucleosomes are not only subjected to remodeling by chromatin remodelers, but are also post-translationally modified by dedicated enzymes. Each histone harbors an amino-terminal part rich in basic residues, called histone “tails”, which protrude from the nucleosome surface and are targeted by histone-modifying enzymes (Figure 19) (Peterson and Laniel, 2004).

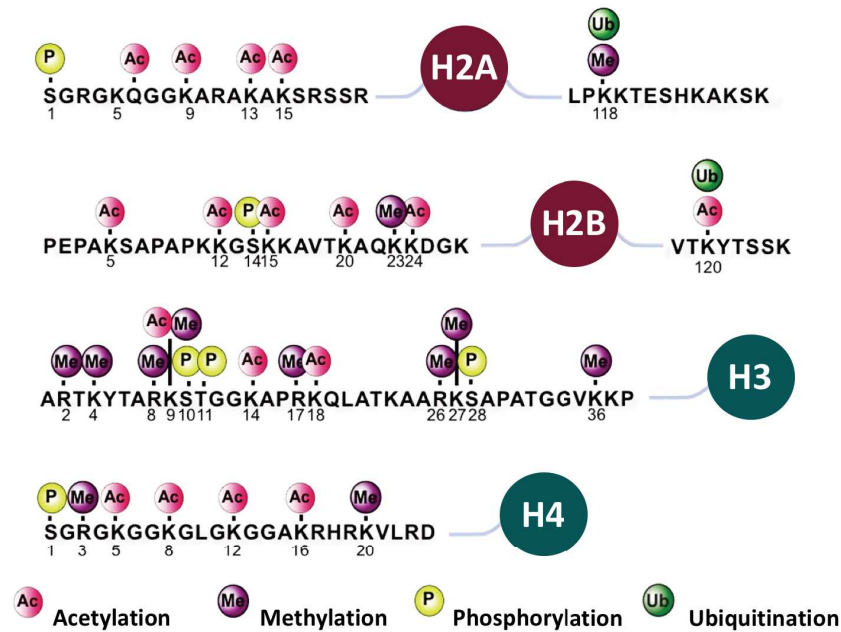


Figure 19: Overview of histone modifications. H2A and H2B (dark red) are modified at both the N-terminal and C-terminal parts. In contrast H3 and H4 (dark green) are subjected to modifications in their amino-terminal tails. Numbers under modified residues indicate their position. Four different modifications are depicted, acetylation (Ac, pink), methylation (Me, purple), phosphorylation (P, yellow), and ubiquitination (Ub, green). Adapted from (Kato et al., 2010).

Similar to a concept put forward in the field of signal transduction, histone post-translational modifications (PTMs) are highly dynamic and deposited by enzymes that act as “writers”, removed by another set of enzymes that act as “erasers”, and specifically recognized by “reader” domains found in many transcription cofactors. Histone tails are modified at many sites by at least eight distinct classes of modifications (Table 1) (Kouzarides, 2007).

CHROMATIN MODIFICATIONS	RESIDUES MODIFIED
Acetylation	K-ac
Methylation	K-me1 K-me2 K-me3 / R-me1 R-me2
Phosphorylation	S-ph / T-ph
Ubiquitination	K-ub
Sumoylation	K-su
ADP-ribosylation	E-ar
Deimination	R > Cit
Proline isomerization	P-cis > P-trans

Table 1: Overview of different classes of chromatin modification. Each residue targeted is depicted in bold. Adapted from (Kouzarides, 2007).

Besides the high diversity of histone PTMs that have been discovered, each accessible histone residue is potentially a target for PTM, resulting in a combinatorial pattern of histone marks. Moreover, methylation exists on different forms. Lysine and arginine can accept one or two methyl groups whereas only lysine can be tri-methylated. This complexity has been proposed to create a so-called histone code, in which the combination of specific histone marks dictates different transcriptional outcomes.

For instance, the spreading of histone modifications establishes a chromatin environment over large regions of DNA, creating two major types of chromatin. Euchromatin is accessible and contains transcriptionally active genes. Heterochromatin is less accessible and contains silenced genes. Each type is associated with different sets of modifications that recruit specific proteins, or “readers”. For instance, Heterochromatin Protein 1 binds the methylated lysine 9 of histone 3 (H3K9me3) and mediates transcriptional repression by compacting chromatin and maintaining the heterochromatin state. As a consequence, modifications are generally classified as either activating or repressing. However, this distinction has been challenged by numerous studies. Indeed, the same mark affects transcription differently, depending the context. One such example is H3K36me which is implicated in transcription activation as well as repression (Wagner and Carpenter, 2012).

In contrast, histone acetylation appears invariably associated with transcription activation. Acetylation is thought to establish a more open and permissive environment for transcription by neutralizing the charge of the histone tail, weakening the interaction between histone and DNA (Roth et al., 2001). Histone acetylation is directed by histone acetyltransferases (HATs) enzymes which are classified into several families based on the structural and functional similarities of their catalytic domain. For instance, Gcn5 and PCAF belong to the GNAT (Gcn5-related-N-acetyltransferase) family and TIP60 is a member of the MYST (Moz, Ybf2, Sas2, and Tip60) (Table 2).

HAT family	Members	Histone substrate
GNAT	GCN5, PCAF, ELP3	H3K9, 14, 18, 36
MYST	TIP60, MOZ, MORF, HBO1, HMOF	H4K5, 8, 12, 16, H3K14
p300/CBP	p300, CBP	H2AK5, H2BK12, 15, H3K14, 18, H4K5, 8
Transcription factor related	TFIIC, TAF1	H3K9, 14, 18
Nuclear receptor co-activators	SRC, ACTR, P160, CLOCK	H3/4

Table 2: HAT families. Members of each family and their specific histone substrates are indicated. Adapted from (Lu et al., 2015; Roth et al., 2001).

Importantly, several monomeric HAT enzymes can only acetylate free histones and fail to acetylate nucleosomal histones (Grant et al., 1997), so that HAT enzymes are often found within larger, macromolecular complexes which harbour others regulatory activities. Such an example is the SAGA coactivator complex, on which I will now focus.

3. The SAGA coactivator complex

The SAGA (Spt-Ada-Gcn5-Acetyltransferase) complex was first discovered in yeast by Workman and colleagues, as a large complex of about 1.8-2 MDa harboring the histone H3 acetyltransferase Gcn5. Initial studies also identified proteins of the Ada and Spt families within yeast SAGA (Grant et al., 1997). In humans, Gcn5 has two distinct paralogues, Gcn5 and PCAF (p300/CBP-associated factor) (E R Smith et al., 1998; Yang et al., 1996), which have defined seemingly distinct complexes, using related but different experimental strategies. These complexes have been independently coined as the PCAF complex, the STAGA complex (Spt3-TAFII31-Gcn5L-acetylase), or the TFTC complex (TBP-free TAFII-containing complex) (Brand et al., 1999; Martinez et al., 2001; Ogryzko et al., 1998). It has now become clear that these complexes are functionally and structurally equivalent, and correspond to the human counterpart of the yeast SAGA complex (Nagy et al., 2009).

3.1. SAGA composition

SAGA is as a co-activator complex that contains multiple subunits and presents a typical modular organization. SAGA is composed of 18-20 subunits organized into five different modules (Figure 20, Table 3).

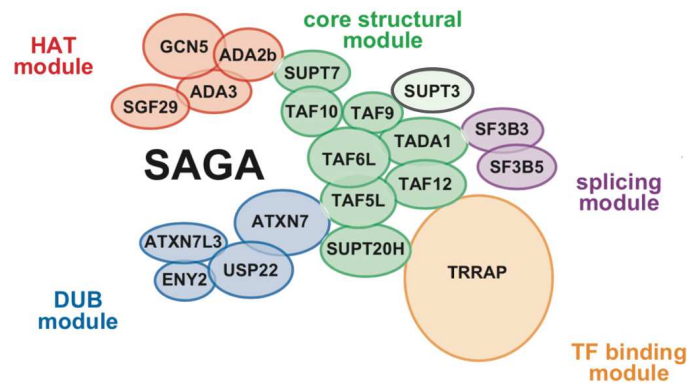


Figure 20: Modular organization of the SAGA complex. Schematic illustration of the subunit composition of each SAGA module. HAT (in red), Histone deubiquitinase (DUB) module (in blue), Core (in green), Splicing module (in purple) and Transcription factor binding module (in orange). Adapted from (Helmlinger and Tora, 2017).

Functional tools	Orthologous SAGA complexes			
	<i>H. sapiens</i>	<i>S. cerevisiae</i>	<i>S. pombe</i>	<i>D. melanogaster</i>
HAT module	KAT2A/KAT2B (GCN5/PCAF)	Gcn5	Gcn5	KAT2 (GCN5)
	TADA2b	Ada2	Ada2	Ada2b
	TADA3	Ngg1 (Ada3)	Ngg1 (Ada3)	Ada3
	SGF29	Sgf29	Sgf29	Sgf29
DUB module	USP22 (UBP22)	Ubp8	Ubp8	dNonstop
	ATXN7L3	Sgf11	Sgf11	dSgf11
	ATXN7/ATXN7L1/L2	Sgf73	Sgf73	dATXN7
	ENY2	Sus1	Sus1	dE(y)2
Core structural module	TAF5L	Taf5	Taf5	WDA/TAF5L
	TAF6L	Taf6	Taf6	SAF6/TAF6L
	TAF9/TAF9b	Taf9	Taf9	TAF9
	TAF10	Taf10	Taf10	TAF10b
	TAF12	Taf12	Taf12	TAF12
	SUPT7L (STAF65G)	Spt7	Spt7	Spt7
	TADA1	Hfi1 (Ada1)	Hfi1 (Ada1)	Ada1
	SUPT20H	Spt20	Spt20	Spt20
TBP binding	SUPT3H	Spt3	Spt3	Spt3
	-	Spt8	Spt8	-
TF binding module	TRRAP	Tra1	Tra1	Nipped-A
Splicing module	SF3B3	-		SF3B3
	SF3B5	-		SF3B5

Table 3: SAGA domain organization in different organisms. SAGA overall organization is highly conserved. Names of each subunit from *H. sapiens*, *S. cerevisiae*, *S. pombe* and *D. melanogaster* are indicated. Names in brackets are alternative, commonly used names, and “/” signs separate paralogous subunits. From (Helmlinger and Tora, 2017).

3.1.1. Histone acetyltransferase module

As previously mentioned, histone acetylation results in chromatin decompaction, which increases the accessibility of factors that promote transcription. Gcn5 was isolated from *Tetrahymena* as the first HAT, which functions in transcriptional activation, providing the first, much awaited link between histone acetylation and transcriptional regulation (Brownell et al., 1996). The HAT module of SAGA is composed of GCN5 which harbors the enzymatic HAT activity, as well as the TADA3, TADA2b, and SGF29 subunits. TADA2B/Ada2 anchors the HAT module to the remainder of the SAGA complex (Gamper et al., 2009; Lee et al., 2011). The HAT module of SAGA preferentially acetylates histone H3 on lysines residues 9 and 14 (H3K9, H3K14) (Feller et al., 2015; Grant et al., 1999; Jin et al., 2011). Nevertheless, contrary to H3K9ac which is severely reduced in Gcn5/PCAF depleted cells, H3K14ac global levels do not change, suggesting redundancy or compensation with others HAT. Interestingly, H3K9ac is detected at the promoters of all transcribed genes, suggesting a broad genome-wide recruitment of SAGA (Bonnet et al., 2014).

3.1.2. Histone deubiquitinase module

SAGA harbors a second catalytic module which displays deubiquitinase activity. This activity is carried out by the ubiquitin protease USP22, which interacts with ATXN7, ATXN7L3, and ENY2 subunits to form the DUB module of SAGA. The ZnF-sgf73 domain of ATXN7 subunit connects the DUB to the rest of SAGA and all subunits of the module are required for USP22 enzymatic activity (Lang et al., 2011). H2B is monoubiquitinated on lysine 123 in yeast and lysine 120 in humans. Ubiquitinated H2B (H2Bub) is associated with the transcribed regions of all expressed genes but is excluded from promoter regions and rather appears at gene bodies (Bonnet et al., 2014; Minsky et al., 2008). The H2Bub mark is removed by SAGA in an extremely dynamic manner. Indeed, Bonnet and colleagues have shown that after only 10 minutes of transcription inhibition, H2Bub is completely removed, suggesting that SAGA associates with active genes very transiently and dynamically. Moreover, the DUB activity is proportional to the levels of H2Bub and gene expression, suggesting a sequential ubiquitylation and deubiquitylation of H2B, required for optimal gene activation (Bonnet et al., 2014; Henry, 2003).

3.1.3. Core structural module

The structural integrity of SAGA relies essentially on two families of proteins: TAFs and SPTs. After the discovery of Gcn5, a subset of TAFs proteins were identified as part of SAGA (Grant et al., 1998a). TAFs proteins, as already addressed in the first part, form the TFIID complex. Some TAFs proteins contain histone fold domain (HFD) responsible for heterodimerization, which constitute a crucial structural element of TFIID (Gangloff et al., 2001). The core complex of TFIID is constituted by TAF5 and the following heterodimers: TAF4/12, TAF6/9, TAF8/10, TAF11/13. Interestingly the same strategy has been conserved in SAGA. Indeed, SAGA contains five TAFs: TAF5L, TAF6L, TAF9, TAF10 and TAF12 which adopt a TFIID-like core structure. Unlike TFIID,

SAGA does not contain TAF4 and TAF8, both subunits have been replaced by two others HFD-containing proteins, TADA1 and SPT7, respectively. Yeast two-hybrid assay, co-expression systems, and crosslinking mass-spectrometry studies have demonstrated that Ada1 forms a heterodimer with TAF12, and SPT7 with TAF10 (Gangloff et al., 2001, 2000; Han et al., 2014). Moreover, SPT3 subunit curiously harbors two HFD in its N-terminal and C-terminal regions, which resemble those found in the TFIID heterodimer TAF11/13, however no study has provided any evidence that SPT3 dimerizes within SAGA (Birck et al., 1998). The last subunit which belongs to the core module is SUPTH20, identified by Nagy and colleagues (Nagy et al., 2009).

3.1.4. TBP binding module

There is several functional and biochemical evidence demonstrating that, in the yeast *S. cerevisiae*, SAGA plays an important role in TBP recruitment, through the Spt3 and Spt8 subunits. Although genetic studies revealed the importance of the SAGA–TBP interaction in PIC assembly and transcription initiation, biochemical studies have shown that this interaction is very weak (reviewed in (Grünberg and Hahn, 2013)). In mammals, the exact function of SUPT3H remains to be determined and an ortholog of yeast Spt8 does not exist. Furthermore, studies in mammalian cells have indicated that SAGA plays a role after PIC recruitment (Chen et al., 2012). Therefore, whether a TBP-binding module exists in mammalian SAGA remains to be determined.

3.1.5. Splicing module

The splicing module of SAGA contains two subunits: SF3B3, from the SF3b splicing factor that associates with U2 snRNP, was the first described (Martinez et al., 2001) and SF3B5 identified recently in *Drosophila* (Stegeman et al., 2016). This module appears specific to metazoan SAGA complexes but its exact function is not well understood yet. It has been speculated that this splicing module promotes co-transcriptional splicing at SAGA-dependent genes, but experimental work in *Drosophila* suggest that this module has a splicing-independent function when incorporated in SAGA. Indeed, SF3B3 and SF3B5 are independently associated with the U2 snRNP and SAGA, moreover their association within SAGA does not require RNA, indicating that both factors function in SAGA in a splicing-independent manner (Stegeman et al., 2016).

3.1.6. Transcription factor binding module

One key feature of co-activators is that they typically cannot bind DNA directly or specifically. Therefore, co-activator complexes require promoter-bound activators for their recruitment to chromatin. Although SAGA harbors several others subunits or domains that ensure its recruitment on chromatin, the TF binding module of SAGA allows its recruitment to chromatin through direct interactions with activators. This function is mostly dependent on one subunit, TRRAP. Yeast Tra1 or human TRRAP is the largest component of SAGA and is shared with another co-activator with HAT

activity, NuA4/TIP60. TRRAP was first identified as an interacting partner for c-MYC and E2Fs transcription factors (Steven B McMahon et al., 1998) and quickly found to be part of SAGA (Grant et al., 1998; Saleh et al., 1998).

TRRAP harbors several structural domains, characteristics of a family of serine-threonine kinases; the phosphatidylinositol 3-kinase-related protein kinases (PIKKs). TRRAP is the sixth member of this family, but contrary to the five others members which are true kinases, TRRAP is a pseudokinase because its kinase domain lacks catalytic residues required to be active. Consequently, TRRAP was first suggested to serve as a scaffolding protein for the SAGA assembly since it is a pseudokinase and the largest subunit of SAGA. However, it was shown in *S. pombe* that Tra1 is not required for SAGA assembly (Helmlinger et al., 2011). This observation has been confirmed by recent structural work from the Schultz and Cheung laboratories, which have shown that Tra1 folds independently of SAGA and occupies a defined lobe within the complex, interacting with the rest of SAGA through a limited number, 1 or 2, surface contacts (Díaz-Santín et al., 2017; Sharov et al., 2017). Therefore, instead of having structural roles within the SAGA complex, TRRAP displays regulatory roles and constitutes the TF binding module of SAGA. Interestingly, similar approaches suggest that, contrary to SAGA, the yeast NuA4 complex requires Tra1 for its overall assembly and stabilization ((Xuejuan Wang et al., 2018) and unpublished work from our lab) (Figure 21).

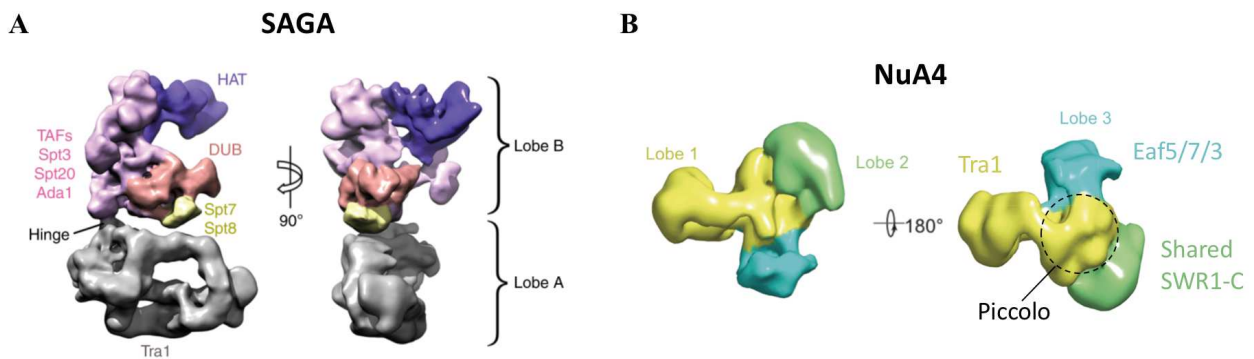


Figure 21: Structural comparison of Tra1 subunit within SAGA and NuA4 complexes. (A) Cryo-EM structure of SAGA obtained from *Pichia Pastoris* at 11.7 Å resolution. SAGA is organized into two lobes; the lower lobe (lobe A, in grey) is fully occupied by Tra1 whereas the upper lobe (lobe B, colored) contains enzymatic and chromatin recognition modules. Tra1 interacts with the second lobe through a single and narrow interface forming the hinge region. (B) Structure of fully assembled native yeast NuA4 complex determined by single-particle electron microscopy. NuA4 adopts a trilobal overall architecture. Lobe 1 (in yellow) adopts a hollow cradle like shape characteristic of the PIKK proteins that Tra1 belongs to. In contrast lobe 2 (in green) and lobe 3 (in blue) which correspond to shared SWR1-C and TINTIN modules respectively, are more globular and attached peripherally to lobe 1. The piccolo module is positioned between lobe 2 and lobe 3. Adapted from (Setiaputra et al., 2018; Sharov et al., 2017).

3.2. SAGA, a paradigm to illustrate the redundancy and the diversity in form and function of a coactivator

Although coactivator complexes display highly specialized and coordinated functions, it seems increasingly clear that there is an important structural and functional overlap between them. Indeed, coactivator share many subunits or modules. In addition, many coactivator subunits have duplicated and exist as one or more paralogs, particularly in metazoans. Therefore, in the case of SAGA, cells might assemble a plethora of slightly different SAGA complexes with separate and/or overlapping activities. SAGA represents a perfect paradigm to illustrate this tool sharing phenomenon, which might allow cells to expand the range of their transcriptional responses.

3.2.1. PCAF and ATAC complex

The HAT module of SAGA represents the first example of module sharing and diversity. First, human Gcn5 (hGcn5) differs from its counterpart in yeast (yGcn5) in the N-terminal region, where it contains an extension harboring a PCAF homology domain (Figure 22). In vertebrate organisms, Gcn5 and PCAF are two paralogous proteins sharing 73% of identity and encoded by the *KAT2A* and *KAT2B* genes, respectively.

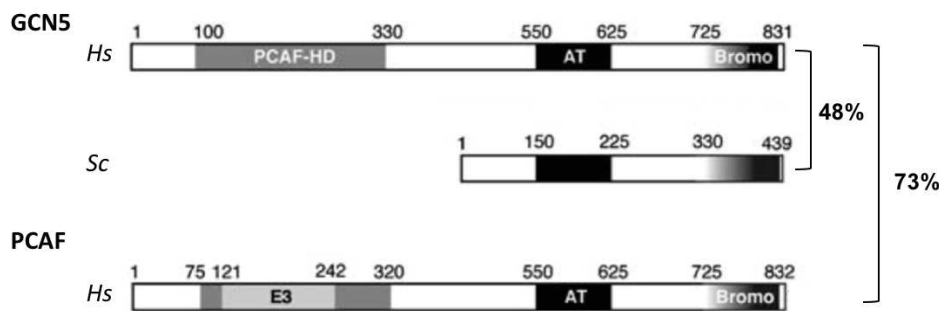


Figure 22: Structure of GCN5 and PCAF. Schematic representation of the domain organization of Gcn5 in human (*Hs*) and yeast (*Sc*), and PCAF in human (*Hs*). hGcn5 and yGcn5 share 48% of identity and differ in their amino-terminal parts, where hGcn5 harbors an extension containing a PCAF homology domain (PCAF-HD, in grey). hGcn5 shares 73% of identity with PCAF, which displays also a PCAF-HD. The acetyltransferase domain (AT, in black) and the bromodomain (Bromo, shaded) are indicated. Numbers over the boxes indicate the boundaries of each domain. The ubiquitin E3 ligase domain specific of PCAF (E3, in light grey) is also indicated. Adapted from (Nagy and Tora, 2007).

Interestingly, although both proteins form similar SAGA complexes, are similar in structure, HAT activity and substrate specificity, they show important differences in their spatial and temporal expression. Indeed, GCN5 is highly expressed early during embryonic development, 7.5 days after fertilization. In contrast, PCAF starts to be expressed around 12.5 days after fertilization, at low levels (Xu et al., 2000; Yamauchi et al., 2000). Moreover, in adult mice, the expression of GCN5 and PCAF is rather ubiquitous, with some additional tissue specificity (Xu et al., 2000, 1998). Accordingly, *Pcaf* is dispensable for early mouse development, whereas *Gcn5* loss leads to embryonic lethality (Xu et al.,

2000). However, embryos from double mutant die earlier, with more severe defects, than single *Gcn5* deletion mutants, indicating that the functions of GCN5 and PCAF are not partially redundant (Nagy and Tora, 2007; Xu et al., 2000). Consequently, GCN5 and PCAF are involved in specific developmental processes.

Besides development, GCN5 and PCAF display pro- and anti-oncogenic functions, respectively. GCN5 potentiates the growth of cancer cells, in urothelial carcinoma cells (Koutsogiannouli et al., 2017), in non-small lung cell cancer (Chen et al., 2013), in glioma cells (Liu et al., 2015), in hepatocellular carcinoma (Majaz et al., 2016) but also in colorectal cancer (Yin et al., 2015). Interestingly, we serendipitously observed a negative correlation between the mRNA expression of *GCN5* and *PCAF*, comparing samples from normal tissues and primary tumor (Figure 23).

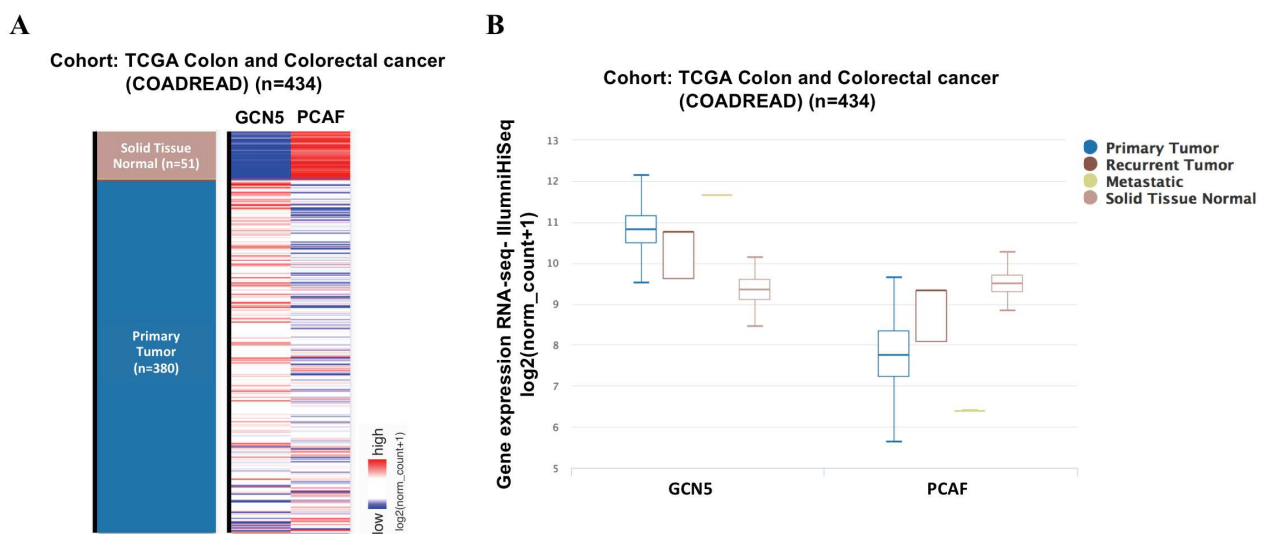


Figure 23: Negative correlation between *GCN5* and *PCAF* expression in colorectal cancer. (A) Heat map of *GCN5* and *PCAF* gene expression from RNA-seq data obtained in 51 normal tissue samples and 380 primary tumor samples. (High expression, in red; low expression, in blue). (B) Xena chart view showing box plots of *GCN5* and *PCAF* expression from 434 samples divided into four different types: primary tumor (in blue), recurrent tumor (in brown), metastatic (in yellow), and normal tissue (in pink). Data are retrieved from The Cancer Genome Atlas (TCGA) COAD-READ project.

Second, in metazoans, GCN5/PCAF are part of two co-activator complexes: SAGA and ATAC (Ada-Two-A-Containing) (Muratoglu *et al.*, 2003; Guelman et al., 2006; Wang *et al.*, 2008). Besides GCN5, ATAC shares also TADA3 and SGF29 subunits with the HAT module of SAGA. Interestingly, two paralogues of TADA2 exist in metazoans: TADA2B and TADA2A. Each is specific to the HAT module of either SAGA or ATAC, respectively, and both stimulate Gcn5 catalytic activity (Riss et al., 2015). If both complexes preferentially target histone H3 (Nagy *et al.*, 2010), one might legitimately wonder what is the rationale of having two different complexes to realize the same activity. This could provide a way for cells to assign different genomic locations at both complexes, allowing to fine-tune transcription. However, clearly, some differences might exist and need further investigations.

3.2.2. *DUB variants*

The SAGA DUB module is subjected to fine-tune regulation by a wide array of paralogues and variants, which are involved in the modulation of its composition and activity. Therefore, the SAGA DUB constitutes another example of coactivator diversity and redundancy.

First, the study of USP22 depletion in mammalian cells unveiled the existence of two USP22-related deubiquitinating enzymes, namely USP27X and USP51, which function independently of SAGA, but in cooperation with ENY2 and ATXN7L3 (Atanassov et al., 2016). Against all expectations, the ablation of USP22 leads to a decrease in H2Bub global level instead of a global increase, whereas the depletion of ENY2 or ATXN7L3 components result in increased H2Bub. These observations suggested that additional DUBs are involved in the deubiquitination of H2B and that their activities require ENY2 and ATXN7L3 adaptors. Biochemical work showed that USP27X, USP51, and USP22 compete for ENY2 and ATXN7L3 adaptor proteins. To conclude, the imbalance of one enzyme affects the activity of the others, representing a mechanism to modulate DUBs activity and substrate specificity.

Second, besides its incorporation within DUB-related modules, ENY2 subunit is also part of another complex associated to the nuclear pore and involved in the mRNA export: the transcription and export complex 2 (TREX-2). Interestingly in yeast, TREX-2 and SAGA interact through the Sus1 (ENY2) subunit, which acts as a bridging factor between both complexes. This has led to the suggestion that SAGA-dependent transcription is coupled to mRNA export (Rodríguez-Navarro, 2009). However, such interaction seems to be too dynamic and unstable to be detected in mammalian cells (Umlauf et al., 2013). Recently, a new functional interaction between TREX-2 and the DUB module of SAGA has been described and plays a role in DNA repair. The interplay between both complexes is required to maintain the H2B/H2Bub balance, which is critical for correct double strand break (DSB) repair during homology directed repair (Evangelista et al., 2018).

Third, an additional level of complexity is brought by the diversity of other DUB component paralogues that exist in mammalian cells. For instance, ATXN7 has two paralogues of unknown function, ATXN7L1 and ATXN7L2. In contrast, ATXN7L3 has one paralog, ATXN7L3B, which localizes to the cytoplasm and affects H2Bub levels indirectly by competing with ATXN7L3 for ENY2 binding. Therefore, the sequestration of ENY2 by ATXN7L3B changes its subcellular localization, limiting SAGA DUB activity (Li et al., 2016).

3.2.3. *TRRAP-containing complexes*

The TRRAP subunit is shared with another HAT-containing coactivator complex called TIP60 (Doyon et al., 2004). Like SAGA, TRRAP is believed to be the subunit by which the TIP60 complex is recruited to chromatin, through direct contacts with activators (Frank et al., 2003). However, contrary to SAGA, TIP60 acetylates histones H4, H2A and the histone variants H2AZ and H2AX.

Therefore, TRRAP constitutes a platform of recruitment for two distinct HAT-containing complexes allowing to regulate different cellular processes.

Nevertheless, the identification of genes requiring SAGA or TIP60 through a TRRAP-dependent recruitment has been complicated by the fact that TRRAP is an essential protein for viability and that no ‘separation-of-function’ allele has been isolated from structure-function or genetic studies, despite intense efforts, particularly from the Brandl and Hahn laboratories (Hoke et al., 2010; Knutson and Hahn, 2011; Mutiu et al., 2007). Indeed, a Tra1 deletion mutant in the yeast *S. cerevisiae* is inviable (Saleh et al., 1998) and TRRAP disruption in mice leads to early embryonic lethality (Herceg et al., 2001). Therefore, it appears difficult to decipher the exact contribution of TRRAP to the recruitment of each complex. Interestingly, the yeast *S. pombe* has two TRRAP homologs, providing the unique advantage to address the specificity of each complex. Indeed, the genome of *S. pombe* encodes two paralogous proteins Tra1 and Tra2, which are specifically incorporated in SAGA and NuA4 (TIP60) complexes, respectively (Helmlinger, 2012). Remarkably, a Tra1 deletion mutant is viable whereas Tra2 is essential for viability in *S. pombe*, indicating that TRRAP/Tra1 is essential in *S. cerevisiae* and in mice likely because of its role within TIP60/NuA4 complex.

3.2.4. SAGA and TFIID as general cofactors of RNA pol II

SAGA and TFIID display structural and functional common features, suggesting a redundancy in their function or at least in their structural organization.

Indeed, both complexes share five subunits in yeast, including TAF5, TAF6, TAF9, TAF10 and TAF12. In metazoans SAGA and TFIID share TAF9, TAF10 and TAF12 but two gene duplication events led to diversification of the *TAF5* and *TAF6* genes, such that TAF5 and TAF6 are specific to TFIID, whereas TAF5L and TAF6L proteins are specifically found in SAGA.

These shared subunits participate in the core structure of each complex, indicating a conserved strategy in complex scaffold formation. Besides a structural resemblance, TFIID and SAGA complexes are functionally similar to the extent that both are involved in TBP loading on promoters.

These observations raise the questions as to how both complexes cooperate to regulate transcription and whether they have identical or distinct roles in this process. Several laboratories have addressed such issues and most significant achievements have been obtained in the yeast *S. cerevisiae*. For instance, early transcriptome studies have defined two major classes of genes: SAGA- and TFIID-dominated genes. Interestingly, each class display specific characteristics. SAGA-dominated genes represent 10% of the *S. cerevisiae* genome, corresponding mainly to stress-responsive genes with TATA-containing promoters whereas TFIID-dominated genes account for 90% of the yeast genome, representing mostly housekeeping genes that lack a consensus TATA-box (Basehoar et al., 2004; Huisinga and Pugh, 2004). Additional studies have then provided other distinctions between both classes, such as the level of acetylation, regulation and positioning of nucleosomes, such that SAGA-dominated genes tend to have TATA box-containing, hypoacetylated promoters that lack a defined NDR and are highly regulated.

However, by taking advantage of technical improvements, this classical dichotomy has been challenged recently by the studies of the Tora and Hahn laboratories, providing a more comprehensive

analysis of SAGA and TFIID genome occupancy and their effect on RNA polymerase II transcription (Baptista et al., 2017; Warfield et al., 2017). Both studies convincingly demonstrated that SAGA and TFIID are in fact recruited genome-wide at all promoters, regardless of the previous distinction SAGA-dominated or TFIID-dominated genes. Importantly, using fast, conditional loss-of-function alleles together with nascent transcriptomics, the authors showed that both SAGA and TFIID contribute to the transcription of nearly all yeast genes, consistent with their genome-wide occupancy of most promoters. Nevertheless, promoter context may still account for the distinctive functional roles of each complex, particularly in cells that are challenged by external cues known to induce a specific class of genes. In other words, it is possible that, contrary to previous assumptions, SAGA functions as a general co-activator for RNA polymerase II and, on top of that contribution, SAGA becomes more important for the transcriptional induction of specific genes in response to various stimuli.

These studies provide better insights on transcription regulation and raise several exciting questions for future work. How do SAGA activities control RNA polymerase II transcription? At which step: PIC assembly, RNA polymerase II pausing and release, or even elongation as suggested by the presence of a highly dynamic, DUB-dependent histone modification along gene bodies? Furthermore, is the general effect of SAGA on transcription conserved in metazoans? Although SAGA complex is highly conserved from yeast to mammals, as shown previously, SAGA is characterized by a wide diversity which is mainly based on paralogous proteins and module variants; and might thus contribute to differences between both species. Interestingly, the study of Bonnet and colleagues suggests conservation of this function of SAGA. SAGA from budding yeast and HeLa cells is indeed broadly distributed at promoters and control histone modification pattern at all genes (Bonnet *et al.*, 2014).

3.3. SAGA recruitment to chromatin

In order to regulate transcription activation, SAGA needs first to be recruited to gene promoters. This step is achieved by several subunits or domains.

3.3.1. Recruitment mediated by activators

As discussed previously, one way to recruit SAGA to chromatin is through TRRAP, which is able to interact with transcription factors (Figure 24A), such as c-MYC, E2F and E1A in mammals (Deleu et al., 2001; Lang and Hearing, 2003; Liu et al., 2003; McMahon et al., 2000; Steven B McMahon et al., 1998) or Gal4, Gcn4, or VP16 in yeast (Bhaumik and Green, 2001; Knutson and Hahn, 2011; Lin et al., 2012).

However, Helmlinger and colleagues have nicely revealed that SAGA does not rely entirely on Tra1/TRRAP to be recruited on chromatin. Indeed, Tra1 in *S. pombe* was shown to recruit SAGA at certain promoters but surprisingly SAGA binds other promoters in a Tra1-independent manner. Other subunits of SAGA may therefore trigger its recruitment on chromatin (Helmlinger et al., 2011).

3.3.2. Interaction with the basal transcription machinery

In yeast, genetic and crosslinking studies revealed that SAGA interacts with the basal transcription machinery, representing therefore another mechanism for SAGA to be recruited to promoters. Indeed, Spt3 and Spt8, two subunits of the core structural module of SAGA were shown to interact with TBP (Figure 24B) (Eisenmann et al., 1992; Mohibullah and Hahn, 2008). However, functional studies of Spt3-TBP interaction, suggests a role of SAGA in assisting the recruitment of TBP at promoters, as a coactivator does, rather than a role of TBP in recruiting SAGA at chromatin to activate transcription (Dudley et al., 1999; Larschan and Winston, 2001). Therefore, SAGA is recruited by activators and uses its Spt3 subunit to mediate the recruitment of TBP impacting the transcription efficiency at particular promoters. The interaction SAGA-TBP would not cause the recruitment of SAGA on chromatin but instead represents one consequence of the SAGA recruitment on chromatin

Moreover, so far, no Spt8 homologue has been identified in mammals and an interaction between SUPT3H and TBP is not detectable in human cells (Martinez et al., 1998). Nevertheless, one possibility is that the interaction between TBP and SUPT3H is weak and/or transient, and requires additional components to be stabilized and detectable, such as promoter DNA and GTFs.

3.3.3. Recruitment through chromatin-interacting domains

In addition to Tra1/TRRAP and Spt3-Spt8, which can recruit SAGA to chromatin by direct interaction with activators and TBP, respectively, SAGA subunits harbor several histone mark reader domains.

a) Bromodomain

GCN5 and SUPT7H contains bromodomains that display an acetyl-lysine binding activity (Figure 24C). Therefore, SAGA is potentially recruited on chromatin through specific histone marks and SAGA binds the product of its own enzymatic activity.

However, it's a 'chicken *versus* the egg' question, because acetylated lysines on histone H3 are a prerequisite for the binding of bromodomain-containing proteins, such as GCN5 and this histone mark can be deposited by GCN5 itself. Thus, histone H3 acetylation mediated by SAGA not only represents an anchor to stabilize its own occupancy but also a way to form a self-sustaining epigenetic marks, capable of spreading, at least locally (Hassan et al., 2002).

Gcn5 and SUPT7H bromodomains are therefore involved in the retention of SAGA on chromatin in an activator-independent manner. It is worth mentioned here that GCN5 acetylates many non-histone proteins and it is formally possible that GCN5 and SUPT7H bromodomains can also recognize such modifications, for example to stabilize SAGA complex assembly or interaction with members of the PIC.

b) SCA7

ATXN7 and ATXN7L3 subunits harbor atypical zinc fingers, referred to as SCA7 domains. However, both SCA7 domains show sequence divergence which leads to a structural rearrangement of their helical structures, accounting for distinct functions. The orientation and the composition of the C-terminal helix in the ATXN7 SCA7 domain differs from the one of the ATXN7L3 protein, resulting in a loss of nucleosome binding property of ATXN7L3. In contrast, the ATXN7-SCA7 domain binds H2A-H2B dimers (Figure 24D), but not H3-H4 tetramers, facilitating therefore the recruitment of SAGA to the specific substrate of the DUB module (Bonnet et al., 2010).

c) Tudor

SGF29 contains in its C-terminus a unique and conserved tandem-Tudor domain, which binds methylated histones. Specifically, SGF29 interacts with H3K4me2/3 (Figure 24E) (Vermeulen et al., 2010). Therefore, SGF29 acts as a chromatin reader and constitute another mechanism for SAGA recruitment on chromatin (Bian et al., 2011).

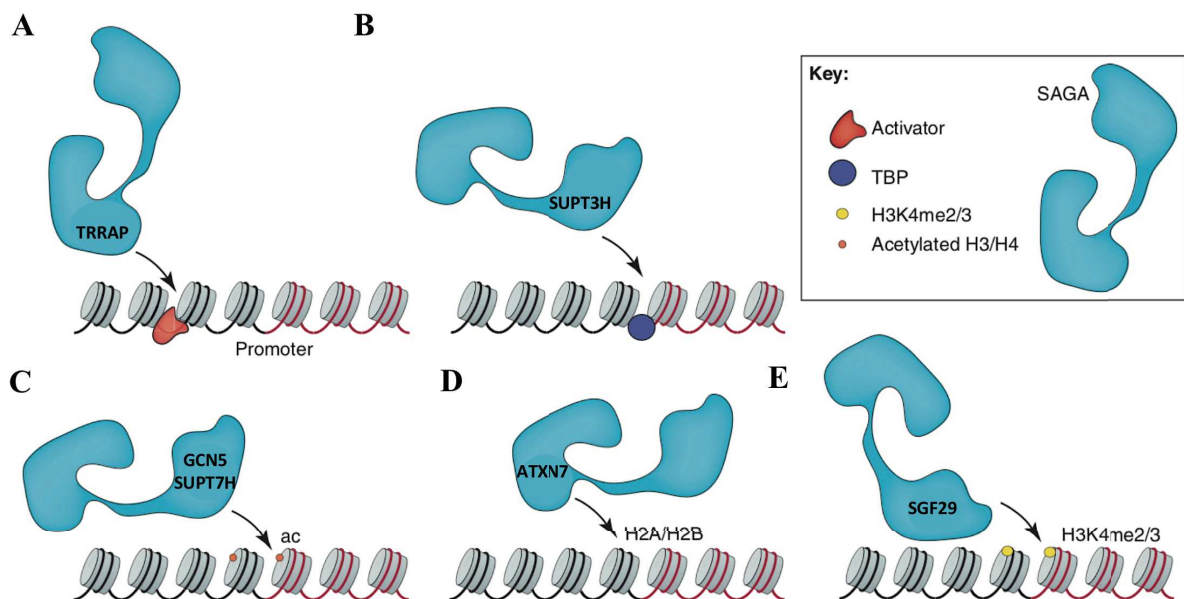


Figure 24: SAGA recruitment to chromatin. SAGA recruitment/retention to promoters is mediated through multiple interactions. (A) TRRAP subunit recruits SAGA to promoters by contacting directly transcription factors. (B) SUPT3H might interact with TBP as reported in yeast. (C) GCN5 and SUPT7H contain bromodomains that mediate the retention of SAGA on acetylated nucleosomes. (D) ATXN7 through its SCA7 domain binds H2A-H2B dimers. (E) SGF29 binds H3K4me2/3 through a tandem-tudor domain. Adapted from (Weake and Workman, 2012).

4. TIP60/NuA4, another HAT-containing complex

NuA4 was initially purified from *S. cerevisiae* using the same in-gel acetyltransferase assay that allowed the discovery of SAGA (Grant et al., 1997). Through multiple chromatographic steps, Workman and colleagues identified four native high molecular weight complexes containing HAT activity on polynucleosomal substrates. Two of them were reported to contain the HAT Gcn5 and to primarily acetylate H3 and to a lesser extent H2B and correspond to the SAGA and ADA complexes. The two others were not further characterized aside from their histone substrate specificity and were therefore named NuA4 (Nucleosome acetyltransferase of histone H4) and NuA3 (Allard et al., 1999). The purification and determination of the subunit composition of the NuA4 complex was first reported by Jacques Côté and colleagues in yeast (Allard et al., 1999). This study identified the catalytic subunit of the complex as the product of the *ESA1* gene, and also observed the presence of Tra1 in the complex.

The human ortholog of *Esa1*, TIP60, was originally identified as a protein interacting with the HIV-1 Tat transactivator, and was thus called TIP60 for Tat interactive protein 60 KDa (Kamine et al., 1996). Later Yamamoto and Horikoshi brought biochemical evidence that TIP60 has histone acetyltransferase activity, by showing that recombinant TIP60 effectively acetylates H2A and H4 (Yamamoto and Horikoshi, 1997). Subsequently, through a purification of TIP60 acetyltransferase, the TIP60 complex was characterized in human cells as homolog of the yeast NuA4 complex (Doyon et al., 2004; Ikura et al., 2000).

4.1. TIP60/NuA4 composition

NuA4 is a ~ 1 MDa complex composed of 13 subunits highly conserved in eukaryotes and organized into four distinct functional modules (Figure 25).

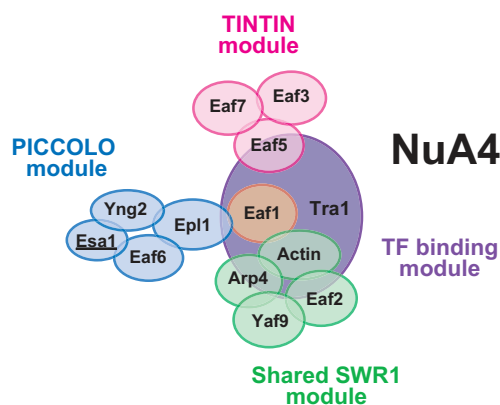


Figure 25: Modular organization of the NuA4 complex. Schematic illustration of the subunit composition of each NuA4 module. The Piccolo module (in blue) containing the HAT (subunit underlined), the Tintin module (in pink), the shared SWR1 module (in green), and the Transcription factor binding module (in purple). All four modules assemble around Eaf1 subunit (in orange).

In metazoans, the homologous TIP60 complex contains at least five additional subunits, as compared to yeast NuA4 (Cai et al., 2005, 2003; Doyon et al., 2004; Obri et al., 2014). TIP60 harbors two types of chromatin-modifying activities: a histone acetyltransferase and an ATP-dependent chromatin remodeler, which are separated in two distinct complexes in yeast, NuA4 and SWR1, respectively. Based on subunit composition comparisons and biochemical assays using hybrid fusion proteins, the metazoan TIP60 complex has been proposed to result from a near-perfect fusion of the yeast NuA4 and SWR1 complexes (Figure 26) (Doyon and Côté, 2004). However, a human ortholog of SWR1, namely SRCAP (SNF-2-related CREB-binding protein activator protein), exists in human cells and catalyzes the ATP-dependent replacement of histone H2A in canonical nucleosomes with H2A.Z (Table 4) (Ruhl et al., 2006).

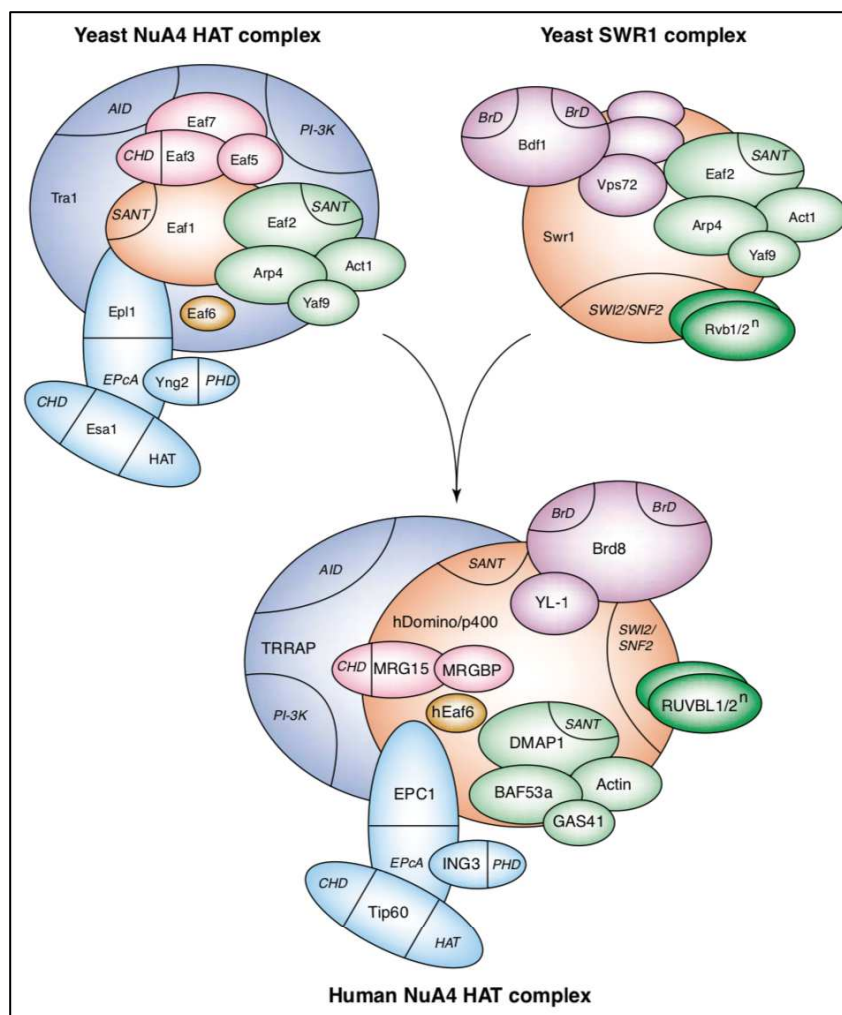


Figure 26: Origin model of human NuA4 complex. TIP60 complex (down) is suggested to result from a merge between NuA4 (top left) and SWR1 (top right) yeast complexes. Protein domains of each subunit are shown in *italic*. Adapted from (Doyon and Côté, 2004).

Modules or Function	<i>H. sapiens</i>		<i>S. cerevisiae</i>	
	TIP60	SRCAP	NuA4	SWR1
PICCOLO module	TIP60	-	Esa1	-
	EPC1/EPC2	-	Elp1	-
	ING3	-	Yng2	-
	MEAF6	-	Eaf6	-
TINTIN module	MRGBP	-	Eaf7	-
	MRG15	-	Eaf3	-
	(MRGX)	-	(Eaf5)	-
Shared SWR1 module	ACTIN	ACTIN	Act1	Act1
	DMAP1	DMAP1	Eaf2	Eaf2
	BAF53	BAF53	Arp4	Arp4
	GAS41	GAS41	Yaf9	Yaf9
TF binding module	TRRAP	-	Tra1	-
ATPase or scaffold	P400	SRCAP	Eaf1	Swr1
Bromodomain- containing protein	BRD8	-	-	Brd1
(Helicases)	RUVBL1	RUVBL1	-	Rvb1
	RUVBL2	RUVBL2	-	Rvb2
H2AZ chaperones	YL-1	YL-1	-	Vps72
	ANP32E	-	-	Chz1

Table 4: NuA4 conservation from yeast to human. Names of each TIP60 subunit from *H. Sapiens* and *S. cerevisiae* are indicated. TIP60 complex in human (*H. Sapiens*) corresponds to a near-perfect merge between NuA4 and SWR1 yeast complexes. TIP60 subunits shared with SRCAP complex are indicated as well as their homologs in yeast. Brackets indicate speculative information and “/” signs separate paralogous subunits. SRCAP and SWR1 complexes contain others specific subunits that are not found in TIP60/NuA4 and hence are not present in this table.

Interestingly, according to the domain architecture of human P400 and SRCAP proteins, and their counterparts in *S. cerevisiae* Eaf1 and Swr1, it is tempting to speculate that in higher eukaryotes Swr1 and Eaf1 have fused and evolved into P400 protein (Figure 27). This is further supported by a recent elegant study performed in the fungal pathogen *Candida albicans*, that showed a dynamic

fusion and separation of the NuA4 and Swr1 complexes that correlates with cell fate transition from a unicellular yeast state to a multicellular hyphal state (Xiongjun Wang et al., 2018).



Figure 27: Model of merger between NuA4 and SWR1 complexes. Domain architecture of Swr1 and Eaf1 in yeast (*S. cerevisiae*) and their orthologs in Human (*H. sapiens*), P400 and SRCAP. Helicase/SANT-associated (HSA, in blue), Swi3, Ada2, N-Cor, and TFIIB (SANT, in green) and ATPase (in red) domains are indicated.

Like SAGA, TIP60 is a transcriptional co-activator complex and shares many components with other complexes. For instance, as previously discussed, yeast Tra1 and human TRRAP are also present in SAGA (*cf* 3.2.3.). Additionally, RUVBL1/2, BAF53, GAS41, Actin, YL-1, and DMAP1 are shared with the yeast SWR1 or human SRCAP complexes (Table 4). Although the SRCAP and TIP60 complexes are both implicated in the deposition of H2AZ into chromatin in human cells, they appear to regulate distinct processes (Lu et al., 2009).

4.2. NuA4/TIP60 structure

The previously reported yeast NuA4 structure determined by cryo-EM reconstruction showed a single modular architecture (Chittuluru et al., 2011). Strikingly, this structure resembles the lobe A of SAGA structure which is predominantly occupied by the Tra1 subunit (Figure 28) (Sharov et al., 2017).

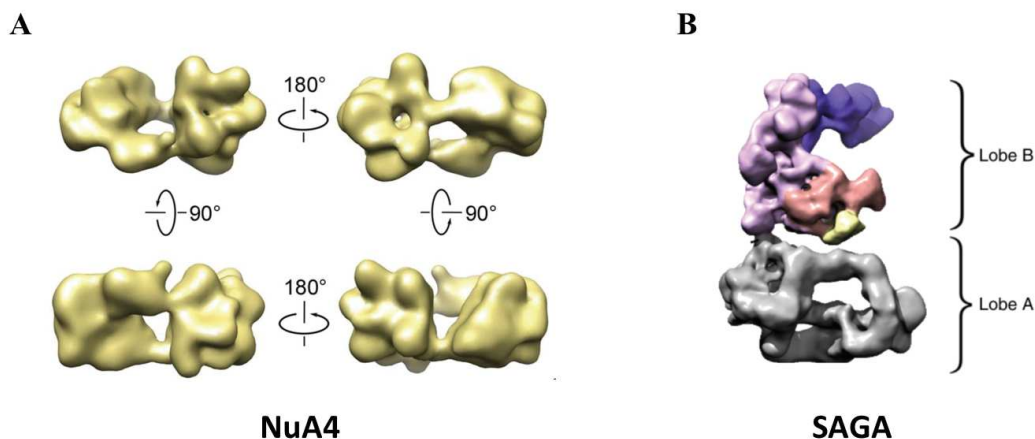


Figure 28: NuA4 structure resembles SAGA lobe A. (A) 3D-cryoEM map reconstruction of NuA4 complex from *S. cerevisiae* obtained by Chittuluru and colleagues and showed in different views (Chittuluru et al., 2011). (B) Cryo-EM structure of SAGA obtained from *Pichia Pastoris* at 11.7 Å resolution, showing lobe A (in gray) which corresponds to Tra1 subunit. Lobe B (colored) correspond to the rest of SAGA (Sharov et al., 2017).

Recently, the high resolution cryo-EM structure of Tra1 obtained in *S. cerevisiae* clearly revealed that the entirety of NuA4 structure, as proposed by Chittuluru and colleagues, corresponds in fact to Tra1 structure (Figure 29) (Díaz-Santín et al., 2017). The rest of NuA4 subunits might have therefore dissociated in this reconstruction and/or are highly dynamic.



Figure 29: NuA4 and Tra1 structure comparison. Representative 2D class average of Tra1 (left panel) obtained by the Cheung lab., filtered to 21 Å (middle panel) to allow visual comparison with the 2D class average obtained for NuA4 complex by Chittuluru and colleagues. Those 2D structures clearly revealed that NuA4 structure (right) closely matches Tra1 appearance (middle). Scale bar represents 5 nm.

Recently, the structure of NuA4/TIP60 subcomplexes as well as a partially assembled NuA4 complex from *S. cerevisiae* were reported (Setiaputra et al., 2018; Xuejuan Wang et al., 2018). These structures revealed a trilobal overall architecture (Figure 30). The lobe 1 houses the structural core with the Eaf1 subunit acting as a scaffold for the other modules. Interestingly, Tra1 is also found in lobe 1 and, contrary to SAGA complex, Tra1 mediates interactions with several NuA4 subunits. The Piccolo module located between lobe 2 and 3 is anchored to NuA4 through Efp1 which interacts with Eaf1. The shared SWR1 and TINTIN modules occupy the two peripheral lobes, lobe 2 and lobe 3, respectively. SWR1 contacts lobe 1 at multiple sites whereas TINTIN is anchored to NuA4 through Eaf5 which interacts with the N-terminal region of Eaf1 (Figure 30).

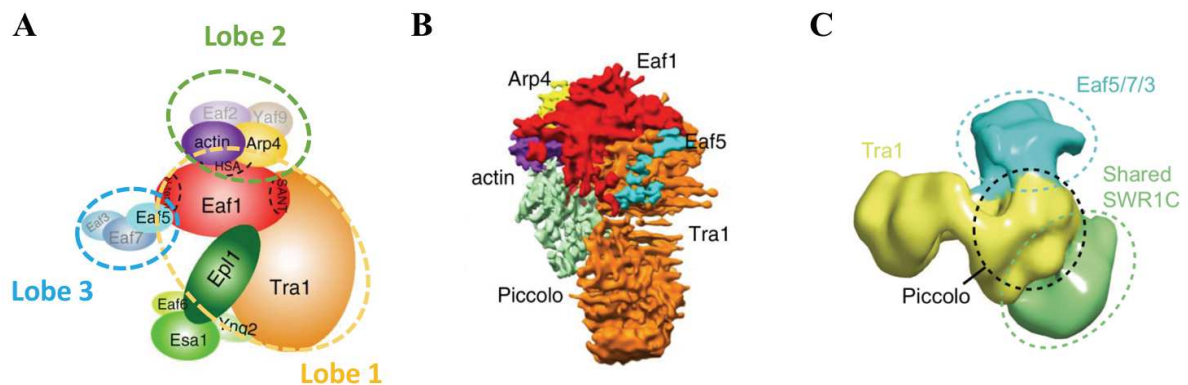


Figure 30: Overall structure of NuA4. (A) Schematic representation of subunit and modular organization of the NuA4 complex, subunits present in the TEEAA (Tra1-Eaf1-Eaf5-Actin-Arp4)-piccolo assembly (B) are highlighted. The dashed circles depict the three distinct lobes. (B) Cryo-EM structure of the TEEAA-piccolo assembly. (C) Trilobal architecture of the fully assembled NuA4 complex. Lobe 1 (yellow), lobe 2 (green), and lobe 3 (blue) are indicated, as shown in (A). Adapted from (Setiaputra et al., 2018; Xuejuan Wang et al., 2018).

4.3. Cellular functions of TIP60

TIP60 complex is involved in several key cellular processes, including chromatin remodeling, gene transcription, DNA repair, apoptosis and tumorigenesis (Ghobashi and Kamel, 2018). Those functions are mainly mediated through its two types of chromatin-modifying activities, the HAT and the ATP-dependent chromatin remodeler, carried out by TIP60 and P400 subunits, respectively. Interestingly, opposing roles for TIP60 and P400 have been described upon DNA damage (Tyteca et al., 2006), as well as on Wnt-pathway in the context of colorectal cancer (Chevallard-Briet et al., 2014).

4.3.1. The histone acetyltransferase activity of TIP60

The TIP60 HAT is a member of the MYST family of acetyltransferases. Homozygous ablation of *Tip60* in mice causes embryonic lethality near the blastocyst stage of development (Hu et al., 2009). Interestingly, Esa1, the yeast TIP60 homolog, is the only essential HAT in yeast (E. R. Smith et al., 1998), which emphasizes the critical role of TIP60 for cell proliferation.

TIP60 mediates its functions by acetylating several substrates. TIP60 preferentially acetylates histones H2A and H4, as well as the histone variant H2A.Z (Figure 31) (Corujo and Buschbeck, 2018; Kimura and Horikoshi, 1998). TIP60 acetylates also several non-histone proteins, such as ATM and p53, and therefore contributes to maintain genome integrity (Sun et al., 2005; Tang et al., 2006). Suppression of TIP60 sensitizes cells to ionizing radiation by blocking ATM kinase activity and impairing the ATM-dependent phosphorylation of p53 and chk2 downstream effectors. Upon DNA damage, TIP60 mediates the acetylation of ATM on its lysine residue 3016 located in its FATC domain, which is critical for its subsequent auto-phosphorylation and activation (Sun et al., 2007, 2005).



Figure 31: Histone substrates of TIP60. TIP60 acetylates canonical H2A, H4 and H2AZ variant. Beginning of histones tail sequences of H2A (in red), H4 (in green), and H2AZ (in pink) are indicated. Residues acetylated are in bold. Numbers below residues indicate their positions.

TIP60 associates with a large number of transcription factors to catalyze histone acetylation and activating transcription, including c-MYC, E2Fs, p53, and nuclear receptors (Brady et al., 1999; Frank et al., 2003; Taubert et al., 2004). Remarkably, TIP60 can also regulate gene transcription independently of its HAT activity. For instance, TIP60 was shown to repress differentiation genes in embryonic stem cells and to promote their self-renewal by limiting promoter-proximal chromatin

accessibility in a HAT-independent manner (Acharya et al., 2017). Consequently, TIP60 might act as a transcriptional co-activator in a HAT-dependent manner and mediates repression independently of its HAT activity.

4.3.2. ATP-dependent histone variant deposition

P400 catalyzes the ATP-dependent incorporation of H2AZ variant into chromatin by exchanging H2A-H2B dimers within nucleosomes with free H2A.Z-H2B dimers (Gévry et al., 2007). Interestingly, P400 was also shown to incorporate H3.3 variant into chromatin (Pradhan et al., 2016). Both variants are important in gene regulation. However, the exact function of each variant remains controversial and likely context-dependent.

Depending on the gene, cell type or site of deposition, the H2A.Z histone variant appear to either repress or activate transcription. For instance, in the ciliated protozoan *Tetrahymena thermophila*, H2A.Z has been found in the transcriptionally active macronucleus and not the micronucleus, which is transcriptionally inactive, suggesting a positive role of H2AZ in gene transcription (Stargell et al., 1993). In *S. cerevisiae* H2A.Z is involved in both activation and repression of transcription, as well as other processes such as heterochromatin formation and genomic stability (Adam et al., 2001; Guillemette et al., 2005; Larochelle and Gaudreau, 2003; Meneghini et al., 2003; Santisteban et al., 2000; Zhang et al., 2005).

Consistent with an important role in transcriptional regulation, genome-wide localization of H2A.Z revealed that it is highly enriched at promoters, at the -1 and +1 nucleosomes, flanking the nucleosome-depleted region and the transcription start site (Guillemette et al., 2005; Li et al., 2005; Raisner et al., 2005; Zhang et al., 2005). Several evidences suggest that H2A.Z modulates nucleosome stability, thereby impacting transcription both positively and negatively (Abbott et al., 2001; Albert et al., 2007; Li et al., 2005; Meneghini et al., 2003; Suto et al., 2000; Zhang et al., 2005).

H2A.Z is a prime example of a crosstalk between the regulatory activities of chromatin regulatory complexes. Indeed, although P400 catalyzes its nucleosomal incorporation in an ATPase-dependent reaction, TIP60 has crucial roles in H2A.Z function too. First, in yeast, NuA4-dependent acetylation of H4 is crucial for the recruitment of SWR1-C and, consequently H2A.Z deposition to chromatin (Babiarz et al., 2006; Durant and Pugh, 2007; Raisner et al., 2005). Second, NuA4/TIP60 catalyzes H2A.Z acetylation, which seems to occur following its deposition by SWR1-C/P400.

In summary, work in yeast suggests a model in which NuA4 regulates SWR1-C recruitment, histone variant deposition and modification to promoter regions to fine-tune transcription initiation. Such intricate, coordinated activities perhaps explain the fact that, in metazoans, both the NuA4 and SWR1-C complexes have merged into the TIP60 complex, which is capable of targeting, depositing and modifying H2A.Z in a single recruitment event (Lu et al., 2009).

II. TTT complex, a co-chaperone of HSP90

Molecular chaperones define multidomain proteins that are essential in maintaining proteostasis. Chaperones have evolved to assist protein folding from their nascent state until they reach their active conformation. The main chaperones rely on cycles of ATP binding and hydrolysis to mediate their functions. Chaperones are involved in protein quality control by contributing to the folding, stabilization, activation and by preventing aggregation of several of their substrates referred to as clients. Proper regulation of these different steps ensures protein homeostasis which plays critical roles in normal cell physiology but also during stress responses and human diseases.

Many chaperones are upregulated in response to a heat stress, and therefore have been called heat shock proteins (HSPs). HSP chaperones have been classified according to their molecular weight ranging from 10 kDa to more than 100 kDa (HSP40, HSP60, HSP70, HSP90, HSP110 and the small HSPs). The most conserved HSP is HSP90, which acts mainly at the late stages of client folding, downstream of HSP70, which binds to nascent and newly synthesized polypeptides. Therefore, protein folding involves the collaboration between HSP70 and HSP90, as well as a multitude of proteins referred to as “co-chaperones”. Moreover HSP70/HSP90 act in concert with the ubiquitin-proteasome system to ensure protein quality control through the degradation of misfolded proteins.

1. HSP90 chaperone: from conformational dynamics to co-chaperone regulation

HSP90 forms a highly dynamic homodimer of elongated proteins. HSP90 is ubiquitously found in cells and is one of the most abundant cytoplasmic protein representing 1-2% of total protein content (Taipale et al., 2010), while nuclear HSP90 represents only a small fraction of the nuclear proteins.

Organisms in all kingdoms of life express at least one gene encoding HSP90. In eukaryotes, HSP90 can be divided into four subfamilies depending on its localization: HSP90 A, B, C and TRAP family, corresponding to cytosolic, endoplasmic reticulum-localized, chloroplast-specific and mitochondrial HSP90, respectively. HSP90A represents the largest and the best-described group of the HSP90 families. In contrast to the other major chaperones, such as HSP60, HSP70 and HSP110, the mechanism of action of HSP90 is less-well understood and remains elusive. As a matter of fact, HSP90 is intensively subjected to regulation, notably through post-translational modifications, transcription, as well as conformational rearrangements and various co-chaperone interactions.

1.1. Structure and function of HSP90 define a conformational cycle

In order to facilitate the folding and activation of its clients, HSP90 relies on an ATP-driven conformational cycle. During each cycle, HSP90 undergoes several conformational changes triggered by ATP hydrolysis and regulated by co-chaperones. HSP90 mediates its chaperone activity through an ATP-hydrolysis dependent process which governs the binding, the conformational rearrangements

required for activation and release of its clients. The HSP90 conformational cycle encompasses several steps during which specific domains of HSP90 are involved.

Each HSP90 monomer consists of three domains: an amino-terminal domain (NTD) required for the ATP binding, a middle domain (MD) responsible for ATP hydrolysis and clients binding, and a carboxy-terminal domain (CTD) involved in HSP90 dimerization (Figure 32).

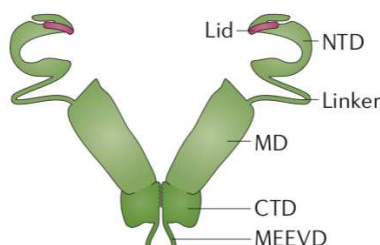


Figure 32: The HSP90 domain organization. Schematic representation showing that HSP90 adopts a dimeric structure with a V-shape conformation, in which each monomer is composed of three domains. An amino-terminal domain (NTD), connected by a linker region to a middle domain (MD), and a carboxy-terminal domain (CTD) which contains a Met-Glu-Glu-Val-Asp (MEEVD) motif. Adapted from (Schopf et al., 2017).

The NTD encompasses the ATP-binding site constituted of an α/β sandwich motif and a molecular lid that, in its ATP-bound state, closes over the nucleotide-binding pocket. The lid closure results in an intermediate state that then will go through a closed 1 and closed 2 states, consisting of the dimerization between the NTD of each monomer and their twisting after association with their middle domains, respectively (Figure 33).

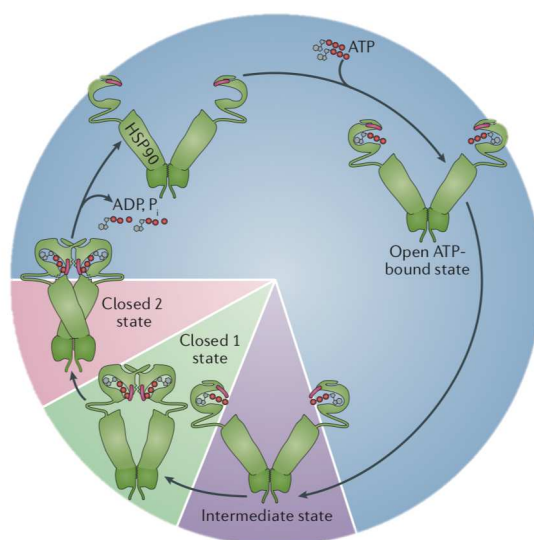


Figure 33: The HSP90 conformational cycle. During each cycle, HSP90 goes through different states characterized by specific conformational rearrangements. Each cycle starts with HSP90 in an open-state, competent for ATP binding, and ends with the ATP hydrolysis. Adapted from (Schopf et al., 2017).

ATP hydrolysis occurs once NTD have dimerized to form the closed state, and the catalytic loop of the MD has been repositioned. Although the NTD provides all structural requirements for ATP

binding as well as a conserved catalytic glutamate residue involved in the activation of a water molecule for attacking the γ -phosphate during ATP hydrolysis reaction, it has only a negligible ATPase activity. NTD needs the medium domain which harbors structural features involved in the ATPase activity, notably a catalytic loop that contacts the γ -phosphate of ATP through a conserved arginine residue and orientates it for the attack (Cunningham et al., 2012; Meyer et al., 2003). In order to achieve ATP hydrolysis, HSP90 relies on several residues found in its different domains and hence is part of the “split ATPases” superfamily (Meyer et al., 2003).

Besides its implication in ATP hydrolysis, the MD plays important roles in client recognition, notably through its hydrophobic patch. The NTD and the MD are connected by a flexible and charged linker region which appears to be important for two distinct purposes; it provides flexibility allowing domain rearrangements and it modulates the activity of co-chaperones (Hainzl et al., 2009; Tsutsumi et al., 2012).

Regarding the CTD, it provides several surfaces of interaction. First, it mediates dimerization between both monomers via two long helices, helix 4 and 5 which form the bulk of the dimerization interface (Figure 34) (Harris et al., 2004). Second, the helix 2 of the CTD is an exposed, mobile and amphipathic helix, that is likely providing a substrate binding site. Finally, the last five residues of the CTD constitute the MEEVD motif which serves as docking site for interaction with tetratricopeptide repeat domain (TPR)-containing co-chaperones (*cf* 1.2.1.).

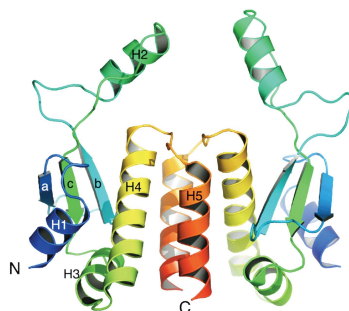


Figure 34: Cartoon of the CTD of the E. Coli HSP90 homolog, high temperature protein G (hptG). The structure reveals the surface of dimerization between the CTD of each monomer. The dimerization interface consists of two pairs of helices (H4 and H5) which form a four-helix bundle. The mobility of H2 helices allows the interaction between the CTD and substrates. Adapted from (Harris et al., 2004).

Through their specific structural and functional organizations, all three domains of HSP90 participate in and define a conformational HSP90 cycle which ends by the NTD dissociation after ATP hydrolysis, releasing ADP and inorganic phosphate. Henceforth, HSP90 returns to an open V-shape conformation (Figure 33). Clients are tethered to HSP90 *via* adaptors which usually bind to the MEEVD motif, but they make additional, low-affinity and transient contacts within the middle region of HSP90. ATP-driven conformational cycle thus allows HSP90 to act as a “molecular forceps” on its clients to assist their folding.

Each cycle is extremely dynamic and allows the processing of clients. Nevertheless, to be completed, each cycle requires the action of specific co-chaperones.

1.2. HSP90 regulation by co-chaperones

Although HSP90 is regulated by several post-translational modifications as well as transcription, the major regulators of HSP90 activity are co-chaperones (Schopf et al., 2017). So far, more than 20 co-chaperones of HSP90 have been identified. Co-chaperones bind to HSP90 and regulate its function in many different ways, covering all steps of its conformational cycle. Mainly, co-chaperones act as modulators of the HSP90 ATPase-associated conformational changes and/or as adaptors for client recruitment.

1.2.1. TPR-containing co-chaperones

Co-chaperones bind HSP90 at different locations, for instance the one that contain TPR domains interact with the MEEVD motif in the CTD of HSP90. These TPR-containing co-chaperones represent the largest subset of HSP90 co-chaperones. TPR domain consists of 3 to 16 tandem-repeats of 34 amino-acid motif. Each repeat forms a helix-turn-helix structure, leading to an overall “super-coil” TPR structure that is involved in protein-protein interactions (Cortajarena and Regan, 2006).

Interestingly, despite a shared HSP90-binding mechanism, TPR-containing co-chaperones act differentially to modulate HSP90 function. Some of them contain enzymatic activities involved in the progression of the HSP90 conformational cycle, such as a PP5 co-chaperone which is a protein phosphatase activated once bound to HSP90 (Haslbeck et al., 2015). Others interact with HSP90 in order to mediate the import of substrates into a specific cellular compartment, such as the mitochondria by TOM70 co-chaperone (Young et al., 2003).

One prominent role of TPR-containing co-chaperones is to facilitate the interplay between HSP90 and the others chaperone systems. Such example has been well described for the HSC70 and HSP90-organizing protein (HOP) co-chaperone which contains multiple TPR allowing the simultaneous binding of HSP70 and HSP90 chaperones, therefore HOP participates in the maturation of the clients by coordinating the successive actions of each chaperone (Taipale et al., 2010).

1.2.2. Non-TPR co-chaperones

Co-chaperones without TPR bind to the N-terminal and middle domains of HSP90. Therefore, some of them regulate the HSP90 ATPase activity. For instance, activator of HSP90 ATPase 1 (AHA1) co-chaperone is a strong activator of the HSP90 ATPase activity by binding to the middle domain as well as the NTD of HSP90 and promoting the closed 1 state (Figure 35A). In contrast, p23 co-chaperone, by binding the NTD, stabilizes the closed 2 state of HSP90 which inhibits ATP hydrolysis and client release, therefore facilitating their maturation (Figure 35B). CDC37 co-chaperone represses also the ATPase activity of HSP90, by blocking the ATP-binding pocket and preventing the lid closure (Figure 35C).

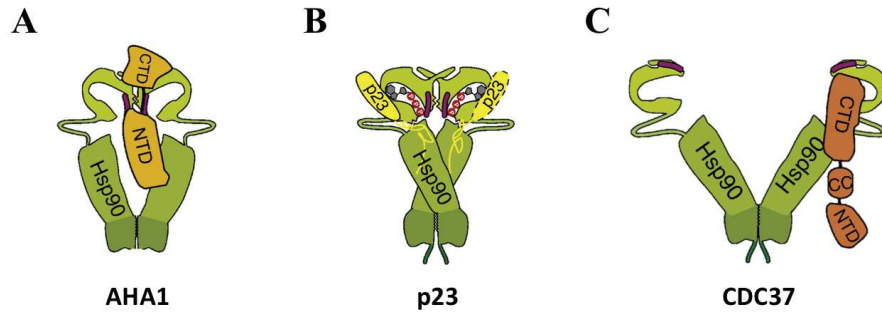


Figure 35: HSP90 regulation by non-TPR containing co-chaperone. (A) AHA1 co-chaperone binds to the NTD and MD domains of HSP90 promoting its closed 1 state. (B) p23 stabilizes the closed 2 state of HSP90 by binding the NTD. (C) CDC37 through its C-terminal domain interacts with the HSP90 NTD, preventing the lid closure. Adapted from (Li et al., 2012).

Besides their roles in regulating conformational states of HSP90 and therefore the maturation of clients, co-chaperones are essential in bringing the substrate specificity. Indeed, some co-chaperone serve as adaptors that deliver specific class of clients to HSP90.

1.2.3. Client specificity

Protein that physically interacts with HSP90 and whose level usually decreases upon HSP90 inhibition, is defined as an HSP90 client.

Currently, more than 200 clients of HSP90 have been identified. The clientele of HSP90 covers a broad range of proteins with diverse structures and functions, within which kinases represent the major group (Taipale et al., 2012).

Despite this large diversity, so far, no common sequence or structural motif has emerged as recognition motif for HSP90. Therefore, to deal with this plethora of clients, HSP90 is assisted by co-chaperones, which play an important role in client recognition and recruitment.

For instance, CDC37 co-chaperone - besides its regulatory role in HSP90 ATPase activity- acts as an specific adaptor for kinases clients including notably receptor tyrosine kinases and serine-threonine kinases (Gray et al., 2008).

1.2.4. R2TP co-chaperone

Most of the HSP90 co-chaperones act as single polypeptide proteins, however co-chaperones can exist as multiprotein complexes such as the Ruvbl1-Ruvbl2-Tah1-Pih1 (R2TP) complex. R2TP was first discovered in *S. cerevisiae* in a large-scale screen for HSP90-interacting proteins (Zhao et al., 2005). Subsequently, through a proteomic analysis the human ortholog of R2TP was identified. In mammalian cells, the R2TP complex comprises four subunits, two ATPases RUVBL1 and RUVBL2, which form an hexameric ring, and a heterodimer constituted of RPAP3 (Tah1) and PIH1D1(Pih1) proteins. RPAP3 harbors several domains which mediate multiple interactions. For instance, the

second TPR domain of RPAP3 anchors the R2TP complex to HSP90 (Henri et al., 2018; Martino et al., 2018), whereas its C-terminal region directly binds RUVBL1/2 hexamers (Maurizy et al., 2018). In mammals, the R2TP complex associates with additional subunits of the prefoldin-like module to form the R2TP/PFDL complex (Sardiu et al., 2008), recently re-named PAQosome (particle for arrangement of quaternary structure) (Houry et al., 2018; Kakihara and Houry, 2012) (Figure 36).

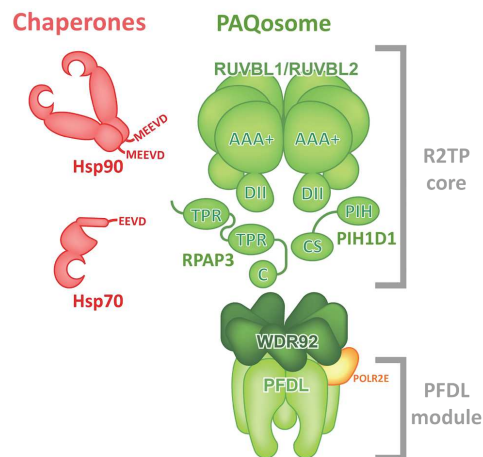


Figure 36: Schematic representation of the PAQosome co-chaperone. The PAQosome is the new name of the R2TP/PFDL complex. It is composed of a R2TP core consisting of four subunits: RPAP3, PIH1D1 and a hexamer of RUVBL1/2, associated to a prefoldin module. TPR domains in RPAP3 are involved in chaperone HSP70 and HSP90 interactions through their “EEVD” conserved motif. Adapted from (Houry et al., 2018).

Therefore, HSP90 *via* the PAQosome regulates the cellular stability, activation and assembly of diverse multiprotein complexes such as the RNA polymerases and the small nucleolar ribonucleoproteins (snRNPs) and the RNA polymerases (Boulon et al., 2010, 2008; Zhao et al., 2008) (Figure 37). Interestingly, the PAQosome relies on additional proteins to interact with its clients, these adaptor proteins act as “co-co-chaperone” and provide a unique mechanism of client selection by a co-chaperone. For instance, ECD and ZNHIT2 are specific adaptors that regulate the assembly of U5snRNP by the PAQosome (Cloutier et al., 2017); whereas NUFIP1, ZNHIT3, and ZNHIT6 promote the interaction between PAQosome and box C/D snoRNPs subunits (Bizarro et al., 2015; Boulon et al., 2008). Through its PIH1D1 subunit, the PAQosome was shown to interact with TELO2, another adaptor protein which forms the TTT co-chaperone (Horejsí et al., 2010). Therefore, through the TTT co-chaperone, the PAQosome is also involved in the stability and assembly of members of a specific kinase family, the PIKKs (Takai et al., 2010) (Figure 37).

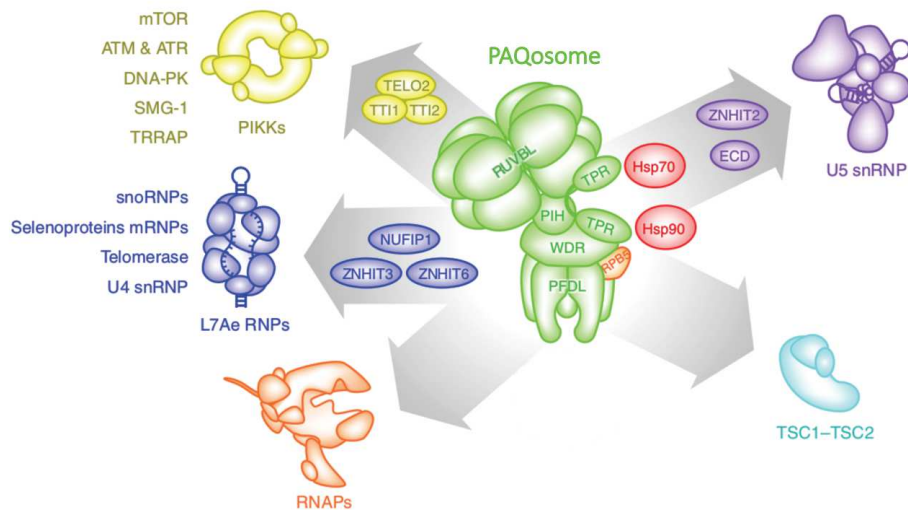


Figure 37: Schematic representation of the PAQosome interactors. The PAQosome co-chaperone (in green) interacts with chaperones (in red) but also adaptors (represented inside the arrows) that bring the specificity of clients (found at the extremity of the arrows). Adapted from (Cloutier et al., 2017).

2. TTT, co-chaperone dedicated to PIKKs

2.1. Discovery of the TTT complex as a novel HSP90 co-chaperone

Telomere maintenance 2 (TELO2), as its name suggests, was initially discovered as a protein altering telomere length in the yeast *S. cerevisiae* (Runge and Zakian, 1996). Much later, TELO2 was for the first time described as an interacting partner for PIKKs in the yeast *S. pombe* through a study of TOR complexes (Hayashi et al., 2007). Interestingly, Hayashi and colleagues identified by mass-spectrometry TTI1, as well as members of the PIKK family including TOR kinases, specifically associated with TELO2 protein. Simultaneously, the laboratory of Titia de Lange reported that TELO2 deletion in mouse correlated with a significant reduction in all PIKKs protein levels, revealing a function of TELO2 as a regulator of PIKKs stability (Takai et al., 2007).

TELO2 partners were first identified in 2008 by Shevchenko and colleagues through an accurate mapping of the *S. cerevisiae* “proteomic environment”. This approach allowed them to confirm existing data but also to nicely uncover a new protein complex containing Tel2 with two uncharacterized Tel2-interacting proteins (Tti1 and Tti2), as well as Tra1, Rvb1/2 and a protein of unknown function Asa1, forming altogether the ASTRA complex (for assembly of Tel, Rvb and Atm-like kinase) (Shevchenko et al., 2008). In 2010, through a genome-wide RNAi screen for genes required for ionizing radiation (IR) resistance in mammalian cells, Hurov and colleagues identified TTI1 as a novel regulator of the DNA damage response, in association with TTI2 and TELO2 proteins. The complex formed was therefore called Triple T also referred to as TTT complex and shown to act as a critical regulator of PIKK abundance (Hurov et al., 2010). Finally, ASTRA, the TTT

homolog in *S. cerevisiae*, was found in a genome-wide screen for chromosome instability, as a regulator of Tel1 and Tor1, ATM and mTOR homologs, respectively (Stirling et al., 2011).

Strikingly, the impairment of PIKK stability is not due to a defect in mRNA stability but in the accumulation of the newly synthesized protein (Takai et al., 2007). TTT allows the newly synthesized PIKKs to assemble into their functional complexes. For instance, the absence of TELO2 impaired the formation of TORC1 and TORC2 complexes (Takai et al., 2010). Moreover, TELO2 dissociates from the mature PIKKs: as an example, TELO2 does not bind phosphorylated-ATM which corresponds to the activated and mature form of ATM (Takai et al., 2010). Soon after their synthesis, TTT binds the PIKKs to regulate their maturation so that PIKKs can complete their overall folding for the assembly into their respective complexes.

Remarkably, TTT was defined as a PIKK-specific co-chaperone. Indeed, TTT was shown to not only interact with R2TP (PAQosome) complex (Horejsí et al., 2010; Takai et al., 2010), but also to function in coordination with HSP90 (Izumi et al., 2011; Takai et al., 2010). TTT coordinates the activities of PAQosome and HSP90 chaperone to integrate newly synthesized PIKK in their native complex.

The involvement of HSP90 was revealed through the use of specific HSP90 inhibitors such as 17-AAG and geldanamycin, which impaired PIKK stability (Hurov et al., 2010; Izumi et al., 2011; Takai et al., 2007). Nevertheless, TTT seems to cooperate with HSP90 in a PIKK specific manner. Indeed, the protein levels of ATR, ATM, DNAPKcs and TRRAP appear to be more affected in HeLa cells treated with HSP90 inhibitor than mTOR and SMG1, which are less impacted (Izumi et al., 2011; Takai et al., 2007). Remarkably, the opposite effects are observed in MEFs expressing a CK2-phosphosite mutated TELO2 protein unable to recruit the PAQosome. Indeed, TELO2 was shown to be phosphorylated on two serine residues by the CK2 kinase, on S487 and S491 (Horejsí et al., 2010) and interestingly, these phosphorylations have been shown to mediate the interaction between TELO2 and the PAQosome complex through the PIH1D1 subunit (Horejsí et al., 2010). Hence, in a mutant in which serines have been replaced by alanines, namely TELO2-2A, the PAQosome dissociates, leading to a clear impairment in mTOR and SMG1 stability, but a minor effect on ATM, ATR and DNAPKcs steady-state levels (Horejsí et al., 2010). Remarkably, the interaction of TELO2-2A with PIKKs or HSP90 is not affected, suggesting that the PAQosome is critical for mTOR and SMG1 assembly. Overall, these data suggest that the TTT might rely on different mechanisms to regulate the different PIKKs, some involving the PAQosome (such as for mTOR or SMG1) and some independently. This hypothesis is strengthened by the fact that in the yeast *S. pombe*, homologs of PIH1D1 and RPAP3 have not been identified so far, only RUVBL1/2 ATPases are conserved. In addition, a CK2-phosphosite mutant of TELO2 in *S. pombe* does not affect PIKK stability (Inoue et al., 2017). Surprisingly however, this mutant keeps interaction with RUVBL1/2, contrary to its homolog in mammals (Horejsí et al., 2010), suggesting that TTT regulates HSP90 and/or RUVBL1/2 activities to direct the folding of PIKKs. Today, our understanding of TTT is still very limited: plenty of questions remain, regarding the structure and the organization of TTT, and how it connects PIKKs with HSP90 and RUVBL1/2 activities.

2.2. Structure and function of the PIKK family

During the mid-1990's a novel family of kinases, structurally related to the phosphatidylinositol 3-kinases (PI3Ks), have been identified and hence named phosphatidylinositol 3-kinase-related protein kinases (PIKKs). Against all expectations PIKKs do not relay signals through phosphorylation of inositol phospholipids as PI3Ks kinases do, instead PIKKs mediate phosphorylations of others substrates. Indeed, PIKKs are unconventional serine/threonine kinases that play fundamental roles in numerous key cellular processes, establishing themselves as “big” players in stress responses (Abraham, 2004).

The PIKK family comprises six members: Ataxia-Telangiectasia Mutated (ATM), Ataxia- and Rad3-Related (ATR), DNA-dependent Protein Kinase catalytic subunit (DNA-PKcs), mammalian Target Of Rapamycin (mTOR), Suppressor of Morphogenesis in Genitalia (SMG1) and Transformation/transcription domain-Associated Protein (TRRAP), which are involved in a variety of cellular pathways. All of them require to be assembled with cognate partners in order to function accurately.

2.2.1. General domain organization and regulation

All PIKKs share a common linear structural organization, consisting in several domains, among which the FAT (FRAP, ATM, TRRAP) domain, the kinase domain (KD) and the FAT-C terminal (FATC) domain (Figure 38) are salient features (Lempiäinen and Halazonetis, 2009). Together the FAT and the kinase domain constitute the conserved core of the PIKKs.

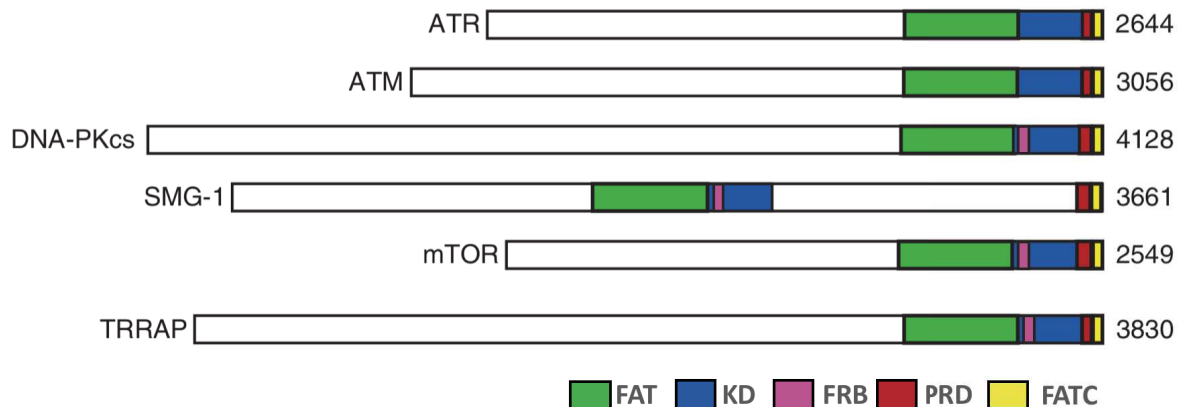


Figure 38: Schematic representation of the general domain organization of the PIKK family. The PIKK family encompasses six members sharing a common domain organization. From the N-terminus to the C-terminus, PIKK structure consists in a long stretch of HEAT repeats (white box), followed by the FAT (FRAP-ATM-TRRAP) domain (in green), the kinase domain (KD, in blue), the PIKK regulatory domain (PRD, in red) and the FAT-C terminal domain (FATC, in yellow). Some PIKKs, harbor a specific feature at the N-terminal part of their kinase domain, the FKBP12-rapamycin binding domain (FRB, in pink). The number indicated correspond to the total length of the respective PIKK. Adapted from (Lempiäinen and Halazonetis, 2009).

Interestingly, despite their large sizes ranging from about 290 kDa for mTOR to 470 kDa for DNA-PKcs, the kinase domain of PIKKs accounts for only 5-10% of total sequence (Abraham, 2004). In fact, the bulk of PIKK sequence resides in an extended amino-terminal part composed of 40-54 HEAT (Huntingtin, Elongation factor 3, A subunit of protein phosphatase 2 and TOR1) repeats which form an alpha-helical solenoid involved in protein-protein interactions (Perry and Kleckner, 2003).

The FATC domain corresponds to the extreme C-terminal region of PIKKs and consists in 33-35 residues, and represents another domain that mediates protein-protein interactions. The FATC domain is highly evolutionary conserved across species and among PIKKs, making it exchangeable in some of them. For instance, domain-swapping experiments have shown that the FATC of ATM can be replaced by that of ATR, DNA-PKcs or TRRAP without affecting functionality (Jiang et al., 2006). However, FATC domains can trigger inherent specificity for each PIKK, so that in some cases swapping does not restore PIKK function (Takahashi et al., 2000). The FATC domain has been shown to be critical for PIKK function, since substitution of a single amino-acid is enough to abrogate the function of SMG-1 (Morita et al., 2007) as well as mTOR (Takahashi et al., 2000). Moreover, in the yeast *S. cerevisiae* a single substitution of the last residue of the FATC of Tra1 (TRRAP) was shown to impair cell growth and transcriptional activity. Strikingly, mutations in the *Tti2* gene were able to rescue the FATC-mutant phenotype, suggesting that the FATC domain is essential for PIKK folding and/or stabilization mediated by the TTT complex (Genereaux et al., 2012). Remarkably, the FATC domain is enriched in hydrophobic and aromatic residues allowing thus interactions with lipids and membranes. Therefore, the FATC provides an anchor to membranes for PIKKs, allowing to spatially separate signaling events (Sommer et al., 2013).

Other domains, more diverse in sequence and length, are shared between PIKKs, such as the PRD, a linker region between the kinase and the FATC domains, which represents a site of post-translational modifications and therefore is important for the regulation of the kinase activity (Mordes et al., 2008; Sun et al., 2007). In addition, in some but not all PIKKs, a FRB-like domain which characterizes mTOR has been defined (Baretić and Williams, 2014). However, the FRB-like domain differs from the canonical FRB domain as it neither binds nor is inhibited by FKBP12-rapamycin (Brumbaugh et al., 2004).

2.2.2.mTOR, a PIKK responsible for cell proliferation, growth and protein synthesis

a) mTOR function overview

mTOR kinase is a central signaling hub within the cell, which integrates several extracellular and intracellular cues. mTOR assembles into two distinct multisubunit complexes, TORC1 and TORC2, defined by the presence of specific subunits, RAPTOR and RICTOR respectively, but also common subunit such as mammalian lethal with SEC13 protein 8 (mLST8). Within both complexes mTOR responds to several inputs and mediates specific downstream events through phosphorylations of several substrates, which are specific to each catalytic complexe.

For instance, mTORC1 senses and responds to nutrient availability by regulating translation, ribosome biogenesis and autophagy, to promote cell growth. mTORC2 controls cell proliferation and survival, as well as actin cytoskeleton by responding primarily to growth factors.

Besides the specificity of signals, both complexes display substrate specificity. mTORC1 promotes mRNA translation initiation through its major effectors p70S6 Kinase 1 (S6K1) and eIF4E-binding protein 1 (4EBP1) and mTORC2 substrates essentially include members of the AGC kinase family, such as AKT and PKC kinases (Saxton and Sabatini, 2017).

b) Structural organization of mTOR complexes

Cryo-EM structures of human mTORC1 and mTORC2 complexes have been obtained recently (Aylett et al., 2016; Chen et al., 2018; Yang et al., 2016). Interestingly, these studies revealed a dimerization mechanism of mTOR kinase in both complexes. mTOR monomers pack against each other to form a central scaffold, providing binding surfaces for the others components of the complex. mTORC1 and mTORC2 complexes adopt a hollow rhombohedral shape with a 2-fold symmetry (Figure 39).

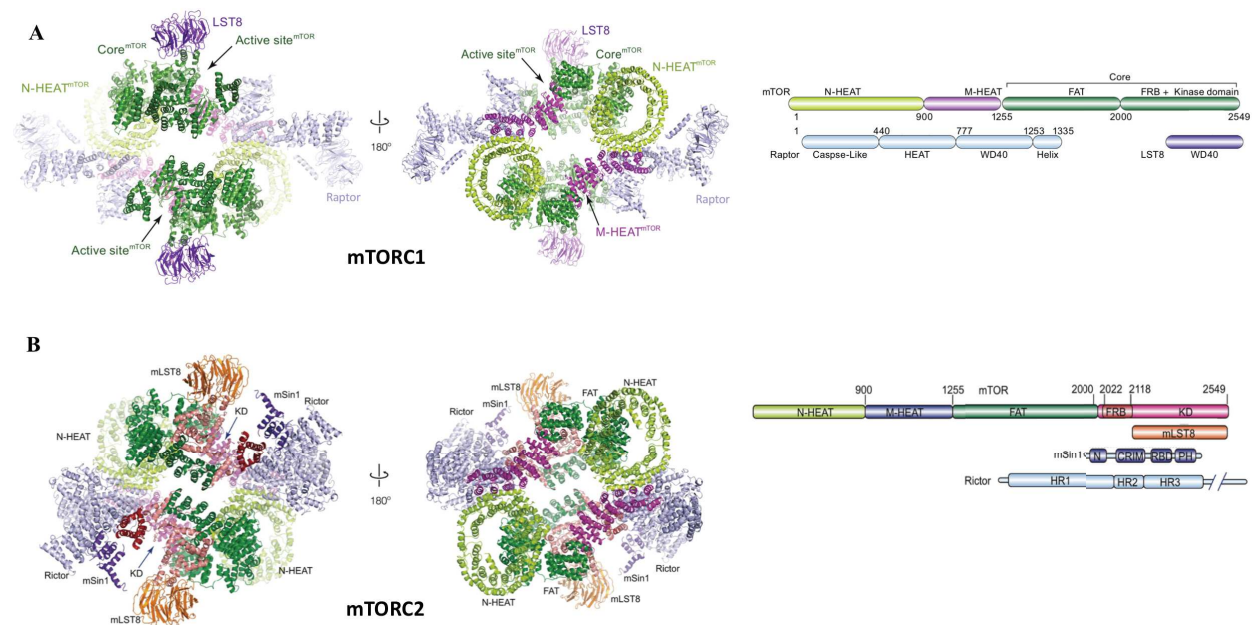


Figure 39: Overall structure of human mTOR complexes. Ribbon representations in two different views of mTORC1 (A), and mTORC2 (B). Proteins and domains composing each complex are indicated. The color matching of each component and their specific domains is depicted in the linear representation of the domain architecture (on the right). Both complex adopt a 2-fold symmetry with a central core formed by two mTOR molecules. Adapted from (Aylett et al., 2016; Yang et al., 2016).

Although mTORC1 and mTORC2 adopt a similar overall conformation they exhibit some specific features (Figure 40A). For instance, their specific components RAPTOR and RICTOR, which have no sequence similarity, adopt distinct conformations within each complex (Figure 40A), consequently their binding to mTOR is mutually exclusive. Moreover, mTORC2 differs from

mTORC1 by a narrower central hole, forming therefore a more compact fold. Indeed, the height of the inner hole, which is defined by the distance between both arginine 1966 located in the FAT domain of each mTOR monomer, is reduced of 12 Å in mTORC2 compare to mTORC1 (Figure 40A, B). Finally, one critical difference between mTORC1 and mTORC2 is their sensitivity to rapamycin. Structural comparisons of the two complexes, clearly showed that the insensitivity of mTORC2 to rapamycin resides in a steric hindrance generated by the existence of five α -helices in its mSin1 subunit (Figure 40A, B). Hence FKBP12-rapamycin cannot get access to the FRB domain in mTORC2, which in addition is pushed forward as compared to its position in mTORC1 (Figure 40B).

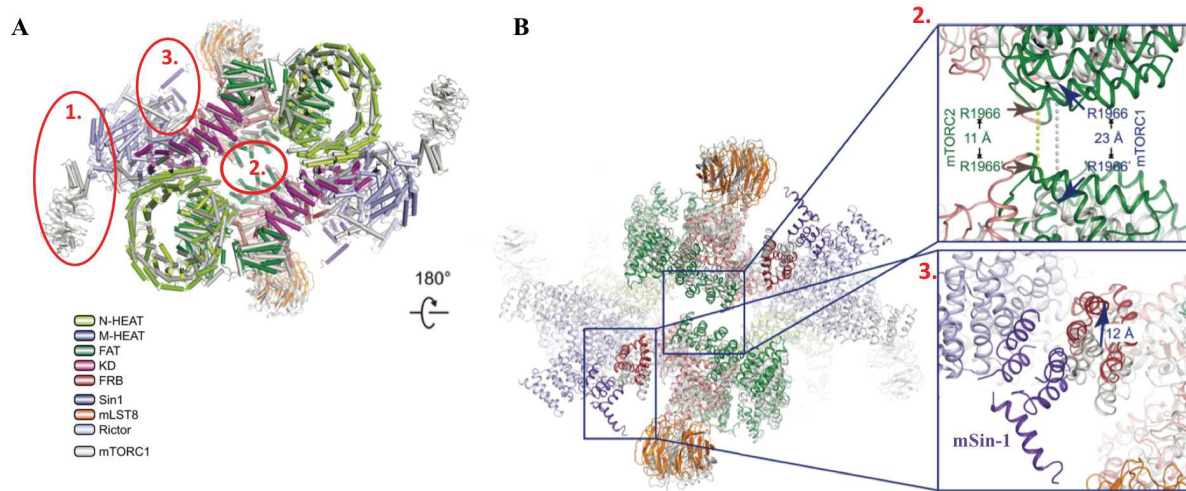


Figure 40: Structural distinctions between mTORC1 and mTORC2 complexes. Superimposition of mTORC1 and mTORC2 structures in two different views, with helices shown in cylinders (A) and ribbon (B) representations. The color scheme is indicated for each component and domain. Three main differences are highlighted by a red circle (A) and two of them are depicted in a closed-up view (B). 1- RAPTOR and RICTOR adopt distinct conformations. 2- The central hole is narrower in mTORC2, as depicted in the closed-up view (B), the distance between R1966 residues of both monomers is shorter in mTORC2. 3- Steric hindrance generated by Sin1 subunit in mTORC2, the closed-up view shows in details the presence of five α -helices in Sin1 blocking the access of the FRB domain which in addition moves upward. Adapted from (Chen et al., 2018).

c) Regulation of mTOR complex assembly

As mentioned previously, mTOR assembles within mTORC1 and mTORC2 complexes, which respond to distinct environmental cues by regulating specific signaling pathways. Incorporation of mTOR into both complexes is highly regulated. However, mechanisms that drive the dynamic assembly of mTOR in one complex *versus* the other are still poorly defined.

Remarkably, some studies have revealed a clear involvement of the energy status of the cell, which ultimately impacts, directly or indirectly, the TTT co-chaperone activity. For instance, Fernandez-Saiz and colleagues showed that upon serum deprivation, TELO2 and TTI1 proteins are targeted for degradation within the mTORC1 complex in a CK2-dependent manner by the SCF^{Fbxo9} ubiquitin ligase, thereby impacting mTORC1 activity and favoring mTORC2 signaling. They identified a mechanism which allows cells to minimize energy-consuming events and to avoid early cell death after growth factors withdrawal (Fernández-Sáiz et al., 2013). In addition, the lab of John

Blenis reported that glucose and glutamine depletion lead to a decrease of mTOR and TTT interaction, resulting in the disruption of mTORC1 lysosomal localization, dimerization and thus activity (Kim et al., 2013). Interestingly, in a screen for autophagy regulators David-Morrison and colleagues identified the WAC protein as an adaptor to facilitate the dimerization of mTOR loaded with TTT on one side, and RUVBL/2 on the other. WAC responds to energy stimulation to promote mTORC1 activity (David-Morrison et al., 2016). Thus, TTT is regulated by the metabolic state of the cells and represents a central regulator of mTOR complexes assembly and activity.

Besides TTT, components of mTORC1 and mTORC2 can be involved in the preferential assembly and activation of one complex *versus* the other. Recently, Wang and colleagues revealed that the assembly of mTORC2 is modulated by a mLST8-ubiquitination-dependent switch. They showed that the polyubiquitination of mLST8 by the ubiquitin ligase TRAF2 disrupts its interaction with mSIN-1, an mTORC2 subunit, favoring thus mTORC1 formation. Conversely, in response to growth signals, the deubiquitinase OTUD7B removes the polyubiquitin chains from mLST8, facilitating thus the activation of mTORC2/AKT signaling (B. Wang et al., 2017).

2.2.3.ATR, ATM and DNAPKcs, PIKKs involved in DNA damage response

a) Overview of ATR, ATM and DNA-PKcs function

The DNA damage response (DDR) encompasses several signaling pathways that sense and repair damages in DNA, ensuring genome integrity. Upon DNA damage, “sensors” bind to the injury site and recruit PIKKs that act as “transducers” which in turn activate downstream “effectors” to mediate DNA repair. PIKKs transduce the signal by phosphorylating hundreds of targets to orchestrate repair.

Depending on the type of DNA damage encountered, a specific PIKK is involved. For instance, ATM and DNA-PKcs respond mainly to double-strand DNA breaks (DSBs) while ATR is activated upon replication-stress by single-stranded DNA (ssDNA) (Pancholi et al., 2017).

To be repaired, DSBs rely on two different mechanisms: the homologous recombination (HR) mediated by ATM and the non-homologous end-joining (NHEJ) requiring DNA-PKcs activity. The choice between both is influenced by the cell-cycle. Therefore, DSBs that occur during S and G2 phases are predominantly repaired by HR, whereas the one formed during G1 phase are mainly repaired through NHEJ (Branzei and Foiani, 2008).

ssDNA, which is mostly generated during replication at stalled-replication forks and at resected DSBs, is immediately bound by Replication Protein A, which represents the major ssDNA-binding protein and constitutes a key signal for ATR recruitment. Once recruited, ATR activates specific downstream effectors such as p53 and CHK1 triggering cell-cycle arrest or apoptosis.

b) Structure and regulation of DDR-specific PIKKs

DNA-PKcs contains in its N-terminal part HEAT repeats which are divided into two portions, an N-terminal and a middle-HEAT repeats, N-HEAT and M-HEAT respectively. Both portions pack against each other and adopt a hollow double-ring structure (Figure 41B).

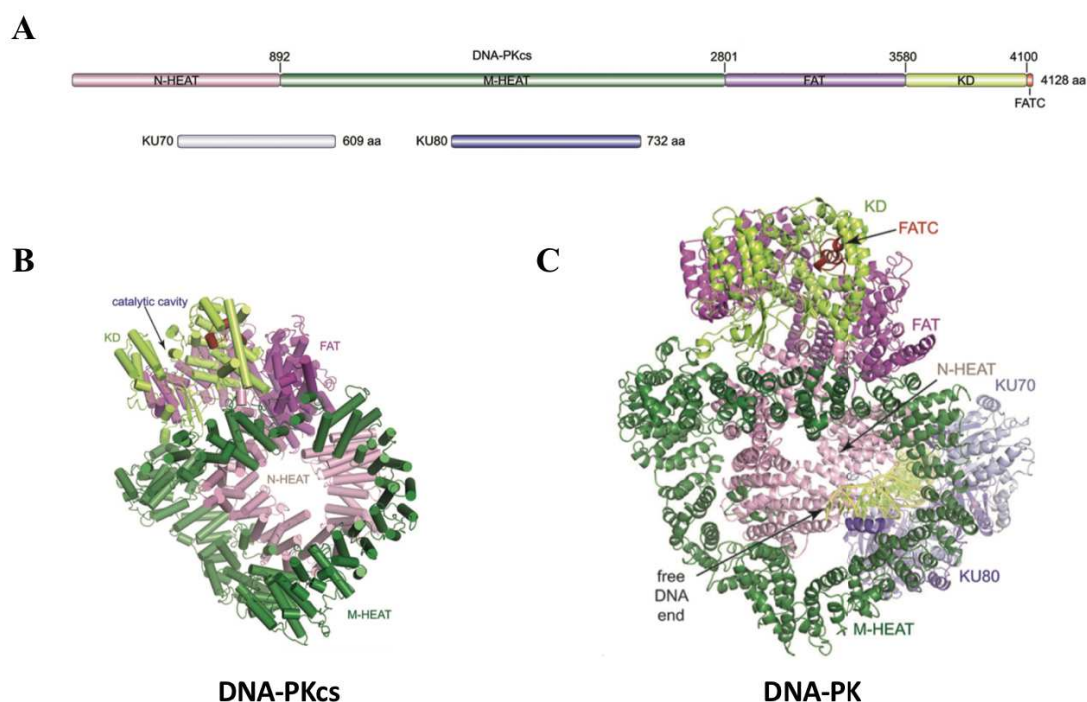


Figure 41: Overall structure of DNA-PKcs and DNA-PK. (A) Linear representation of DNA-PKcs domain architecture, KU70 and KU80 proteins, with the specific color scheme used hereafter in the structures. (B) The N-terminal α -solenoid of DNA-PKcs adopts a hollow double-ring structure which connects KU70/80 heterodimer forming altogether the DNA-binding tunnel of the DNA-PK complex (C). Adapted from (Yin et al., 2017).

DNA-PKcs forms the DNA-PK complex or holoenzyme with Ku70/80 heterodimer bound to DNA. Ku70/80 heterodimer recognizes double-stranded DNA (dsDNA) ends and then recruits DNA-PKcs. Ku70/80 and DNA-PKcs together form a DNA-binding tunnel which surrounds ~ 30 bp of DNA (Figure 41C). Interestingly, the kinase activity of DNA-PKcs is allosterically stimulated by Ku70/80 and DNA which coordinately induce conformational changes (Yin et al., 2017).

ATM is also activated by conformational changes. Indeed, ATM forms a homodimer in which active sites of both ATM molecules are buried and thus substrates cannot get access (Figure 42) (Lau et al., 2016). Therefore, in unstressed cells, ATM was described to adopt an homodimeric structure catalytically inactive. However, recently, the cryo-EM analysis of ATM published by Baretić and colleagues uncovers an equilibrium between two types of dimers, a symmetric “closed” dimer and an asymmetric “open” dimer (Baretić et al., 2017). Surprisingly, the structure of the “open” dimer

suggests that it might be enzymatically active. They showed that the transition between the “closed” to the “open” dimers involves several C-terminal structural elements, that altogether form a compact arrangement called the FLAP (FATC, LBE, Activation loop, PRD), as well as two specific helices forming the FLAP-BE (FATC, LBE, Activation loop, PRD, Binding Element). In the “closed” dimer, the FLAP/FLAP-BE interaction restricts access to the ATM substrate-binding site. This interaction is lost in the “open” dimer and thus might allow substrate binding.

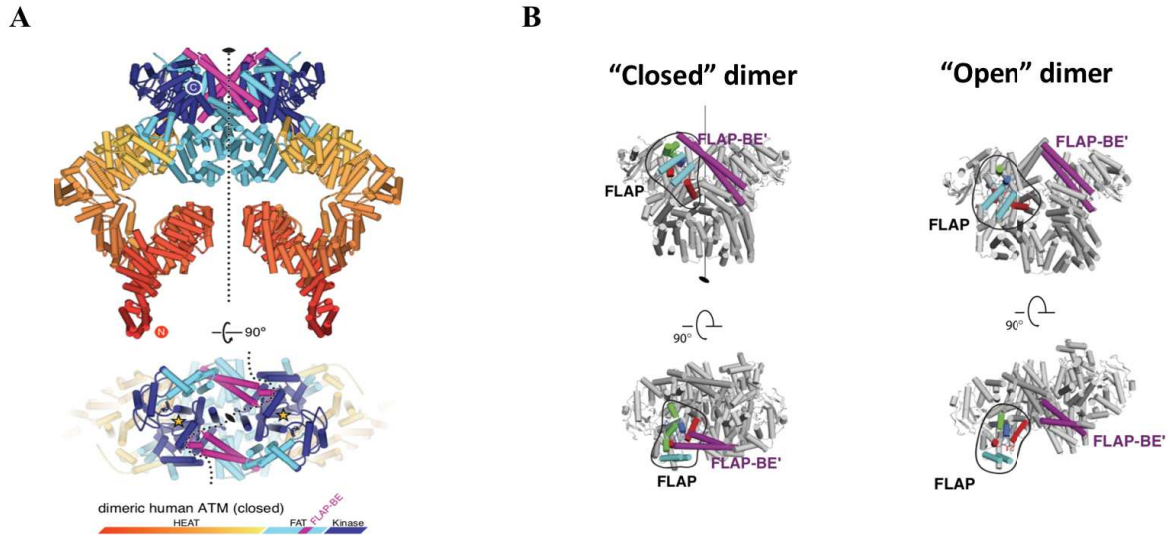


Figure 42: Structure of human ATM dimers. (A) Model of the cryo-EM structure of the human ATM “closed” dimer. The HEAT repeats of each monomer form a helical structure while the C-terminal part participates in the dimerization interface. (B) The FLAP-BE (purple) interacts with the FLAP and restricts ATM to a conformation that blocks the substrate from entering the active site (left panel). The loss of this interaction, leads to the “open” dimer structure leaving sufficient space for a substrate to bind (right panel). Adapted from (Baretić et al., 2017; Imseng et al., 2018).

Upon DNA damage, the Mre11-Rad50-Nbs1 (MRN) complex acts as a sensor of DSBs and recruits ATM. Once recruited, ATM undergoes intermolecular autophosphorylation leading to its activation. In fact, autophosphorylation on serine 1981 was shown to induce the dissociation of the complex, releasing phosphorylated and activated-ATM monomers (Bakkenist and Kastan, 2004). The MRN complex not only recruits ATM but also stimulates its kinase activity through conformational changes that increase its substrate affinity (Lee and Paull, 2004). ATM is also stimulated by TIP60 acetylation of Lys3016, in the FATC domain (Sun et al., 2005).

ATR also adopts a dimeric structure with a hollow “heart” shape (Figure 43). ATR forms an obligate complex with its binding partner ATRIP (ATR interacting protein). The cryo-EM structure obtained from human ATR-ATRIP complex revealed a dimerization between two ATR monomers which adopt distinct conformation within the complex thanks to a switch point located in their N-HEAT allowing the binding of ATRIP (Figure 43) (Rao et al., 2018).

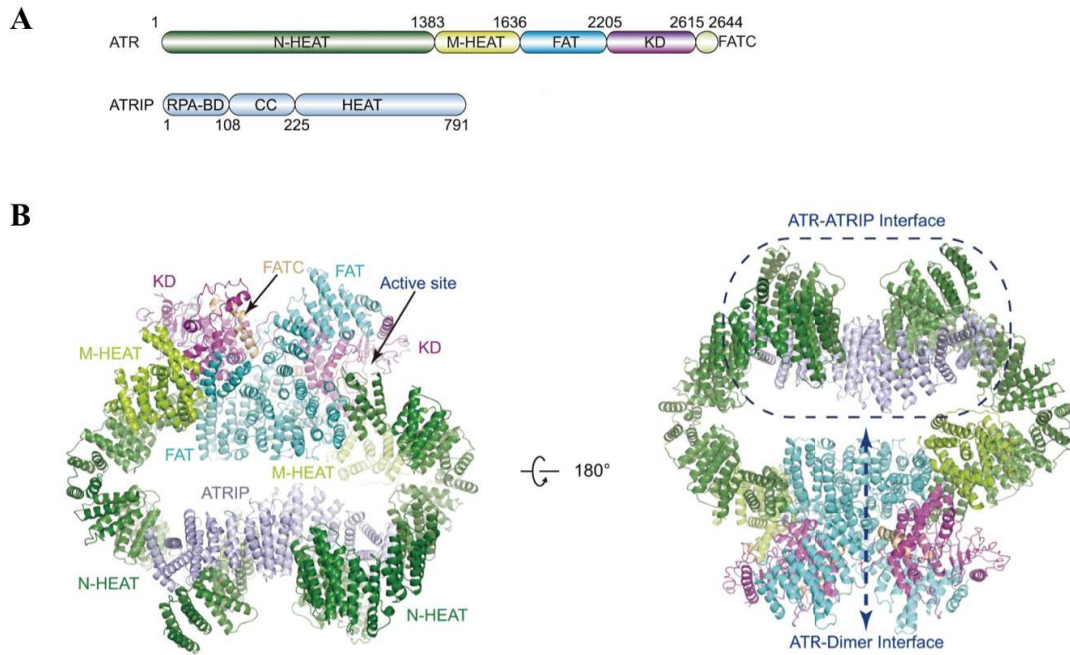


Figure 43: Overall structure of ATR-ATRIP complex. (A) Linear representation of ATR and ATRIP domain structure with the corresponding color scheme used in the ribbon representations (B). ATR-ATRIP form a dimeric complex with a hollow “heart” shape. Each ATR monomer adopts a distinct overall conformation within the complex, critical for the binding of ATRIP. The dimerization interface encompasses intermolecular contacts between both ATR monomers (ATR-Dimer interface) but also between ATRIP and the N-termini of both ATR (ATR-ATRIP interface) (B, right). Adapted from (Rao et al., 2018).

Recently, the structure of the yeast homolog of ATR-ATRIP, namely Mec1-Dcd2 has been determined by cryo-EM at 3.9 Å in *S. cerevisiae* and also revealed a dimeric structure but they were able to discriminate two molecules of Dcd2 (ATRIP), as compared to human complex (X. Wang et al., 2017).

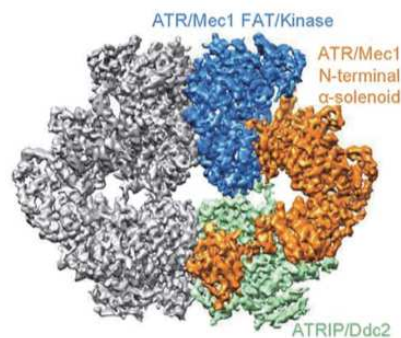


Figure 44: Overall structure of Mec1-Dcd2, the yeast homolog of ATR-ATRIP. Mec1 and Dcd2 form a dimer of heterodimers. The FAT-KD-PRD-FATC domains of Mec1 are in blue, the α-solenoid in orange and Dcd2 in green. The other monomer is colored in grey. Adapted from (X. Wang et al., 2017).

Although ATR-ATRIP complex is catalytically active, its kinase activity might be stimulated by Topoisomerase DNA II Binding Protein 1 (TopBP1), which acts by facilitating substrate access or favoring catalytic reaction through conformational changes of the kinase domain (Rao et al., 2018).

2.2.4. SMG1 and the NMD process

Translation of a messenger RNA starts from a methionine START codon and ends with the presence of a STOP codon. Cells display a post-transcriptional surveillance pathway that ensures that mRNAs harboring premature translation termination codons, which may lead to toxic truncated proteins, are removed before translation. In addition to a quality control role, this surveillance mechanism, named nonsense-mediated mRNA decay (NMD), is also involved in transcript abundance regulation. SMG1 forms a complex, the so-called SMG1 complex (SMG1C), with SMG8 and SMG9 (Figure 45).

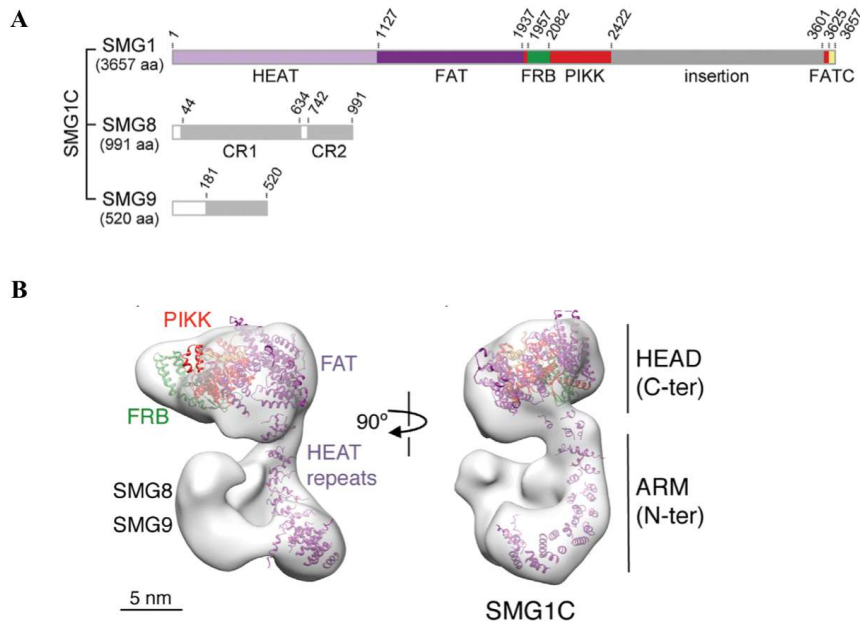


Figure 45: SMG1 complex structure. (A) Schematic representation of SMG1, SMG8, and SMG9 domain organization, with the corresponding color scheme used in the EM structure (B). (B) EM structure of SMG1C (grey transparent density), revealing that SMG1 structures into a compact head (at the top of the molecule) and a thinner arm (at the bottom of the molecule). Adapted from (Melero et al., 2014).

Premature termination codon (PTC) recognition results in aberrant translation termination, which induces the fixation of UPF1, a central regulator of NMD, on the terminating ribosome and the assembly of the transient SURF complex comprising the SMG1, UPF1, eRF1 and eRF3 proteins (Causier et al., 2017). If an exon junction complex (EJC) is located 50–55 or more nucleotides downstream from the termination codon, the SURF complex associates with the downstream EJC through UPF2 and UPF3, two NMD factors. SURF association with UPF2-UPF3-EJC induces SMG1-mediated UPF1 phosphorylation, which is central to NMD (Yamashita et al., 2009). Little is known about the molecular events leading to this activation.

2.2.5. TRRAP and the transcription

TRRAP is the PIKK involved in transcription regulation. As addressed previously, TRRAP is part of two transcriptional co-activator complexes, SAGA and TIP60, in which it acts as an activator-interacting protein. TRRAP was originally identified as an interacting partner for c-MYC and E2F transcription factors (Steven B. McMahon et al., 1998). It represents an important mediator for MYC and E1A oncogenic activities, notably for their transforming function (Deleu et al., 2001). TRRAP activates genes involved in important processes, including cell cycle progression (Herceg et al., 2001), mitotic checkpoint control (Li et al., 2004), maintenance of stem cell niches (Loizou et al., 2009; Sawan et al., 2013; Tapias et al., 2014; Tauc et al., 2017; Wurdak et al., 2010), or multiciliated cell differentiation (Z. Wang et al., 2018).

TRRAP is highly conserved throughout evolution with 20-25% of identity and 55-60% of similarity between homologs in different species (Steven B McMahon et al., 1998). Genetic studies revealed that *Tra1* is essential for cell viability and gene-specific transcription in yeast, and disruption of *Trrap* in mice led to peri-implantation lethality indicating an essential function in embryonic development and cell cycle control (Brown et al., 2001; Herceg et al., 2001; Saleh et al., 1998).

Although TRRAP retains a kinase domain in which are preserved the relative positions of the catalytic, activation and phosphate-binding loops, as found in mTOR and DNA-PKcs (Figure 46), it lacks critical residues required for ATP/Mg binding and catalysis. Moreover, the relative position of the Tra1 FRB domain occludes the active site as compared with the FRB of mTOR and DNA-PKcs which in contrast are positioned away from the active site cleft. These conformational and structural differences support that TRRAP is catalytically inactive and represents the only pseudo-kinase of the PIKK family (Díaz-Santín et al., 2017; Saleh et al., 1998).

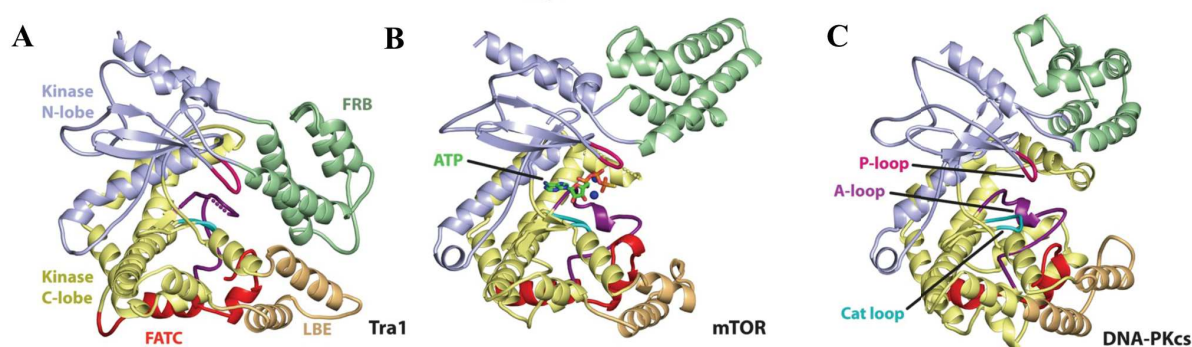


Figure 46: TRRAP is a pseudo-kinase. Kinase domain comparison between Tra1 (A), mTOR (B), and DNA-PKcs (C). The relative positions of the phosphate binding loop (P-loop, pink), catalytic loop (Cat loop, cyan) and activation loop (A-loop, purple) are conserved in Tra1. The position of the Tra1 FRB domain (in green) differs from those of mTOR and DNA-PKcs.

Remarkably, Tra1 overall structure resembles DNA-PKcs (Figure 47), suggesting functional similarities between both PIKKs, which might not engage the kinase activity. As described previously, DNA-PKcs is recruited by Ku70/80 to sites of DSBs. Interestingly, TIP60 is also recruited to DSBs in a TRRAP-dependent manner to mediate H4 acetylation, and TRRAP depletion was shown to impair DSBs repair (Murr et al., 2006). Moreover, TRRAP was reported to interact with the MRN complex, a known sensor of DSBs (Robert et al., 2006). Altogether, these observations point out toward a direct role of TRRAP in DNA damage repair which might involve the structural homology of Tra1 with DNA-PKcs.

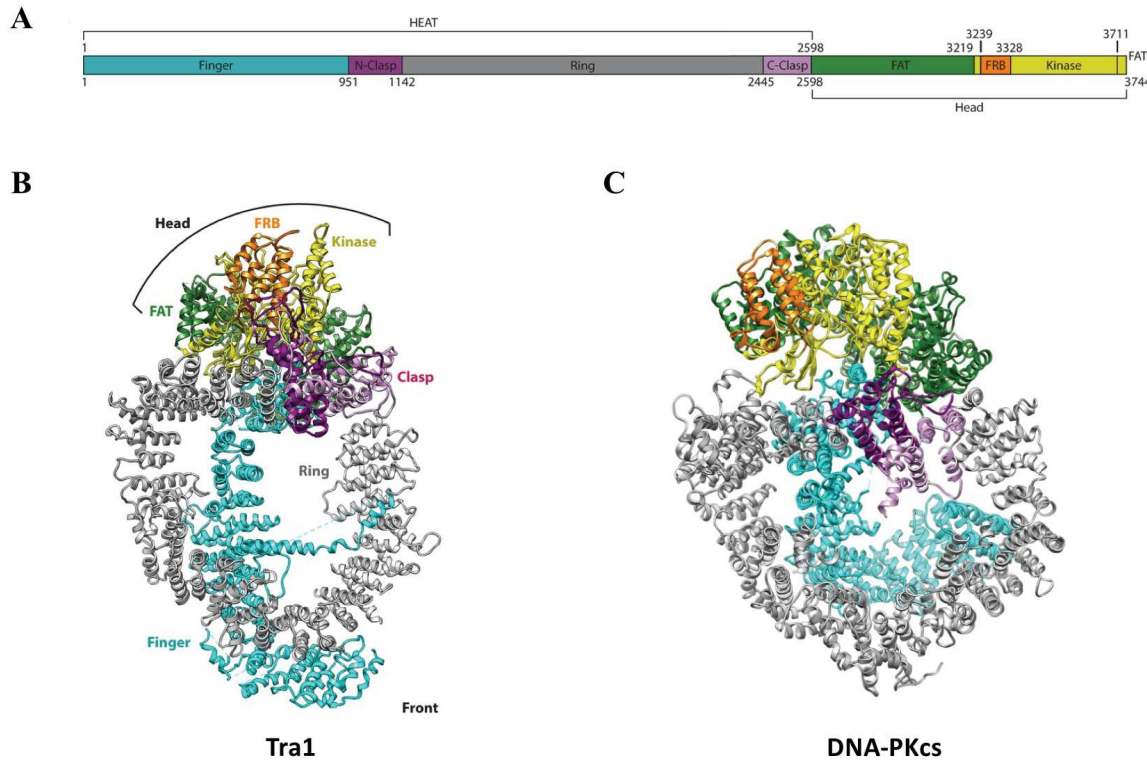


Figure 47: Overall structure of Tra1 structurally homologous to DNA-PKcs. (A) Schematic representation of Tra1 domain organization with the color scheme used in (B). (B) Cryo-EM structure of Tra1 which adopts a ring structure similar to DNA-PKcs (C).

OBJECTIVES

OBJECTIVES

The cofactor TRRAP is part of two co-activator complexes, SAGA and TIP60. TRRAP interacts with transcription factors, such as c-MYC and E2Fs and participates in the recruitment of SAGA and TIP60 on chromatin. Although TRRAP was reported to activate several genes involved in a number of important cellular processes, its direct targets remain poorly described.

Interestingly, TRRAP is the sole pseudo-kinase of the PIKK family to which it belongs. The folding, stability and assembly of the PIKKs is ensured by a co-chaperone of HSP90, the TTT complex composed of TELO2, TTI1 and TTI2 subunits.

Despite clear evidence that TTT interacts and stabilizes TRRAP as for other PIKKs, any study demonstrated so far, the effect of TTT on the assembly of TRRAP within SAGA and TIP60 complexes nor its role in transcription regulation. Surprisingly, TTT and TRRAP are overexpressed in colorectal cancer, raising the hypothesis that TTT could represent a key regulator of tumorigenesis by regulating a specific transcriptional program mediated by TRRAP.

In line with this, the objectives of my PhD work were the followings:

- 1) Examine the role of TTT co-chaperone in the regulatory activities of TRRAP pseudo-kinase in colorectal cancer.
- 2) Identify and characterize the direct targets of TRRAP.

RESULTS

RESULTS

PART 1:

Transcriptional repression of interferon-stimulated genes by the TRRAP transcriptional co-activator and its chaperone TTT

Dylane Detilleux¹, Peggy Raynaud¹, Boris Bonaventure², Emeric Dubois³, Samia Guendouz³, Caroline Goujon², Bérengère Pradet-Balade¹ and Dominique Helmlinger¹

¹CRBM, CNRS, University of Montpellier, Montpellier, France

²IRIM, CNRS, University of Montpellier, Montpellier, France

³MGX-Montpellier GenomiX, CNRS, Montpellier, France.

Keywords: transcription; chromatin; interferon; oncogenesis; chaperones

ABSTRACT

Gene expression regulation is essential for cells to respond to signaling cues. Transcription represents a crucial regulatory step and involves several factors with multiple distinct activities. One such factor, TRRAP (Transformation/transcription domain associated protein), was first discovered as an interacting partner for the MYC oncogenic transcription factor. TRRAP was then shown to be part of two co-activator complexes, SAGA and TIP60. Interestingly, TRRAP is the sole pseudokinase of the PIKK family, which encompasses five kinases playing critical roles during key cellular processes. The PIKKs are folded and assembled into their active complexes by a dedicated co-chaperone of HSP90, namely TTT. We used CRISPR-Cas9 to construct fast, inducible degron alleles of both TRRAP and the TTT co-chaperone in colorectal cancer cells. Transcriptomic analysis revealed a significant overlap between genes which expression depends on TRRAP and TTT. Remarkably, most of these genes are MYC and E2Fs targets, suggesting that TTT has an important role in sustaining the activities of these oncogenic transcription factors in colorectal cancer cells. Surprisingly, TTT and TRRAP depletion also induced a common Type I Interferon gene expression signature. Antibody-targeted chromatin profiling (CUT&RUN) and kinetic analyses revealed that TRRAP directly represses the expression of IRF9, which acts as a master regulator for the expression of interferon stimulated genes. To conclude, we have uncovered an unexpected repressive role of TTT and TRRAP at interferon-stimulated genes in colorectal cancer cells, revealing a previously unidentified mechanism by which TRRAP contributes to tumorigenesis.

INTRODUCTION

Transcriptional regulation is crucial for cells to adjust to external changes, for example during development or to maintain homeostasis, and occurs at multiple steps. Transcription initiation is controlled by large, multimeric complexes that remodel or modify nucleosomes at promoters. Two such complexes, the SAGA and TIP60 co-activators, modulate target gene expression through several regulatory activities, including histone H3 and H4 acetylation, H2B de-ubiquitination, or deposition of the histone variant H2A.Z (Lu et al. 2009; Spedale et al. 2012; Helmlinger and Tora 2017). Although SAGA and TIP60 have distinct regulatory roles, they share one component, named Tra1 in yeast or TRRAP in metazoans (Grant et al. 1998; Vassilev et al. 1998; Allard et al. 1999; Ikura et al. 2000). Its primary role is to mediate the recruitment of SAGA and TIP60 to promoters by direct interaction with a diverse range of transcription factors.

TRRAP was indeed initially discovered as a co-activator for the c-MYC and E2Fs transcription factors and is essential for their oncogenic activities (McMahon et al. 1998; Park et al. 2001; Nikiforov et al. 2002; Taubert et al. 2004). Biochemical evidence then established that yeast Tra1 directly contacts several transcription activators (Brown et al. 2001; Bhaumik et al. 2004; Fishburn et al. 2005; Reeves and Hahn 2005; Herbig et al. 2010; Lin et al. 2012). Accordingly, TRRAP activates genes involved in number of important processes, including cell cycle progression (Herceg et al. 2001), mitotic checkpoint control (Li et al. 2004), maintenance of stem cell niches (Loizou et al. 2009; Wurdak et al. 2010; Tapias et al. 2014; Tauc et al. 2017; Sawan et al. 2013), or multiciliated cell differentiation (Wang et al. 2018). However, the direct regulatory roles of TRRAP have been challenging to study, because genetic analyses relied on partial depletion or conditional knock-out strategies and its enrichment by conventional chromatin immunoprecipitation (ChIP) approaches is weak, as compared to background signals.

The domain architecture of TRRAP is typical of phosphoinositide 3 kinase-related kinases (PIKK), but TRRAP lacks catalytic residues and is the sole pseudokinase of that

family (McMahon et al. 1998; Saleh et al. 1998; Vassilev et al. 1998). PIKKs are atypical kinases implicated in diverse processes, including DNA repair and telomere homeostasis, through ATM, ATR, and DNA-PKcs, coordination of cell growth with metabolic inputs, through mTOR, or non-sense mediated mRNA decay, via SMG1 (Lempiäinen and Halazonetis 2009; Imseng et al. 2018). Several elegant studies have demonstrated that PIKKs require a dedicated HSP90 co-chaperone, the triple T complex (TTT), for their stabilization, maturation, and incorporation into active complexes (Takai et al. 2007; Anderson et al. 2008; Takai et al. 2010; Hurov et al. 2010; Kaizuka et al. 2010; Izumi et al. 2010).

TTT was initially discovered in fission yeast and is composed of three conserved, specific subunits, TELO2, TTI1, and TTI2 (Hayashi et al. 2007; Shevchenko et al. 2008; Takai et al. 2010). Biochemical evidence suggest a model in which TTT directs the pleiotropic HSP90 chaperone to PIKKs specifically. TTT recruits HSP90 through the phosphorylation-dependent interaction of TELO2 with the R2TP complex, formed by RPAP3, PIH1D1 and the AAA+ ATPases RUVBL1 and RUVBL2 (Hořejší et al. 2010, 2014; Pal et al. 2014). Numerous functional studies in different organisms have implicated TTT, particularly TELO2, in PIKK signaling in response to DNA damage or metabolic stress (Ahmed et al. 2001; Takai et al. 2007; Shikata et al. 2007; Anderson et al. 2008; Hurov et al. 2010; Izumi et al. 2012; Kaizuka et al. 2010; Kim et al. 2012). More recent studies have shown that TTT itself can respond to various signaling cues, such as nutrient levels, to modulate PIKK levels, localization, or substrate binding (Kim et al. 2012; Rao et al. 2014; David-Morrison et al. 2016; Brown and Gromeier 2017). In contrast, the effect of TTT on the incorporation of the TRRAP pseudokinase into the SAGA or TIP60 complexes and in transcriptional regulation remains unknown, despite clear evidence that TTT interacts with and stabilizes TRRAP (Takai et al. 2007; Kaizuka et al. 2010; Hurov et al. 2010; Izumi et al. 2012). In addition, little is known about how the SAGA and TIP60 complexes are assembled, which chaperones are

required, and whether TRRAP is incorporated into each complex by similar or distinct mechanisms.

To examine the role of TTT in the regulatory activities of TRRAP, we used CRISPR-Cas9 genome editing to fuse an auxin-inducible degron (AID) to the endogenous *TELO2* and *TRRAP* genes in HCT116 colorectal cancer cells. Their rapid, robust, and reversible depletion allowed us to demonstrate that *TELO2* controls TRRAP activity. First, we found that *TELO2* promotes the incorporation of TRRAP into both SAGA and TIP60 complexes. Second, transcriptomic analyses revealed that *TELO2* regulates the expression of a large fraction of TRRAP-dependent genes. Remarkably, most of these genes were previously annotated as targets of c-MYC and E2Fs, suggesting that TTT has an important role in sustaining the activities of these oncogenic transcription factors in colorectal cancer. We then used an innovative chromatin profiling strategy, Cleavage Under Targets and Release Using Nuclease (CUT&RUN) (Skene et al. 2018), to identify genes that are directly regulated by TRRAP. Unexpectedly, TRRAP contributes to the inhibition of interferon-stimulated gene (ISG) expression in the absence of any pathogen. In particular, we observed robust binding of TRRAP to the promoters of the genes encoding the IRF7, IRF9, and STAT2 transcription factors. Kinetic analyses showed that their expression is rapidly and tightly modulated by TRRAP. To conclude, we report here an unexpected repressive role of TRRAP at interferon-stimulated genes in colorectal cancer cells, revealing a previously unidentified mechanism by which TRRAP might contribute to tumorigenesis. In addition, we present evidence that TRRAP, although a pseudokinase, shares a dedicated chaperone machinery, TTT, with its cognate kinases for its stability and function.

RESULTS and DISCUSSION

Acute and rapid depletion of TELO2 and TRRAP using an auxin-inducible degron

Previous work has reported that the TTT components TELO2, TTI1, and TTI2 stabilize steady-state TRRAP levels (Takai et al. 2007; Kaizuka et al. 2010; Hurov et al. 2010; Izumi et al. 2012). We therefore sought to determine whether and how TTT contributes to TRRAP-dependent transcriptional regulation. For this aim, we first asked if TTT promotes the incorporation of TRRAP into both the SAGA and TIP60 coactivator complexes.

Our initial attempts to knockdown TTT using RNA interference failed to reproduce the effect on PIKK stability in HCT116 colorectal cancer cells (data not shown). We reasoned that, to observe the effects of a chaperone on its clients, we need an inducible depletion strategy that targets protein stability directly and rapidly. In addition, a conditional approach was dictated by the observations that both TELO2 and TRRAP are essential for early embryonic development or cell proliferation (Herceg et al. 2001; Takai et al. 2007). To that end, we used CRISPR-Cas9-mediated genome editing to generate HCT116 cell lines in which an auxin-inducible degron (AID) is fused to the C-terminal of TELO2 (Figure 1A). Using the same strategy, we fused an AID to the N-terminal extremity of TRRAP (Figure 1B), because the C-terminal FATC domain is critical for the function of yeast Tra1 (Hoke et al. 2010; Helmlinger et al. 2011).

The AID system mediates proteasomal-dependent degradation of AID-tagged proteins through the F-box protein transport inhibitor response 1 (TIR1). Upon auxin treatment, TIR1 recruits the SCF E3 ubiquitin ligase complex to proteins harboring a degron sequence derived from AtIAA17 (Nishimura et al. 2009). We thus first generated a human colorectal cancer cell line stably expressing TIR1. For this, HCT116 cells were transduced with a lentiviral vector expressing TIR1, derived from *Oriza sativa* (OsTIR1), which is reported to be more stable at higher temperatures, as compared to its *Arabidopsis thaliana* ortholog AtTIR1. We selected and amplified a clone expressing OsTIR1, which was then transiently

transfected with four distinct plasmids to achieve bi-allelic insertion of the AID coding sequence at either the *TELO2* or *TRRAP* locus. Specifically, we used a mutant D10A nickase version of SpCas9, which generates only single strand breaks and thus requires two single guide RNAs (sgRNAs) for editing, each on a separate plasmid, hence reducing off target cleavage and repair. Finally, we combined gene synthesis, high-fidelity PCR, and molecular cloning to construct two distinct donor plasmids. Both comprised the sequence encoding a full-length IAA17-derived degron (Nishimura et al. 2009). We also included repeated HA epitopes and a YFP fluorescent tag, to allow protein detection and selection following transfection and editing, respectively. Finally, to lower the risks of affecting the levels or function of TRRAP with a long fusion sequence at its N-terminal end, we inserted a 2A peptide (P2A) between the HA-AID and YFP sequences, which is then cleaved off during translation (Figure 1B). Selection was performed using fluorescence-activated cell sorting, keeping cells that showed moderate YFP expression levels, as compared to background fluorescence (Supplemental Figure 1A,B). Clonal populations of cells were obtained by serial dilutions. Following amplification, about 60 clones showing normal proliferation rates were isolated and screened by Western blot for a complete size shift of *TELO2* or *TRRAP*, using antibodies against the endogenous proteins (Supplemental Figure 1C,D). Approximately 10% clones showed homozygous insertion of the donor sequence at the desired loci. We then amplified and characterized 3 distinct homozygous clones for each tagged protein (Supplemental Figure 1E,F).

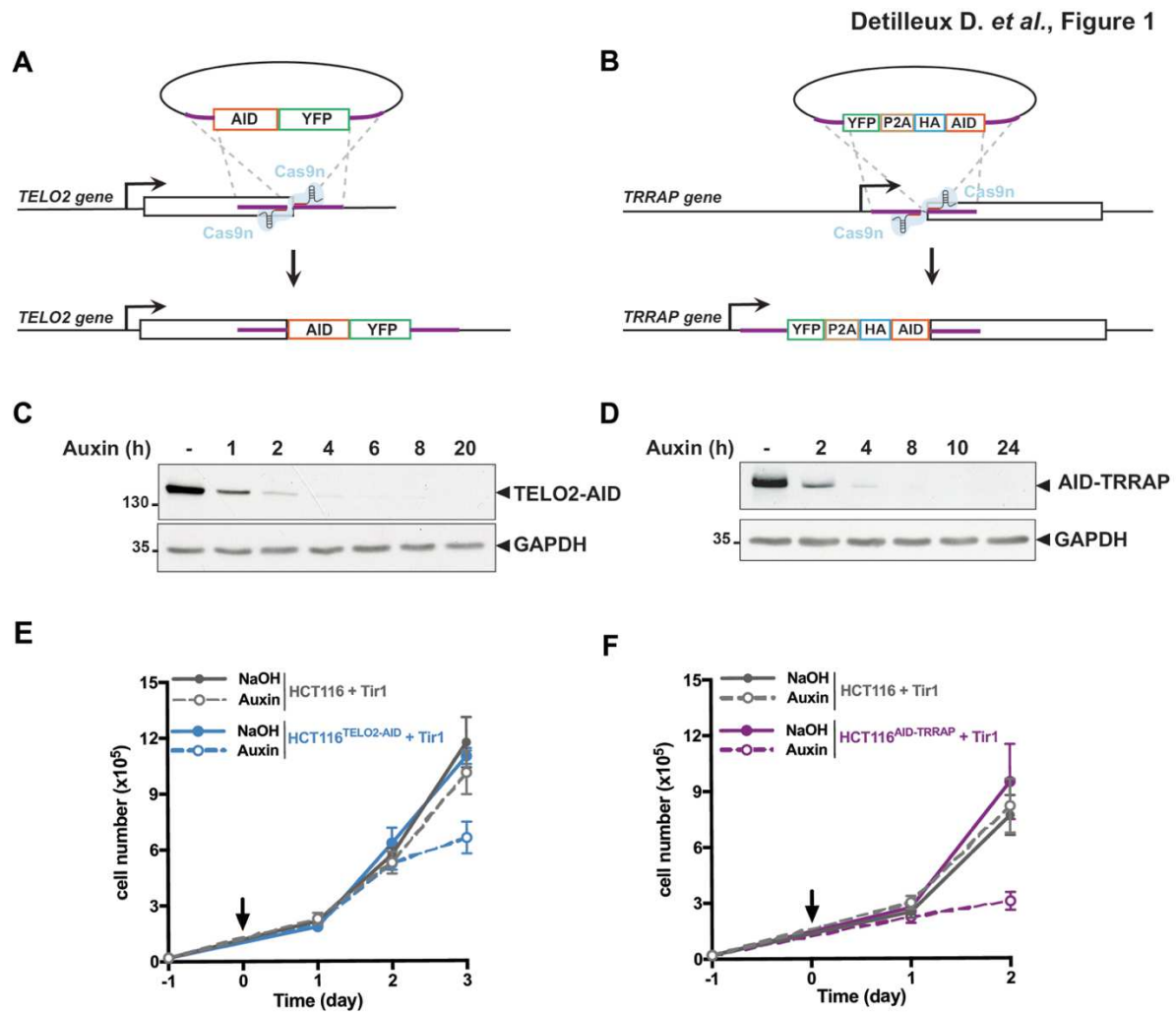
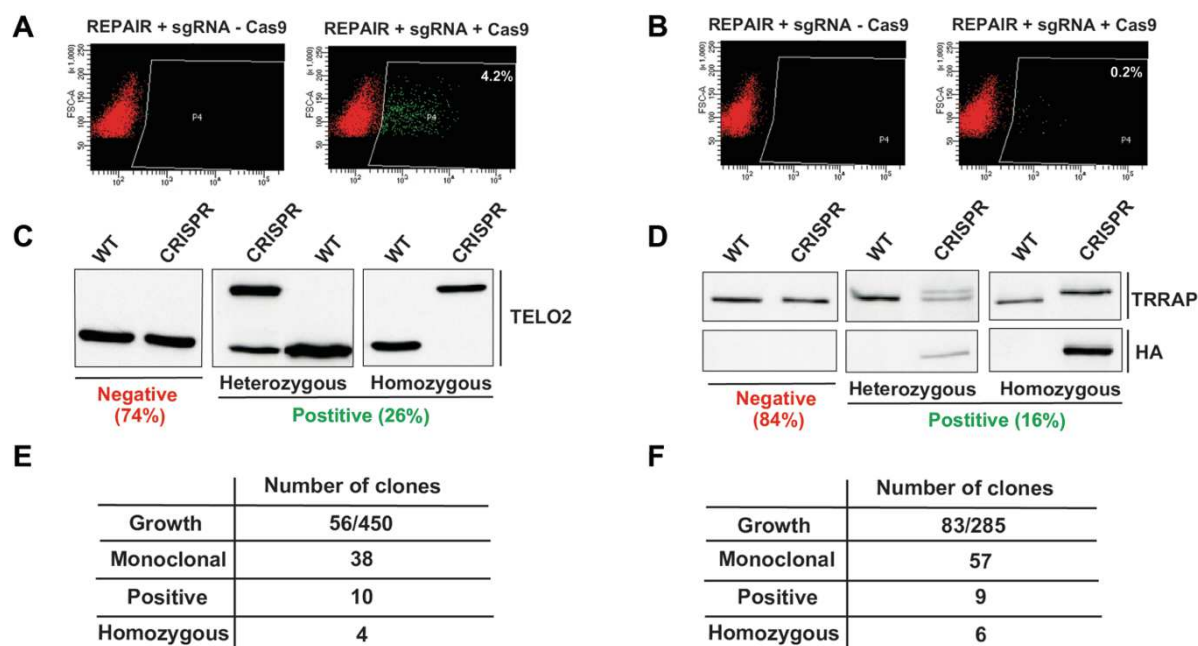
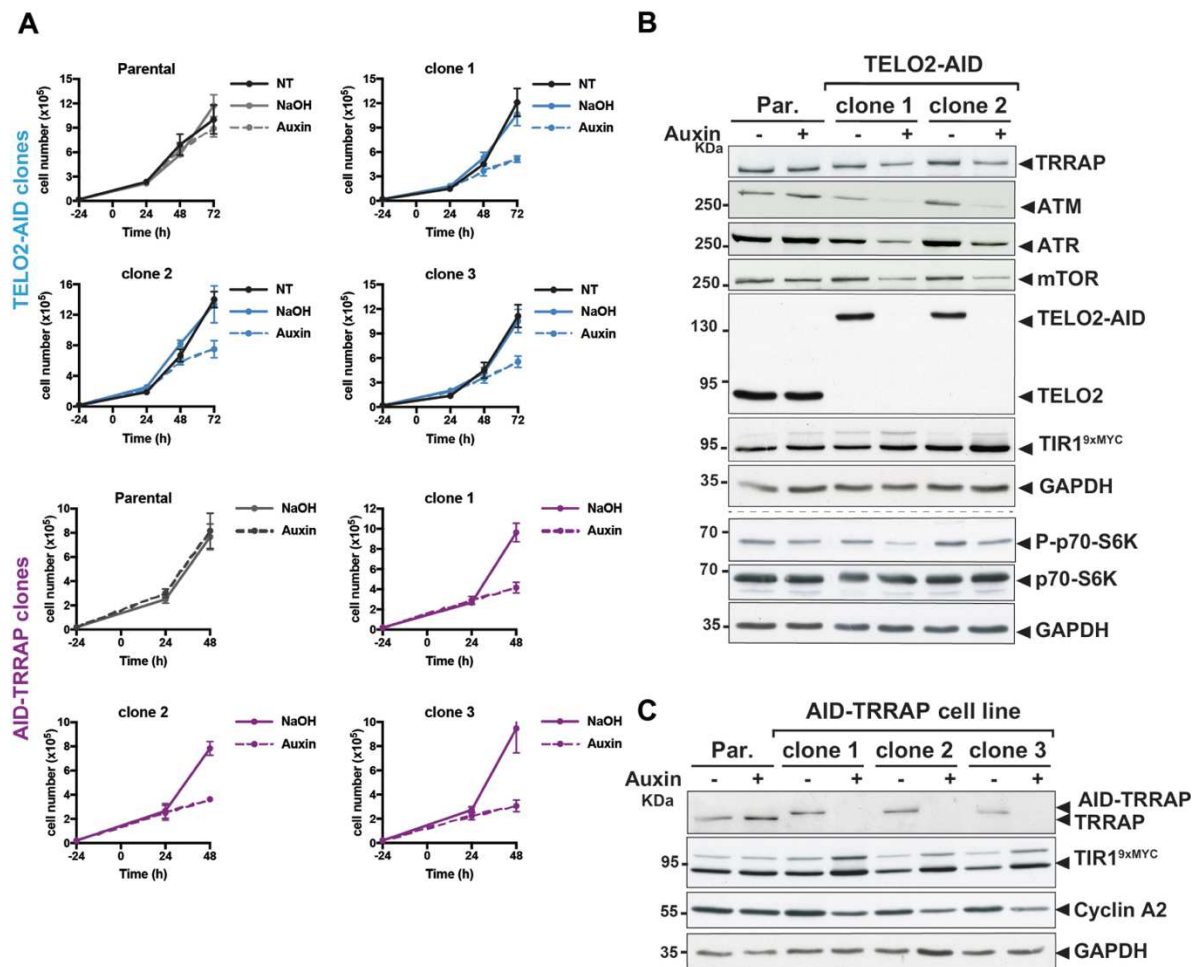


Figure 1: Acute and rapid depletion of TELO2 and TRRAP proteins using an AID system. (A,B) Schematic overview of the CRISPR-Cas9 strategy used to achieve the bi-allelic insertion of an auxin-inducible degron (AID) to the C-terminus of *TELO2* (**A**) or the N-terminus of *TRRAP* (**B**). A cassette comprising the full length AtIAA17 sequence and the YFP ORF, flanked by 800-bp homology arms (purple) was cloned into a donor plasmid that serves as template for homology-directed repair. (**C,D**) Western-blot analyses of protein extracts from TELO2-AID (**C**) or AID-TRRAP (**D**) cells harvested at different time points after auxin addition, as indicated. Blots were probed using an anti-TELO2 antibody (**C**) or an anti-HA antibody (**D**). GAPDH is used as loading control. (**E,F**) Proliferation rate of cells treated with NaOH (full line) or auxin (dashed line) was assessed by trypan blue exclusion assay. Parental (grey) and TELO2-AID (blue) or AID-TRRAP (purple) cell lines were seeded at day -1. Auxin or its vehicle alone were added at day 0 (black arrow) and cell counting was performed at the indicated time points.

Detilleux D. *et al.*, Supplemental Figure 1

Supplemental Figure 1: Overview of the strategy for selecting, screening and amplifying TELO2-AID and AID-TRRAP clones. (A,B) Snapshots of YFP-fluorescent measurements performed two days after transfecting either the donor plasmid (REPAIR) and both sgRNA plasmids alone (left panels) or together with the Cas9 nickase expressing plasmid (right panels). A small percentage of YFP+ cells was detected following TELO2-AID (4.2%) (A) and AID-TRRAP (0.2%) (B) editing. (C,D) Representative Western blots of negative, heterozygous, and homozygous clones. Blots were probed with either an anti-TELO2 antibody (C) or an anti-TRRAP antibody (D). Given the high molecular weight of TRRAP (400kDa), correct fusion of the HA-AID tag to TRRAP was confirmed using an anti-HA antibody. (E,F) Summary of the number of clones that grew following FACS (Growth) from a single cell (Monoclonal), showing a size-shift by Western-blot screening (Positive), including those showing bi-allelic recombination (Homozygous).

Within a few hours of auxin treatment we observed a fast, progressive, and acute degradation of TELO2 and TRRAP (Figure 1C,D). As expected, depletion of either TELO2 or TRRAP severely impaired cell proliferation (Figure 1E,F and Supplemental Figure 2A), consistent with the essential role of each protein in cell proliferation (Herceg et al. 2001; Takai et al. 2007). Furthermore, prolonged TELO2 depletion reduced steady-state protein levels of the TRRAP, ATM, ATR, and mTOR PIKKs (Supplemental Figure 2B) and triggered a decrease in mTORC1 activity, as illustrated with p70-S6K phosphorylation (Supplemental Figure 2B). Similarly, TRRAP conditional depletion was accompanied by a decrease in the levels of Cyclin A2 (Supplemental Figure 2C), which levels are regulated by TRRAP (Herceg 2003; Wurdak et al. 2010; Tapias et al. 2014). Finally, PIKK levels and cell growth of parental HCT116 cells, which express TIR1 alone, were unaffected by auxin treatment, indicating that neither auxin nor its vehicle inhibit cell growth (Figure 1E,F and Supplemental Figure 2A). In conclusion, the power of CRISPR-Cas9-mediated editing allowed the fusion of an AID to TELO2 or TRRAP, for their rapid and acute depletion in HCT116 cells.

Dettelleux D. *et al.*, Supplemental Figure 2

Supplemental Figure 2: Effect of auxin-mediated depletion of TELO2 or TRRAP on proliferation and PIKK stability. **(A)** The proliferation rate of parental cells (grey) and three distinct TELO2-AID clones (blue) or AID-TRRAP clones (purple) was monitored using trypan blue exclusion assay. Cells were plated at day -1. At day 0 (arrow), cells were treated with auxin (dashed line), its vehicle only (NaOH, full line), or untreated (NT, black) and counted daily. **(B)** Immunoblots for the indicated proteins in parental cells (Par.) and two distinct TELO2-AID clones treated for 48 hours with or without auxin. **(C)** Immunoblots for the indicated proteins in parental cells (Par.) and three distinct AID-TRRAP clones treated for 24 hours with or without auxin. **(B,C)** The F-box TIR1 protein is detected using an anti-MYC antibody. GAPDH is used as loading control between samples.

TELO2 promotes the incorporation of TRRAP into the SAGA and TIP60 complexes

We then asked whether TELO2 stabilizes TRRAP directly at chromatin, where TRRAP functions. However, cellular fractionation followed by Western blot analysis revealed that endogenous TELO2 is localized in the cytoplasm and clearly absent from the nucleus (Figure 2A). We observed a similar pattern for the YFP fluorescence signal of TELO2-AID cells using live microscopy (data not shown). As expected, TRRAP is predominantly nuclear (Figure 2A), consistent with its role in transcription and with published immunofluorescence microscopy staining (Wurdak et al. 2010; Wang et al. 2018). Nonetheless, TRRAP was also detectable in the cytoplasmic fraction (Figure 2A). Immunoprecipitation of TRRAP from each compartment showed that TELO2 interacts specifically with the cytoplasmic fraction of TRRAP, but not the nuclear fraction of TRRAP (Figure 2B). Surprisingly, TELO2 depletion primarily affected the steady-state levels of TRRAP from the nuclear fraction, but not from the cytoplasmic fraction (Figure 2A,B). We interpret this discrepancy as suggesting that TELO2 controls TRRAP stability in the cytoplasm, but TRRAP nuclear localization is coupled to its stabilization and incorporation into SAGA and/or TIP60.

We therefore assessed TRRAP incorporation into the SAGA complex upon TELO2 depletion. After 24 hours of auxin treatment, we observed a reduced interaction between TRRAP and SAGA components in nuclear extracts (Figure 2C). Consistent with our observation that TELO2 does not affect cytoplasmic TRRAP levels, TELO2 depletion did not affect TRRAP interaction with SUPT3H in cytoplasmic extracts, although this interaction is weak (Figure 2D). This population of TRRAP still interacting with SAGA may exist due to residual TELO2 activity or TTT-independent folding. Overall, our results indicate that the TELO2 co-chaperone is required for TRRAP stability, nuclear localization, and incorporation into SAGA. These processes are likely tightly coupled, such that non-incorporated TRRAP is rapidly degraded prior to nuclear import.

Interestingly, Western blot analysis showed that the reduced levels of TRRAP in SAGA did not affect the interaction between SUPT3H, the bait, and several other SAGA subunits,

namely SUPT7L, TADA1, TADA3, SGF29, and TAF10 (Figure 2C). This observation suggests that, similar to fission yeast (Helmlinger et al. 2011), TRRAP is not essential for the assembly and scaffolding of the SAGA complex in human cells. Furthermore, TRRAP interacts with SUPT3H and several core SAGA components in the cytoplasm (Figure 2D), which was observed using tandem mass spectrometry analysis of anti-TRRAP immunoprecipitates from HeLa cytoplasmic extracts (László Tora, personal communication).

Altogether, conditional and rapid depletion of the TELO2 co-chaperone allowed us to better characterize its functional role in TRRAP stability and complex assembly. Our results suggest a model in which TTT contributes to the folding and incorporation of TRRAP within the SAGA complex in the cytoplasm, prior to its import, and TRRAP is dispensable for the overall assembly of SAGA.

Dettileux D. et al., Figure 2

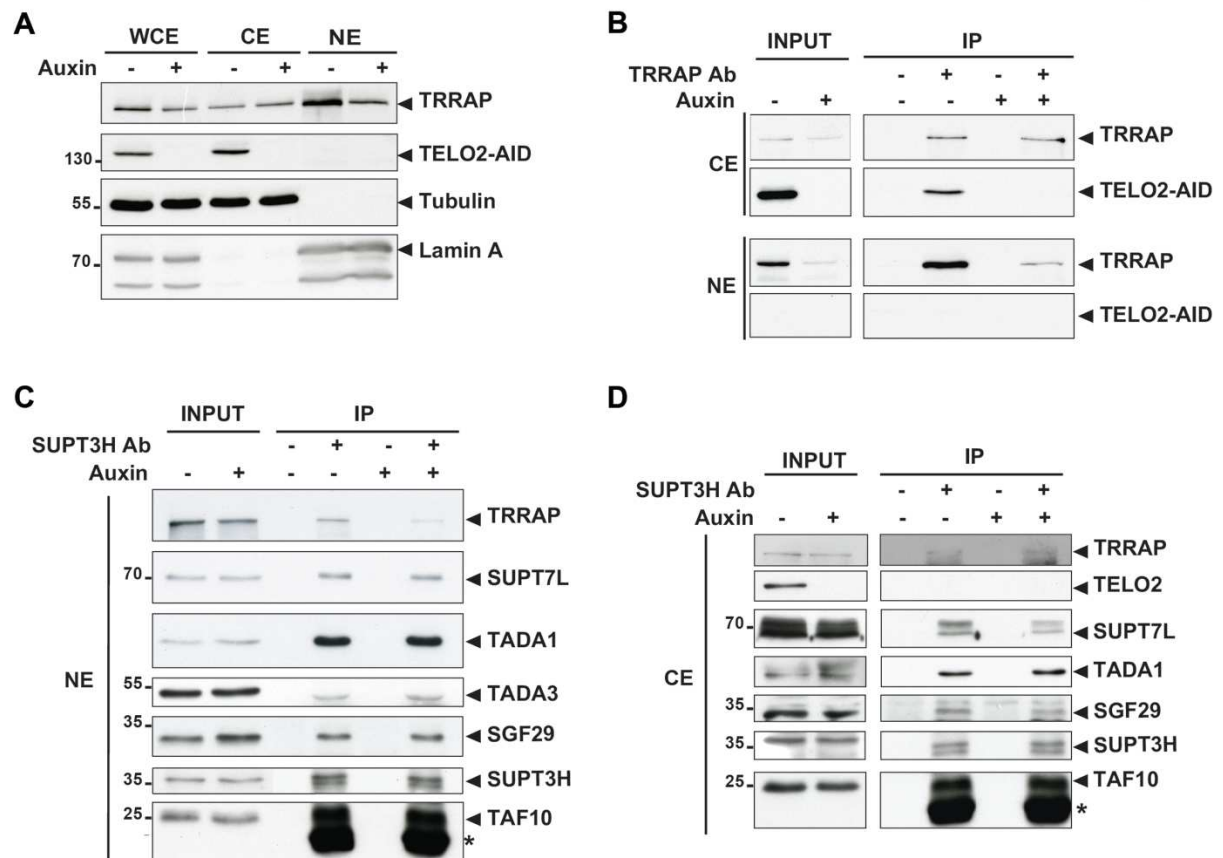


Figure 2: TELO2 promotes TRRAP stabilization, SAGA complex incorporation and nuclear localization. (A) Western blot analysis of total (WCE), cytoplasmic (CE), or nuclear (NE) extracts from TELO2-AID cells treated with NaOH (-) or with auxin (+) for 48 hours. Blots were probed with anti-TRRAP and -TELO2 antibodies. Lamin A and tubulin were used as nuclear and cytoplasmic markers, respectively. (B-D) Immunoprecipitation (IP) of endogenous TRRAP (B) and SUPT3H (C,D) from cytoplasmic and nuclear extracts prepared from TELO2-AID cells treated with NaOH or auxin for either 48h (B) or 24h (C,D). Western blot analysis of the baits and their interaction partners were performed using the relevant antibodies, as indicated. 2% of starting material was loaded (INPUT). Control IPs (Ab -) were performed using beads alone. The star (*) symbol labels antibody light chains.

TELO2 contributes to TRRAP function in gene expression regulation

These results prompted us to determine the contribution of TTT to TRRAP transcriptional activity. We performed RNA sequencing (RNA-seq) analyses in TELO2- or TRRAP-depleted cells to identify genes regulated by both factors. Based on the growth curves of each loss-of-function allele (Figure 1E,F), three distinct TELO2-AID or AID-TRRAP clones were treated with auxin for either 48 or 24 hours, respectively, from which polyA tail-enriched RNAs were extracted and sequenced. Visualization of aligned reads immediately revealed several transcripts which levels changed upon both TELO2 and TRRAP depletion (Supplemental Figure 3A). For example, *MCIDAS*, which is a direct target of TRRAP in multiciliated cells (Wang et al., 2018), is activated by both TELO2 and TRRAP. We then compared the entire transcriptome of TELO2- with TRRAP-depleted cells. Differential expression analyses based on the negative binomial distribution was performed using the DESeq2 package (Love et al. 2014). This analysis revealed a statistically significant positive correlation between the transcriptome of TELO2- and TRRAP-depleted cells (Spearman's $\rho = 0.6723$) (Figure 3A). However, differentially expressed genes were overall more severely affected upon TRRAP depletion than following TELO2 depletion (Figure 3A). Additionally, TRRAP regulates the expression of a higher number of genes than TELO2 (Supplemental Figure 3B). These differences are consistent with TRRAP acting more directly in transcription and with the partial destabilization of TRRAP after 48 hours of TELO2 depletion (Supplemental Figure 2B). Specifically, using a two-fold change threshold and a 1% false discovery rate (FDR) cut-off, we identified 2,227 transcripts which levels are regulated by TRRAP, whereas only 470 transcripts are regulated by TELO2. Importantly, over half of the genes that were differentially expressed upon TELO2 depletion (272/470) were also affected upon TRRAP depletion (Figure 3B). Such substantial overlap supports our conclusion that TELO2 significantly contributes to TRRAP functions.

Dettelleux D. et al., Figure 3

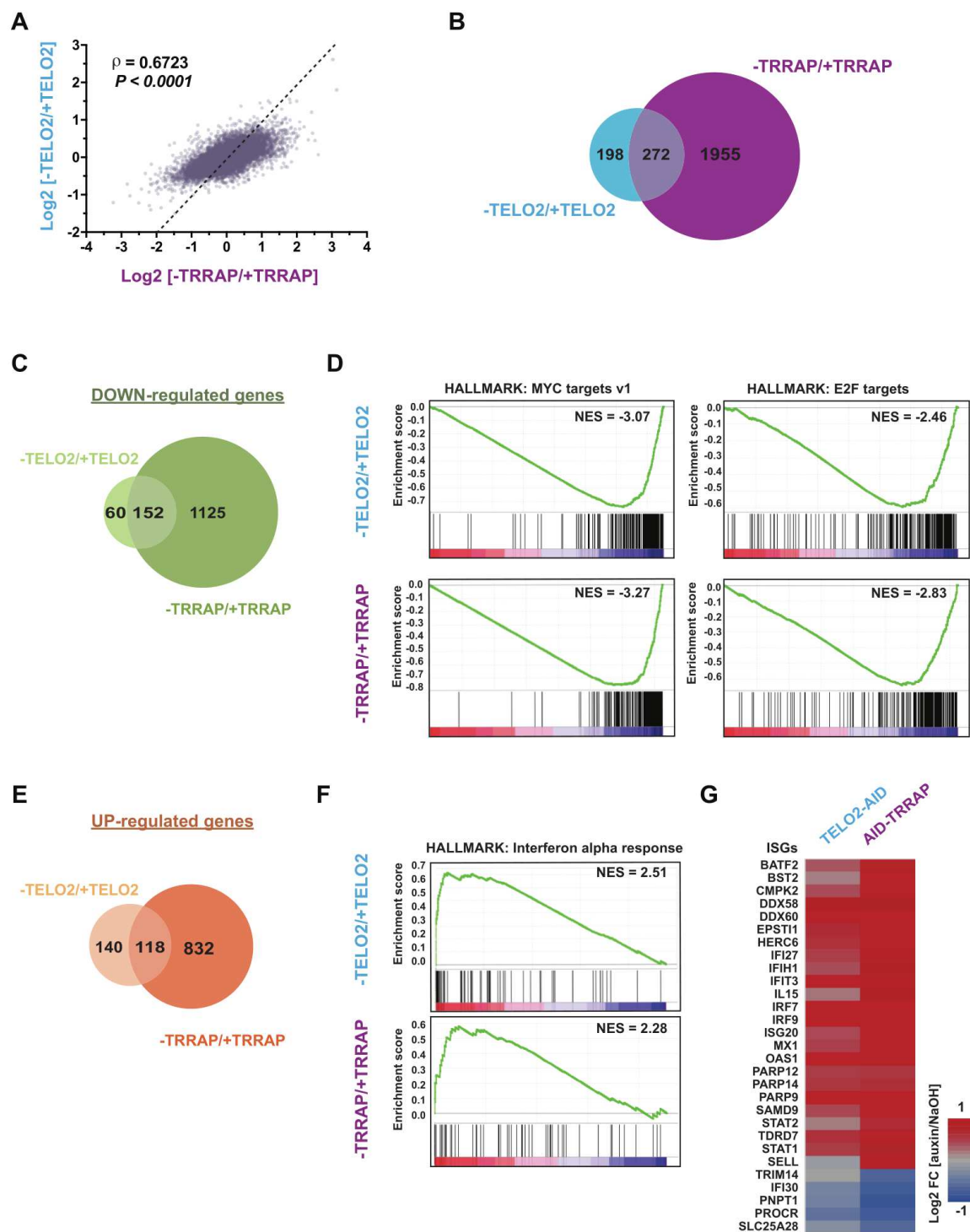


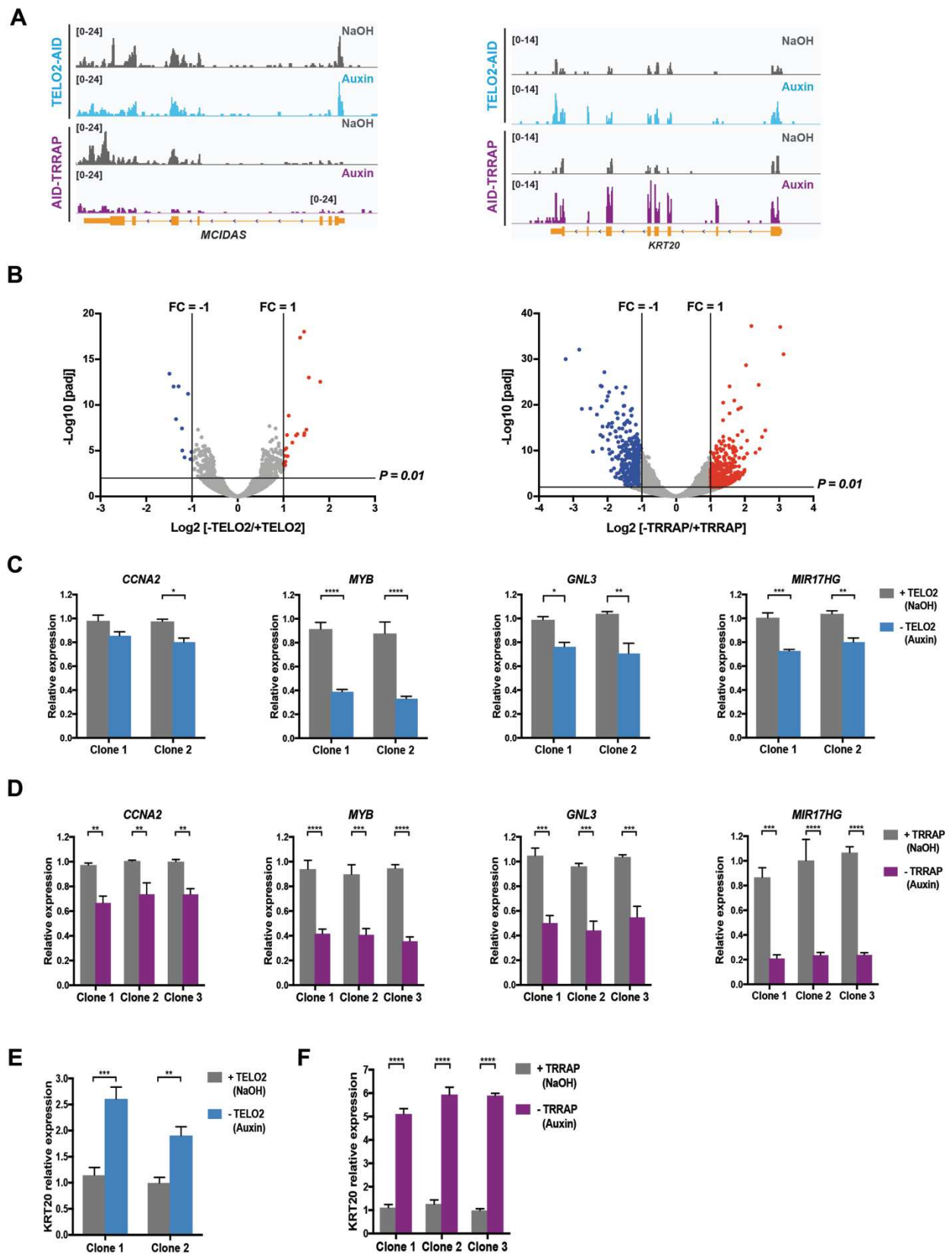
Figure 3: TELO2 contributes to TRRAP function in gene expression regulation. (A)

Scatter plot representing the correlation of transcripts levels between TELO2 and TRRAP-depleted cells. Spearman's correlation ($\rho = 0.6723$) indicates that 67% of the variation observed upon TRRAP depletion explains the variation observed upon TELO2 depletion.

(B,C,E) Venn diagrams showing the overlap between TELO2- and TRRAP-dependent genes (adjusted $P < 0.01$). **(B)** Venn diagram for all differentially expressed genes (470 TELO2-dependent and 2,227 TRRAP-dependent transcripts). **(C)** Venn diagram for down-regulated genes (212 TELO2-dependent and 1,277 TRRAP-dependent transcripts). **(E)** Venn diagram for up-regulated genes (258 TELO2-dependent and 950 TRRAP-dependent transcripts).

(D,F) Gene set enrichment analysis (GSEA) graphs of the most highly enriched hallmarks in either the TELO2- or TRRAP-depleted transcriptomes. A positive normalized enrichment score (NES) indicates enrichment in the set of up-regulated genes, whereas a negative NES indicates enrichment within down-regulated genes. The enrichment profile is represented by a green line and each gene hit is indicated by a vertical black bar under the plot with its fold change color-coded (red = up-regulated, blue = downregulated). **(G)** Heat map of the expression change of ISGs in TELO2 and TRRAP-depleted cells. Log2 fold change between auxin and NaOH treated cells is shown according to a scaled color code as indicated.

Dettelleux D. et al., Supplemental Figure 3



Supplemental Figure 3: TELO2 and TRRAP regulate the expression of a common set of genes. (A) Scaled IGV (Integrative Genomics Viewer) snapshots of two differentially expressed genes, *MCIDAS* (left panel) and *KRT20* (right panel), from RNA-seq performed in

TELO-AID and AID-TRRAP cells after auxin treatment for 48h or 24h, respectively. (B) Volcano plots of mRNA level fold-change (FC) against statistical significance (adjusted P value), for TELO2 (left panel) and TRRAP (right panel) depletion. FC is calculated as the Log2 of the ratio between NaOH- (+TELO2 or +TRRAP) and auxin-treated (-TELO2 or -TRRAP) cells. Thresholds of a 2-fold change and adjusted P value of 0.01 are indicated. Blue dots represent mRNAs whose level decrease at least 2-fold and red dots represent mRNAs whose level increase at least 2-fold. (C-F) RT-qPCR analysis of genes whose levels decrease (C,D) or increase (E,F) in both RNA-seq. mRNA levels were measured in two TELO2-AID clones treated for 48h with NaOH or auxin (C,E) and in three AID-TRRAP clones treated for 24h with NaOH or auxin (D,F). Results were normalized to *PPIB* expression and to one NaOH-treated control sample, set to 1. Each column represents the mean value of at least 3 independent experiments, overlaid with error bars showing the standard error of the mean (SEM). Statistical significance was determined by two-way ANOVA followed by Bonferroni's multiple comparison tests *P ≤ 0.05, ** P ≤ 0.01, *** P ≤ 0.001, **** P ≤ 0.0001.

Although TELO2 and TRRAP both activate and inhibit gene expression, we detected a larger overlap between the TELO2- and TRRAP-dependent transcriptomes for downregulated genes (152/212), than for upregulated genes (118/258) (Figure 3C,E). Reverse transcriptase followed by quantitative PCR (RT-qPCR) analyses confirmed these findings for a few selected genes. For example, TELO2 and TRRAP activates the expression of *CCNA2*, *MYB* and the MYC targets genes *GNL3* and the MiR-17-92a-1 Cluster Host Gene *MIR17HG* (Jaenicke et al. 2016; Li et al. 2014) (Supplemental Figure 3C,D). Conversely, *KRT20* expression is repressed by both TELO2 and TRRAP (Supplemental Figure 3A,E,F).

Finally, we performed a gene set enrichment analysis (Subramanian et al. 2005) to get an overview of the functional categories enriched in TELO2- and TRRAP-dependent genes. Remarkably, the set of genes down-regulated upon TELO2 depletion was enriched for hallmarks defined in the molecular signature database (MSigDB) as either MYC or E2Fs target genes (Figure 3D, upper panels). Identical hallmarks with similar enrichment scores

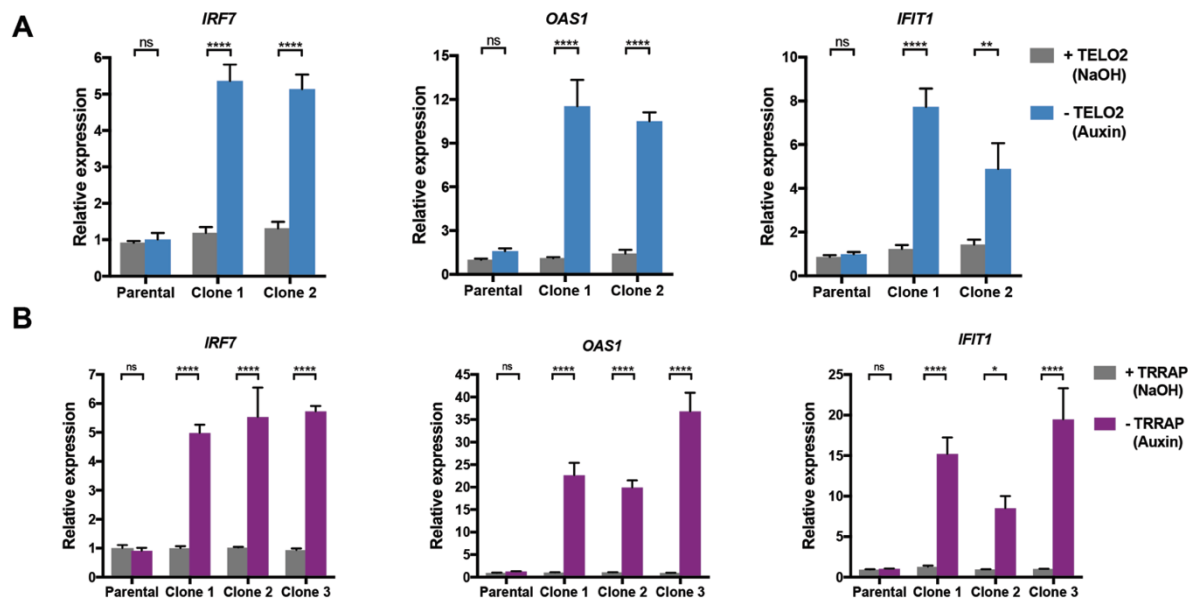
were found in the set of genes down-regulated upon TRRAP depletion, as expected for a co-activator of the c-MYC and E2Fs transcription factors (Figure 3D, lower panels).

Furthermore, a TORC1 signaling hallmark was specifically enriched in the set genes regulated by TELO2 (not shown), consistent with its well-characterized roles in TORC1 stability. In conclusion, TELO2 appears as a novel, important regulator of the c-MYC and E2Fs transcriptional factors, presumably through its role in promoting TRRAP incorporation into the SAGA and TIP60 co-activator complexes.

TELO2 and TRRAP represses interferon-stimulated genes

We noticed a significant enrichment of interferon-stimulated genes (ISGs) in the set of transcripts which levels increase upon depletion of both TELO2 and TRRAP (Figure 3F). Indeed, about one third of the 97 genes constituting this specific hallmark in MSigDB were differentially expressed at least two-fold upon TELO2 depletion (NES = 2.51) or TRRAP depletion (NES = 2.28). Strikingly, TELO2 and TRRAP appear to repress most differentially expressed ISGs (24/29), whereas only a few genes require TELO2 and TRRAP for their activation (5/29) (Figure 3G). To confirm these transcriptomic results, we performed RT-qPCR of selected ISGs, including *IRF7*, which encodes a transcription factor acting as a master regulator in type I interferon (IFN) production and signaling. We also measured the expression of two downstream effectors of this pathway, 2'-5'-Oligoadenylate Synthetase 1 *OAS1* and Interferon Induced Protein With Tetratricopeptide Repeats 1 *IFIT1* (Honda and Taniguchi 2006; Schoggins and Rice 2011). All three genes exhibited an increase in their mRNA expression levels upon depletion of both TELO2 and TRRAP (Supplemental Figure 4A,B). We noted that the de-repression of several ISGs, including *OAS1* and *IFIT1*, was stronger upon TRRAP depletion than upon TELO2 depletion (Figure 3G and Supplemental Figure 4A,B).

Detilleux D. et al., Supplemental Figure 4



Supplemental Figure 4: ISGs are repressed by TELO2 and TRRAP. RT-qPCR analysis of selected ISGs, *IRF7*, *OAS1*, and *IFIT1*, upon depletion of TELO2 (**A**) or TRRAP (**B**). mRNA levels were measured in two TELO2-AID clones treated for 48h with NaOH or auxin (**A**) and in three AID-TRRAP clones treated for 24h with NaOH or auxin (**B**), as well as in parental HCT116 cells (**A,B**). Results were normalized to *PPIB* expression and to one parental replicate treated with NaOH, set to 1. Each column represents the mean value of at least 3 independent experiments, overlaid with error bars showing the standard error of the mean (SEM). Statistical significance was determined by two-way ANOVA followed by Bonferroni's multiple comparison tests * $P \leq 0.05$, ** $P \leq 0.01$, *** $P \leq 0.001$, **** $P \leq 0.0001$, ns: not significant.

TRRAP is best characterized for its positive role on transcription. Our observation that many ISGs appear coordinately induced upon the loss of TRRAP prompted us to explore this phenotype further. We first established that auxin does not trigger a type I IFN response, directly or indirectly. First, treatment of HCT116 TIR1 parental cells with auxin did not induce the expression of *IRF7*, *OAS1*, and *IFIT1* (Supplemental Figure 4A,B). Second, their expression levels did no change upon auxin-mediated protein degradation of an unrelated AID-tagged protein (data not shown). Third, RNAseq and RT-qPCR analyses identified a small, specific set of genes, including two genes, *CYP1A1* and *CYP1B1*, which encode

enzymes involved in drug metabolism and are up-regulated in response to the addition of the plant hormone auxin to HCT116 cells (data not shown). Altogether, these observations suggest that, unexpectedly, TELO2 and TRRAP contribute to the repression of ISGs in unstimulated HCT116 cells.

Genome-wide analysis of TRRAP binding reveal direct regulatory targets.

Our observation that TRRAP regulates many genes both positively and negatively prompted us to determine the binding of TRRAP genome-wide, in order to distinguish direct from indirect regulatory effects. Chromatin immunoprecipitation of TRRAP followed by high-throughput sequencing (ChIP-seq) has been reported previously (Sawan et al. 2013; Wang et al. 2018). However, both studies identified a relatively small number of TRRAP-bound loci: 1,962 peaks in mouse embryonic stem cells (Sawan et al. 2013) and 5,109 peaks in differentiated multiciliated cells (Wang et al. 2018). Furthermore, in the latter study, only about 26% of TRRAP-regulated genes were actually bound by TRRAP, likely in part because TRRAP-containing complexes, which do not bind to DNA directly, are notoriously difficult to capture in ChIP experiments and ChIP has an inherent low signal-to-noise ratio.

In contrast, recent work in yeast successfully used chromatin endogenous cleavage followed by high-throughput sequencing (ChEC-seq) to discover that SAGA is, in fact, recruited to RNA polymerase II promoters genome-wide (Baptista et al. 2017). We therefore implemented ChEC in mammalian cells using a strategy recently developed by the Henikoff lab and named Cleavage Under Targets and Release Using Nuclease (CUT&RUN) (See Appendix for details). Briefly, CUT&RUN consists in directing micrococcal nuclease (MNase) to a protein using a specific antibody, controlling MNase cleavage activity with calcium, and releasing “foot-printed” protein-DNA complexes into the supernatant for paired-end DNA sequencing (Skene and Henikoff 2017). CUT&RUN therefore avoids formaldehyde crosslinking, which can yield misleading results, and generates very little noise because undigested chromatin and genomic DNA are not extracted.

We determined the genome-wide occupancy of TRRAP in HCT116 cells using CUT&RUN experiments followed by high-throughput sequencing (CUT&RUN-seq). For this, we used an HA antibody that recognizes the repeated HA epitopes fused to the N-terminal end of TRRAP (Figure 1B). As controls, we performed a similar anti-HA CUT&RUN-seq after auxin-mediated TRRAP depletion and performed CUT&RUN-seq using control rabbit IgGs. Visualization of aligned reads immediately identified many TRRAP bound loci, with high signal-to noise ratio, as seen for example with the *MIR17HG* locus (Figure 4A). The remarkable specificity and efficiency of this strategy to detect TRRAP binding was then confirmed by qPCR analyses of independent CUT&RUN experiments (Figure 4B). These analyses showed that TRRAP binding at *MIR17HG* is about 60-fold above that observed using control IgGs. Furthermore, TRRAP enrichment is specific because no HA signal was detected after auxin-mediated TRRAP depletion or downstream in the body of the *MIR17HG* gene (Figure 4B). We therefore validated the CUT&RUN technique for profiling the chromatin binding of TRRAP, a component of large chromatin-modifying and -remodeling complexes, in human cells.

Statistical analysis of enriched genomic regions using the MACS2 algorithm (Zhang et al. 2008) identified 15,429 peaks of TRRAP occupancy, which were assigned to 9,220 unique genes. As expected the number of peaks drastically decreased upon auxin-mediated TRRAP depletion, down to 117 peaks (data not shown). Plotting the frequency distribution of the position of each peak relative to the position of the nearest transcription start site (TSS) revealed that TRRAP binds almost exclusively within about 300 base pairs (bp) of the TSS (Figure 4C). This range corresponds to the median size of nucleosome-depleted regions (NDR) in human cells (Scruggs et al. 2015; De Dieuleveult et al. 2016), suggesting that TRRAP is predominantly found at NDRs in human cells, similar to yeast SAGA (Baptista et al. 2017).

Detilleux D. et al., Figure 4

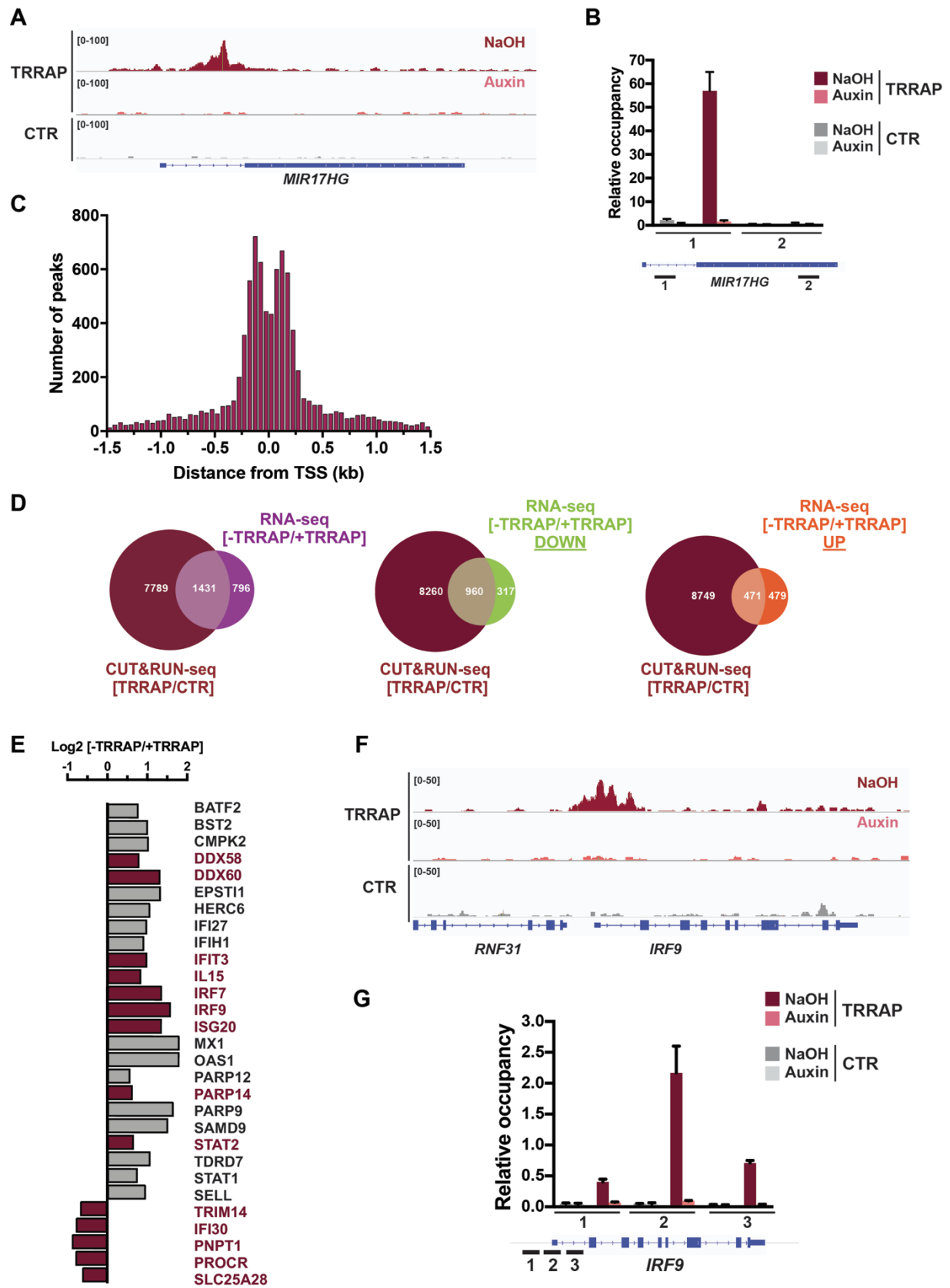


Figure 4: Genome-wide analysis of TRRAP chromatin binding. (A) Scaled IGV snapshot of the CUT&RUN-seq profile of TRRAP occupancy at the *MIR17HG* locus in AID-TRRAP cells treated with NaOH (dark red) or auxin (pink) for 12h. The corresponding control (CTR) CUT&RUN-seq profile is also shown (grey). **(B)** qPCR analysis of TRRAP-footprinted DNA extracted following CUT&RUN performed using either an anti-HA antibody (TRRAP) or control IgG (CTR). CUT&RUN was performed in AID-TRRAP cells treated with NaOH or auxin 24h. qPCR was performed using oligonucleotides that amplified either promoter (amplicon 1) or the gene body (amplicon 2) of *MIR17HG*. Each column represents the mean value of 3 independent experiments, overlaid with error bars showing the standard error of the mean (SEM). **(C)** Frequency distribution histogram representing the number of TRRAP peaks relative to TSS. The distance was calculated by subtracting the coordinate of the peak summit from that of the TSS. **(D)** Venn diagrams showing the overlap between TRRAP-bound genes (9,220 peaks) and all TRRAP-dependent genes (adjusted $P < 0.01$). Left: Venn diagram with all differentially expressed genes (2,227). Middle: Venn diagram with down-regulated genes (1,277). Right: Venn diagram for up-regulated genes (950). **(E)** Overlap between CUT&RUN-seq profile of TRRAP binding and RNA-seq analysis of TRRAP-dependent transcripts for selected ISGs as in **(Figure 3G)**. Each column represents the Log₂ of the ratio between NaOH- (+TRRAP) or auxin-treated cells (-TRRAP) and is colored dark red if TRRAP binding was detected within 1 kb of the corresponding TSS. **(F)** Scaled IGV snapshot of the CUT&RUN-seq profile of TRRAP occupancy at the *IRF9* locus in AID-TRRAP cells treated with NaOH (dark red) or auxin (pink) for 12h. The corresponding control (CTR) CUT&RUN-seq profile is also shown (grey). **(G)** qPCR analysis of TRRAP-bound DNA extracted following CUT&RUN performed using either an anti-HA antibody (TRRAP) or control IgG (CTR). CUT&RUN was performed in AID-TRRAP cells treated with NaOH or auxin 24h. qPCR was performed using oligonucleotides that amplified different regions of the *IRF9* promoter. Each column represents the mean value of 3 independent experiments, overlaid with error bars showing the SEM.

We then analyzed the overlap between TRRAP-bound genes, defined as those having at least one TRRAP peak within ± 1 kb of their TSS, with genes whose expression is regulated by TRRAP (Figure 4D). Remarkably, almost two-third (64%) of TRRAP-regulated genes are directly bound by TRRAP and therefore are strong candidates for being direct transcriptional targets of TRRAP. Importantly, a substantial overlap was observed for both TRRAP-activated and -repressed genes. As expected, the number of genes directly activated by TRRAP is about twice higher the number of genes directly repressed by TRRAP (Figure 4D). Conversely, only 25% of genes are indirectly downregulated upon TRRAP depletion, whereas 51% of genes are indirectly upregulated (Figure 4D). To summarize, combining RNA-seq and CUT&RUN-seq analyses in a conditional depletion allele of TRRAP allowed us to identify about 960 and 471 genes that are directly activated or repressed by TRRAP, respectively, in proliferating colorectal cancer cells.

TRRAP directly represses master regulators of ISG expression

Among the 29 ISGs whose expression levels were significantly affected upon TRRAP depletion (Figure 3G), half of them were directly bound by TRRAP (Figure 4E). We therefore conclude that TRRAP has a direct inhibitory role in the expression of several ISGs in HCT116 cells. Interestingly, we observed that TRRAP binds and contributes to the repression of several genes with pivotal roles in innate immune responses. These include the double-stranded (ds) RNA sensor DDX58 (RIG-I), as well as the IRF7, IRF9, and STAT2 transcription factors (Figure 4E), which mediate the transcriptional induction of downstream effectors of type I IFN signaling (Honda and Taniguchi 2006; Chan and Gack 2016). Notably, TRRAP binds robustly and specifically to the proximal core promoter region of *IRF9*, which we verified using qPCR analysis of independent CUT&RUN experiments (Figure 4F,G).

Western blotting confirmed that TRRAP depletion causes a progressive accumulation of the RIG-I, IRF7, IRF9 proteins, suggesting that a functional innate immune response might be triggered (Figure 5A). RIG-I activation culminates in the TBK1-mediated phosphorylation

and nuclear translocation of the IRF3 and IRF7 transcription factors. Whereas IRF3 is constitutively expressed, IRF7 is strongly activated in the early phase of infection. IRF7 has an essential role in the induction of the genes encoding the interferon- α and - β cytokines, which are then secreted to activate autocrine or paracrine type I IFN signaling (Honda and Taniguchi 2006). The *IRF7* gene is later itself transcriptionally induced by the IFN-stimulated gene factor 3 (ISGF3); a heterotrimer of STAT1, STAT2 and IRF9, to establish a positive feedback regulatory loop in IFN signaling.

TRRAP inhibits ISG expression without activating an innate immune response

Our observation that the conditional loss of TRRAP induces a type I interferon signature raised the possibility that RIG-I, IRF7, or an intermediate signaling component is activated upon TRRAP depletion. Indeed, several studies have recently shown that defects in nuclear processes can induce cytosolic innate immune signaling and type I interferon production, for instance upon the loss of heterochromatin and silencing at endogenous retroviral elements (ERVs) (Roulois et al. 2015; Chiappinelli et al. 2015; Cuellar et al. 2017). We therefore hypothesized that TRRAP might have a yet unidentified role in heterochromatin silencing, as suggested for TIP60 (Rajagopalan et al. 2018). A preliminary RT-qPCR analysis of a few unique ERVs indeed showed that TRRAP depletion induces their expression, although at later time points than ISG induction (data not shown). Alternatively, TRRAP may contribute to the modulation of TBK1 activity by GCN5/PCAF (Jin et al. 2014). Last, induction of a type I IFN signature may result from the direct repression of RIG-I expression by TRRAP.

To test these different possibilities and establish whether ISGs are induced because the dsRNA-sensing pathway is activated upon TRRAP depletion, we performed epistasis analyses between TRRAP and components of the innate immune response. For this, CRISPR-Cas9 was used to generate several different knockout mutants in AID-TRRAP HCT116 cells, because we wanted complete deletion mutants to facilitate the interpretation

of genetic interactions. We targeted key genes in cytosolic pathogen recognition and immune signaling, namely the dsRNA sensors RIG-I and MDA5, the downstream mitochondrial adaptor MAVS, and the TBK1 kinase, which mediates IRF7 activation (Figure 5B).

Western blot analyses confirmed the complete loss of each targeted protein following CRISPR-Cas9-mediated editing of the corresponding gene and clonal selection (Figure 5C). We then measured the expression of a downstream effector of type I IFN signaling, *OAS1*, which is one of the most strongly induced gene upon TRRAP depletion (Supplemental Figure 4B). Here, we depleted TRRAP for a shorter amount of time, 10 hours, because we reasoned that such an innate immune response would be activated early upon TRRAP depletion and that the later positive feedback regulation triggered by IFN signaling would complicate our interpretation of the results. We observed that TRRAP depletion induced *OAS1* expression at similar levels in *RIG-I*, *MDA5*, *MAVS*, and *TBK1* knockout mutants, as compared to control AID-TRRAP cells (Figure 5D). The I κ B kinase- ϵ (IKK ϵ) can be activated by MAVS and function redundantly with TBK1 in certain conditions (Chan and Gack 2016). Pharmacological inhibition of IKK ϵ in TBK1 knockout cells did not affect *OAS1* induction upon TRRAP depletion (Figure 5D), indicating that TRRAP inhibits ISG expression downstream of TBK1/ IKK ϵ . Altogether, these genetic analyses establish that TRRAP is epistatic to the RIG-I/MDA5-MAVS-TBK1 signaling axis in the regulation of ISG expression.

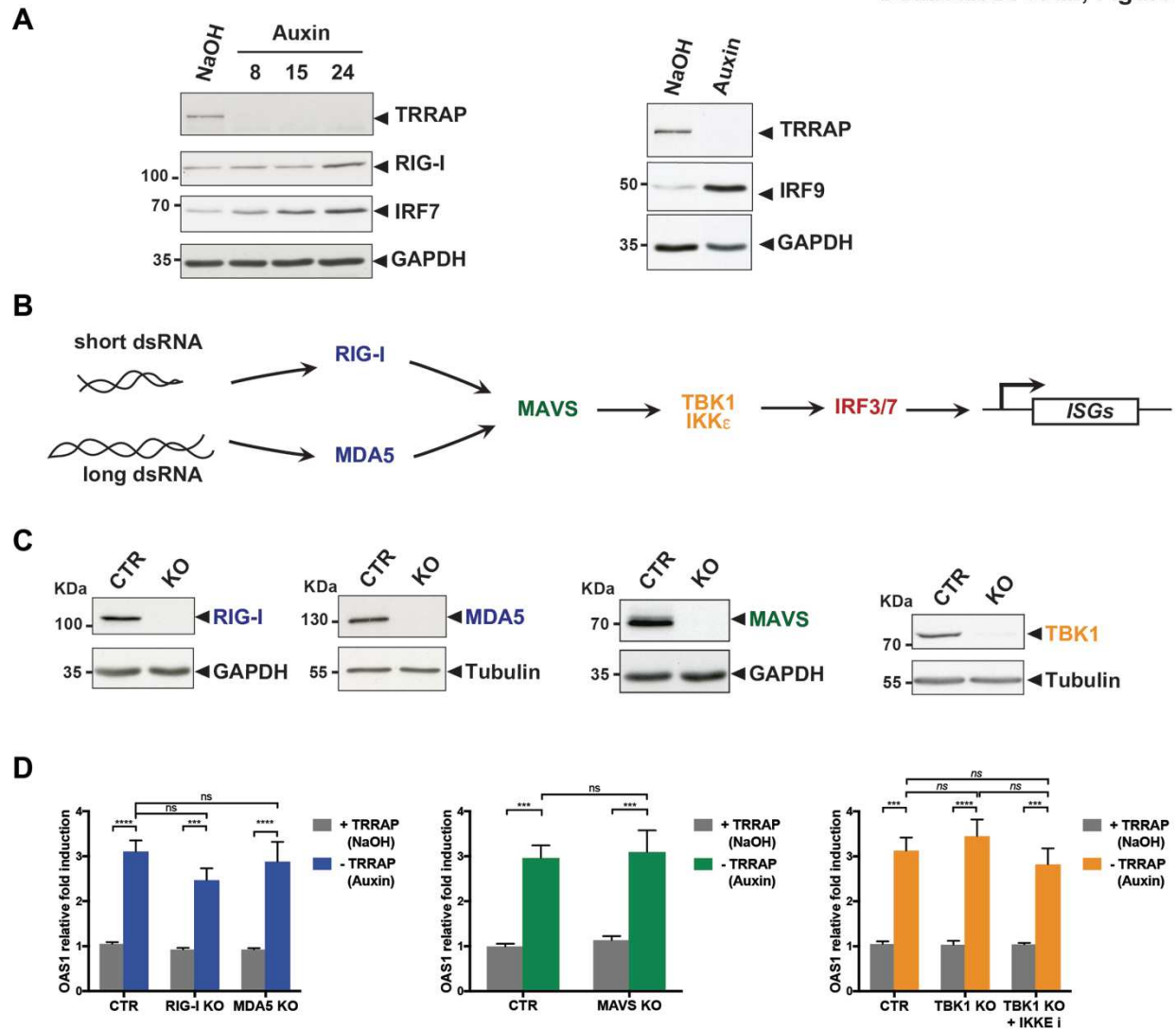


Figure 5: Epistasis analysis between TRRAP and innate immune response factors. (A)

Western blot analyses of TRRAP, RIG-I, IRF7, and IRF9 in protein extracts from AID-TRRAP cells treated with NaOH for 24h or auxin for various time points, as indicated. **(B)** Schematic representation of the activation of the innate immune signaling pathway by dsRNAs. **(C)** Western blot analyses of each targeted protein with the corresponding antibodies. Extracts were prepared from either clonal cell lines (RIG-I, MDA5, MAVS) or a polyclonal population of cells (TBK1) following the transduction of either control sgRNA (CTR) or specific sgRNA (KO). Tubulin and GAPDH were used to control for equal loading across samples. **(D)** RT-qPCR analysis of *OAS1* mRNA levels in AID-TRRAP control (CTR), RIG-I, MDA5, MAVS, TBK1 knockout cells (KO), treated for 10h with NaOH (+TRRAP) or auxin (-TRRAP). In addition, AID-TRRAP TBK1-KO cells were treated with a TBK1/IKK ϵ pharmacological inhibitor, BX795, concomitantly with auxin addition. Results were normalized to *PP1B* expression. To visualize the fold induction of *OAS1* caused by TRRAP depletion in each

knockout cell line, values were normalized to the NaOH condition, set to 1. Each column represents the mean value of at least 5 independent experiments, overlaid with error bars showing the SEM. Statistical significance was determined by two-way ANOVA followed by Tukey's multiple comparison tests *** $P \leq 0.001$, **** $P \leq 0.0001$, ns: not significant.

Our observation that TBK1 does not suppress the TRRAP-dependent derepression of ISG expression is important. First, this result contrasts with the observation that TBK1 knockdown suppresses ISG induction caused by the loss of GCN5/PCAF (Jin et al. 2014), suggesting that TRRAP functions independently of GCN5/PCAF to repress ISG expression. Second, TBK1 is activated by other cytosolic sensors than RIG-I-like receptors, including the dsDNA sensors cGAS and IFI16 and their adapter STING (Chan and Gack 2016), ruling out a possible activation of this response in TRRAP-depleted cells.

Finally, we did not find evidence that the downstream effectors of TBK1, the IRF7 and IRF3 transcription factors, are themselves activated upon TRRAP depletion. First, although we observed a modest, two-fold increase of *IRF3* mRNA levels upon TRRAP depletion, IRF3 protein levels did not accumulate. Furthermore, its phosphorylation on Ser396, which is essential for its activation, did not increase upon TRRAP depletion (data not shown). Second, cell fractionation followed by Western blotting showed that TRRAP depletion did not cause the nuclear translocation of IRF7, a hallmark of its activation, particularly at early time points of auxin treatment (data not shown). We therefore failed to detect an activation of the IRF3 and IRF7 transcription factors upon TRRAP depletion, despite robust ISG induction.

TRRAP dynamically regulates IRF9 expression

RNA-seq and CUT&RUN analyses revealed that two other IFN-responsive transcription factors, STAT2 and IRF9, which form the ISGF3 complex with STAT1, are directly repressed by TRRAP (Figure 3G and Figure 4E-G). Although ISGF3 functions downstream of TBK1 and IRF7 activation, its major transcriptional target is the *IRF7* gene itself, to create a positive feedback loop during IFN signaling (Honda and Taniguchi 2006). We therefore investigated how TRRAP directly represses the expression of *IRF9*. We focused our attention on IRF9, because recent work has revealed that, in HCT116 cells, high expression of IRF9 alone is sufficient to induce many of the ISGs that are up-regulated upon TRRAP depletion (Kolosenko et al. 2015). In addition, another study has shown that unphosphorylated ISGF3 (U-ISGF3) has a basal transcriptional activity that drives the prolonged expression of a specific subset of ISGs (Cheon et al. 2013). Remarkably, most of the U-ISGF3-dependent genes (21/28) are up-regulated at least 1.5-fold upon TRRAP depletion.

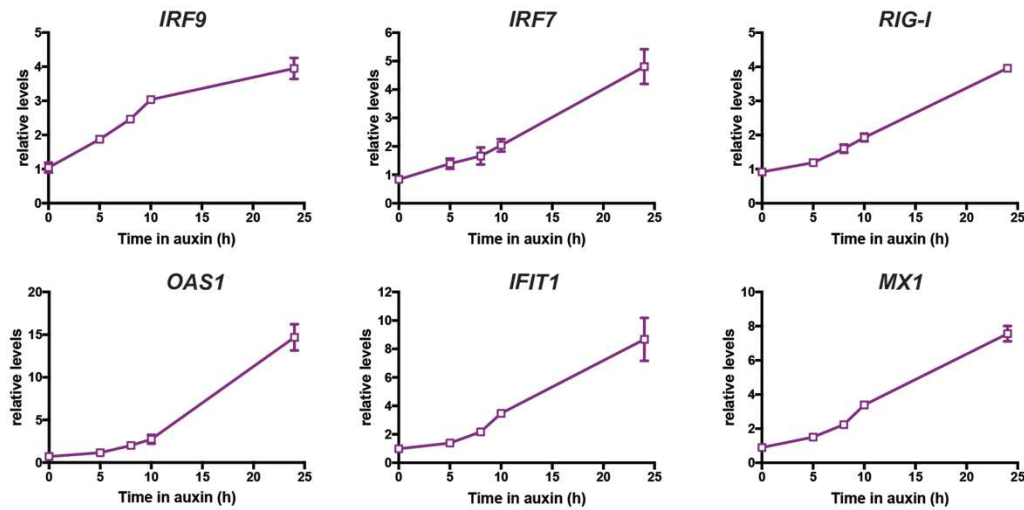
To better characterize the effect of TRRAP on IRF9 and ISG expression and rule out late, indirect effects, we followed their expression upon TRRAP depletion in a time-course experiment. As shown in Figure 6A, *IRF9* mRNA levels increased rapidly and progressively upon TRRAP depletion. Specifically, expression of *IRF9* was about two-fold higher already 5 hours after auxin treatment (Figure 6A), which is concomitant with the loss of a detectable TRRAP signal (Figure 1D). The expression levels of IRF9 target genes, including *IRF7*, *RIG-I*, *OAS1*, *IFIT1*, and *MX1* showed a similar, progressive up-regulation upon TRRAP depletion, although with a slight delay, as compared to *IRF9* (Figure 6A). Altogether, these results provides additional evidence for a direct regulatory role of TRRAP on the expression of ISGs, particularly *IRF9*.

We then assessed the dynamics with which TRRAP modulates *IRF9* expression, taking advantage of the reversibility of the auxin degron system. Indeed, TRRAP re-accumulated within a few hours after washing out auxin from the media (Figure 6B). RT-qPCR analysis of *IRF9* mRNA levels showed that its expression ceased to increase upon auxin removal, in

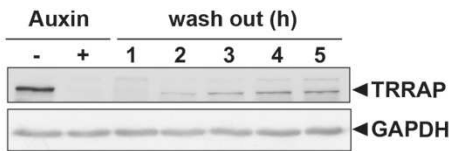
parallel to the recovery of TRRAP. At later time points, *IRF9* mRNA levels progressively decreased back to basal levels (Figure 6C). Similarly, recovering TRRAP quickly stabilized the levels of *IRF7*, *OAS1*, and *IFIT1* mRNAs, while their expression continued to increase if TRRAP depletion is maintained (Figure 6C). In agreement with these observations, CUT&RUN followed by qPCR analysis showed that TRRAP binding at the *IRF9* promoter increased rapidly upon auxin removal (Figure 6D). In conclusion, recovering TRRAP leads to a rapid reversion of the ISG expression phenotype. Altogether, these kinetic analyses indicate that TRRAP and IRF9 levels dynamically anti-correlate in HCT116 cells.

Detilleux D. et al., Figure 6

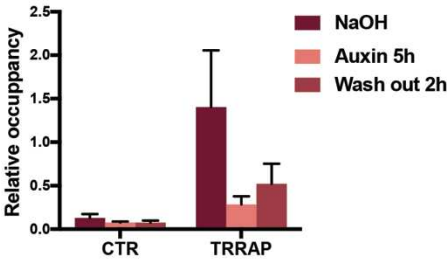
A



B



D



C

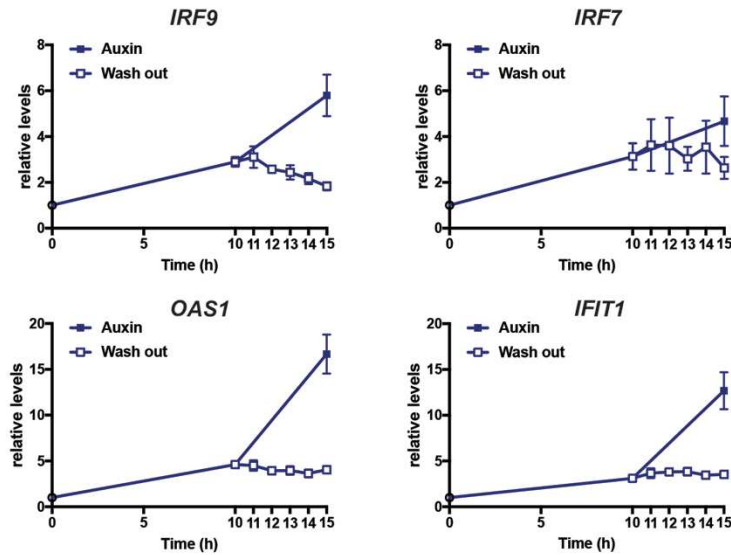


Figure 6: Dynamic anti-correlation between TRRAP levels and IRF9 and ISG

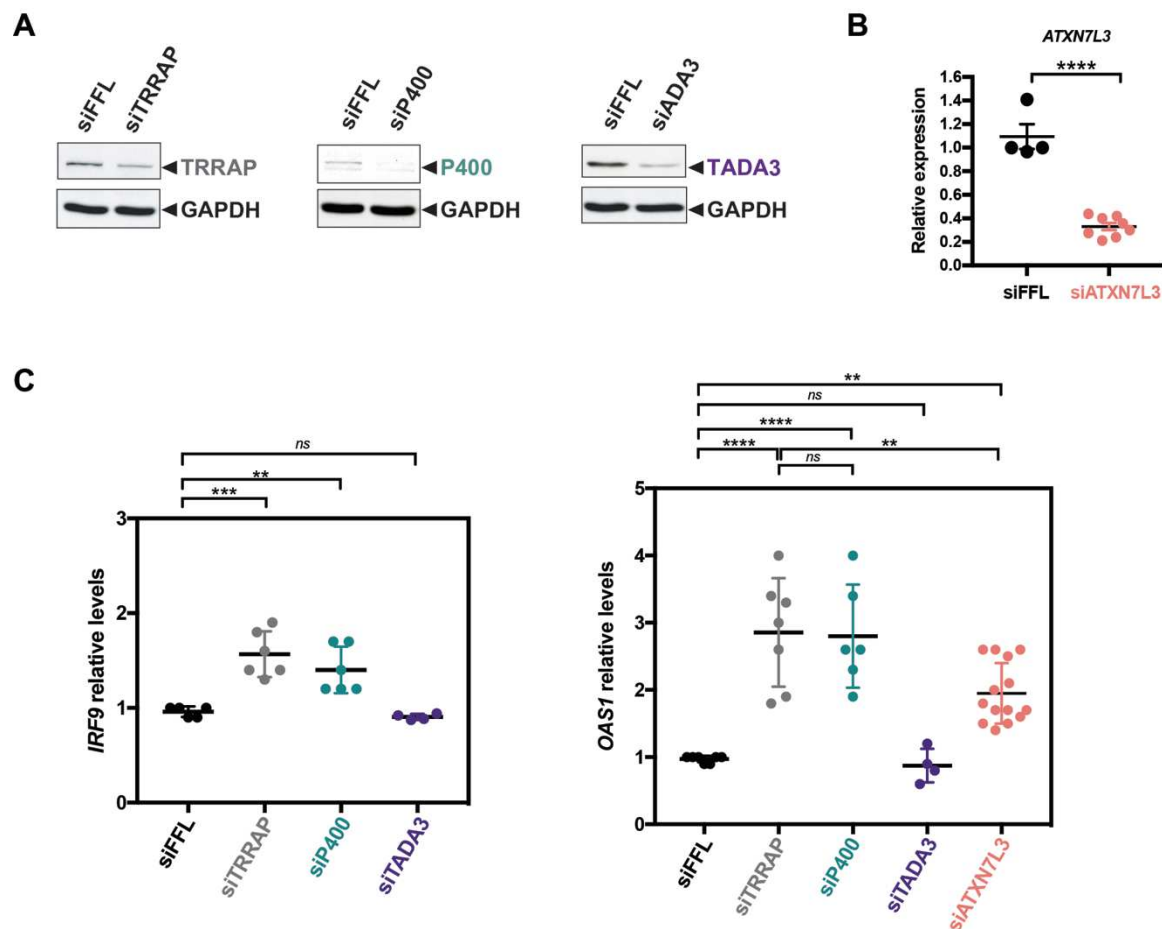
expression. (A) RT-qPCR analysis of *IRF9*, *IRF7*, *RIG-I*, *OAS1*, *IFIT1*, and *MX1* mRNA levels in AID-TRRAP cells over a time course of TRRAP depletion. RNAs were extracted from cells treated with auxin and harvested at various time points, as indicated. **(B)** Western blot analysis of TRRAP protein levels in AID-TRRAP cells, which were first treated with auxin for 12h, then washed out from auxin, and harvested at various time points, as indicated. Blots were probed with an anti-TRRAP antibody and an anti-GAPDH antibody was used to control for equal loading. **(C)** RT-qPCR analysis of *IRF9*, *IRF7*, *OAS1*, and *IFIT1* mRNA levels in AID-TRRAP cells over a time course of either TRRAP depletion (auxin) or recovery (wash out). RNAs were extracted from cells first treated with auxin for 10h, then washed out from auxin, and harvested at various time points, as indicated (open square). As a positive control, cells were also harvested following 15h of auxin treatment. treated with auxin and harvested at various time points, as indicated (closed square). **(A,C)** Expression levels were normalized to *PPIB* levels and to non-auxin treated control samples, set to 1. Each point represents the mean value of 3 clones, overlaid with error bars showing the SEM. **(D)** qPCR analysis of TRRAP-bound DNA extracted following CUT&RUN performed using either an anti-HA antibody (TRRAP) or control IgG (CTR). CUT&RUN was performed in AID-TRRAP cells first treated with auxin for 5h, then washed out from auxin for 2h. qPCR was performed using oligonucleotides that amplified the *IRF9* promoter (amplicon 2, Figure 4G). Each column represents the mean value of 3 clones, overlaid with error bars showing the SEM..

The TIP60 component p400 contributes to the repression of ISGs

TRRAP regulates transcription initiation as part of the SAGA and TIP60 co-activator complexes. To determine whether TRRAP requires SAGA or TIP60 to repress ISGs, we knocked down specific subunits for each complex, targeting distinct histone modifying or remodeling activities (Figure 7A,B). These include P400, an ATPase that catalyzes the deposition of histone H2A.Z as part of the TIP60 complex, TADA3, which is required for SAGA acetyltransferase activity (HAT) on nucleosomal histone H3 and H2B, and ATXN7L3, which is essential for SAGA de-ubiquitination (DUB) of histone H2B (Helmlinger and Tora 2017). As a positive control, we measured ISG expression upon siRNA-mediated knockdown of TRRAP. RT-qPCR analyses revealed that *IRF9* and *OAS1* mRNA levels increase upon P400 knockdown, to similar levels as those observed upon TRRAP knockdown (Figure 7C). We noted a modest increase of *OAS1* mRNA levels upon ATXN7L3 knockdown and no change in *IRF9* and *OAS1* expression upon TADA3 knockdown. Under these experimental conditions, the effect of ATXN7L3 on *OAS1* expression was significantly less strong than the repressive effect of TRRAP and P400 (Figure 7C). Altogether, these analyses indicate that TRRAP might cooperate with P400 to repress the expression of ISGs, whereas the HAT and DUB activities of SAGA have minor roles, if any.

Work is currently in progress to determine how TRRAP and p400 modulate the chromatin architecture of the *IRF9* promoter to inhibit their expression in colorectal cancer cells.

Detilleux D. et al., Figure 7

**Figure 7: Contribution of SAGA and TIP60 regulatory activities to ISG expression. (A)**

Western blot analyses of each targeted protein with the corresponding antibodies. Extracts were prepared from HCT116 cells transiently transfected with the corresponding siRNAs, as indicated. An anti-GAPDH antibody was used to control for equal loading across samples.

(B) RT-qPCR analysis of *ATXN7L3* mRNA levels from cells transiently transfected with an siRNA targeting *ATXN7L3*. **(C)** RT-qPCR analysis of *IRF9* (left) and *OAS1* (right) mRNA levels from cells treated as described in **(A,B)**. Expression levels were normalized to *PPIB* levels and to expression in cells transfected with a control siRNA targeting Firefly Luciferase (FFL), set to 1. Each bar represents the mean value of at least 3 independent experiments, overlaid with individual data points and error bars showing the SEM. Statistical significance was determined by one-way ANOVA followed by Dunnett's multiple comparison tests * $P \leq 0.05$, ** $P \leq 0.01$, *** $P \leq 0.001$, **** $P \leq 0.0001$, ns: non-significant.

MATERIALS & METHODS

Cell culture, reagents and transfection

HCT116 cells (a gift from Dr. Vogelstein, Howard Hughes Medical Institute, Baltimore, MD) were cultured in MCCOYS'5A medium (Sigma) supplemented with 10% (v/v) FBS and 100 U/ml Penicillin/Streptomycin in 5% CO₂ at 37 °C.

For siRNA knockdown, HCT116 cells were plated in 6-well plates 24 h before transfection and transfected with 20nM of siRNA using INTERFERin® (Polyplus Transfections) according to the manufacturer's protocol. Cells were then harvested 48 h after transfection for RNA isolation and protein analysis.

Auxin powder was dissolved in NaOH 1N and used at a final concentration of 0.5mM (SIGMA), BX795 inhibitor (Invivogen) was resuspended in DMSO and used at 1µM.

Generation of CRISPR-Cas9-edited cell lines

Single guide RNAs (sgRNAs) were designed using <http://crispr.mit.edu/>. Then, candidate sgRNAs with the highest scores (indicating fewest potential off-targets) were selected and synthesized. Two complementary oligonucleotides of sgRNAs were annealed, and cloned into the BbsI sites of pUC57 vector. The two different sgRNA plasmids, the pX335-U6-Chimeric_BB-CBh-hSpCas9n(D10A) (#42335) and the donor plasmid containing the AID and YFP cassettes were co-transfected into osTIR1-9Myc expressing HCT116 cells using Eugene6 transfection reagent (Promega). 48h after transfection YFP positive cells were selected and FACS-sorted.

Trypan blue exclusion cell viability assay

Cells were plated at 20,000 cells/well in 1mL in 24-well plate. Cells were counted daily using the Countess™ automated cell counter based on trypan blue exclusion assay (Invitrogen).

Cell fractionation

Separation of cytoplasmic and nuclear fractions was achieved using the Rapid, Efficient and Practical (REAP) protocol (Suzuki et al., 2010). Briefly, medium was removed from cell culture dishes and cells were washed twice using ice-cold PBS. 1 ml of PBS was added to

each 10cm dish, cells were scraped and collected in microcentrifuge tubes. Samples were centrifuged (10 s, 2000 x g) and supernatants were discarded. 1 ml of 0.1% NP40 was added to each pellet with pipetting up and down several times. Small aliquots (150µL) were set aside as whole cell lysates (WCE). The rest of the samples were centrifuged (10 s) and supernatants were transferred to new tubes as the cytoplasmic fractions (150µL) (CE). The pellet portions were re-suspended in 1 ml 0.1% NP40 and centrifuged (10 s, 2000 x g). After discarding the supernatants, the nuclear fractions were obtained (NE). Whole lysates were mixed with 4X Laemmli buffer (ratio 3:1), sonicated on ice at level 2 twice (5 min) and boiled (4 min). Additionally, nuclear fractions were re-suspended in 200 µl of 1X Laemmli buffer, sonicated on ice twice (5 min) and boiled (4 min). Cytoplasmic fractions were mixed with 4X Laemmli buffer (ratio 3:1) and boiled (4 min). For western blot analysis 20µL of WCE and CE fractions and 10µL of NE were loaded.

Cell lysis and Western blots

Cells from 6-well plate, were harvested by trypsinization and lysed in RIPA buffer (20 mM Tris, pH 7.5, 150 mM NaCl, 1% Nonidet-P40, 0.5% sodium deoxycholate, protease inhibitors (cOmplete EDTA-free cocktails tablets, Roche). Cell lysates were subjected to 6% or 10% SDS-PAGE and 40µg of protein was loaded per track. The gels were transferred for 2 h onto Nitrocellulose membranes (GE Healthcare Biosciences, Pittsburgh, PA). Detection was performed by diluting primary antibodies in TBS, 0.1% Tween and 5% BSA or non-fat dry milk. After incubation and washing the secondary anti-mouse IgG or anti-rabbit IgG antibodies conjugated to horse-radish-peroxidase (Santa Cruz) were added at a dilution of 1:5,000 in TBS, 0.1% Tween, 5% non-fat drymilk. Detection was performed using Pierce™ ECL western blotting Substrate (ThermoFisher scientific).

RT-qPCR analysis

Total RNA was isolated from HCT116 cells using the TRIzol reagent (Invitrogen) according to the manufacturer's instructions, followed by a DNase digestion step using the TURBO DNA-free™ kit (Ambion). Total RNA (1 µg) was reverse-transcribed using the SuperScript III reverse transcriptase (Invitrogen, Life Technologies). Real-time quantitative PCR (qPCR) was performed using LightCycler® 480 SYBR Green Master Mix and amplified on the LightCycler® 480 instrument (Roche). Relative levels of gene expression were analyzed using the $2\Delta\Delta C_t$ method and compared to the expression of the human housekeeping gene

PPIB. The cycling conditions comprised an initial denaturation phase at 95°C for 5 min, followed by 50 cycles at 95°C for 10 s, 60°C for 30 s and 72°C for 15 s.

Preparation of RNA for RNA-seq

Total RNA was extracted using the TRIzol reagent (Invitrogen) according to the manufacturer's instructions, followed by a DNase digestion step using the TURBO DNA-free™ kit (Ambion). RNA integrity was checked with an Agilent Bioanalyzer 2100 (Agilent Technologies). High-throughput sequencing of RNA libraries was performed following the standard protocol from Fasteris (www.fasteris.com). All sequencing runs were performed on an Illumina HiSeq 2500.

CUT&RUN, CUT&RUN-qPCR

CUT&RUN experiments were performed as described (Skene et al., 2018) and protocol used is detailed in Appendix 1). Briefly, cells were grown up to 80% confluence. Fresh cell cultures were harvested and cells were counted. 250.000 cells per sample were used. Cells were washed and incubated 10' at RT with 10µL of concanavalin A-coated beads. Cells bound to beads were permeabilized and incubated with the appropriate antibody overnight at 4°C. Protein A-MNase at a final concentration of 700ng/mL was mixed and incubated with cells at 4°C for 1h on a tube rotator. pA-MN was activated with 2µL of 100mM CaCl₂, and digestion was performed 30' at 0°C. The reaction was stopped with 100µL of stop buffer containing 2pg/mL of heterologous spike-in DNA. Release of the fragments was achieved at 37°C during 15'. DNA was extracted following option A (fast DNA extraction by spin column) and eluted in 30µL of NE buffer. Extracted DNA was either used for quantitative PCR (qPCR) analysis using a Roche LightCycler 480 with Sybr green master mix, or sequenced.

Statistics

Statistical tests were performed using GraphPad Prism. t-Tests were used when comparing two means. One-way or two-way analyses of variance (ANOVA) were performed for comparing more than two means, across one (for example "genotype") or two distinct variables (for example "genotype" and "treatment"). ANOVAs were followed by Bonferroni or Tukey post hoc pairwise comparisons. Comparisons that are statistically significant ($P \leq 0.05$) are marked with star signs (*), whereas those that are statistically not significant ($P > 0.05$) are labeled n.s.

APPENDIX 1: CUT&RUN protocol

Beads preparation

- Gently resuspend 10 μ L (per sample) of Concanavalin A-coated bead slurry into 1.5 ml Binding buffer in a 2 ml tube.
- Place the tube on a magnet stand to clear (30 s to 2 min). Withdraw the liquid, and remove from the magnet stand.
- Add 1.5 ml Binding buffer, mix by inversion, remove liquid from the cap and side with a quick pulse on a microcentrifuge.
- Resuspend in a volume of Binding buffer equal to the volume of bead slurry (10 μ L per final sample).

Binding cells to beads

- Harvest fresh culture(s) of HCT116 cells (non-treated, treated with NaOH or auxin) at room temperature and count them. Used 250,000 cells per sample.
- Centrifuge 3 min 600 x g at room temperature and withdraw liquid.
- Resuspend in 1.5 ml room temperature Wash buffer by gently pipetting and transfer in a 2 ml tube. (wash 1/2)
- Centrifuge 3 min 600 x g at room temperature and withdraw liquid.
- Again, resuspend in 1.5 ml room temperature Wash buffer by gently pipetting. Centrifuge 3 min 600 x g at room temperature and withdraw liquid. (wash 2/2)
- Resuspend in 1 ml room temperature Wash buffer by gently pipetting.
- While gently vortexing the cells at room temperature, add the bead slurry.
- Rotate 10 min at room temperature.
- Divide into aliquots in 1.5-ml tubes, one for each antibody to be used.
- Place on the magnet stand to clear and pull off the liquid.

Binding primary antibody

- Add antibody to a final concentration of 1:100 in 300 μ L of the Antibody buffer (per sample). Use an anti-rabbit IgG antibody as negative control.
- Place each tube at a low angle on the vortex mixer set to low (~1100 rpm) and squirt the 300 μ L of the Antibody buffer (per sample) along the side. Tap to dislodge the remaining beads.
- Place on the tube rotator overnight at 4°C.

- Remove liquid from the cap and side with a quick pulse on a micro-centrifuge.
- Place on the magnet stand to clear (~30 s) and pull off all of the liquid.
- Add 1 ml Dig-wash buffer, mix by inversion and remove liquid from the cap and side with a quick pulse on a micro-centrifuge.

Binding secondary antibody (not required in our experiments)

The binding efficiency of Protein A to the primary antibody depends on host species and IgG isotype. A secondary antibody such as rabbit α -mouse is recommended if mouse and goat IgG are used. In contrast rabbit and guinea pig IgG are well bound by Protein A, and thus do not require a secondary antibody.

Bind Protein A-MNase fusion protein

- Place each tube at a low angle on the vortex mixer set to low (~1100 rpm) and squirt 100 μ L of the Dig-wash buffer.
- Mix in the pA-MNase to a final concentration of ~700 ng/ml (e.g. 5 μ L/100 μ L of a 1:10 dilution of the 140 μ g/ml glycerol stock kindly provided by the Henikoff lab).
- Place on the tube rotator at 4 °C for ~1h.
- Remove liquid from the cap and side with a quick pulse on a micro-centrifuge.
- Place on the magnet stand to clear and pull off all of the liquid.
- Add 1 ml Dig-wash buffer, mix by inversion.
- Repeat wash steps.

Targeted digestion

- Place on the magnet stand to clear and pull off all of the liquid.
- Place each tube at a low angle on the vortex mixer set to low (~1100 rpm) and add 100 μ L of the Dig-wash buffer along the side while gently vortexing to allow the solution to dislodge most or all of the beads. Tap to dislodge the remaining beads.
- Insert tubes into the 1.5 ml wells of a heater block sitting in wet ice to chill down to 0 °C.
- Remove each tube from the block, mix in 2 μ L of 100mM CaCl_2 (diluted 1:10 from a 1M stock) with gentle vortexing and immediately replace the tube in the 0 °C block.
- Incubate at 0 °C for the 30 min.
- Add 100 μ L of 2XSTOP containing 2pg/mL of heterologous spike-in DNA, and mix by gentle vortexing.

Target chromatin release

- Incubate 15 min at 37 °C to release CUT&RUN fragments from the insoluble nuclear chromatin.
- Centrifuge 5 min at 4 °C and 16,000 x g and place on magnet stand.

DNA extraction

- Place a spin column into a collection tube and add 400µL Buffer NT1 (from NucleoSpin kit).
- Decant the supernatant cleanly from the pellet and transfer (~ 170µL) to the NT1 in the spin column pipetting gently up and down to mix.
- Centrifuge 30 s at 11,000 x g. Discard flow-through.
- Add 700µL Buffer NT3. Centrifuge 30 s at 11,000 x g. Discard flow-through.
- Add 700µL Buffer NT3. Centrifuge 30 s at 11,000 x g. Discard flow-through and replace in rotor.
- Centrifuge for 1 min at 11,000 x g. Let dry 5 min.
- Place in a fresh tube and add 30µL Buffer NE to membrane.
- After 1 min, centrifuge for 1 min at 11,000 x g.
- Decant the supernatant cleanly from the pellet and transfer to a fresh 1.5-ml microcentrifuge tube.

Extracted DNA fragments were either used for quantitative PCR (qPCR) analysis using a Roche LightCycler 480 with SYBR green master mix, or sequenced.

Library preparation and sequencing

- Prepare barcoded libraries for Illumina sequencing with KAPA Single-Indexed Adapters set A&B and the Hyper Prep kit (KAPA Biosystems) following the manufacturer's instructions.
- Amplify for 12 cycles, preferably with a 10 s 60°C combined annealing/extension step.
- Quantify library yield and determine the size distribution of libraries by Bioanalyzer.

REFERENCES

- Ahmed S, Alpi a, Hengartner MO, Gartner a. 2001. C. elegans RAD-5/CLK-2 defines a new DNA damage checkpoint protein. *Curr Biol* **11**: 1934–1944.
- Allard S, Utley RT, Savard J, Clarke A, Grant P, Brandl CJ, Pillus L, Workman JL, Côté J. 1999. NuA4, an essential transcription adaptor/histone H4 acetyltransferase complex containing Esa1p and the ATM-related cofactor Tra1p. *EMBO J* **18**: 5108–5119.
- Anderson CM, Korkin D, Smith DL, Makovets S, Seidel JJ, Sali A, Blackburn EH. 2008. Tel2 mediates activation and localization of ATM/Tel1 kinase to a double-strand break. *Genes Dev* **22**: 854–859.
- Baptista T, Grünberg S, Minoungou N, Koster MJE, Timmers HTM, Hahn S, Devys D, Tora L. 2017. SAGA Is a General Cofactor for RNA Polymerase II Transcription. *Mol Cell* **130**–143.
- Bhaumik SR, Raha T, Aiello DP, Green MR. 2004. In vivo target of a transcriptional activator revealed by fluorescence resonance energy transfer. *Genes Dev* **18**: 333–343.
- Brown CE, Howe L, Sousa K, Alley SC, Carrozza MJ, Tan S, Workman JL. 2001. Recruitment of HAT complexes by direct activator interactions with the ATM-related Tra1 subunit. *Science* **292**: 2333–2337.
- Brown MC, Gromeier M. 2017. MNK Controls mTORC1:Substrate Association through Regulation of TELO2 Binding with mTORC1. *Cell Rep* **18**: 1444–1457.
- Chan YK, Gack MU. 2016. Viral evasion of intracellular DNA and RNA sensing. *Nat Rev Microbiol* **14**: 360–373.
- Cheon H, Holvey-Bates EG, Schoggins JW, Forster S, Hertzog P, Imanaka N, Rice CM, Jackson MW, Junk DJ, Stark GR. 2013. IFN β -dependent increases in STAT1, STAT2, and IRF9 mediate resistance to viruses and DNA damage. *EMBO J* **32**: 2751–2763.
- Chiappinelli KB, Strissel PL, Desrichard A, Li H, Henke C, Akman B, Hein A, Rote NS, Cope

- LM, Snyder A, et al. 2015. Inhibiting DNA Methylation Causes an Interferon Response in Cancer via dsRNA Including Endogenous Retroviruses. *Cell* **162**: 974–986.
- Cuellar L, Herzner AM, Zhang X, Goyal Y, Watanabe C, Friedman BA, Janakiraman V, Durinck S, Stinson J, Amott D, et al. 2017. Silencing of retrotransposons by SET DB1 inhibits the interferon response in acute myeloid leukemia. *J Cell Biol* **216**: 3535–3549.
- David-Morrison G, Xu Z, Rui Y-N, Chang W-L, Jaiswal M, Yamamoto S, Xiong B, Zhang K, Sandoval H, Duraine L, et al. 2016. WAC Regulates mTOR Activity by Acting as an Adaptor for the TTT and Pontin/Reptin Complexes. *Dev Cell* **36**: 139–151.
- De Dieuleveult M, Yen K, Hmitou I, Depaux A, Boussouar F, Dargham DB, Jounier S, Humbertclaude H, Ribierre F, Baulard C, et al. 2016. Genome-wide nucleosome specificity and function of chromatin remodellers in ES cells. *Nature* **530**: 113–116.
- Fishburn J, Mohibullah N, Hahn S. 2005. Function of a eukaryotic transcription activator during the transcription cycle. *Mol Cell* **18**: 369–378.
- Grant PA, Schieltz D, Pray-Grant MG, Yates JR, Workman JL. 1998. The ATM-related cofactor Tra1 is a component of the purified SAGA complex. *Mol Cell* **2**: 863–867.
- Hayashi T, Hatanaka M, Nagao K, Nakaseko Y, Kanoh J, Kokubu A, Ebe M, Yanagida M. 2007. Rapamycin sensitivity of the *Schizosaccharomyces pombe* tor2 mutant and organization of two highly phosphorylated TOR complexes by specific and common subunits. *Genes to cells* **12**: 1357–1370.
- Helmlinger D, Marguerat S, Villén J, Swaney DL, Gygi SP, Bähler J, Winston F, Villen J, Swaney DL, Gygi SP, et al. 2011. Tra1 has specific regulatory roles, rather than global functions, within the SAGA co-activator complex. *EMBO J* **30**: 2843–2852.
- Helmlinger D, Tora L. 2017. Sharing the SAGA. *Trends Biochem Sci* **xx**: 1–12.
- Herbig E, Warfield L, Fish L, Fishburn J, Knutson BA, Moorefield B, Pacheco D, Hahn S. 2010. Mechanism of Mediator recruitment by tandem Gcn4 activation domains and three Gal11 activator-binding domains. *Mol Cell Biol* **30**: 2376–2390.

- Herceg Z. 2003. Genome-wide analysis of gene expression regulated by the HAT cofactor Trrap in conditional knockout cells. *Nucleic Acids Res* **31**.
- Herceg Z, Hulla W, Gell D, Cuenin C, Leonart M, Jackson S, Wang ZQ. 2001. Disruption of Trrap causes early embryonic lethality and defects in cell cycle progression. *Nat Genet* **29**: 206–211.
- Hoke SM, Irina Mutiu A, Genereaux J, Kvas S, Buck M, Yu M, Gloor GB, Brandl CJ. 2010. Mutational analysis of the C-terminal FATC domain of *Saccharomyces cerevisiae* Tra1. *Curr Genet* **56**: 447–465.
- Honda K, Taniguchi T. 2006. IRFs: master regulators of signalling by Toll-like receptors and cytosolic pattern-recognition receptors. *Nat Rev Immunol* **6**: 644–658.
- Hořejší Z, Stach L, Flower TG, Joshi D, Flynn H, Skehel JM, O'Reilly NJ, Ogradowicz RW, Smerdon SJ, Boulton SJ. 2014. Phosphorylation-dependent PIH1D1 interactions define substrate specificity of the R2TP cochaperone complex. *Cell Rep* **7**: 19–26.
- Hořejší Z, Takai H, Adelman CA, Collis SJ, Flynn H, Maslen S, Skehel JM, de Lange T, Boulton SJ, Horejsi Z, et al. 2010. CK2 phospho-dependent binding of R2TP complex to TEL2 is essential for mTOR and SMG1 stability. *Mol Cell* **39**: 839–850.
- Hurov KE, Cotta-Ramusino C, Elledge SJ. 2010. A genetic screen identifies the Triple T complex required for DNA damage signaling and ATM and ATR stability. *Genes Dev* **24**: 1939–1950.
- Ikura T, Ogryzko V V., Grigoriev M, Groisman R, Wang J, Horikoshi M, Scully R, Qin J, Nakatani Y. 2000. Involvement of the TIP60 histone acetylase complex in DNA repair and apoptosis. *Cell* **102**: 463–473.
- Imseng S, Aylett CH, Maier T. 2018. Architecture and activation of phosphatidylinositol 3-kinase related kinases. *Curr Opin Struct Biol* **49**: 177–189.
- Izumi N, Yamashita A, Hirano H, Ohno S. 2012. Heat shock protein 90 regulates phosphatidylinositol 3-kinase-related protein kinase family proteins together with the

- RUVBL1/2 and Tel2-containing co-factor complex. *Cancer Sci* **103**: 50–57.
- Izumi N, Yamashita A, Iwamatsu A, Kurata R, Nakamura H, Saari B, Hirano H, Anderson P, Ohno S. 2010. AAA+ proteins RUVBL1 and RUVBL2 coordinate PIKK activity and function in nonsense-mediated mRNA decay. *Sci Signal* **3**: ra27.
- Jaenicke LA, von Eyss B, Carstensen A, Wolf E, Xu W, Greifenberg AK, Geyer M, Eilers M, Popov N. 2016. Ubiquitin-Dependent Turnover of MYC Antagonizes MYC/PAF1C Complex Accumulation to Drive Transcriptional Elongation. *Mol Cell* **61**: 54–67.
- Jin Q, Zhuang L, Lai B, Wang C, Li W, Dolan B, Lu Y, Wang Z, Zhao K, Peng W, et al. 2014. Gcn5 and PCAF negatively regulate interferon- β production through HAT-independent inhibition of TBK1. *EMBO Rep* **15**: 1192–201.
- Kaizuka T, Hara T, Oshiro N, Kikkawa U, Yonezawa K, Takehana K, Iemura S-I, Natsume T, Mizushima N. 2010. Tti1 and Tel2 are critical factors in mammalian target of rapamycin complex assembly. *J Biol Chem* **285**: 20109–20116.
- Kim SG, Hoffman GR, Poulogiannis G, Buel GR, Jang YJ, Lee KW, Kim B-YY, Erikson RL, Cantley LC, Choo AY, et al. 2012. Metabolic Stress Controls mTORC1 Lysosomal Localization and Dimerization by Regulating the TTT-RUVBL1/2 Complex. *Mol Cell*.
- Kolosenko I, Fryknäs M, Forsberg S, Johnsson P, Cheon H, Holvey-Bates EG, Edsbäcker E, Pellegrini P, Rassoolzadeh H, Brnjic S, et al. 2015. Cell crowding induces interferon regulatory factor 9, which confers resistance to chemotherapeutic drugs. *Int J Cancer* **136**: E51–E61.
- Lempiäinen H, Halazonetis TD. 2009. Emerging common themes in regulation of PIKKs and PI3Ks. *EMBO J* **28**: 3067–3073.
- Li H, Cuenin C, Murr R, Wang Z-QQ, Herceg Z. 2004. HAT cofactor Trapp regulates the mitotic checkpoint by modulation of Mad1 and Mad2 expression. *EMBO J* **23**: 4824–4834.
- Li Y, Choi PS, Casey SC, Dill DL, Felsner DW. 2014. MYC through miR-17-92 suppresses

- specific target genes to maintain survival, autonomous proliferation, and a Neoplastic state. *Cancer Cell* **26**: 262–272.
- Lin L, Chamberlain L, Zhu LJ, Green MR. 2012. Analysis of Gal4-directed transcription activation using Tra1 mutants selectively defective for interaction with Gal4. *Proc Natl Acad Sci U S A* **109**: 1997–2002.
- Loizou JI, Oser G, Shukla V, Sawan C, Murr R, Wang Z-QQ, Trumpp A, Herceg Z. 2009. Histone acetyltransferase cofactor Trrap is essential for maintaining the hematopoietic stem/progenitor cell pool. *J Immunol* **183**: 6422–6431.
- Love MI, Huber W, Anders S. 2014. Moderated estimation of fold change and dispersion for RNA-seq data with DESeq2. *Genome Biol* **15**: 1–21.
- Lu PY, Lévesque N, Kobor MS. 2009. NuA4 and SWR1-C: two chromatin-modifying complexes with overlapping functions and components. *Biochem Cell Biol* **87**: 799–815.
- McMahon SB, Van Buskirk HA, Dugan KA, Copeland TD, Cole MD. 1998. The novel ATM-related protein TRRAP is an essential cofactor for the c-Myc and E2F oncoproteins. *Cell* **94**: 363–374.
- Nikiforov MA, Chandriani S, Park J, Kotenko I, Matheos D, Johnsson A, McMahon SB, Cole MD. 2002. TRRAP-dependent and TRRAP-independent transcriptional activation by Myc family oncoproteins. *Mol Cell Biol* **22**: 5054–63.
- Nishimura K, Fukagawa T, Takisawa H, Kakimoto T, Kanemaki M. 2009. An auxin-based degron system for the rapid depletion of proteins in nonplant cells. ed. Intergovernmental Panel on Climate Change. *Nat Methods* **6**: 917–22.
- Pal M, Morgan M, Phelps SEL, Roe SM, Parry-Morris S, Downs JA, Polier S, Pearl LH, Prodromou C. 2014. Structural basis for phosphorylation-dependent recruitment of Tel2 to Hsp90 by Pih1. *Structure* **22**: 805–818.
- Park J, Kunjibettu S, McMahon SB, Cole MD. 2001. The ATM-related domain of TRRAP is required for histone acetyltransferase recruitment and Myc-dependent oncogenesis.

Genes Dev **15**: 1619–1624.

Rajagopalan D, Tirado-Magallanes R, Bhatia SS, Teo WS, Sian S, Hora S, Lee KK, Zhang Y, Jadhav SP, Wu Y, et al. 2018. TIP60 represses activation of endogenous retroviral elements. *Nucleic Acids Res* 1–15.

Rao F, Cha J, Xu J, Xu R, Vandiver MS, Tyagi R, Tokhunts R, Koldobskiy MA, Fu C, Barrow R, et al. 2014. Inositol Pyrophosphates Mediate the DNA-PK/ATM-p53 Cell Death Pathway by Regulating CK2 Phosphorylation of Tti1/Tel2. *Mol Cell* **54**: 119–132.

Reeves WMW, Hahn S. 2005. Targets of the Gal4 transcription activator in functional transcription complexes. *Mol Cell Biol* **25**: 9092–9102.

Roulois D, Yau HL, Pugh TJ, Brien O, Carvalho DD De, Roulois D, Yau HL, Singhanian R, Wang Y, Danesh A, et al. 2015. DNA-Demethylating Agents Target Colorectal Cancer Cells by Inducing Viral Mimicry by Endogenous Transcripts. *Cell* **162**: 961–973.

Saleh A, Schieltz D, Ting N, McMahon SB, Litchfield DW, Yates JR, Lees-Miller SP, Cole MD, Brandl CJ. 1998. Tra1p is a component of the yeast Ada·Spt transcriptional regulatory complexes. *J Biol Chem* **273**: 26559–26565.

Sawan C, Hernandez-Vargas H, Murr R, Lopez F, Vaissière T, Ghantous AY, Cuenin C, Imbert J, Wang Z-QQ, Ren B, et al. 2013. Histone acetyltransferase cofactor Trapp maintains self-renewal and restricts differentiation of embryonic stem cells. *Stem Cells* **31**: 979–991.

Schoggins JW, Rice CM. 2011. Interferon-stimulated genes and their antiviral effector functions. *Curr Opin Virol* **1**: 519–525.

Scruggs BS, Gilchrist DA, Nechaev S, Muse GW, Burkholder A, Fargo DC, Adelman K. 2015. Bidirectional Transcription Arises from Two Distinct Hubs of Transcription Factor Binding and Active Chromatin. *Mol Cell* **58**: 1101–1112.

Shevchenko AA, Roguev A, Schaft D, Buchanan L, Habermann B, Sakalar C, Thomas H, Krogan NJ, Shevchenko AA, Stewart AF. 2008. Chromatin Central: towards the

comparative proteome by accurate mapping of the yeast proteomic environment.

Genome Biol **9**: R167.

Shikata M, Ishikawa F, Kanoh J. 2007. Tel2 is required for activation of the Mrc1-mediated replication checkpoint. *J Biol Chem* **282**: 5346–5355.

Skene PJ, Henikoff JG, Henikoff S. 2018. Targeted in situ genome-wide profiling with high efficiency for low cell numbers. *Nat Protoc* **13**: 1006–1019.

Skene PJ, Henikoff S. 2017. An efficient targeted nuclease strategy for high-resolution mapping of DNA binding sites. *Elife* **6**: 1–35.

Spedale G, Timmers HT, Pijnappel WW. 2012. ATAC-king the complexity of SAGA during evolution. *Genes Dev* **26**: 527–541.

Subramanian A, Tamayo P, Mootha VK, Mukherjee S, Ebert BL, Gillette MA, Paulovich A, Pomeroy SL, Golub TR, Lander ES, et al. 2005. Gene set enrichment analysis: A knowledge-based approach for interpreting genome-wide expression profiles. *Proc Natl Acad Sci* **102**: 15545–15550.

Takai H, Wang RC, Takai KK, Yang H, de Lange T. 2007. Tel2 Regulates the Stability of PI3K-Related Protein Kinases. *Cell* **131**: 1248–1259.

Takai H, Xie Y, de Lange T, Pavletich NP. 2010. Tel2 structure and function in the Hsp90-dependent maturation of mTOR and ATR complexes. *Genes Dev* **24**: 2019–2030.

Tapias A, Zhou ZW, Shi Y, Chong Z, Wang P, Groth M, Platzer M, Huttner W, Herceg Z, Yang YG, et al. 2014. Trapp-dependent histone acetylation specifically regulates cell-cycle gene transcription to control neural progenitor fate decisions. *Cell Stem Cell* **14**: 632–643.

Taubert S, Gorrini C, Frank SR, Parisi T, Fuchs M, Chan H-M, Livingston DM, Amati B. 2004. E2F-dependent histone acetylation and recruitment of the Tip60 acetyltransferase complex to chromatin in late G1. *Mol Cell Biol* **24**: 4546–4556.

- Tauc HM, Tasdogan A, Meyer P, Pandur P. 2017. Nipped-A/TRRAP regulates intestinal stem cell proliferation in *Drosophila*. *Development* 612–623.
- Vassilev A, Yamauchi J, Kotani T, Prives C, Avantaggiati ML, Qin J, Nakatani Y. 1998. The 400 kDa subunit of the PCAF histone acetylase complex belongs to the ATM superfamily. *Mol Cell* **2**: 869–875.
- Wang Z, Plasschaert LW, Aryal S, Renaud NA, Yang Z, Choo-Wing R, Pessotti AD, Kirkpatrick ND, Cochran NR, Carbone W, et al. 2018. TRRAP is a central regulator of human multiciliated cell formation. *J Cell Biol.*
- Wurdak H, Zhu S, Romero A, Longer M, Watson J, Chiang C-Y yuan, Zhang J, Natu VS, Lairson LL, Walker JR, et al. 2010. An RNAi screen identifies TRRAP as a regulator of brain tumor-initiating cell differentiation. *Cell Stem Cell* **6**: 37–47.
- Zhang Y, Liu T, Meyer CA, Eeckhoute J, Johnson DS, Bernstein BE, Nussbaum C, Myers RM, Brown M, Li W, et al. 2008. Model-based analysis of ChIP-Seq (MACS). *Genome Biol* **9**.

PART II:

TORC1 and TORC2 converge to regulate the SAGA co-activator in response to nutrient availability

Thomas Laboucarié¹, Dylane Detilleux¹, Ricard A Rodriguez-Mias², Céline Faux¹, Yves Romeo¹, Mirita Franz-Wachtel³, Karsten Krug³, Boris Macek³, Judit Villén², Janni Petersen⁴ & Dominique Helmlinger^{1*}

¹ CRBM, CNRS, University of Montpellier, Montpellier, France.

² Department of Genome Sciences, University of Washington, Seattle, WA, USA.

³ Proteome Center Tübingen, Tuebingen, Germany.

⁴ Flinders Centre for Innovation in Cancer, School of Medicine, Faculty of Health Science, Flinders University, Adelaide, SA, Australia.

* Corresponding author.

Keywords: differentiation; fission yeast; SAGA; signal transduction; TOR; transcription

The regulation of gene expression plays a fundamental role in the ability of cells to adapt to fluctuations in their environment and is essential for cell growth, proliferation, and differentiation. Signaling pathways integrate external signals to drive specific gene expression programs and control cell fate decisions. For example, it has been well-characterized that nutrient availability controls the balance between proliferation and quiescence, through a network of signaling pathways and transcription factors.


Previous data from our lab showed that the SAGA coactivator complex regulates the expression of differentiation genes in response to nutrient availability in *S. pombe* (Helmlinger et al, 2008). More particularly, in nutrient rich conditions (proliferation state), the acetyltransferase subunit of SAGA, Gcn5, represses the transcription of genes required for differentiation. Tra1, another SAGA component is also required to repress the expression of differentiation genes in rich conditions. In contrast, the SAGA subunits Spt7 and Spt8 are required for induction of these genes upon nutrient starvation (differentiation state).

These results raised the question of how the SAGA complex is able to sense and respond accurately to nutrient availability, and to act either as an activator or as a transcriptional repressor. The goal of a former PhD student project in our lab, Thomas Laboucarié, was to tackle these specific questions. During my master internship and for the first few months of my thesis, I contributed to this project using genetics and cell biology approaches in the fission yeast *Schizosaccharomyces pombe*.

Through genetic analyses and quantitative proteomic experiments, we discovered that, depending on nutrient levels, *S. pombe* SAGA is controlled by either TORC1 or TORC2 to regulate the expression of differentiation genes. Strikingly, we found that the TORC1 and TORC2 pathways oppose each other in the phosphorylation of the SAGA subunit Taf12 and in the control of SAGA regulatory activities at differentiation genes. When I joined, Thomas identified that the PP2A phosphatase is responsible for Taf12 dephosphorylation in proliferation conditions. Thomas had also shown that PP2A functions downstream of TORC1. The specific aim of my work was to understand how TORC1 modulates PP2A activity towards Taf12. Using a combination of epistasis and biochemical analyses, I demonstrated that TORC1 activates PP2A through the Greatwall kinase, which inhibits PP2A by phosphorylating the endosulfine protein Igo1. I also showed that, when yeast cells stop proliferating and initiate differentiation, the decrease in TORC1 activity activates Greatwall-Igo1, which inhibits PP2A to allow Taf12 phosphorylation.

This work was published in *EMBO Reports* in September 2017 and my contribution is recognized with a second position authorship on the manuscript.

TORC1 and TORC2 converge to regulate the SAGA co-activator in response to nutrient availability

Thomas Laboucarié¹, Dylane Detilleux¹, Ricard A Rodriguez-Mias², Céline Faux¹, Yves Romeo^{1,†}, Mirita Franz-Wachtel³, Karsten Krug³, Boris Maček³, Judit Villén², Janni Petersen⁴ & Dominique Helmlinger^{1,*} 

Abstract

Gene expression regulation is essential for cells to adapt to changes in their environment. Co-activator complexes have well-established roles in transcriptional regulation, but less is known about how they sense and respond to signaling cues. We have previously shown that, in fission yeast, one such co-activator, the SAGA complex, controls gene expression and the switch from proliferation to differentiation in response to nutrient availability. Here, using a combination of genetic, biochemical, and proteomic approaches, we show that SAGA responds to nutrients through the differential phosphorylation of its Taf12 component, downstream of both the TORC1 and TORC2 pathways. Taf12 phosphorylation increases early upon starvation and is controlled by the opposing activities of the PP2A phosphatase, which is activated by TORC1, and the TORC2-activated Gα^{AKT} kinase. Mutational analyses suggest that Taf12 phosphorylation prevents cells from committing to differentiation until starvation reaches a critical level. Overall, our work reveals that SAGA is a direct target of nutrient-sensing pathways and has uncovered a mechanism by which TORC1 and TORC2 converge to control gene expression and cell fate decisions.

Keywords differentiation; fission yeast; SAGA; signal transduction; TOR; transcription

Subject Categories Metabolism; Signal Transduction; Transcription

DOI 10.15252/embr.201744942 | Received 31 July 2017 | Revised 31 August 2017 | Accepted 7 September 2017 | Published online 27 October 2017

EMBO Reports (2017) 18: 2197–2218

Introduction

Gene regulation plays a fundamental role in the ability of cells to adapt to fluctuations in their environment. For example, nutrient availability controls whether cells proliferate or not, through a

network of signaling kinases that drive specific gene expression programs [1]. Nutrient sensing is mediated by several distinct kinases that are part of highly conserved signaling pathways [2]. Of these, the target of rapamycin (TOR) atypical serine/threonine kinase plays a central role in coordinating cell growth with nutrient levels. TOR assembles into two distinct, highly conserved complexes, TORC1 and TORC2, which differ in their composition, regulation, and functions (reviewed in [3,4]). In the fission yeast *Schizosaccharomyces pombe*, TORC1 promotes cell growth and inhibits sexual differentiation when nutrients are present. In contrast, TORC2 induces cell cycle exit and differentiation upon starvation (reviewed in [5–7]). Accordingly, TORC1 and TORC2 oppositely control the expression of *ste11⁺* and *mei2⁺*, which encodes the master regulators of mating and meiosis, respectively [8–12]. However, the mechanism by which TORC1 and TORC2 regulate gene expression in this context is not well understood.

One critical step of gene expression is transcription initiation, which involves many different types of factors, including co-activators [13]. Co-activators are typically large multi-subunit complexes that possess multiple distinct activities, such as histone modification, nucleosome remodeling, and recruitment of general transcription factors. One such co-activator is the SAGA complex (Spt-Ada-Gcn5 acetyltransferase). SAGA is essential for the transcription of many inducible genes and has key roles in cell cycle progression, stress responses, or during development (reviewed in [14,15]). SAGA is composed of 19 conserved subunits that are organized into functional modules with separate activities. For example, the Gcn5 subunit is a nucleosomal histone acetyltransferase (HAT) [16,17], whereas the Spt8 subunit modulates the recruitment of the TATA box-binding protein (TBP) to certain promoters [18,19]. Other subunits, including Spt7 [16], Ada1 [20], and five TBP-associated factors (TAF5, 6, 9, 10, and 12) [21], are required for the integrity of the complex [18,21,22] and serve as structural scaffolds [23–26]. Interestingly, distinct SAGA activities function independently of each other and can have opposing roles in transcriptional regulation [27]. For example, we have previously shown that, in *S. pombe*,

¹ CRBM, CNRS, University of Montpellier, Montpellier, France

² Department of Genome Sciences, University of Washington, Seattle, WA, USA

³ Proteome Center Tübingen, Tuebingen, Germany

⁴ Flinders Centre for Innovation in Cancer, School of Medicine, Faculty of Health Science, Flinders University, Adelaide, SA, Australia

*Corresponding author. Tel: +33 434 35 95 48; Fax: +33 434 35 94 10; E-mail: dhelmlinger@crbm.cnrs.fr

[†]Present address: Laboratoire de Biologie Moléculaire Eucaryote, Université de Toulouse-Paul Sabatier CNRS, UMR 5099, Toulouse, France

SAGA uses distinct activities to either repress or induce the expression of differentiation genes, depending on nutrient levels [28,29]. However, it is not known how SAGA senses nutrient availability and, more generally, whether signaling pathways directly control the regulatory activities of co-activator complexes.

Here, we have addressed these issues in the context of cell fate control by nutrient availability in *S. pombe*. Epistasis analyses established that the SAGA co-activator regulates the expression of differentiation genes downstream of both the TORC1 and TORC2 signaling pathways. Quantitative proteomic and biochemical analyses revealed that the Taf12 subunit is phosphorylated early upon nutrient starvation. We then showed that TORC1 activates the PP2A phosphatase, via the Greatwall (Gwl) kinase, to de-phosphorylate Taf12, whereas the TORC2-Gad8^{AKT} kinase pathway phosphorylates Taf12. Unexpectedly, we found that Taf12 phosphorylation inhibits sexual differentiation. We propose a model in which, upon nutrient starvation, the simultaneous inhibition of TORC1 and activation of TORC2-Gad8^{AKT} induces Taf12 phosphorylation, which modulates the timing and the amplitude of the differentiation response. Overall, our work reveals that Taf12 is a direct target of nutrient-sensing pathways and that the TORC1 and TORC2 pathways converge to control a common effector, allowing the versatile expression of the master regulators of a differentiation program.

Results

The SAGA subunit Gcn5 regulates sexual differentiation downstream of both the TORC1 and TORC2-Gad8^{AKT} pathways

Schizosaccharomyces pombe is an ideal model to address how cells sense nutrients and coordinately regulate gene expression to control cell fate decisions. In the presence of nutrients, *S. pombe* grows and proliferates. Conversely, upon starvation, particularly of nitrogen, cells exit the cell cycle at the G1 phase and commit to sexual differentiation, which sequentially involves mating, meiosis, and sporulation. The Ste11 transcription factor is the master regulator of sexual differentiation and activates the expression of many genes, including *mei2*⁺, which functions as the decisive trigger of meiosis (reviewed in [30]). We have previously identified dual, opposite roles for SAGA in this process [28]. In rich conditions, the SAGA HAT, Gcn5, directly represses the expression of *ste11*⁺ and *mei2*⁺. In contrast, the Spt8 subunit is required for the induction of these genes upon starvation. We reasoned that, if SAGA is able to switch

from a repressor to an activator in response to nutrients, it must be under the regulation of nutrient-sensing signaling pathways.

In rich conditions, the highly conserved TORC1 kinase and cyclic adenosine monophosphate (cAMP)-activated protein kinase A, Pka1, are the two major pathways that both promote growth and inhibit differentiation [7]. We first sought to identify which of these two pathways requires Gcn5 to inhibit differentiation. To do this, we quantified *ste11*⁺ and *mei2*⁺ expression in mutants that constitutively activate (CA) TORC1 signaling. These included point mutations in the TORC1-specific kinase *tor2*⁺ (*tor2-CA*) and in its activating GTPase Rheb, *rhb1*⁺ (*rhb1-CA*), as well as deletion mutants of the tuberous sclerosis complex proteins Tsc1 and Tsc2. We observed that *ste11*⁺ and *mei2*⁺ expression (Fig 1A and B), as well as differentiation (Fig 1E), are weakly induced upon starvation of all mutants, *tsc1Δ*, *tsc2Δ*, *rhb1-CA*, and *tor2-CA*, as compared to wild-type (WT) controls. Therefore, constitutive activation of TORC1 prevents the induction of differentiation upon starvation, as anticipated from previous work [9,10,31–34]. In marked contrast, in *gcn5Δ* mutants, *ste11*⁺ and *mei2*⁺ expression and differentiation are de-repressed in rich conditions and further induced upon starvation, as compared to WT strains (Fig 1A, B and E). Strikingly, we observed that the expression profiles of *ste11*⁺ and *mei2*⁺ are indistinguishable between *gcn5Δ* single mutants and *gcn5Δ tsc1Δ* or *gcn5Δ tsc2Δ* double mutants (Fig 1A and B). Similar results are observed in *gcn5Δ rhb1-CA* or *gcn5Δ tor2-CA* double mutants. Accordingly, *gcn5Δ* mutants suppress the sterility of *tsc1Δ* and *rhb1-CA* mutants (Fig 1E). We noticed that Gcn5 only partially rescues the differentiation phenotype of constitutively active TORC1 mutants, suggesting that TORC1 controls other processes that are important for sexual differentiation, independently of Gcn5. To conclude, the absence of Gcn5 rescues the inability of constitutively active TORC1 mutants to differentiate, indicating that TORC1 requires Gcn5 to inhibit differentiation.

We tested whether Gcn5 is also epistatic to the cAMP-Pka1 pathway, which synergizes with TORC1 to control *ste11*⁺ expression [11]. Activation of Pka1 either by adding cAMP or by deleting the cAMP-specific phosphodiesterase gene, *cgs2*⁺, markedly reduces *ste11*⁺ and *mei2*⁺ expression, both in rich and starved conditions (Appendix Fig S1A–D), as shown previously [35–37]. In contrast to what we observed with TORC1, *gcn5Δ* mutants do not suppress this phenotype (Appendix Fig S1A–D), suggesting that Pka1 does not require Gcn5 to inhibit differentiation. Altogether, our genetic analyses indicate that the SAGA subunit Gcn5 inhibits differentiation downstream of TORC1.

Figure 1. SAGA is epistatic to the TORC1 and TORC2 pathways in the regulation of differentiation in response to nutrient availability.

- A–D Expression of *ste11*⁺ (A, C) and *mei2*⁺ (B, D) using quantitative RT–PCR of RNA extracted from cells grown either in nutrient rich medium (dark gray) or shifted for 4 h to starvation medium (light gray). Cells of the following genotypes were analyzed: wild-type isogenic controls (WT), *gcn5Δ*, *tsc1Δ*, *gcn5Δ tsc1Δ*, *tsc2Δ*, *gcn5Δ tsc2Δ*, *rhb1-DA4*—a constitutively active (CA) *rhb1* mutant [34], *gcn5Δ rhb1-DA4*, *tor2-L1310P*—a CA *tor2* mutant [33], *gcn5Δ tor2-L1310P*, *tor1Δ*, *gcn5Δ tor1Δ*, *gad8Δ*, and *gcn5Δ gad8Δ*. *act1*⁺ served as a control for normalization across samples. Values from a WT strain grown in rich medium were set at 1 to allow comparisons across culture conditions and mutant strains. Each column represents the mean value of 4 (A, B) or 3 (C, D) independent experiments, overlaid with individual data points and error bars showing the standard error of the mean (SEM). Statistical significance was determined by two-way ANOVA followed by Bonferroni's multiple comparison tests (*n* = 4 for A, B; *n* = 3 for C, D); **P* ≤ 0.01.
- E, F Cells were grown to mid-log phase either in rich medium or shifted for 8 h to starvation medium. Zygotes and tetrads, which correspond to differentiated cells, were counted under a light microscope. Cells of the following genotypes were analyzed: WT isogenic controls, *gcn5Δ*, *tsc1Δ*, *gcn5Δ tsc1Δ*, *rhb1-DA4*, *gcn5Δ rhb1-DA4*, *gad8Δ*, and *gcn5Δ gad8Δ*. Each value represents the mean percentage and SEM of differentiating cells to the total number of cells, averaged from four independent experiments. At least 200 cells from the indicated genotypes were counted in each experiment. White arrowheads indicate zygotes. Scale bar, 10 μm.

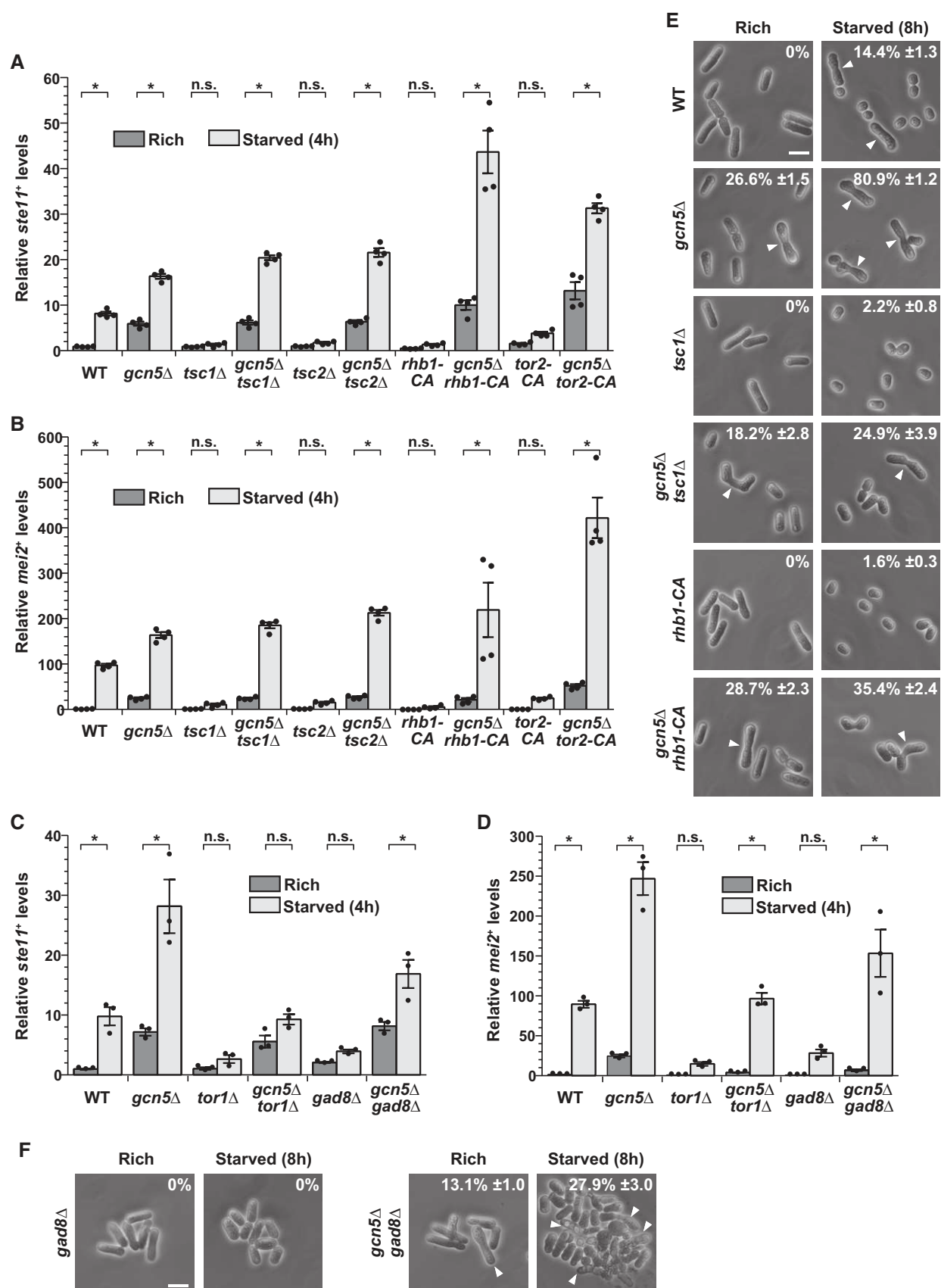


Figure 1.

Upon nutrient starvation, several signaling pathways are activated and required for sexual differentiation in *S. pombe*. Each is defined by a highly conserved kinase, including orthologs of the p38 MAPK, Sty1, and of the TORC2 complex, defined by the Tor1 kinase [7]. Similar to other eukaryotes, *S. pombe* TORC2 mediates many of its functions through the activation of an AKT kinase, Gad8^{AKT} [38–41]. Additionally, one *S. pombe* ortholog of the adenosine monophosphate (AMP)-activated protein kinase, Ssp2, has important roles in starvation responses, notably through the inhibition of TORC1 [42,43].

We determined whether any of these kinases also functionally interacts with Gcn5 to regulate differentiation genes. To do this, we quantified their expression in mutants of each kinase, grown either in rich medium or shifted to starvation conditions. As compared to WT controls, we observed little, if any, induction of both *ste11*⁺ and *mei2*⁺ upon starvation of *tor1Δ* (Fig 1C and D), *gad8Δ* (Fig 1C and D), *sty1Δ* (Appendix Fig S1E and F), or *ssp2Δ* mutants (Appendix Fig S1G and H), as expected from previous work [38,42,44,45]. In contrast, expression of *mei2*⁺, and to a lesser extent of *ste11*⁺, is induced upon starvation of *gcn5Δ gad8Δ* or *gcn5Δ tor1Δ* double mutants (Fig 1C and D). In marked contrast, *gcn5Δ* mutants do not suppress the lack of induction observed in *sty1Δ* or *ssp2Δ* mutants (Appendix Fig S1E–H). Finally, *gcn5Δ*

mutants partially suppress the sterility of *gad8Δ* mutants (Fig 1F) but, surprisingly, not of *tor1Δ* mutants (data not shown). We observed that *gcn5Δ tor1Δ* double mutants exhibit severe cell cycle progression defects, which likely interfere with their ability to exit from G1 and commit to sexual differentiation. To conclude, our genetic analyses suggest that Gcn5 regulates sexual differentiation downstream of the TORC2-Gad8^{AKT} pathway, but not of p38^{Sty1} or Ssp2^{AMPK}. However, the partial suppression of the differentiation phenotypes of *gad8Δ* and *tor1Δ* mutants by *gcn5Δ* mutants suggests that the TORC2-Gad8^{AKT} pathway requires additional effectors to induce sexual differentiation upon starvation.

SAGA is differentially phosphorylated in response to a change in nutrient levels

These genetic analyses prompted us to determine how TORC1 and TORC2 control Gcn5 in response to nutrients. To do this, we used the tandem affinity purification (TAP) procedure to purify Gcn5, as part of SAGA, from cells grown under nutrient rich conditions or shifted to starvation medium for 45 min. Both total protein staining and quantitative mass spectrometry (MS) analysis revealed that SAGA subunit composition does not change upon shifting cells from rich to starved conditions (Fig 2A, Appendix Table S1). To test

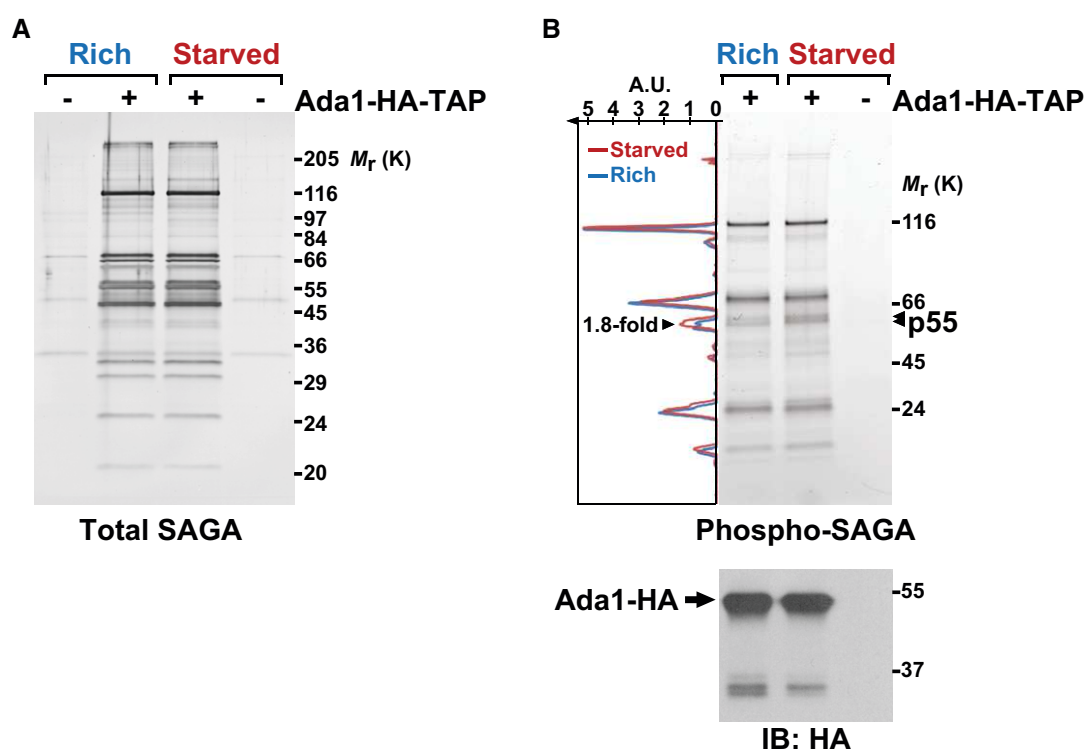


Figure 2. SAGA is phosphorylated in response to nutrient starvation.

A, B 4–20% gradient SDS–polyacrylamide gel electrophoresis analysis of SAGA purified from cells grown either in rich medium (R) or starved for 45 min (S). SAGA was purified using endogenously TAP-tagged Ada1. A fraction of each eluate was loaded and either stained with silver, to detect all proteins (A), or with Pro-Q[®] Diamond, which stains phosphorylated proteins (B). A strain without any TAP tag is shown as a negative control for the purification. The graph to the left of the gel in (B) shows the fluorescence intensity of the phospho-specific stain, which was quantified along the left lane in blue (rich) and the middle lane in red (starved), using ImageJ. The area of one peak, which corresponds to the bands marked with arrowheads and was coined p55, is 1.8-fold larger in SAGA purified from starved cells, as compared to rich conditions. Below is an anti-HA immunoblot (IB) of each eluate, to reveal the amount of Ada1-HA bait recovered. Shown are gels that are representative of three independent experiments. A.U., arbitrary units.

whether SAGA is differentially phosphorylated, we re-analyzed these purifications using an in-gel fluorescent stain, Pro-Q Diamond, which is specific for phosphorylated proteins (Fig 2B). Quantification of each lane indicates that one band, migrating at about 55 kDa and coined p55, is about 1.8-fold more intense in SAGA purified from starved cells, as compared to rich conditions (Fig 2B). The predicted molecular weight of eight out of the 19 subunits of *S. pombe* SAGA falls between 50 and 60 kDa, including Gcn5 [28].

To test whether p55 corresponds to Gcn5, we purified SAGA using a strain in which Gcn5 is tagged with MYC epitopes, such as to slow its migration to a portion of the gel where no other SAGA subunits are detected (Appendix Fig S2A). Although Gcn5 is clearly phosphorylated (Appendix Fig S2B), its normalized levels are similar between rich and starved conditions (Appendix Fig S2C). Importantly, p55 is still detectable in SAGA purified from Gcn5-MYC cells and its phosphorylation increases upon starvation (Appendix Fig S2A–C). Therefore, one SAGA component, but not Gcn5, is differentially phosphorylated in response to nutrients.

Taf12 is phosphorylated in response to nutrient availability

To identify p55, we performed a quantitative MS analysis of phospho-peptides within SAGA, using a SILAC procedure (Fig 3A). We analyzed either whole cell extracts or purified SAGA complexes, comparing cells that were differentially labeled with lysine and arginine isotopes, grown either in rich conditions or shifted to starvation medium for 45 min. Strikingly, the core SAGA subunit Taf12 appeared differentially phosphorylated on several residues in all four independent phospho-SILAC experiments, including when the p55 band was cut and directly analyzed by MS. Specifically, Taf12 shows increased phosphorylation of threonines (Thr

218, 221, and 283 upon starvation (Fig 3B, Appendix Figs S3 and S4).

To confirm and further characterize this observation, we examined the migration of endogenously FLAG-tagged Taf12 by Western blot analysis of extracts from cells grown in rich medium or shifted to starved conditions. We detected an electrophoretic mobility shift of Taf12 following nutrient starvation, either in crude extracts (Fig 3D, lower panel) or after its immuno-purification (Fig 3D, upper panel). We quantified the relative intensity of the phosphorylated form of Taf12, named hereafter P-Taf12, and of total Taf12 from seven independent biological replicates and confirmed that P-Taf12 increases reproducibly upon starvation, whereas total Taf12 levels do not change (Fig 3E). We then demonstrated that this shift is indeed caused by phosphorylation. First, this isoform of Taf12 disappears upon λ -phosphatase treatment of FLAG purified Taf12 (Fig 3D, upper panel). Second, we constructed strains in which either one (Taf12-T283A) or all three Thr were mutated to alanines (Ala) (Taf12-5A). We also mutated the serines (Ser) that are adjacent to Thr218 and Thr221, in order to prevent their possible phosphorylation in the Thr-to-Ala mutant (Fig 3C). Western blotting confirmed that, at most, all five Ser/Thr residues contribute to this mobility shift, without affecting Taf12 steady-state levels (Fig 3F). Altogether, these results indicate that Taf12 becomes phosphorylated upon nutrient starvation in *S. pombe*.

Next, we verified that Taf12 is phosphorylated within SAGA, as suggested by our phospho-SILAC analyses. Similarly, we asked whether Taf12 is phosphorylated as part of the TFIID general transcriptional factor complex, of which *S. pombe* Taf12 is also a core component [46], similar to other eukaryotes. We used either Spt7 or Taf4 to purify SAGA or TFIID, respectively. Anti-FLAG blotting of each eluate indicated that starvation induces Taf12 phosphorylation

Figure 3. The SAGA and TFIID subunit Taf12 is phosphorylated early upon starvation.

- A Overview of the quantitative proteomic approaches used to identify differentially phosphorylated peptides, either in crude extracts or in SAGA purifications. Cells were metabolically labeled using a SILAC procedure and grown either in rich medium or shifted to nutrient starvation conditions. Several independent experiments were carried out with forward and reverse labeling schemes (see Materials and Methods for details).
- B Schematic view of the *S. pombe* (*Sp*) Taf12 protein sequence, including, in red, the three differentially phosphorylated Thr, at positions 218, 221, and 283 and, in gray, the histone-fold domain. Shown below are the starved-to-rich SILAC ratios of the signal intensities observed for the Thr218-Thr221 peptide (Appendix Fig S3) and for the Thr283 peptide (Appendix Fig S4).
- C Summary of the different *taf12*⁺ point mutants that were constructed and analyzed.
- D FLAG-tagged Taf12 was purified from cells grown in rich medium (R) or shifted for 45 min to starvation medium (S). Anti-FLAG immuno-precipitations (IP) were incubated with and without λ -phosphatase or its inhibitor and immunoblotted (IB), together with 1% of whole cell extracts (WCE), using an anti-FLAG antibody.
- E Phospho-Taf12 (P-Taf12), total Taf12, and tubulin levels were quantified from cells grown in rich medium (R) or starved for 45 min (S). P-Taf12 levels were normalized to those of total Taf12, while total Taf12 levels were normalized to those of tubulin. Data points were individually plotted on the graph and overlaid with the mean and SEM. Signal intensities were quantified from IBs of seven independent experiments. Statistical significance was determined using a t-test ($n = 7$, unpaired, two-tailed); * $P \leq 0.01$.
- F P-Taf12 and total Taf12 were followed in WT, *taf12-T283A* and *taf12-5A* mutants, grown in rich medium (R) or starved for 45 min (S).
- G, H SAGA and TFIID were tandem affinity-purified using endogenously TAP-tagged Spt7 (G) or Taf4 (H), from strains containing FLAG-tagged Taf12, grown in rich medium or starved for 45 min. TAP-tagged Spt7 and Taf4 were eluted using the TEV protease, releasing a shorter form of each bait (Spt7-CBP or Taf4-CBP). Eluates were loaded and immunoblotted (IB) using anti-FLAG or anti-CBP antibodies, together with 1% of either whole cell extracts (WCE) or IgG-Sepharose flow-through (FT). Shown are IBs that are representative of two independent experiments.
- I P-Taf12, total Taf12, and Ser546-phosphorylated Gad8^{AKT} were followed in WT cells, grown in rich conditions or over a time-course after a shift to starvation medium. Gad8^{AKT} phosphorylation at Ser546 is a proxy of TORC2 activity in *S. pombe*.
- J P-Taf12 and total Taf12 were followed in WT cells, grown in rich conditions or shifted to different starvation media for 30 min. These include both the removal of the nitrogen source, ammonium chloride (NH₄Cl), and the reduction in the carbon source, glucose, from a concentration of 2–0.5%. Alternatively, cells were either only deprived of NH₄Cl or only exposed to reduced glucose levels (2–0.5%).
- K P-Taf12 and total Taf12 were followed in WT cells, grown in rich conditions or deprived of NH₄Cl for 1 h. Then, NH₄Cl was added back to the medium for 30 or 60 min.

Data information: Shown are IBs that are representative of at least three independent experiments. The number sign (#) symbol identifies antibody heavy chains and the star (*) symbol labels an unspecific band detected by the anti-FLAG antibody in *S. pombe*. Both short and long exposures of the FLAG IBs are shown to detect total Taf12 and P-Taf12, respectively, within the linear range of the chemiluminescence signal. Anti-tubulin IBs are shown as controls for loading between samples.

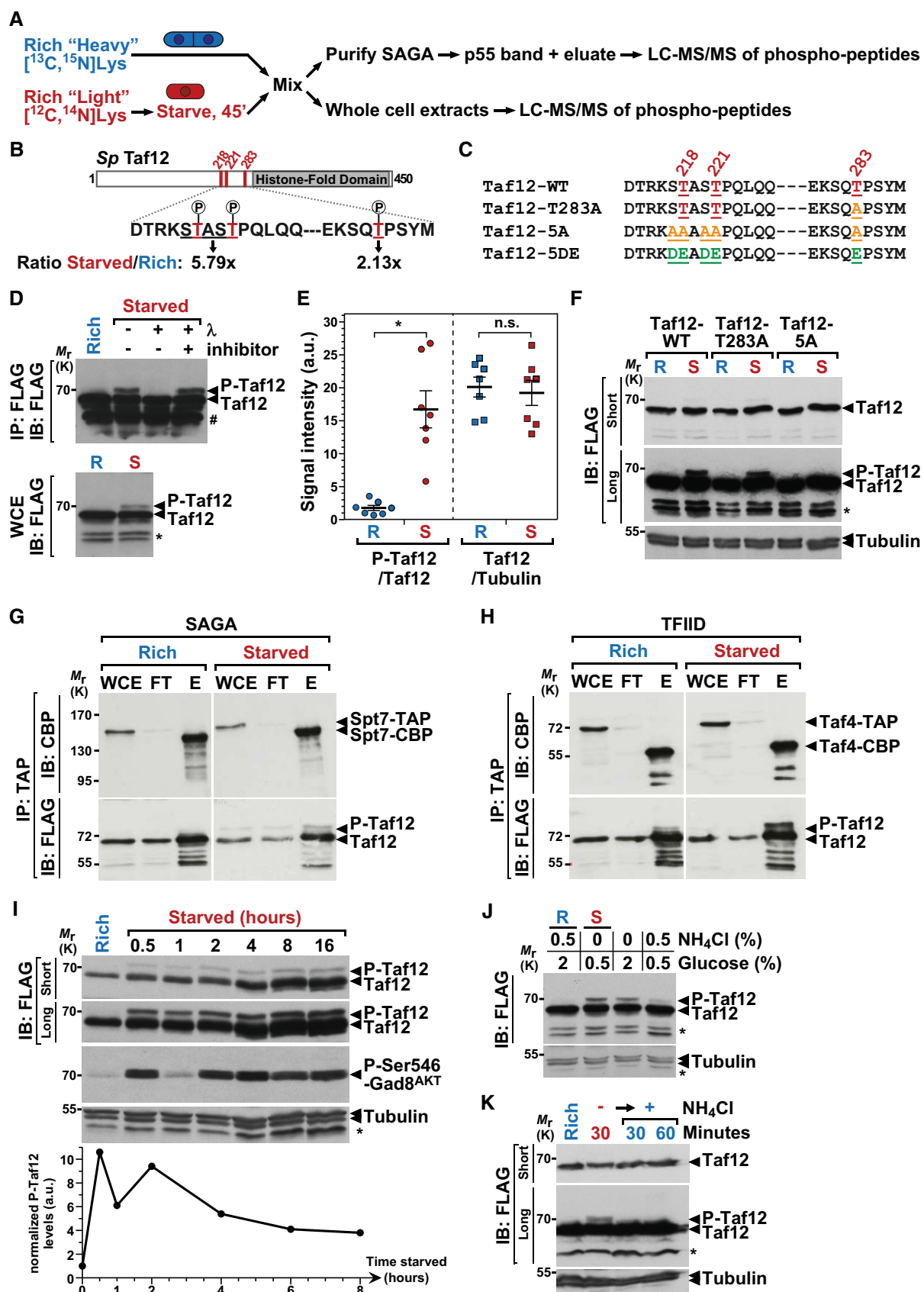


Figure 3.

both within SAGA (Fig 3G) and TFIID (Fig 3H). Total protein staining of purified TFIID showed that its subunit composition does not change upon shifting cells from rich to starved conditions (Appendix Fig S5), similar to SAGA (Fig 2A). To conclude, Taf12 becomes phosphorylated upon nutrient starvation, as part of both the SAGA and TFIID complexes.

Dynamics of Taf12 phosphorylation

To further characterize Taf12 phosphorylation, we monitored its kinetics upon starvation and detected P-Taf12 already 30 min after shifting cells to starved medium (Fig 3I). This observation suggests that Taf12 is directly controlled by nutrient-sensing pathways, which respond to nutrient starvation within this timeframe in *S. pombe*. For example, TORC1 activity is fully inhibited within 30 min of nitrogen starvation [47]. Likewise, we observed that phosphorylation of Ser546 of the AKT kinase, Gad8^{AKT}, is maximal 30 min after removing nutrients (Fig 3I), consistent with previous observations [41]. This modification is a hallmark of TORC2 activation both in *S. pombe* [38,40] and in mammals [48]. Interestingly, only a small fraction of total Taf12 is phosphorylated, about 7%, without further increasing with the duration of starvation, as more cells commit to differentiation (Fig 3I). Rather, we observed that Taf12 phosphorylation proportionally decreases about threefold at later time points of starvation (Fig 3I). To conclude, phosphorylation of Taf12 appears restricted to a small fraction of all Taf12 and peaks early upon nutrient starvation.

Our procedure for starving proliferating cells consists in both completely removing ammonium, a preferred nitrogen source, and lowering glucose levels fourfold. In *S. pombe*, TORC1 mostly responds to the availability of nitrogen. We thus tested which of nitrogen or carbon starvation induces Taf12 phosphorylation. Western blot analysis from cells shifted to various media showed that P-Taf12 levels increase upon nitrogen starvation, whereas

lowering glucose levels has a much weaker effect (Fig 3J). Additionally, P-Taf12 levels rapidly decrease when nitrogen is added back to starved cells (Fig 3K). We thus conclude that Taf12 phosphorylation is dynamically regulated by nitrogen availability.

The PP2A phosphatase represses differentiation downstream of TORC1

We next sought to identify which signaling pathways control Taf12 phosphorylation in response to nutrients. In rich conditions, TORC1 activity is high whereas Taf12 phosphorylation levels are low. We therefore hypothesized that TORC1 activates a phosphatase to prevent Taf12 phosphorylation in rich conditions. Functionally, this phosphatase should inhibit differentiation downstream of TORC1. Little is known about which phosphatases function in nutrient sensing and sexual differentiation in *S. pombe*. However, in *S. cerevisiae*, TORC1 regulates the type 2A and 2A-related protein phosphatases (PP2A) to control nutrient stress responses [3,49], including gametogenesis [50]. PP2A is a conserved heterotrimeric complex formed by catalytic (C), structural (A), and regulatory (B55 or B56) subunits. The latter components are mutually exclusive and dictate substrate specificity [51]. *Schizosaccharomyces pombe* PP2A has important roles in morphogenesis and mitosis [52–55], but it is not known whether it also controls sexual differentiation.

To answer this question, we quantified the expression of differentiation genes and the number of cells undergoing sexual differentiation in PP2A deletion mutants, grown either in rich conditions or shifted to starvation medium. We observed that the expression of both *ste11*⁺ and *mei2*⁺ is de-repressed in a catalytic subunit mutant, *ppa2Δ*, as compared to WT controls (Fig 4A and B). Interestingly, both genes are de-repressed in a mutant of the B55 regulatory subunit, *pab1Δ*, but not in a mutant of the B56 regulatory subunit, *par1Δ* (Fig 4A and B). In agreement, we counted a higher number of differentiated cells in *pab1Δ* mutants, in both rich and

Figure 4. The PP2A phosphatase inhibits differentiation and de-phosphorylates Taf12.

- A, B Expression of *ste11*⁺ (A) and *mei2*⁺ (B) using quantitative RT–PCR of RNA extracted from cells grown either in rich medium (dark gray) or starved for 4 h (light gray). Cells of the following genotypes were analyzed: wild-type isogenic controls (WT), *ppa2Δ*, *par1Δ*, *pab1Δ*, *tsc1Δ*, and *pab1Δ tsc1Δ*. *act1*⁺ served as a control for normalization across samples. Values from a WT strain grown in rich medium were set at 1 to allow comparisons across culture conditions and mutant strains. Each column represents the mean value of four independent experiments, overlaid with individual data points and SEM. Statistical significance was determined by two-way ANOVA followed by Bonferroni's multiple comparison tests ($n = 4$); * $P \leq 0.01$.
- C Cells were grown to mid-log phase either in rich medium or starved for 8 h. Zygotes and tetrads, which correspond to differentiated cells, were counted under a light microscope. Each value represents the mean percentage and SEM of differentiating cells to the total number of cells, averaged from four independent experiments. At least 200 cells from the indicated genotypes were counted in each experiment. White arrowheads indicate zygotes. Scale bar, 10 μ m.
- D P-Taf12 was followed by anti-FLAG IB of protein extracts from WT and *pab1Δ* strains, grown in rich conditions (R) or starved for 45 min (S). An anti-Rpb1 IB is shown as a control for loading. The signal intensities of P-Taf12 and total Taf12 were quantified in each strain and condition. Ratios of P-Taf12 to total Taf12 were calculated from six independent experiments and individually plotted in a graph below the IBs, together with the mean and SEM. Averaged values from all WT controls grown in rich medium were set at 1 to allow comparisons across culture conditions and strains. Statistical significance was determined by two-way ANOVA followed by Bonferroni's multiple comparison tests ($n = 6$; * $P < 0.01$; # $P < 0.05$). A short exposure and a long exposure of the FLAG IB are shown to detect total Taf12 and P-Taf12, respectively, within the linear range of the chemiluminescence signal.
- E FLAG-tagged Taf12 and TAP-tagged Pab1 were affinity-purified separately from cells grown in rich conditions (upper panels). TAP-tagged Pab1 was cleaved off from beads using the tobacco etch virus (TEV) protease, releasing a shorter form of Pab1 (CBP-Pab1) in the eluate (E). CBP-Pab1 was then mixed with beads containing FLAG-Taf12 IPs and incubated in a phosphatase buffer, with and without 0.5 μ M microcystin. Each reaction was then analyzed by IB and simultaneously probed with anti-FLAG or anti-CBP antibodies (lower panel).
- F Exponentially growing cells were treated for 1 h with Torin-1, which was added at increasing concentrations, 7 and 21 μ M, to rich medium. Dimethylsulfoxide (DMSO) was used as the vehicle and added as a negative control. Anti-tubulin IBs are shown as a control for loading between samples.
- G P-Taf12 was followed by anti-FLAG IB of protein extracts from WT and *tor2-ts10* strains, grown in rich conditions at 25°C or shifted to 30°C for 4 and 6 h. Anti-tubulin IBs are shown as a control for loading between samples.

Data information: Shown are IBs that are representative of three independent experiments. The star (*) symbol labels unspecific bands detected by the anti-FLAG or anti-CBP antibodies in *S. pombe*.

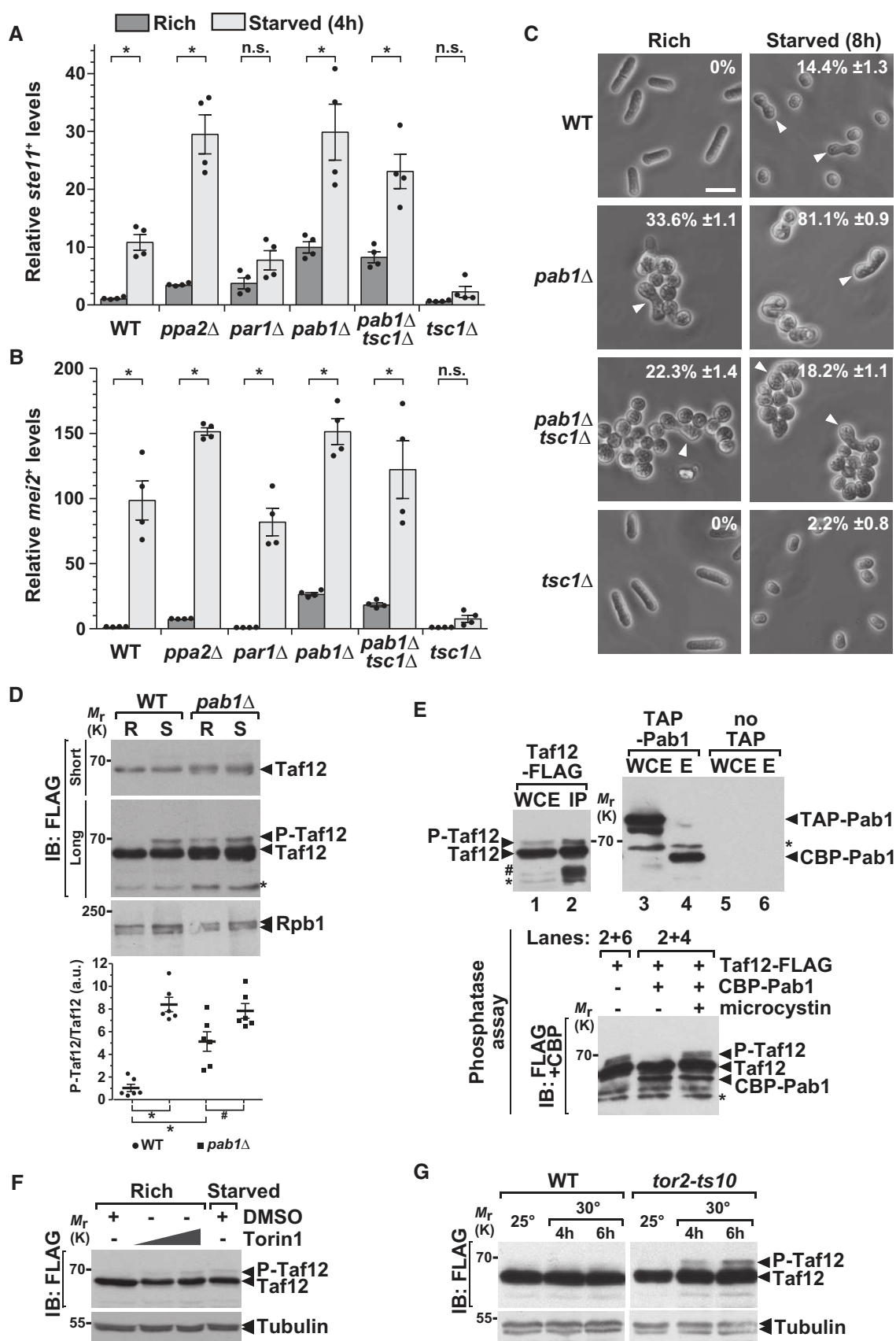


Figure 4.

starved conditions, as compared to WT controls (Fig 4C). Therefore, similar to TORC1 and Gcn5, PP2A inhibits sexual differentiation when cells are grown in rich conditions and this function is specifically mediated by the B55 regulatory subunit Pab1^{B55}.

We then determined whether PP2A-Pab1^{B55} functions downstream of TORC1 in this process, by testing whether a *pab1Δ* mutant suppresses the lack of differentiation observed in a constitutively active TORC1 mutant. We found that the expression profiles of *ste11*⁺ and *mei2*⁺ are similar between a *pab1Δ* single mutant and a *pab1Δ tsc1Δ* double mutant (Fig 4A and B). In agreement, the absence of Pab1^{B55} partially rescues the lack of differentiation of a *tsc1Δ* mutant (Fig 4C). As reported previously [53], *pab1Δ* mutants display severe morphological defects that likely interfere with sexual differentiation. In conclusion, the B regulatory subunit of PP2A, Pab1^{B55}, functions downstream of Tsc1, and likely of TORC1, to inhibit differentiation when cells proliferate. Importantly, a very recent study has shown that TORC1 controls PP2A-Pab1^{B55} to inhibit sexual differentiation in *S. pombe* [56].

The PP2A phosphatase de-phosphorylates Taf12

These results prompted us to test whether PP2A regulates Taf12 phosphorylation in nutrient rich conditions. First, we observed that P-Taf12 levels reproducibly increase in *pab1Δ* mutants, as compared to WT controls, whereas total Taf12 levels do not change (Fig 4D). Interestingly, P-Taf12 levels appear to further increase in starved *pab1Δ* cells, suggesting that, in parallel to inhibiting PP2A, starvation activates a kinase which phosphorylates Taf12. Second, we tested whether PP2A is able to directly de-phosphorylate Taf12. We separately purified Taf12 and Pab1^{B55}, which were endogenously tagged with a FLAG and a TAP epitope, respectively (Fig 4E, upper panels). Incubation of the eluates together in a standard phosphatase buffer revealed that Pab1^{B55} de-phosphorylates Taf12 *in vitro* (Fig 4E, lower panel). To control for the specificity of this assay, we verified that Taf12 is not de-phosphorylated when a PP2A-specific inhibitor, microcystin, is added, or when it is incubated with a control “no TAP” purification. Altogether, these experiments indicate that Taf12 is a substrate of the PP2A-Pab1^{B55} phosphatase, both *in vitro* and *in vivo*.

To determine whether TORC1 modulates Taf12 phosphorylation, we followed P-Taf12 levels upon addition of Torin-1, which inhibits TOR kinase activity. Western blot analyses revealed that P-Taf12 levels increase with the amount of Torin-1 added to cells grown in rich medium (Fig 4F). We noticed that total Taf12 levels decreased upon Torin-1 addition, possibly because TORC1 inhibition reduces translation. However, Torin-1 is an ATP-analogue inhibitor of TOR and therefore inhibits both TORC1 and TORC2 [57,58]. We thus examined Taf12 phosphorylation in a temperature-sensitive mutant of the TORC1-specific kinase, *tor2-ts10* [10]. Western blot analyses showed that P-Taf12 levels increase upon shifting *tor2-ts10* mutants to the restrictive temperature, as compared to WT controls (Fig 4G), indicating that Taf12 phosphorylation is specifically inhibited by TORC1.

It is possible that higher P-Taf12 levels are an indirect consequence of the de-repression of differentiation which is observed in both PP2A-Pab1^{B55} and TORC1 mutants (Fig 4A–C) [10]. However, Taf12 phosphorylation profile is normal in *gcn5Δ* cells (Appendix Fig S6A), even though a *gcn5Δ* mutant phenocopies a

pab1Δ mutant (Figs 1 and 4A–C). Furthermore, constitutive activation of Pka1 does not affect Taf12 phosphorylation in both rich and starved conditions (Appendix Fig S6B and C), consistent with our genetic analyses, which indicated that SAGA does not function downstream of the cAMP-Pka1 pathway (Appendix Fig S1A–D). In conclusion, we show that PP2A-Pab1^{B55} is a crucial effector of TORC1 to prevent both differentiation and Taf12 phosphorylation.

The Ppk18^{Gwl}-Igo1 pathway promotes differentiation through PP2A and SAGA

Our data indicate that P-Taf12 levels inversely correlate with TORC1 and PP2A-Pab1^{B55} activities. We next investigated the mechanism by which TORC1 inhibits PP2A to allow Taf12 phosphorylation upon starvation. PP2A activity and substrate specificity are controlled by its interaction with distinct regulatory proteins. Of these, the essential PP2A-associated protein Tap42 is a major effector of TORC1 signaling in *S. cerevisiae* [3,49]. BLAST searches identified one *S. pombe* protein, SPCC63.05, as the *bona fide* ortholog of *S. cerevisiae* Tap42 (E-value = 2.3^{−27}). However, conditional depletion of Tap42 had no effect on Taf12 phosphorylation (Appendix Fig S7).

In *S. cerevisiae*, another major effector of TORC1 signaling is the S6 kinase ortholog, Sch9, which regulates PP2A through the Great-wall (Gwl) kinase ortholog, Rim15. As in other eukaryotes, Rim15^{Gwl} inhibits PP2A activity by phosphorylating proteins of the α -endosulfine family [59,60]. Remarkably, this regulatory cascade is essential to induce quiescence upon starvation in *S. cerevisiae* [59]. A recent study has identified a similar pathway in *S. pombe*, in which the Ppk18^{Gwl} kinase phosphorylates Ser64 of the Igo1 α -endosulfine to inhibit PP2A-Pab1 and coordinate cell growth with mitosis [61].

To characterize the role of this pathway upon starvation in *S. pombe*, we first monitored the migration pattern of endogenously MYC-tagged Igo1 in response to nutrient availability. Western blotting of a Phos-tag-containing acrylamide gel revealed several bands that migrated slower in extracts from starved cells (Fig 5A). This starvation-induced shift is not observed in *ppk18Δ* mutants or in Ser64-to-Ala *igo1* knock-in mutants. We then quantified *ste11*⁺ and *mei2*⁺ expression and the number of differentiated cells in *ppk18Δ*, *igo1Δ* and *igo1-S64A* mutants, grown either in rich conditions or shifted to starvation medium. We observed that the expression of both genes (Fig 5B and C) and sexual differentiation (Appendix Fig S8) are weakly induced upon starvation of all three mutants, as compared to wild-type (WT) controls. Therefore, starvation induces the phosphorylation of Igo1-Ser64, most likely through the Ppk18^{Gwl} kinase, and this pathway is required to promote differentiation, analogous to its role in *S. cerevisiae*.

This function of Ppk18^{Gwl}-Igo1 opposes that of PP2A-Pab1^{B55} and of SAGA-Gcn5, which both inhibit differentiation when cells proliferate. We thus tested whether Ppk18^{Gwl} and Igo1 genetically interact with Pab1^{B55} and Gcn5 to control differentiation. We observed that *ste11*⁺ and *mei2*⁺ expression profiles are similar between *gcn5Δ* single mutants and *gcn5Δ ppk18Δ* or *gcn5Δ igo1-S64A* double mutants (Fig 5B and C). Likewise, the expression profiles of *pab1Δ* single mutant are similar to those of *pab1Δ ppk18Δ* and *pab1Δ igo1-S64A* double mutants (Fig 5B and C). Accordingly, *gcn5Δ* and *pab1Δ* mutants suppress the sterility of *ppk18Δ* and

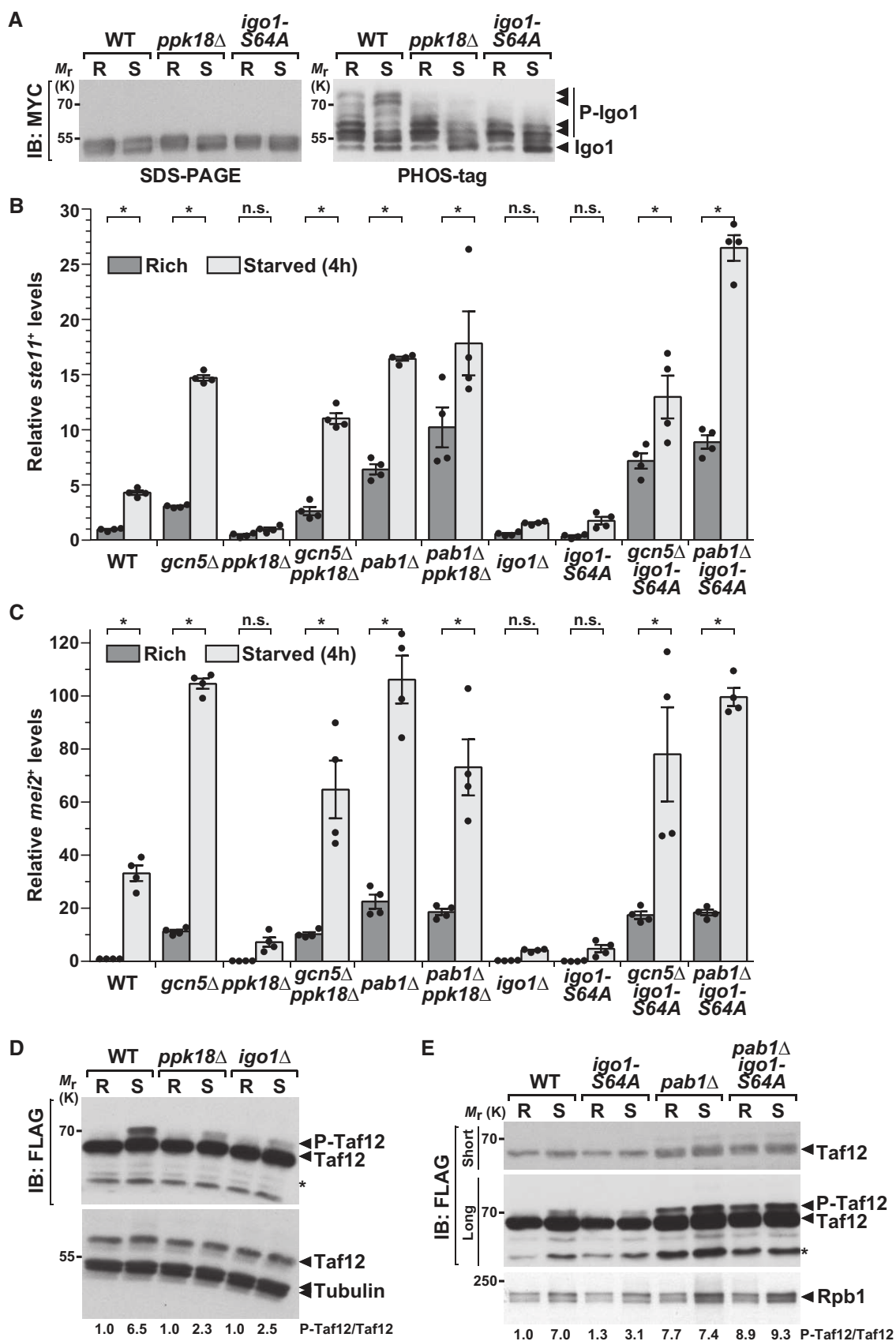


Figure 5.

Figure 5. PP2A activity is regulated by the Ppk18^{Gwl}-Igo1 pathway to control differentiation and Taf12 phosphorylation, in response to nutrient availability.

- A Igo1 phosphorylation (P-Igo1) was followed by anti-MYC IB of protein extracts from WT, *ppk18Δ*, and *igo1-S64A* strains, grown in rich conditions (R) or starved for 45 min (S). Igo1 migration was analyzed by electrophoresis of both a 12% SDS–polyacrylamide gel containing the Phos-tag™ molecule (right panel) and a standard 10% SDS–polyacrylamide gel (left panel). Arrowheads indicate the various phosphorylated isoforms of Igo1-MYC in each strain and condition. Shown is an IB representative of two independent experiments.
- B, C Expression of *ste11⁺* (C) and *mei2⁺* (D) using quantitative RT–PCR of RNA extracted from cells grown either in rich medium (dark gray) or starved for 4 h (light gray). Cells of the following genotypes were analyzed: wild-type isogenic controls (WT), *gcn5Δ*, *ppk18Δ*, *gcn5Δ ppk18Δ*, *pab1Δ*, *pab1Δ ppk18Δ*, *igo1Δ*, *igo1-S64A*, *gcn5Δ igo1-S64A*, and *pab1Δ igo1-S64A*. *act1⁺* served as a control for normalization across samples. Values from a WT strain grown in rich medium were set at 1 to allow comparisons across culture conditions and mutant strains. Each column represents the mean value of four independent experiments, overlaid with individual data points and SEM. Statistical significance was determined by two-way ANOVA followed by Bonferroni's multiple comparison tests ($n = 4$); $*P \leq 0.01$.
- D P-Taf12 was followed by anti-FLAG IB of protein extracts from WT, *ppk18Δ*, and *igo1Δ* strains, grown in rich conditions (R) or starved for 45 min (S). An anti-tubulin IB is shown as a control for loading.
- E P-Taf12 was followed in WT, *igoS64A*, *pab1Δ*, and *pab1Δ igoS64A* strains, grown in rich conditions (R) or starved for 45 min (S). An anti-Rpb1 IB is shown as a control for loading.

Data information: In (D and E), the signal intensities of P-Taf12 and total Taf12 were quantified in each strain and condition. Shown below each blot are average measurements of three independent experiments ($n = 3$). A short exposure and a long exposure of the FLAG IB are shown to detect total Taf12 and P-Taf12, respectively, within the linear range of the chemiluminescence signal. The star (*) symbol labels an unspecific band detected by the FLAG antibody in *S. pombe*.

igo1-S64A mutants (Appendix Fig S8). Thus, the absence of either Pab1^{B55} or Gcn5 suppresses the inability of *ppk18Δ* or *igo1-S64A* mutants to differentiate upon starvation. We conclude that Ppk18^{Gwl}-Igo1 inhibits PP2A-Pab1^{B55} to allow sexual differentiation in response to starvation and that Gcn5 functions downstream of this pathway.

The Ppk18^{Gwl}-Igo1 pathway inhibits Taf12 de-phosphorylation by PP2A-Pab1^{B55}

We next determined whether Taf12 phosphorylation is modulated by the Ppk18^{Gwl}-Igo1-PP2A cascade, by analyzing P-Taf12 levels in *ppk18Δ* and *igo1Δ* mutants, grown either in rich conditions or shifted to starvation medium. Western blot analyses and quantifications revealed that Taf12 phosphorylation is reduced in starved *ppk18Δ*, *igo1Δ*, and *igo1-S64A* mutants, as compared to WT controls (Fig 5D and E). Therefore, Ppk18^{Gwl}-Igo1 contributes to Taf12 phosphorylation upon starvation. Our genetic analyses (Fig 5B and C) predicted that this function of Ppk18^{Gwl}-Igo1 would require PP2A-Pab1^{B55} activity. Indeed, we observed that the pattern of Taf12 phosphorylation is similar between *pab1Δ* single mutants and *pab1Δ igo1-S64A* double mutants (Fig 5E). Therefore, the absence of PP2A-Pab1^{B55} rescues the inability of *igo1-S64A* mutants to induce Taf12 phosphorylation. These observations indicate that, upon starvation, Ppk18^{Gwl}-Igo1 is important to inhibit PP2A-Pab1^{B55} activity toward Taf12 and allow its phosphorylation.

The TORC2-Gad8^{AKT} pathway induces Taf12 phosphorylation upon starvation

Our results show that, in rich conditions, Taf12 is de-phosphorylated by PP2A-Pab1^{B55} downstream of TORC1. Upon starvation, inhibition of PP2A-Pab1^{B55} by Ppk18^{Gwl}-Igo1 prevents Taf12 de-phosphorylation. However, Taf12 phosphorylation is expected to result from the opposing activities of the PP2A-Pab1^{B55} phosphatase, whose activity decreases upon starvation, and a kinase, whose activity should increase concomitantly. Indeed, we noticed that P-Taf12 levels still increase upon starvation of both starved PP2A-Pab1^{B55} and Ppk18^{Gwl}-Igo1 mutants (Figs 4D and 5D and E).

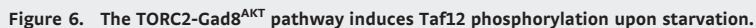
Our genetic analyses suggested that the TORC2-Gad8^{AKT} functionally interacts with SAGA to regulate differentiation (Fig 1C, D and F). We thus tested whether the TORC2-Gad8^{AKT} pathway

controls Taf12 phosphorylation upon starvation. Western blot analyses and quantifications revealed that, upon shifting cells to starvation conditions, Taf12 phosphorylation is reduced both in *tor1Δ* and in *gad8Δ* mutants, as compared to WT controls, whereas total Taf12 levels do not change (Fig 6A). We verified that this reduction is not an indirect consequence of the defects in G1 arrest and sexual differentiation of *tor1Δ* and *gad8Δ* mutants [38,62,63]. Both *sty1Δ* and *ssp2Δ* mutants are also unable to arrest in G1 and to differentiate upon starvation [42,45]. However, Taf12 phosphorylation remains unchanged in either *sty1Δ* or *ssp2Δ* mutants (Fig 6B), in agreement with our genetic analyses (Appendix Fig S1E–H).

We then determined whether Gad8^{AKT} interacts with Taf12, using a strain in which Taf12 and Gad8^{AKT} were tagged with a FLAG and a TAP epitope, respectively. Affinity purification and elution of TAP-tagged Gad8^{AKT} specifically recover FLAG-tagged Taf12, only in extracts from starved cells, suggesting that nutrient starvation promotes the interaction between Taf12 and Gad8^{AKT} *in vivo* (Fig 6C). We then tested whether Gad8^{AKT} is able to directly phosphorylate Taf12, by incubating affinity-purified endogenous Gad8^{AKT} with a recombinant fragment of Taf12, as well as a fragment of its well-characterized substrate Fkh2 as a positive control (Fig 6D, left and middle panels). Kinase assays revealed that Gad8^{AKT} phosphorylates Taf12 *in vitro*, as compared to a control “no tag” purification (Fig 6D, right panel). Importantly, using a Taf12-5A mutant substrate, we found that Gad8^{AKT} targets the same Ser/Thr residues that are phosphorylated upon starvation and de-phosphorylated by PP2A-Pab1^{B55}. We conclude that Taf12 is a substrate of the Gad8^{AKT} kinase, both *in vitro* and *in vivo*. Altogether, these results indicate that the TORC2-Gad8^{AKT} pathway mediates Taf12 phosphorylation in response to nutrient starvation.

Role of Taf12 phosphorylation during sexual differentiation

We next addressed the role of Taf12 phosphorylation *in vivo*. To do this, we quantified *ste11⁺* and *mei2⁺* expression and the number of differentiated cells in non-phosphorylated *taf12-5A* mutants. Surprisingly, both genes are more strongly induced upon starvation of *taf12-5A* mutants, as compared to WT controls (Fig 7A and B). In agreement with Gad8^{AKT} controlling Taf12 phosphorylation, the absence of Gad8^{AKT} does not suppress the increased expression of *ste11⁺* and *mei2⁺* in starved *taf12-5A* mutants (Appendix Fig S9). We then quantified the differentiation response of *taf12-5A* mutants,



A P-Taf12 was followed by anti-FLAG IB or protein extracts from WT, *tor1Δ*, and *gad8Δ* strains, grown in rich conditions (R) or starved for 45 min (S). An anti-tubulin IB is shown as a control for loading. The signal intensities of P-Taf12 and total Taf12 were quantified in each strain and condition. P-Taf12 to Taf2 ratios were calculated from three independent experiments and individually plotted in a graph below the IBs, together with the mean and SEM. Averaged values from all WT controls grown in rich medium were set at 1 to allow comparisons across culture conditions and mutant strains. Statistical significance was determined by two-way ANOVA followed by Bonferroni's multiple comparison tests ($n = 3$); $*P \leq 0.01$.

B P-Taf12 was followed by anti-FLAG IB of protein extracts from *sty1Δ* cells (left panel) or *ssp2Δ* cells (right panel), grown in rich conditions (R) or starved for 45 min (S). An anti-tubulin IB is shown as a control for loading. Shown are IBs that are representative of two independent experiments.

C TAP-tagged Gad8 was immuno-precipitated using IgG-Sepharose beads (IP) from strains containing FLAG-tagged Taf12, grown either in rich medium (left panels) or starved for 45 min (right panels). TAP-tagged Gad8 was eluted from beads using the TEV protease, releasing a shorter form of Gad8 (CBP-Gad8). Eluates were loaded and immunoblotted (IB) using anti-FLAG or anti-CBP antibodies, together with 1% of whole cell extracts (WCE), to detect Taf12 co-precipitation with Gad8. A strain which does not contain any TAP tag is shown as a negative control for the IP. Shown is an IB representative of two independent experiments.

D Endogenous Gad8-HA was affinity-purified from starved cells, in order to activate its kinase activity (left and middle panels), and mixed with recombinant, purified GST-Taf12, GST-Taf12-5A, or GST-Fkh2 proteins (right panels) in a kinase assay buffer. Each assay was then analyzed by IB and probed with an anti-phospho-AKT substrate antibody.

Data information: The star (*) symbols label unspecific bands detected by the FLAG or the CBP antibodies in *S. pombe*.

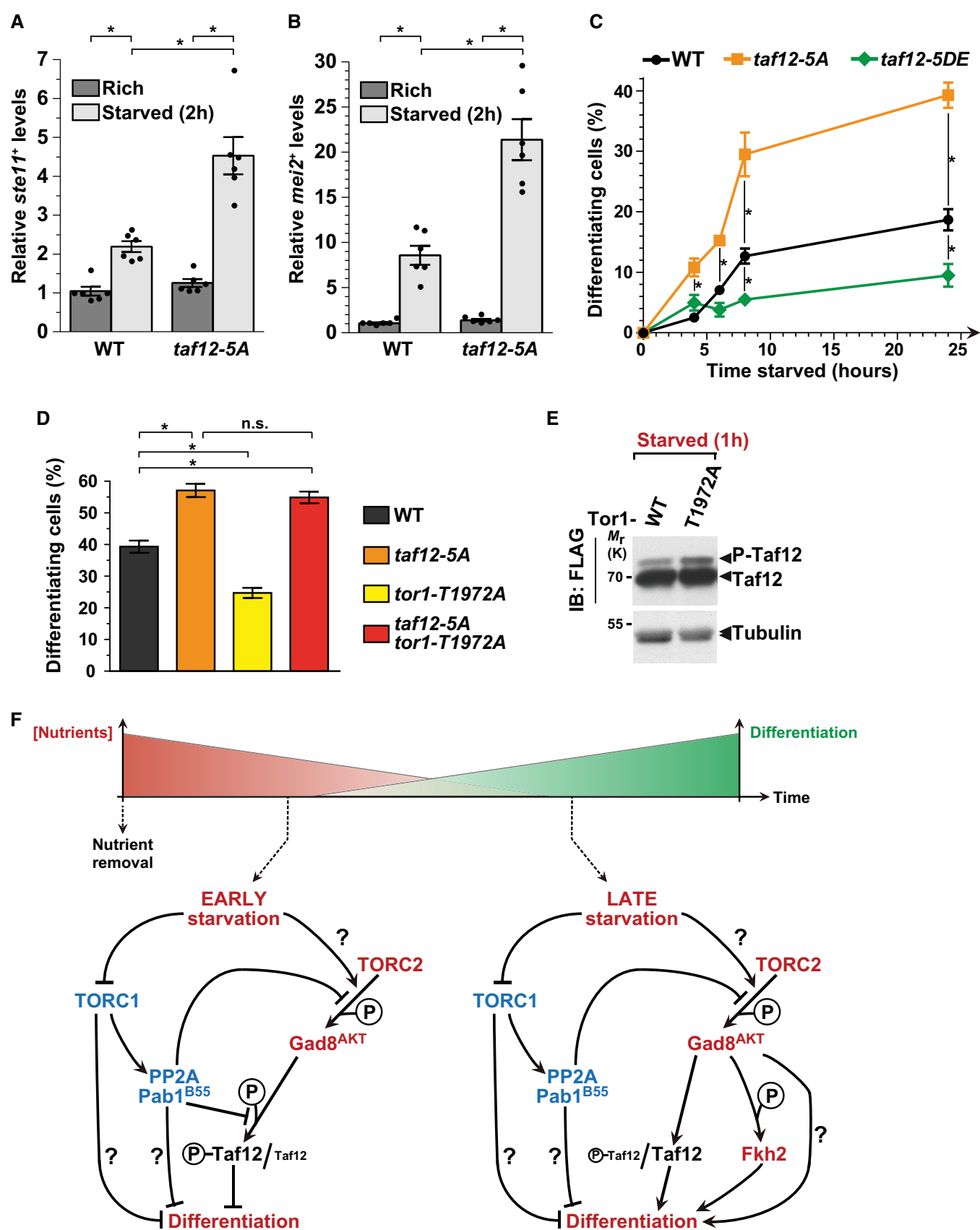


Figure 7.

Figure 7. Taf12 phosphorylation inhibits sexual differentiation downstream of TORC2.

- A, B Expression of *ste11⁺* (A) and *mei2⁺* (B) using quantitative RT-PCR of RNA extracted from cells grown either in rich medium (dark gray) or starved for 2 h (light gray). Cells of the following genotypes were analyzed: wild-type isogenic controls (WT) and *taf12-5A* mutants. *act1⁺* served as a control for normalization across samples. Values from a WT strain grown in rich medium were set at 1 to allow comparisons across culture conditions and mutant strains. Each column represents the mean value of six independent experiments, overlaid with individual data points and SEM. Statistical significance was determined by two-way ANOVA followed by Bonferroni's multiple comparison tests ($n = 6$); $*P \leq 0.01$.
- C, D Zygotes and tetrads, which correspond to differentiated cells, were counted from cultures of homothallic cells grown to mid-log phase in rich medium (t0) and shifted to starvation medium for up to 24 h (C) or from heterothallic cells mixed and incubated for 2 days on mating medium (D). Cells of the following genotypes were analyzed: wild-type isogenic controls (WT), *taf12-5A*, *taf12-5DE*, *tor1-T1972A*, and *taf12-5A tor1-T1972A*. Each value represents the mean percentage and SEM of differentiating cells to the total number of cells, averaged from six independent experiments. At least 200 cells from the indicated genotypes were counted in each experiment. Statistical significance was determined by two-way ANOVA followed by Tukey's multiple comparison tests ($n = 6$); $*P \leq 0.01$.
- E P-Taf12 was followed by anti-FLAG IB of protein extracts from WT and *tor1-T1972A* strains, grown in rich medium and shifted to starved conditions for 60 min. An anti-tubulin IB is shown as a control for loading. Shown is an IB which is representative of two independent experiments.
- F Proposed model for the regulation and role of Taf12 phosphorylation during the early and late steps following nutrient starvation in *S. pombe*. Question marks represent unknown regulatory pathways. See Discussion for details.

at various time points upon nutrient starvation. In agreement with our previous observations, *taf12-5A* mutants commit to differentiation more efficiently than WT cells (Fig 7C). To confirm this inhibitory role of Taf12 phosphorylation, we repeated this analysis using a strain in which all 5 Ser/Thr were mutated into aspartates (Asp) and glutamates (Glu) (*taf12-5DE*), to mimic the negative charge of phosphorylation (Fig 3C). Indeed, in contrast to *taf12-5A* mutants, we observed less differentiating cells in starved *taf12-5DE* mutants, as compared to WT controls (Fig 7C). We noticed, however, that Taf12 phosphorylation represses differentiation genes only in the early time points of starvation (Appendix Fig S9 and data not shown), consistent with P-Taf12 levels peaking early after starving cells (Fig 3I).

We did not expect Taf12 phosphorylation to inhibit differentiation because we showed that it is induced upon starvation, by TORC2-Gad8^{AKT}, which promotes differentiation. However, a previous study has shown that constitutive activation of the TORC2 kinase Tor1 inhibits differentiation, similarly to a loss of Tor1 function [41]. Therefore, although a basal level of TORC2-Gad8^{AKT} activity is required for cells to differentiate, it appears that TORC2-Gad8^{AKT} also buffers the differentiation response, for example to prevent too many cells from exiting the cell cycle immediately upon starvation. To address whether this function of TORC2 requires Taf12 phosphorylation, we determined the levels of P-Taf12 in a constitutively active mutant of Tor1, *tor1-T1972A* [41]. Western blotting of FLAG-tagged Taf12 revealed that its phosphorylation increases in starved *tor1-T1972A* mutants, as compared to WT controls (Fig 7E). Altogether, our results show that TORC2 activity positively correlates with Taf12 phosphorylation (Figs 6A and 7E). We then asked whether *tor1-T1972A* mutants differentiate less because of this increase in Taf12 phosphorylation. For this, we quantified sexual differentiation upon starvation of *taf12-5A tor1-T1972A* double mutants, as compared to single mutants and WT controls. We counted a similar number of differentiated cells between *taf12-5A tor1-T1972A* double mutants and *taf12-5A* single mutants, indicating that *taf12-5A* mutants rescue the reduced differentiation phenotype of *tor1-T1972A* single mutants (Fig 7D). To conclude, upon nutrient starvation, TORC2 functions as both an activator and an inhibitor of sexual differentiation, the latter being mediated by Taf12 phosphorylation.

Importantly, we did not find any evidence of a loss of Taf12 function in either *taf12-5A* or *taf12-5DE* mutants. First, although *S. pombe* Taf12 is essential for viability [29], both mutants are

viable and grow normally. Second, total protein staining of SAGA and TFIID complexes purified from either *taf12-5A* or *taf12-5DE* mutants, grown either in rich or starved conditions, revealed that the subunit composition of all mutant complexes is similar to that of WT cells, regardless of nutrient levels (Appendix Fig S10). Third, we did not observe any changes in the HAT activity of SAGA purified from either *taf12-5A* or *taf12-5DE* mutants, as compared to WT cells (Appendix Fig S11). Altogether, our results suggest that TORC2-Gad8^{AKT}-mediated phosphorylation of Taf12 is important to modulate the timing and the amplitude of the sexual differentiation response upon nutrient starvation.

Discussion

Although it is well established that transcriptional co-activator complexes regulate inducible genes, less is known about how they sense and respond to signaling cues. Here, we show that the SAGA and TFIID component Taf12 is differentially phosphorylated, depending on nutrient levels. Genetic and biochemical evidence support a model by which the opposing activities of the TORC1-PP2A^{B55} and TORC2-Gad8^{AKT} pathways control the level of Taf12 phosphorylation, differentiation gene expression, and the switch from proliferation to mating and meiosis, in response to nutrient availability (Fig 7F).

Convergence of the TORC1 and TORC2 pathways on a transcriptional regulator

Nutrient availability is sensed by a network of regulatory pathways, many of which control proliferation through the TOR kinase. TOR forms two distinct complexes, TORC1 and TORC2, which differ in their composition, regulation, and function [3,4]. Here, we uncovered a previously unknown feature of the TORC1 and TORC2 pathways, which activate distinct effectors, the PP2A phosphatase, and the Gad8^{AKT} kinase, respectively, to control the phosphorylation of the same target, Taf12. Taf12 is therefore an effector of the known, opposing regulatory roles of TORC1 and TORC2 in the control of gene expression and sexual differentiation in response to nutrients in *S. pombe* [7]. However, our genetic analyses also indicate that TORC1 and TORC2 regulate sexual differentiation through other effectors than Taf12 and SAGA. For example, the absence of Gcn5 cannot completely rescue the lack of differentiation observed when

TORC1 is constitutively activated or upon the loss of TORC2 (Fig 1). Future work will determine which other transcription factors and chromatin regulators contribute to the regulation of differentiation gene expression downstream of TORC1 and TORC2 in *S. pombe*.

Studies in various organisms have demonstrated that TORC1 promotes growth both by stimulating anabolic processes and by inhibiting stress responses, including through the regulation of RNA polymerase I-, II-, and III-dependent transcription [3]. For example, *S. cerevisiae* TORC1 represses nutrient stress-responsive genes by sequestering transcription factors in the cytoplasm, primarily through the Tap42-dependent inhibition of PP2A-related phosphatases. Likewise, when nutrients are present, *S. pombe* TORC1 represses the expression of the master regulators of sexual differentiation, but the mechanism of this regulation is less well characterized [8–12]. A previous study suggested that TORC1 inhibits meiosis through the phosphorylation-dependent degradation of Mei2 [12]. Our work establishes that SAGA, a co-activator of RNA polymerase II, is another important effector of TORC1 to regulate differentiation genes.

We found that TORC1 controls SAGA through Ppk18^{Gwl}-mediated inhibition of the PP2A^{B55} phosphatase. A very recent study proposed that a similar TORC1-activated signaling cascade inhibits sexual differentiation, through the de-phosphorylation of Gad8^{AKT} by PP2A^{B55}, thereby counteracting TORC2 activity [56]. Our work reveals that an additional substrate of the TORC1-PP2A^{B55} pathway contributes to control this process. However, we observed that Taf12 phosphorylation does not modulate sexual differentiation when cells are grown in nutrient rich conditions, indicating that PP2A^{B55} requires other effectors, possibly additional SAGA subunits, to inhibit differentiation when nutrients are present (Fig 7F).

TORC2 is also known to regulate RNA polymerase II-dependent transcription, through the activation of the AKT kinase, which phosphorylates and inhibits FOXO transcription factors in mammals [4]. In *S. pombe*, TORC2 and Gad8^{AKT} are activated upon starvation and required for cells to arrest in G1 and initiate sexual differentiation (Fig 1) [38,41,62,63]. Interestingly, an *S. pombe* FOXO transcription factor, Fkh2, is also required for *ste11*⁺ induction and sexual differentiation upon nitrogen starvation [64] and is phosphorylated by Gad8^{AKT} *in vitro* [39]. Recently, a mutational analysis revealed that Gad8^{AKT}-dependent phosphorylation of Fkh2 is critical for sexual differentiation [56]. Our results show that Taf12 phosphorylation is induced early upon starvation, positively correlates with TORC2 activity, but not any other nutrient-sensing pathway, and negatively correlates with sexual differentiation. We therefore propose that the TORC2-Gad8^{AKT} pathway coordinates the opposing activities of Fkh2 and Taf12 at the promoters of differentiation genes to synchronize their expression with starvation response and allow the sequential induction of cell cycle exit, conjugation, and meiosis (Fig 7F).

Role of Taf12 phosphorylation in sexual differentiation

Intriguingly, phenotypic analyses revealed that Taf12 phosphorylation inhibits sexual differentiation upon starvation (Figs 7A–E and Appendix Fig S9). This function appears contradictory with our observation that Taf12 becomes phosphorylated upon starvation, by TORC2-Gad8^{AKT}. However, hyper-activation of TORC2 upon

starvation inhibits differentiation, similar to a loss of TORC2 [41]. Here, we show that this inhibitory role of TORC2 is mediated, at least in part, by Taf12 phosphorylation (Fig 7D and E).

One possible interpretation is that the phosphorylated form of Taf12 buffers the amplitude of the sexual differentiation response until cells reach a critical level of starvation. Similar functions have been described for two RNA-binding proteins in *S. pombe* [65,66]. We propose that the ability of the TORC2-Gad8^{AKT} pathway to activate both a positive and a negative regulator of differentiation, Fkh2 and Taf12, respectively, contributes to buffering the differentiation response. Such a regulatory motif is reminiscent of an incoherent feedforward loop (Fig 7F), which can indeed establish pulse-like dynamics [67]. *Schizosaccharomyces pombe* may have evolved such regulation to ensure that not all cells in a population commit to meiosis and sporulation, particularly during a transient starvation event, because these processes are irreversible.

Another non-mutually exclusive possibility is that Taf12 phosphorylation sequesters it in the cytoplasm, therefore preventing it from inducing differentiation genes early upon starvation. Then, Taf12 protein levels increase, reducing the proportion of phosphorylated Taf12 (Fig 3I) and, possibly, promoting its nuclear translocation. The TORC2-Gad8^{AKT} pathway might be required for this increase in Taf12 levels. De-phosphorylated, nuclear Taf12 would induce the transcription of differentiating genes at later time points of starvation, to promote sexual differentiation once starvation has reached a critical level (Fig 7F).

Finally, we found that *ste11*⁺ and *mei2*⁺ expression is affected only at early time points of starvation in Taf12 phosphorylation mutants. Although this result is in agreement with our observation that P-Taf12 levels peak early after starvation, it is conceivable that Taf12 phosphorylation regulates the transcription of other important differentiation genes. Transcriptome analyses of differentiating *S. pombe* cells have indeed identified approximately 2,000 genes whose expression changes in successive waves that correlate with the timing of each step of sexual differentiation [68–70]. Finally, as opposed to Taf12 phosphorylation, we noted that Gad8^{AKT} does not modulate the expression of differentiation genes early upon starvation (Appendix Fig S9). This observation might reflect the fact that Gad8^{AKT} phosphorylates other substrates with an opposite function, such as Fkh2. Alternatively, Taf12 phosphorylation may be catalyzed by another kinase, which would be only active during the early steps following starvation.

Regulation of SAGA by Taf12 phosphorylation in response to environmental cues

We have previously shown that SAGA regulates the expression of differentiation genes and cell fate decisions in response to nutrient availability [28]. Here, we provide genetic and biochemical evidence that SAGA functions downstream of TORC1 and TORC2, but not of any other nutrient-sensing kinases. Several signaling pathways have already been shown to involve SAGA, consistent with its prominent role in the expression of stress-regulated genes. Proteomic analyses of SAGA purified from *S. cerevisiae* or human cells have identified several phosphorylation sites on distinct subunits, including Taf12 [71–73]. However, few studies, if any, have explored whether these modifications vary in response to specific cues or signaling pathways. Our work shows that Taf12, a core component of both SAGA

and TFIID, is rapidly and dynamically phosphorylated in response to changes in nutrient levels.

It is well established that co-activator complexes are primarily regulated through their recruitment by promoter-bound transcription factors. However, we showed that *S. pombe* SAGA is recruited to the promoters of differentiation genes regardless of nutrient levels, suggesting a different mode of regulation [28]. Importantly, Taf12 is also phosphorylated as part of the TFIID general transcriptional factor complex, which functions both redundantly and specifically with SAGA in the regulation of transcription initiation [74,75]. Future studies will elucidate the exact contribution of *S. pombe* TFIID to the regulation of differentiation genes and cell fate decisions in response to nutrient availability.

Regardless, we show here that nutrient availability dictates whether Taf12 is phosphorylated or not. However, we found that neither Taf12 phosphorylation nor nutrient availability affect SAGA or TFIID subunit composition. Similarly, SAGA HAT activity remains unchanged in Taf12 phosphorylation mutants. We therefore propose that Taf12 phosphorylation causes a conformational change within SAGA and/or TFIID, for example to coordinate their regulatory activities at specific promoters. Taf12 is indeed an integral component of the core TAF module of both SAGA and TFIID, in which it forms a histone-like dimer either with Ada1 or with Taf4, respectively [23,25,76–79]. This interaction is mediated by the histone-fold domain (HFD) of Taf12, which is highly conserved and supports its essential functions in *S. cerevisiae* [80]. All three phosphorylated Thr are outside, N-terminal to the HFD (Fig 3B). We therefore speculate that these modifications will not impact the overall assembly of the complex but, rather, cause a subtle structural reorganization of specific modules. High-resolution structural studies will determine whether Taf12 phosphorylation induces such structural rearrangements and how it modulates SAGA and TFIID regulatory functions.

Materials and Methods

Schizosaccharomyces pombe procedures, growth conditions, and differentiation tests

Standard culture media and genetic manipulations were used, as described in [81]. For all nutrient starvation experiments, prototrophic cells were inoculated in rich minimal medium (Edinburgh Minimal Medium, EMM + 5 g/l NH₄Cl and 2% glucose) and grown at 30°C to mid-log phase ($\sim 0.5 \times 10^7$ cells/ml). Cells were then pelleted at room temperature, washed once with starvation minimal medium (EMM without NH₄Cl and 0.5% glucose), inoculated in either rich or starved medium, and incubated for various times at 30°C. In the text, “nutrient starvation” thus refers to the complete removal of the nitrogen source and to a fourfold decrease in glucose concentration in the medium. For mating assays, homothallic prototrophs were grown as described above and the number of zygotes and asci was counted under differential interference contrast microscopy. Alternatively, heterothallic prototrophs were grown as described above, mixed in equal proportion, plated onto mating medium (SPAS), and incubated for 2 days at 25°C. The proportion of differentiating cells (%) was calculated by dividing the sum of zygotes (one zygote counted as two cells) plus asci (one ascus

counted as two cells) by the total number of cells (at least 200 cells). Torin-1 (4247/10, Tocris Bioscience), cAMP (A9501, Sigma), or thiamine (T4625, Sigma) were added to the medium at the time points and concentrations indicated.

Strain and plasmid constructions

All *S. pombe* strains used are listed in Appendix Table S2. Genetic crosses were performed by mating strains at 25°C on SPAS medium. Strains with gene deletions or epitope-tagged proteins were constructed by targeting the respective open reading frame (ORF) with *kanMX6*, *natMX6*, or *hphMX6* cassettes, using PCR-based gene targeting and lithium-acetate transformation, as described in [82–85]. For epitope tagging, the corresponding tag was fused to either the 5′ or 3′ end of the targeted ORF, removing either the initiating ATG or the stop codon, respectively. In each case, PCR amplification was performed using primers of 100 bases, with 80 bases to direct homologous recombination. All primers used are listed in Appendix Table S3. Transformants were screened for correct integration by PCR and Western blot analyses. Point mutations were knocked within specific genes using a pop in, pop out allele replacement strategy, as described in [86]. The integrating plasmids were constructed using the pKS-ura4 vector, in which PCR products, restriction digest products, or synthesized DNA fragments were sub-cloned using a Gibson assembly kit, according to the manufacturer’s instructions (New England Biolabs). Plasmids and strains containing point mutations were eventually verified by Sanger sequencing.

We generated several plasmids to generate distinct Taf12 phospho-mutant strains. First, DHB60 was synthesized with a fragment of the *taf12*⁺ gene, ranging from nucleotides (nt) +547 to +1,150 (+1 is defined as the A from the initiating codon) and comprising an A-to-T mutation, designed at nt +847 to replace Thr283 with an Ala283 residue. The DHO744-745 primer pair was then used to amplify *taf12*⁺ from DHB60. This product was assembled into pKS-ura4 together with three distinct PCR products, generated from *S. pombe* genomic DNA using DHO854-855, DHO856-857, and DHO858-859, to create DHB62. These PCR products encompass the first 566 base pairs (bp) of *taf12*⁺, the last 251 bp of *taf12*⁺ fused to an NdeI restriction site for genomic integration, and 590 bp of *taf12*⁺ 3′UTR, respectively. DHB62 was digested with NdeI and integrated into *S. pombe* using lithium-acetate transformation to generate DHP1205.

We then introduced additional single base-pair changes using the QuikChange Site-Directed Mutagenesis kit, according to the manufacturer’s instructions (Agilent Technologies). First, we used DHO909-910 and the DHB62 plasmid template to mutate *taf12*⁺ codons so that the Ser217, Thr218, Ser220, and Thr221 residues are each replaced with Ala residues, creating DHB63. Second, we used DHO1035-1036 and the DHB63 plasmids to replace these Ala residues with Asp217, Glu218, Asp220, and Glu221 residues, creating DHB64. Last, we used DHO1037-1038 and the DHB64 plasmids to replace the Thr283 residue of *taf12*⁺ with a Glu283 residue, creating DHB65. The DHB63 and DHB65 plasmids were digested with NdeI and integrated into *S. pombe* using lithium-acetate transformation to generate DHP1221 and DHP1222, respectively.

The *igo1-S64A* knock-in mutant strain was obtained using the two-step *delitto perfetto* procedure [87]. For this, a portion of the *igo1*⁺ gene, ranging from nt +29 to +571, was synthesized with a

TCA-to-GCT mutation at nt +499 to +501 to replace Ser64 with an Ala residue, generating DHB61. The DHO1120-1121 primer pair was then used to amplify *igo1*⁺ from DHB61, for *S. pombe* transformation and generation of DHP1210 and DHP1287.

RT-qPCR analysis

Quantitative PCR analyses of cDNA were performed using RNA extracted from 50 ml of exponentially growing cells. Total RNA was purified using hot, acidic phenol, and contaminating DNA was removed by DNase I digestion, using the TURBO DNA-free™ kit (Ambion). 1 µg of RNA was then reverse-transcribed (RT) at 55°C with random hexa-nucleotide primers or an oligo-dT primer, using the Invitrogen SuperScript III first-strand synthesis kit (Invitrogen). Fluorescence-based quantitative PCR was performed with SYBR Green, using Stratagene Mx3005P systems. The thermal cycling conditions comprised an initial denaturation at 95°C for 10 min, followed by 40 cycles at 95°C for 30 s, 60°C for 1 min, and 72°C for 1 min. All analyses were performed according to the MIQE guidelines [88]. Relative cDNA quantities were calculated using the Stratagene MxPro software, from the slope produced by standard curves. These were performed for each primer pair on at least one cDNA sample in each experiment. Standard curve slopes were comprised between −3.5 (90% efficiency) and −3.15 (110% efficiency), with an $r^2 > 0.9$. All primer sequences used are listed in Appendix Table S3.

Protein extractions

Protein extracts were prepared from 25 or 10 ml of exponentially growing cells, using either standard lysis buffer (LB: 40 mM HEPES-NaOH pH 7.4, 350 mM NaCl, 0.1% NP-40, and 10% glycerol) or trichloroacetic acid (TCA) precipitation, respectively. For standard lysis, LB was supplemented with protease inhibitors, including cOmplete EDTA-free cocktails tablets (04693132001, Roche), 100 mM PMSF, 1 mg/ml Bestatin, and 1 mg/ml pepstatin A, as well as phosphatase inhibitors, including 50 mM β-glycerophosphate, 1 mM NaF, and 1 mM Na₃VO₄. Glass beads were added to the cell suspension, and lysis was performed using FastPrep (MP Biomedicals). Beads were removed by centrifugation, and extracts were then cleared by centrifugation at 15,000 g, 4°C, for 10 min. For TCA extraction, cell pellets were washed once in 1 ml of 20% TCA and re-suspended in 100 µl of 20% TCA. Glass beads were added, and cells were lysed using a FastPrep (MP Biomedicals). 400 µl of 5% TCA was added to the homogenates that were then vortexed and spun at 15,000 g for 10 min. The pellet was re-suspended in 4× protein sample loading buffer, and the pH was adjusted with 1 M Tris base before boiling. 5 µl of each sample was loaded on a 10% SDS-acrylamide gel, which was stained with Coomassie blue or to normalize for protein amounts across samples.

Immuno-precipitations

Of 50–100 ml of exponentially growing cells was harvested and re-suspended in IP lysis buffer (IP-LB: 50 mM HEPES-NaOH pH 7.4, 150 mM NaCl, 0.5% NP-40, 1 mM EDTA, 10% glycerol), supplemented with protease inhibitors and, when necessary, with phosphatase inhibitors, as described for protein extraction. Following

lysis and extract clarification, 4–5 mg of total proteins was incubated first with 1–5 µg of anti-FLAG antibody (M2, Sigma), for 2 h at 4°C, and then with 50 µl of a 1:1 protein G Sepharose 4 Fast Flow slurry (GE Healthcare Life Sciences), for 1 h at 4°C. Three washes were performed in IP-LB without any protease or phosphatase inhibitors. Beads were eluted in 1× protein sample loading buffer and processed for Western blotting.

For TAP-Gad8 or TAP-Pab1 immuno-precipitations, proteins extracts were incubated overnight with 50 µl of a 1:1 IgG-Sepharose 6 Fast Flow slurry (GE Healthcare Life Sciences), for 2 h at 4°C. Three washes were performed in IP-LB without any protease or phosphatase inhibitors, followed by one wash in TEV buffer (10 mM Tris pH 8.0, 150 mM NaCl, 0.1% NP-40, 0.5 mM EDTA, 10% glycerol, 1 mM DTT). IgG beads were incubated for 1.5 h at room temperature in 100 µl of TEV buffer and 20 U of AcTEV protease (Invitrogen). IgG beads were then pelleted, and the supernatant was processed for Western blotting.

Tandem affinity purifications

Protein complexes were purified by the tandem affinity purification (TAP) method, as described previously [28,89], with minor modifications. 2–4 l of exponentially growing cells was harvested, snap-frozen, and ground in liquid nitrogen using a Freezer/Mill® (Spex SamplePrep). Following purifications, 20 mM EGTA eluates were concentrated and separated on 4–20% gradient SDS-polyacrylamide Tris-glycine gels (Bio-Rad). Total protein content was visualized either by silver staining, using the SilverQuest kit (Invitrogen), or using the SYPRO Ruby/Red protein stains (Molecular Probes), following the manufacturer's instructions. Stained gels were scanned and imaged using either direct light (Amersham Imager 600, GE Healthcare Life Sciences) or a fluorescence imaging system (Typhoon Trio, GE Healthcare Life Sciences). For analysis of phospho-protein content, EGTA eluates were delipidated and desalted using chloroform and methanol precipitation before loading. Phosphorylated proteins were visualized in gel by Pro-Q® Diamond staining, according to the manufacturer's instructions (Molecular Probes). Stained gels were imaged using a Typhoon Trio imager (GE Healthcare Life Sciences) (532 nm laser excitation, 580 nm emission filter). Quantification of signal intensity was performed from scanned gels using ImageJ [90].

Western blots

Western blotting was performed using a peroxidase-anti-peroxidase (PAP) antibody for detection of the TAP tag (P1291, Sigma), an anti-Calmodulin binding protein (CBP) antibody (RCBP-45A-Z, ICLab), an anti-Rpb1 antibody (8WG16, Covance), an anti-tubulin antibody (B-5-1-2, Sigma), an anti-FLAG antibody (M2, Sigma), an anti-MYC antibody (9E10, Agrobio), an anti-HA antibody (12CA5, Agrobio), an anti-phospho-AKT substrate (PAS, Cell Signaling Technology), and an anti-phospho-Ser546-Gad8^{AKT} antibody [40]. Protein concentrations were measured by the Bradford method and used to load equal amounts of proteins across samples. Quantification of signal intensity was performed using film exposures that were within the linear range of ECL detection, as verified by loading serial dilutions of one sample, and analyzed with Image Studio™ Lite 4.0 (LI-COR Biosciences). Typically, P-Taf12 levels were measured from longer

exposures, whereas total Taf12 levels were measured from shorter exposures.

For Phos-tag gels, 12% resolving SDS-acrylamide gels were supplemented with 50 μ M Phos-tagTM-acrylamide (AAL-107, Wako) and 100 μ M MnCl₂. TCA-extracted samples were run at 30 mA for 2 h. Gels were washed twice in transfer buffer (25 mM Tris-HCl, 250 mM glycine) containing 1 mM EDTA and once without EDTA, before being processed for Western blotting.

Phosphatase assays

TAP-Pab1 and Taf12-FLAG were affinity-purified separately, as described above, from 100 to 200 ml of exponentially growing cells. For TAP-Pab1, IgG beads were washed three times in IP-LB, once in phosphatase buffer (50 mM HEPES-NaOH pH 7.4, 100 mM NaCl, 0.1% NP-40, 2 mM MnCl₂, 2 mM DTT), re-suspended in 100 μ l phosphatase buffer containing 10 U of AcTEV protease, and incubated at room temperature for 1.5 h. Equal amounts of the supernatant, normalized on the signal intensity of CBP-Pab1, were mixed with Taf12-FLAG-bound protein G Sepharose beads, with and without 0.5 μ M microcystin. Reactions were incubated for 40 min at 30°C, before processing for Western blotting. For λ -phosphatase treatment of Taf12-FLAG immuno-precipitates, protein G Sepharose beads were re-suspended in 100 μ l λ -phosphatase buffer containing 1 mM MnCl₂, with and without 1 μ l of λ -phosphatase enzyme, and incubated for 35' at 30°C. As a control, 1 mM NaF and 1 mM Na₃VO₄ were added to inhibit phosphatase activity. Reactions were stopped by adding 4 \times protein sample loading buffer and boiling at 95°C for 10 min.

Kinase assays

PCR fragments ranging from nucleotides (nt) +439 to +1011, corresponding to residues Leu147 to Asp337, of the *S. pombe* *taf12* gene were amplified from genomic DNA of either DHP148 (WT) or DHP1221 (*taf12*-5A mutants), using DHO1393-1394. These fragments were sub-cloned into pGEX-4T2 (GE Healthcare Life Sciences), 3' and in frame to the GST coding sequence, using a Gibson assembly kit (New England Biolabs) to generate the DHB82 and DHB83 plasmids, respectively. Recombinant GST-Taf12 and GST-Taf12-5A were produced by IPTG induction of transformed BL21 strains, purified on a column of 200 μ l of glutathione Sepharose 4B (GE Healthcare Life Sciences) for 2 h at 4°C, and eluted using 10 mM reduced glutathione. As a positive control, a fragment corresponding to amino acid residues 209–411 of Fkh2 [39] was cloned, expressed, and purified using an identical strategy. Endogenous Gad8-HA was affinity-purified, as described above, from 100 ml of *S. pombe* cells that were grown in rich medium and starved for nitrogen for 30 min, to activate Gad8^{AKT}. 10 μ g of recombinant GST-Taf12 or GST-Taf12-5A was mixed with Gad8-HA-bound protein G Sepharose beads and incubated for 30 min at 30°C, in kinase buffer (25 mM Tris-HCl pH 8.0, 10 mM MgCl₂, 100 μ M ATP, 1 mM DTT). Reactions were stopped by adding 4 \times protein sample loading buffer and boiling at 95°C for 10 min.

HAT assays

Histone acetyltransferase (HAT) assays were performed with 10% of TEV eluates of purified SAGA complexes, using the EpiQuikTM

HAT Activity/Inhibition Assay Kit (Epigentek), according to the manufacturer's instructions.

SILAC and mass spectrometry analyses

SILAC procedure for SAGA purification analyses

For SILAC analyses of purified SAGA, lysine auxotrophs (DHP828: *h⁻lys1-131 spt7-HA3-TAP2::kanMX6*) were pre-cultured in minimal rich medium (EMM) supplemented with 225 mg/l of either "light" L-lysine or "heavy" L-lysine (¹³C₆-¹⁵N₂-L-lysine, Cambridge Isotope Laboratories), for more than twelve doublings, to maximize metabolic labeling of proteins. Cells were grown to mid-logarithmic phase, either in 2 l of EMM supplemented with 45 mg/l of either "light" L-lysine or "heavy" L-lysine. The "light" L-lysine culture was then shifted to starved medium, without any L-lysine, for 45 min. A reverse labeling scheme was used in an independent replicate of this experiment. Cells were harvested, snap-frozen, and weighted. Equal quantities of dried cells were pooled before TAP purification, which was performed as described above, using Spt7-TAP as the bait. EGTA eluates were processed for silver staining and for mass spectrometry analysis.

Mass spectrometry (MS) analysis

Peptides were re-suspended in 5% formic acid, 5% acetonitrile and loaded onto a 100- μ m ID \times 3-cm precolumn packed with Maccel C18 1.9- μ m, 200-Å particles (The Nest Group) for nRPLC-MS/MS analysis in a Velos Orbitrap mass spectrometer (Thermo Fisher). Peptides were eluted over a 100- μ m ID \times 30-cm analytical column packed with the same material. Gradient conditions were tailored to the complexity and chemical properties of each sample; generally, the gradient was 9–32% acetonitrile in 0.15% formic acid over the course of 90 min. All MS spectra were collected with Orbitrap detection. MS/MS spectra were collected in the linear ion trap; the 20 most abundant ions were selected in a data-dependent manner.

Identification and quantification of peptides, proteins, and modifications

MS/MS spectra were searched with Comet [91] against the *S. pombe* proteome (downloaded November 19, 2015). The precursor mass tolerance was set to 50 p.p.m., and the fragment ion tolerance was set to 0.36 Da with a 0.11-Da offset. Variable modification of methionine oxidation (15.994914 Da), serine, threonine, and tyrosine phosphorylation (79.966331 Da) was used for all searches. For SILAC experiments, an additional variable modification of heavy lysine (8.014198 Da) was considered. Search results were filtered to a 1% FDR at PSM level using Percolator [92]. Phosphorylation sites were localized using an in-house implementation of the Ascore algorithm [93]. Phosphorylation sites with an Ascore > 13 (*P* < 0.05) were considered confidently localized. Peptides were quantified using in-house software measuring chromatographic peak maximum intensities. The peak maxima for peptides with the same combination of modification sites were summed before calculating a ratio. Proteins were quantified by first summing maximum peak intensities of all unmodified peptides for a given protein. The ratio was calculated between the sum of all peptides for a protein from heavy-labeled cells and the sum from light-labeled cells. In instances in which only the light or heavy form was identified, the noise signal level was used as the signal of the missing peptide.

SILAC and mass spectrometry analyses of total protein extracts

For SILAC analyses of total protein extracts, auxotrophic strains were cultured in minimal medium (EMM) supplemented with 225 mg/l of either “light” L-lysine and L-arginine (Lys-0/Arg-0) or “medium” L-lysine and L-arginine ($^2\text{H}_4$ -L-lysine/ $^{13}\text{C}_6$ -arginine, Lys4/Arg6). Supernatants derived from the “light”- and “medium”-labeled cell cultures were combined, and proteins were precipitated at -20°C using ice-cold acetone/methanol left on ice overnight. The proteins were pelleted by centrifugation (2,200 g, 20 min, 4°C) and washed with 80% ice-cold acetone. Dried proteins were resolved in digestion buffer (6 M urea, 2 M thiourea, 10 mM Tris, pH 8.0) and mixed in 1:1 ratio according to measured protein amounts. The mixtures were digested in solution with trypsin as described previously [94]. For proteome analyses, 100 μg of the mixtures was fractionated by isoelectric focusing on an OffGel 3100 Fractionator (Agilent) according to the manufacturer’s instructions. Focusing was performed using 13-cm (12-well) Immobiline DryStrips pH 3–10 (Bio-Rad) at a maximum current of 50 μA for 24 kVh. Peptide fractions were collected and desalted separately using C18 StageTips [95].

For phospho-proteome analyses, 8 mg of each peptide mixture was subjected to phospho-peptide enrichment as described previously [96], with minor modifications: Peptides were separated by strong cation-exchange (SCX) chromatography with a gradient of 0–35% SCX solvent B resulting in seven fractions that were subjected to phospho-peptide enrichment by TiO_2 beads. Elution from the beads was performed three times with 100 μl of 40% ammonia hydroxide solution in 60% acetonitrile (pH > 10.5). Fractions rich in peptides were subjected to multiple TiO_2 enrichment. Enrichment of phospho-peptides from the SCX flow-through was completed in five cycles.

LC-MS/MS analyses were performed on an EasyLC nano-HPLC (Proxeon Biosystems) coupled to an LTQ Orbitrap XL (Thermo Scientific) for phospho-peptide analyses, or an LTQ Orbitrap Elite mass spectrometer (Thermo Scientific) for proteome analyses as described previously [97]. The peptide mixtures were injected onto the column in HPLC solvent A (0.5% acetic acid) at a flow rate of 500 nl/min and subsequently eluted with a 87-min (proteome) or a 127-min (phospho-proteome) segmented gradient of 5–33–90% HPLC solvent B (80% ACN in 0.5% acetic acid). During peptide elution, the flow rate was kept constant at 200 nl/min. For proteome analysis, the twenty most intense precursor ions were sequentially fragmented in each scan cycle. For the phospho-proteome analysis, the five most intense precursor ions were fragmented by multistage activation of neutral loss ions at -98 , -49 , and -32.6 Th relative to the precursor ion [98]. In all measurements, sequenced precursor masses were excluded from further selection for 90 s. Full scans were acquired at resolution of 60,000 (Orbitrap XL) or 120,000 (Orbitrap Elite). The target values were set to 5,000 charges for the LTQ (MS/MS) and 106 charges for the Orbitrap (MS), respectively; maximum allowed fill times were 150 ms (LTQ) and 1,000 ms (Orbitrap). The lock mass option was used for real-time recalibration of MS spectra [96].

The MS data of all SILAC experiments were processed using default parameters of the MaxQuant software (v1.2.2.9) [99]. Extracted peak lists were submitted to database search using the Andromeda search engine [100] to query a target-decoy [101] database of *S. pombe* proteome (<http://www.pombase.org/>, Protein

Dataset in FASTA format, downloaded on the April 6, 2011), containing 5,076 protein entries and 248 commonly observed contaminants.

Statistics

Statistical tests were performed using GraphPad Prism. *t*-Tests were used when comparing two means. One-way or two-way analyses of variance (ANOVA) were performed for comparing more than two means, across one (for example “genotype”) or two distinct variables (for example “genotype” and “nutrients”). ANOVAs were followed by Bonferroni or Tukey *post hoc* pairwise comparisons. An α level of 0.01 was used *a priori* for all statistical tests, except otherwise indicated. Comparisons that are statistically significant ($P \leq 0.01$) are marked with the star sign (*), whereas those that are statistically not significant ($P > 0.01$) are labeled n.s.

Expanded View for this article is available online.

Acknowledgements

We thank Sandra Lopez-Aviles for sharing strains, protocols, and ideas, as well as Bérengère Pradet-Balade and Fred Winston for critical reading of the manuscript. We thank an anonymous referee for contributing to the proposed model in Fig 7F. We also thank Gwendaline Lledo for invaluable technical assistance and all members of the Helmlinger laboratory for helpful suggestions and discussions. We are grateful to Fuyu Tamanoi (UCLA, USA), Tomohiro Matsumoto (Kyoto University, Japan), and Masayuki Yamamoto (University of Tokyo, Japan) for sharing strains. T.L. is a recipient of graduate fellowships from the Labex EpiGenMed and from the Fondation ARC pour la Recherche Contre le Cancer. D.D. is a recipient of a graduate fellowship from the Ligue Contre le Cancer. Y.R. was a recipient of post-doctoral fellowships from the University of Montpellier and the Fondation pour la Recherche Médicale. This work has benefited from support by the Labex EpiGenMed, an “Investissements d’avenir” program (ANR-10-LABX-12-01). This work was supported by funds from the CNRS (ATIP-Avenir), the FP7 Marie Curie Actions (FP7-PEOPLE-2012-CIG/COACTIVATOR), the Fondation ARC (PJA-20131200471), and the Agence Nationale de la Recherche (ANR-15-CE12-0009-01) to D.H.

Author contributions

DH designed and supervised the project; TL, DD, CF, YR, and DH designed experiments, performed research, and analyzed data; RAR-M performed the SILAC analyses of purified SAGA, supervised by JV; MF-W and KK performed the SILAC analyses of total protein extracts, supervised by BM and JP; DH wrote the manuscript, and all authors reviewed and approved the manuscript.

Conflict of interest

The authors declare that they have no conflict of interest.

References

- de Nadal E, Ammerer G, Posas F (2011) Controlling gene expression in response to stress. *Nat Rev Genet* 12: 833–845
- Yuan H-XX, Xiong Y, Guan K-LL (2013) Nutrient sensing, metabolism, and cell growth control. *Mol Cell* 49: 379–387
- Loewith R, Hall MN (2011) Target of rapamycin (TOR) in nutrient signaling and growth control. *Genetics* 189: 1177–1201

4. Laplante M, Sabatini DM (2012) mTOR signaling in growth control and disease. *Cell* 149: 274–293
5. Otsubo Y, Yamamoto M (2008) TOR signaling in fission yeast. *Crit Rev Biochem Mol Biol* 43: 277–283
6. Davie E, Petersen J (2012) Environmental control of cell size at division. *Curr Opin Cell Biol* 24: 838–844
7. Otsubo Y, Yamamoto M (2012) Signaling pathways for fission yeast sexual differentiation at a glance. *J Cell Sci* 125: 2789–2793
8. Shinozaki-Yabana S, Watanabe Y, Yamamoto M (2000) Novel WD-repeat protein Mip1p facilitates function of the meiotic regulator Mei2p in fission yeast. *Mol Cell Biol* 20: 1234–1242
9. Alvarez B, Moreno S (2006) Fission yeast Tor2 promotes cell growth and represses cell differentiation. *J Cell Sci* 119: 4475–4485
10. Matsuo T, Otsubo Y, Urano J, Tamanoi F, Yamamoto M (2007) Loss of the TOR kinase Tor2 mimics nitrogen starvation and activates the sexual development pathway in fission yeast. *Mol Cell Biol* 27: 3154–3164
11. Valbuena N, Moreno S (2010) TOR and PKA pathways synergize at the level of the Ste11 transcription factor to prevent mating and meiosis in fission yeast. *PLoS One* 5: e11514
12. Otsubo Y, Yamashita A, Ohno H, Yamamoto M (2014) *Schizosaccharomyces pombe* TORC1 activates the ubiquitin-proteasomal degradation of the meiotic regulator Mei2 in cooperation with Pat1 kinase. *J Cell Sci* 127: 2639–2646
13. Rando OJ, Winston F (2012) Chromatin and transcription in yeast. *Genetics* 190: 351–387
14. Koutelou E, Hirsch CL, Dent SY (2010) Multiple faces of the SAGA complex. *Curr Opin Cell Biol* 22: 374–382
15. Weake VM, Workman JL (2012) SAGA function in tissue-specific gene expression. *Trends Cell Biol* 22: 177–184
16. Grant PA, Duggan L, Côté J, Roberts SM, Brownell JE, Candau R, Ohba R, Owen-Hughes T, Allis CD, Winston F et al (1997) Yeast Gcn5 functions in two multisubunit complexes to acetylate nucleosomal histones: characterization of an Ada complex and the SAGA (Spt/Ada) complex. *Genes Dev* 11: 1640–1650
17. Grant PA, Eberharter A, John S, Cook RG, Turner BM, Workman JL (1999) Expanded lysine acetylation specificity of Gcn5 in native complexes. *J Biol Chem* 274: 5895–5900
18. Sterner DE, Grant PA, Roberts SM, Duggan LJ, Belotserkovskaya R, Pacella LA, Winston F, Workman JL, Berger SL (1999) Functional organization of the yeast SAGA complex: distinct components involved in structural integrity, nucleosome acetylation, and TATA-binding protein interaction. *Mol Cell Biol* 19: 86–98
19. Bhaumik SR, Green MR (2002) Differential requirement of SAGA components for recruitment of TATA-box-binding protein to promoters *in vivo*. *Mol Cell Biol* 22: 7365–7371
20. Horiuchi J, Silverman N, Piña B, Marcus GA, Guarente L (1997) ADA1, a novel component of the ADA/GCN5 complex, has broader effects than GCN5, ADA2, or ADA3. *Mol Cell Biol* 17: 3220–3228
21. Grant PA, Schieltz D, Pray-Grant MG, Steger DJ, Reese JC, Yates JR, Workman JL (1998) A subset of TAF(II)s are integral components of the SAGA complex required for nucleosome acetylation and transcriptional stimulation. *Cell* 94: 45–53
22. Wu P-YJ, Winston F (2002) Analysis of Spt7 function in the *Saccharomyces cerevisiae* SAGA coactivator complex. *Mol Cell Biol* 22: 5367–5379
23. Wu P-YJ, Ruhlmann C, Winston F, Schultz P (2004) Molecular architecture of the *S. cerevisiae* SAGA complex. *Mol Cell* 15: 199–208
24. Durand A, Bonnet J, Fournier M, Chavant V, Schultz P (2014) Mapping the deubiquitination module within the SAGA complex. *Structure* 22: 1553–1559
25. Han Y, Luo J, Ranish J, Hahn S (2014) Architecture of the *Saccharomyces cerevisiae* SAGA transcription coactivator complex. *EMBO J* 33: 2534–2546
26. Setiawati D, Ross JD, Lu S, Cheng DT, Dong MQ, Yip CK (2015) Conformational flexibility and subunit arrangement of the modular yeast Spt-Ada-Gcn5 acetyltransferase complex. *J Biol Chem* 290: 10057–10070
27. Yu Y, Eriksson P, Bhoite LT, Stillman DJ (2003) Regulation of TATA-binding protein binding by the SAGA complex and the Nhp6 high-mobility group protein. *Mol Cell Biol* 23: 1910–1921
28. Helmlinger D, Marguerat S, Villén J, Gygi SP, Bähler J, Winston F (2008) The *S. pombe* SAGA complex controls the switch from proliferation to sexual differentiation through the opposing roles of its subunits Gcn5 and Spt8. *Genes Dev* 22: 3184–3195
29. Helmlinger D, Marguerat S, Villén J, Swaney DL, Gygi SP, Bähler J, Winston F (2011) Tra1 has specific regulatory roles, rather than global functions, within the SAGA co-activator complex. *EMBO J* 30: 2843–2852
30. Anandhakumar J, Fauquenoy S, Materne P, Migeot V, Hermand D (2013) Regulation of entry into gametogenesis by Ste11: the endless game. *Biochem Soc Trans* 41: 1673–1678
31. Mach KE, Furge KA, Albright CF (2000) Loss of Rhb1, a Rheb-related GTPase in fission yeast, causes growth arrest with a terminal phenotype similar to that caused by nitrogen starvation. *Genetics* 155: 611–622
32. Nakase Y, Fukuda K, Chikashige Y, Tsutsumi C, Morita D, Kawamoto S, Ohnuki M, Hiraoka Y, Matsumoto T (2006) A defect in protein farnesylation suppresses a loss of *Schizosaccharomyces pombe* tsc2+, a homolog of the human gene predisposing to tuberous sclerosis complex. *Genetics* 173: 569–578
33. Urano J, Sato T, Matsuo T, Otsubo Y, Yamamoto M, Tamanoi F (2007) Point mutations in TOR confer Rheb-independent growth in fission yeast and nutrient-independent mammalian TOR signaling in mammalian cells. *Proc Natl Acad Sci USA* 104: 3514–3519
34. Murai T, Nakase Y, Fukuda K, Chikashige Y, Tsutsumi C, Hiraoka Y, Matsumoto T (2009) Distinctive responses to nitrogen starvation in the dominant active mutants of the fission yeast Rheb GTPase. *Genetics* 183: 517–527
35. Watanabe Y, Lino Y, Furuhashi K, Shimoda C, Yamamoto M (1988) The *S. pombe* mei2 gene encoding a crucial molecule for commitment to meiosis is under the regulation of cAMP. *EMBO J* 7: 761–767
36. Sugimoto A, Iino Y, Maeda T, Watanabe Y, Yamamoto M (1991) *Schizosaccharomyces pombe* ste11+ encodes a transcription factor with an HMG motif that is a critical regulator of sexual development. *Genes Dev* 5: 1990–1999
37. Davidson MK, Shandilya HK, Hirota K, Ohta K, Wahls WP (2004) Atf1-Pcr1-M26 complex links stress-activated MAPK and cAMP-dependent protein kinase pathways via chromatin remodeling of cgs2+. *J Biol Chem* 279: 50857–50863
38. Matsuo T, Kubo Y, Watanabe Y, Yamamoto M (2003) *Schizosaccharomyces pombe* AGC family kinase Gad8p forms a conserved signaling module with TOR and PDK1-like kinases. *EMBO J* 22: 3073–3083
39. Ikeda K, Morigasaki S, Tatebe H, Tamanoi F, Shiozaki K (2008) Fission yeast TOR complex 2 activates the AGC-family Gad8 kinase essential for stress resistance and cell cycle control. *Cell Cycle* 7: 358–364

40. Du W, Hálová L, Kirkham S, Atkin J, Petersen J (2012) TORC2 and the AGC kinase Gad8 regulate phosphorylation of the ribosomal protein S6 in fission yeast. *Biol Open* 1: 884–888
41. Hálová L, Du W, Kirkham S, Smith DL, Petersen J (2013) Phosphorylation of the TOR ATP binding domain by AGC kinase constitutes a novel mode of TOR inhibition. *J Cell Biol* 203: 595–604
42. Valbuena N, Moreno S (2012) AMPK phosphorylation by Ssp1 is required for proper sexual differentiation in fission yeast. *J Cell Sci* 125: 2655–2664
43. Davie E, Forte GM, Petersen J (2015) Nitrogen regulates AMPK to control TORC1 signaling. *Curr Biol* 25: 445–454
44. Kato T, Okazaki K, Murakami H, Stettler S, Fantes PA, Okayama H (1996) Stress signal, mediated by a Hog1-like MAP kinase, controls sexual development in fission yeast. *FEBS Lett* 378: 207–212
45. Shiozaki K, Russell P (1996) Conjugation, meiosis, and the osmotic stress response are regulated by Spc1 kinase through Atf1 transcription factor in fission yeast. *Genes Dev* 10: 2276–2288
46. Elmlund H, Baraznenok V, Linder T, Szilagy Z, Rofougaran R, Hofer A, Hebert H, Lindahl M, Gustafsson CM (2009) Cryo-EM reveals promoter DNA binding and conformational flexibility of the general transcription factor TFIID. *Structure* 17: 1442–1452
47. Nakashima A, Sato T, Tamanoi F (2010) Fission yeast TORC1 regulates phosphorylation of ribosomal S6 proteins in response to nutrients and its activity is inhibited by rapamycin. *J Cell Sci* 123: 777–786
48. Sarbassov DD, Guertin DA, Ali SM, Sabatini DM (2005) Phosphorylation and regulation of Akt/PKB by the rictor-mTOR complex. *Science* 307: 1098–1101
49. De Virgilio C, Loewith R (2006) Cell growth control: little eukaryotes make big contributions. *Oncogene* 25: 6392–6415
50. Sarkar S, Dalgaard JZ, Millar JB, Arumugam P (2014) The Rim15-endo-sulfine-PP2ACdc55 signalling module regulates entry into gametogenesis and quiescence via distinct mechanisms in budding yeast. *PLoS Genet* 10: e1004456
51. Janssens V, Goris J (2001) Protein phosphatase 2A: a highly regulated family of serine/threonine phosphatases implicated in cell growth and signalling. *Biochem J* 353: 417–439
52. Kinoshita N, Ohkura H, Yanagida M (1990) Distinct, essential roles of type 1 and 2A protein phosphatases in the control of the fission yeast cell division cycle. *Cell* 63: 405–415
53. Kinoshita K, Nemoto T, Nabeshima K, Kondoh H, Niwa H, Yanagida M (1996) The regulatory subunits of fission yeast protein phosphatase 2A (PP2A) affect cell morphogenesis, cell wall synthesis and cytokinesis. *Genes Cells* 1: 29–45
54. Jiang W, Hallberg RL (2000) Isolation and characterization of par1(+) and par2(+): two *Schizosaccharomyces pombe* genes encoding B' subunits of protein phosphatase 2A. *Genetics* 154: 1025–1038
55. Grallert A, Boke E, Hagting A, Hodgson B, Connolly Y, Griffiths JR, Smith DL, Pines J, Hagan IM (2015) A PP1-PP2A phosphatase relay controls mitotic progression. *Nature* 517: 94–98
56. Martin R, Portantier M, Chica N, Nyquist-Andersen M, Mata J, Lopez-Aviles S (2017) A PP2A-B55-mediated crosstalk between TORC1 and TORC2 regulates the differentiation response in fission yeast. *Curr Biol* 27: 175–188
57. Thoreen CC, Kang SA, Chang JW, Liu Q, Zhang J, Gao Y, Reichling LJ, Sim T, Sabatini DM, Gray NS (2009) An ATP-competitive mammalian target of rapamycin inhibitor reveals rapamycin-resistant functions of mTORC1. *J Biol Chem* 284: 8023–8032
58. Atkin J, Halova L, Ferguson J, Hitchin JR, Lichawska-Cieslar A, Jordan AM, Pines J, Wellbrock C, Petersen J (2014) Torin1-mediated TOR kinase inhibition reduces Wee1 levels and advances mitotic commitment in fission yeast and HeLa cells. *J Cell Sci* 127: 1346–1356
59. De Virgilio C (2012) The essence of yeast quiescence. *FEMS Microbiol Rev* 36: 306–339
60. Lorca T, Castro A (2013) The Greatwall kinase: a new pathway in the control of the cell cycle. *Oncogene* 32: 537–543
61. Chica N, Rozalen AE, Perez-Hidalgo L, Rubio A, Novak B, Moreno S (2016) Nutritional control of cell size by the greatwall-endosulfine-PP2A.B55 pathway. *Curr Biol* 26: 319–330
62. Kawai M, Nakashima A, Ueno M, Ushimaru T, Aiba K, Doi H, Uritani M, Not Available Not A (2001) Fission yeast tor1 functions in response to various stresses including nitrogen starvation, high osmolarity, and high temperature. *Curr Genet* 39: 166–174
63. Weisman R, Choder M (2001) The fission yeast TOR homolog, tor1+, is required for the response to starvation and other stresses via a conserved serine. *J Biol Chem* 276: 7027–7032
64. Shimada M, Yamada-Namikawa C, Murakami-Tonami Y, Yoshida T, Nakanishi M, Urano T, Murakami H (2008) Cdc2p controls the forkhead transcription factor Fkh2p by phosphorylation during sexual differentiation in fission yeast. *EMBO J* 27: 132–142
65. Tsukahara K, Yamamoto H, Okayama H (1998) An RNA binding protein negatively controlling differentiation in fission yeast. *Mol Cell Biol* 18: 4488–4498
66. Jeong HT, Ozoe F, Tanaka K, Nakagawa T, Matsuda H, Kawamukai M (2004) A novel gene, msa1, inhibits sexual differentiation in *Schizosaccharomyces pombe*. *Genetics* 167: 77–91
67. Alon U (2007) Network motifs: theory and experimental approaches. *Nat Rev Genet* 8: 450–461
68. Mata J, Lyne R, Burns G, Bähler J (2002) The transcriptional program of meiosis and sporulation in fission yeast. *Nat Genet* 32: 143–147
69. Mata J, Bähler J (2006) Global roles of Ste11p, cell type, and pheromone in the control of gene expression during early sexual differentiation in fission yeast. *Proc Natl Acad Sci USA* 103: 15517–15522
70. Amorim MJ, Cotobal C, Duncan C, Mata J (2010) Global coordination of transcriptional control and mRNA decay during cellular differentiation. *Mol Syst Biol* 6: 380
71. Mischerikow N, Spedale G, Altelaar AF, Timmers HT, Pijnappel WW, Heck AJ (2009) In-depth profiling of post-translational modifications on the related transcription factor complexes TFIID and SAGA. *J Proteome Res* 8: 5020–5030
72. Chen SH, Albuquerque CP, Liang J, Suhandynata RT, Zhou H (2010) A proteome-wide analysis of kinase-substrate network in the DNA damage response. *J Biol Chem* 285: 12803–12812
73. Spedale G, Timmers HT, Pijnappel WW (2012) ATAC-king the complexity of SAGA during evolution. *Genes Dev* 26: 527–541
74. Lee TI, Causton HC, Holstege FC, Shen WC, Hannett N, Jennings EG, Winston F, Green MR, Young RA (2000) Redundant roles for the TFIID and SAGA complexes in global transcription. *Nature* 405: 701–704
75. Huisinga KL, Pugh BF (2004) A genome-wide housekeeping role for TFIID and a highly regulated stress-related role for SAGA in *Saccharomyces cerevisiae*. *Mol Cell* 13: 573–585
76. Gangloff YG, Werten S, Romier C, Carre L, Poch O, Moras D, Davidson I (2000) The human TFIID components TAF(II)135 and TAF(II)20 and the yeast SAGA components ADA1 and TAF(II)68 heterodimerize to form histone-like pairs. *Mol Cell Biol* 20: 340–351

77. Selleck W, Howley R, Fang Q, Podolny V, Fried MG, Buratowski S, Tan S (2001) A histone fold TAF octamer within the yeast TFIID transcriptional coactivator. *Nat Struct Biol* 8: 695–700
78. Brand M, Leurent C, Mallouh V, Tora L, Schultz P (1999) Three-dimensional structures of the TAFII-containing complexes TFIID and TFTC. *Science* 286: 2151–2153
79. Bieniossek C, Papai G, Schaffitzel C, Garzoni F, Chaillet M, Scheer E, Papadopoulos P, Tora L, Schultz P, Berger I (2013) The architecture of human general transcription factor TFIID core complex. *Nature* 493: 699–702
80. Moqtaderi Z, Yale JD, Struhl K, Buratowski S (1996) Yeast homologues of higher eukaryotic TFIID subunits. *Proc Natl Acad Sci USA* 93: 14654–14658
81. Forsburg SL, Rhind N (2006) Basic methods for fission yeast. *Yeast* 23: 173–183
82. Bahler J, Wu JQ, Longtine MS, Shah NG, McKenzie A 3rd, Steever AB, Wach A, Philippsen P, Pringle JR (1998) Heterologous modules for efficient and versatile PCR-based gene targeting in *Schizosaccharomyces pombe*. *Yeast* 14: 943–951
83. Sato M, Dhut S, Toda T (2005) New drug-resistant cassettes for gene disruption and epitope tagging in *Schizosaccharomyces pombe*. *Yeast* 22: 583–591
84. Hentges P, Van Driessche B, Tafforeau L, Vandenhaute J, Carr AM (2005) Three novel antibiotic marker cassettes for gene disruption and marker switching in *Schizosaccharomyces pombe*. *Yeast* 22: 1013–1019
85. Van Driessche B, Tafforeau L, Hentges P, Carr AM, Vandenhaute J (2005) Additional vectors for PCR-based gene tagging in *Saccharomyces cerevisiae* and *Schizosaccharomyces pombe* using nourseothricin resistance. *Yeast* 22: 1061–1068
86. Gao J, Kan F, Wagnon JL, Storey AJ, Protacio RU, Davidson MK, Wahls WP (2013) Rapid, efficient and precise allele replacement in the fission yeast *Schizosaccharomyces pombe*. *Curr Genet* 60: 109–119
87. Storici F, Lewis LK, Resnick MA (2001) *In vivo* site-directed mutagenesis using oligonucleotides. *Nat Biotechnol* 19: 773–776
88. Bustin SA, Benes V, Garson JA, Hellemans J, Huggett J, Kubista M, Mueller R, Nolan T, Pfaffl MW, Shipley GL et al (2009) The MIQE guidelines: minimum information for publication of quantitative real-time PCR experiments. *Clin Chem* 55: 611–622
89. Rigaut G, Shevchenko A, Rutz B, Wilm M, Mann M, Seraphin B (1999) A generic protein purification method for protein complex characterization and proteome exploration. *Nat Biotechnol* 17: 1030–1032
90. Schneider CA, Rasband WS, Eliceiri KW (2012) NIH Image to ImageJ: 25 years of image analysis. *Nat Methods* 9: 671–675
91. Eng JK, Jahan TA, Hoopmann MR (2013) Comet: an open-source MS/MS sequence database search tool. *Proteomics* 13: 22–24
92. Kall L, Canterbury JD, Weston J, Noble WS, MacCoss MJ (2007) Semi-supervised learning for peptide identification from shotgun proteomics datasets. *Nat Methods* 4: 923–925
93. Beausoleil SA, Villen J, Gerber SA, Rush J, Gygi SP (2006) A probability-based approach for high-throughput protein phosphorylation analysis and site localization. *Nat Biotechnol* 24: 1285–1292
94. Borchert N, Dieterich C, Krug K, Schutz W, Jung S, Nordheim A, Sommer RJ, Macek B (2010) Proteogenomics of *Pristionchus pacificus* reveals distinct proteome structure of nematode models. *Genome Res* 20: 837–846
95. Rappsilber J, Mann M, Ishihama Y (2007) Protocol for micro-purification, enrichment, pre-fractionation and storage of peptides for proteomics using StageTips. *Nat Protoc* 2: 1896–1906
96. Olsen JV, de Godoy LM, Li G, Macek B, Mortensen P, Pesch R, Makarov A, Lange O, Horning S, Mann M (2005) Parts per million mass accuracy on an Orbitrap mass spectrometer via lock mass injection into a C-trap. *Mol Cell Proteomics* 4: 2010–2021
97. Koch A, Krug K, Pengelley S, Macek B, Hauf S (2011) Mitotic substrates of the kinase aurora with roles in chromatin regulation identified through quantitative phosphoproteomics of fission yeast. *Sci Signal* 4: rs6
98. Schroeder MJ, Shabanowitz J, Schwartz JC, Hunt DF, Coon JJ (2004) A neutral loss activation method for improved phosphopeptide sequence analysis by quadrupole ion trap mass spectrometry. *Anal Chem* 76: 3590–3598
99. Cox J, Mann M (2008) MaxQuant enables high peptide identification rates, individualized p.p.b.-range mass accuracies and proteome-wide protein quantification. *Nat Biotechnol* 26: 1367–1372
100. Cox J, Neuhauser N, Michalski A, Scheltema RA, Olsen JV, Mann M (2011) Andromeda: a peptide search engine integrated into the MaxQuant environment. *J Proteome Res* 10: 1794–1805
101. Elias JE, Gygi SP (2007) Target-decoy search strategy for increased confidence in large-scale protein identifications by mass spectrometry. *Nat Methods* 4: 207–214

DISCUSSION & PERSPECTIVES

DISCUSSION & PERSPECTIVES

1. TRRAP is an evolutionarily conserved PIKK family member and requires the TTT co-chaperone to function.

The first objective of my PhD thesis was to analyze the role of the TTT co-chaperone on TRRAP, the only pseudokinase of the PIKK family. The effect of TTT on TRRAP stability was previously reported, however the effect of TTT on TRRAP transcriptional activity had not been addressed then (Hurov et al., 2010; Izumi et al., 2011; Kaizuka et al., 2010; Takai et al., 2007). Although TRRAP is a pseudokinase, it retains the typical domain organization shared among PIKKs and is highly conserved throughout evolution (Helmlinger, 2012). So far, there hasn't been a single eukaryotic genome that does not have a TRRAP ortholog and all have lost the PI3K-like catalytic residues (personal communication, Philippe Fort). Therefore, besides losing these residues, TRRAP, which is a large protein of about 3,800 amino acids, seems to be under strong evolutionary pressure to resemble a PIKK. The reason why has remained obscure, in particular because of the lack of structural information about TRRAP and more generally PIKKs, until recently. We propose that findings reported by us, in this thesis, and others, bring an answer to that question. TRRAP is under pressure to conserve PIKK structural determinants so that it will be recognized, folded and stabilized by the specific, dedicated chaperone machinery, the TTT complex.

Results obtained during my thesis showed that the transcriptional consequences induced upon TRRAP depletion correlate well with those induced upon TELO2 depletion, when examining both the overlap and the enrichment of specific functional signatures in each data set. Although TTT regulates five others PIKKs, namely ATM, ATR, DNA-PKcs, mTOR, and SMG1, half of the genes affected upon TELO2 depletion were also affected in TRRAP-depleted cells, suggesting that TTT affects gene expression mainly through TRRAP. Nevertheless, we cannot rule out that some genes affected upon TRRAP depletion and found to be TTT-dependent, might also be regulated by other PIKKs. Indeed, TRRAP could regulate the signaling of other PIKKs such as ATM, which relies on TIP60-dependent acetylation to be activated (Sun et al., 2005). Interestingly, among the 272 common genes affected upon TELO2 and TRRAP depletion, about 2/3 (181) are bound by TRRAP. To demonstrate that TTT is involved in TRRAP transcriptional activity, one could examine the transcriptional consequences of rescuing TELO2 depletion with TRRAP over-expression, using transient transfection of a plasmid, for example. In addition, it would be important to show that TRRAP binding at these 181 promoters is lost upon TELO2 depletion. I actually attempted to answer this question but CUT&RUN-qPCR using antibodies against endogenous TRRAP (generous gifts from László Tora) failed to give robust and reproducible enrichment at *MIR17HG*.

Besides genes that were highlighted in the overlap between the TTT and TRRAP-dependent transcriptomes, our comparison revealed that TRRAP depletion affects much more genes than the depletion of TELO2. We argue that this difference can be explained by the fact that TRRAP is differently affected in each situation. In AID-TRRAP cells, TRRAP is directly targeted for degradation, whereas in TELO2-AID cells TRRAP is indirectly affected and therefore is destabilized with a much slower kinetic. Thus, in our RNA-seq performed in cells depleted for TELO2, a significant fraction of TRRAP is still present, making such comparisons more complex. Another explanation is that TELO2 targeting might not recapitulate a complete loss of TTT activity, in fact we cannot rule out the possibility that the TTI1 and/or TTI2 subunits could still assemble TRRAP, but less efficiently. This could support an observation which I made, that suggested that TTI1 might interact more strongly with TRRAP upon TELO2 depletion (not shown). It is tempting to speculate that each TTT subunit might affect PIKK differently, leading to distinct outcomes. Alternatively, it is possible that there is a problem in the release of TRRAP by TTI1, when TELO2 is absent, explaining the lack of its incorporation into the SAGA complex. Finally, it would be interesting to separate the TRRAP-dependent genes between those that are regulated by SAGA from those that are TIP60-specific, in order to determine if TTT depletion affects equally both classes of genes. On one hand, we hypothesize that, as shown for mTOR complexes, TTT could be differentially regulated by environmental or signaling cues, which might result in a preferential incorporation of TRRAP within SAGA in some conditions *versus* its incorporation within TIP60 in others. On the other hand, however, if TRRAP is bound to all active promoters, it may be that SAGA, TIP60, or both show the same profile and participate in the transcription of all mRNAs and ncRNAs.

2. Unexpected direct inhibitory roles for TRRAP in transcription

The results obtained and presented in this thesis provide a detailed analysis of the contribution of TRRAP to the regulation of gene expression in colorectal cancer cells. Through a combination of transcriptomic analyses and genome-wide binding studies, we identified direct targets of TRRAP.

Remarkably, although TRRAP is mainly described as a co-activator of transcription, we identified several genes whose expression is induced upon TRRAP depletion, with half of them bound by TRRAP. We decided therefore to focus on those genes, particularly on a set of genes involved in the type I interferon (IFN) response, which corresponds to the most significantly enriched signature found by GSEA analyses.

The IFN signaling pathway is divided into two branches corresponding to an early and to a late response, and involves five major transcription factors. The early response is characterized by the detection of pathogens or more generally something detected as “non-self”. Once triggered, this pathway leads to the activation of the IRF3 and IRF7 transcription factors, which are essential for the transcription of IFN alpha and beta genes. Then, the IFN alpha and beta cytokines activate the

JAK/STAT pathway by binding to dedicated receptors, IFNAR1 and IFNAR2, in an autocrine and paracrine manner. Activation of the JAK kinases eventually results in the formation of the ISGF3 complex, which triggers the late response. ISGF3 comprises the IRF9, STAT1, and STAT2 transcription factors, and is responsible for the transcription of several ISGs, such as *MX1* and *OAS1* but also *IRF7*, to constitute a positive feedback loop (Chan and Gack, 2016; Honda et al., 2006; Schoggins and Rice, 2011) (Figure 48).

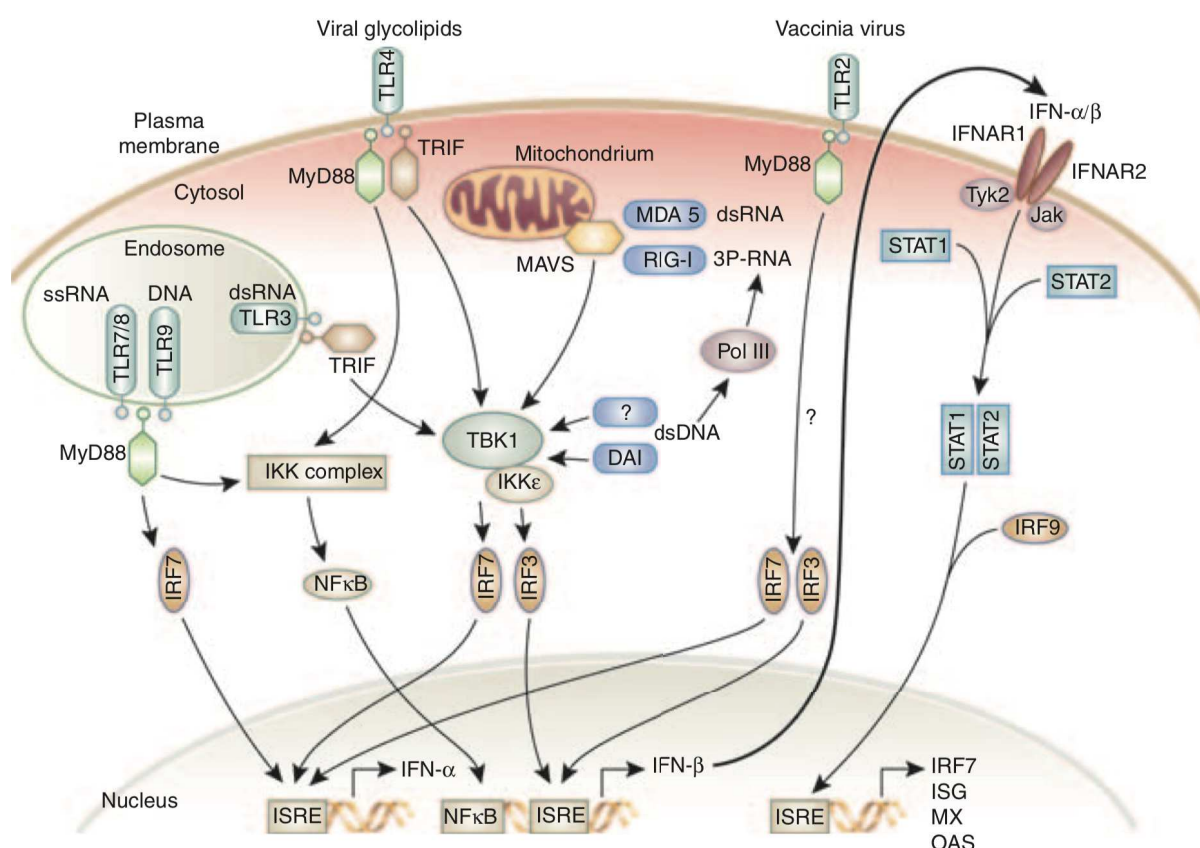


Figure 48: Type I interferon signaling. Schematic representation of the early and late responses of the IFN signaling pathway, showing all membrane and cytosolic receptors, adaptors, kinases and transcription factors involved in. From (Anders et al., 2010)

We showed that components of the early response, such as the central kinase TBK1, are not involved in the ISG induction caused by TRRAP depletion, indicating that TRRAP depletion is unlikely triggering the production of “non-self” elements. Moreover, we could not gather clear evidence that IRF3 and IRF7 are activated. However, although we could neither observe the translocation of IRF3 and IRF7 into the nucleus nor their phosphorylation, we have not formally proven that TRRAP functions downstream of IRF3 or IRF7. We attempted to knock out *IRF7* in AID-TRRAP HCT116 cells using our CRISPR-Cas9 strategy. Unfortunately, we only obtained what may be a hypomorphic allele, as a shorter, truncated version of IRF7 appeared on Western blot analysis of selected clones (not shown). We also measured the production of IFN alpha and beta cytokines in the

media from auxin-treated AID-TRRAP cells, using a dedicated reporter cell line, but were not able to detect significant amounts, as compared to the supernatant from virus-infected cells. The sensitivity of these reporters might not be high enough, though. Finally, we have not directly tested yet whether components from the late response pathway, IFNARs and JAKs, are activated or functionally involved in ISG induction upon TRRAP depletion.

Rather, our CUT&RUN-seq experiments demonstrated that TRRAP binds robustly to the promoters of nearly half of the ISG that are upregulated upon TRRAP depletion, suggesting that ISG promoters are directly repressed by TRRAP. Thus, upon TRRAP depletion, the repression would be relieved and ISGs induced in an IFN-independent manner.

Strikingly, *IRF7*, *IRF9*, and *STAT2* promoters are all bound by TRRAP while their expression is repressed by TRRAP. We suspect therefore that several other upregulated ISGs, which are not bound by TRRAP, are in fact induced as a consequence of increased IRF9/STAT2 expression and activity. Two recent publications support this hypothesis. First, Kolosenko *et al.* reported that IRF9 overexpression alone is sufficient to induce the expression of several ISGs in HCT116 cells (Kolosenko *et al.*, 2015). Second, a heterodimer of unphosphorylated, non-activated IRF9/STAT2 can drive the expression of a subset of ISGs that are remarkably similar to those detected upon TRRAP depletion (Cheon *et al.*, 2013) (see below for details). Nevertheless, at this stage, we cannot formally exclude that TRRAP might activate the transcription of a repressor of ISGs and that upon TRRAP depletion this repressor is not transcribed anymore resulting in ISGs induction. However, I performed an RNA-seq experiment after a shorter depletion of TRRAP (5 hours) to identify a potential ISG repressor. We did not find an obvious candidate in the list of genes which expression decreased 5 hours upon TRRAP depletion, *ie.* before ISGs were induced (not shown).

3. Mechanism of ISG repression by TRRAP

Our results using RNA interference to delineate the involvement of SAGA and TIP60, revealed a clear effect of the TIP60 ATPase, P400. P400 is the catalytic subunit responsible for H2A.Z incorporation. This prompts us to now investigate a potential role of H2A.Z in ISG repression. Our working model predicts that less H2AZ will occupy the +1 and -1 nucleosomes of TRRAP-bound ISG promoters upon TRRAP depletion (Figure 49). In contrast, we should observe no difference on those not bound by TRRAP. We then expect to detect more IRF9 and STAT2 at these promoters, upon TRRAP depletion. Thus, certain ISGs might be repressed through the TRRAP-dependent regulation of the master transcription factors IRF9 and STAT2 in colorectal cancer cells.

To test this hypothesis, we are currently performing chromatin immunoprecipitation (ChIP) and CUT&RUN experiments using anti-H2AZ, -IRF9, and -STAT2 antibodies in cells depleted for TRRAP. Then, we could target INO80 (responsible for H2A.Z removal) by RNA interference, to test

if we can rescue the derepression of ISGs observed upon TRRAP depletion, by restoring the balance of H2AZ occupancy at these promoters.

The involvement of SAGA and TIP60 in the IFN signaling pathway has already been reported by the laboratories of Sharon YR Dent / Kai Ge and Sudhakar Jha, respectively (Jin et al., 2014; Rajagopalan et al., 2018). However, our results do not support an involvement of TRRAP in the mechanisms described in their studies. First, Jin and colleagues showed that GCN5/PCAF repress IFN response by inhibiting TBK1 kinase. In contrast, we observed that the effect of TRRAP depletion on ISG expression does not involve TBK1. Second, Rajagopalan and colleagues identified TIP60 as repressor of ERVs and showed that its depletion leads to IRF7 up-regulation in HCT116 cells. ERV production and detection was actually one of the first hypothesis that we considered to explain the ISG-induction phenotype observed after TRRAP depletion. But here again, our genetic analysis of components of the early response, notably the dsRNA sensors RIG-I and MDA5, did not support the possibility that ERVs were produced and activated an innate immune response in TRRAP-depleted cells. Moreover, besides IRF7, Rajagopalan and colleagues reported that the depletion of TIP60 neither induces an increase of IRF9 nor ISGs, suggesting a distinct mechanism of action.

Altogether, our results suggest that ISG induction upon TRRAP depletion is due to the relief of a direct repression mediated by TRRAP itself at ISG promoters in a TBK1-, ERV-independent, IFN-independent and therefore STAT-phosphorylation independent manner. As mentioned previously, this idea is supported by several studies that revealed that an unphosphorylated form of STAT2 (U-STAT2) binds to IRF9 to form an unphosphorylated ISGF3 complex (U-ISGF3). U-ISGF3 activates the expression of a subset of specific ISGs in the absence of any IFN stimulation (Błaszczyk et al., 2015; Cheon et al., 2013; Kraus et al., 2003). U-ISGF3 was shown to bind distinct interferon stimulated response elements (ISREs) with flanking sequences that differ from canonical ISREs (Cheon et al., 2013). Remarkably, those non-canonical, U-ISGF3-specific ISGs overlap strongly with the TRRAP-repressed ISGs (21/28). Altogether, we propose two working models to explain how TRRAP represses ISG induction. Although both models are different, they are not exclusive, it is possible that both coexist and might explain the ISG induction observed upon the depletion of TRRAP (Figure 49 and 50).

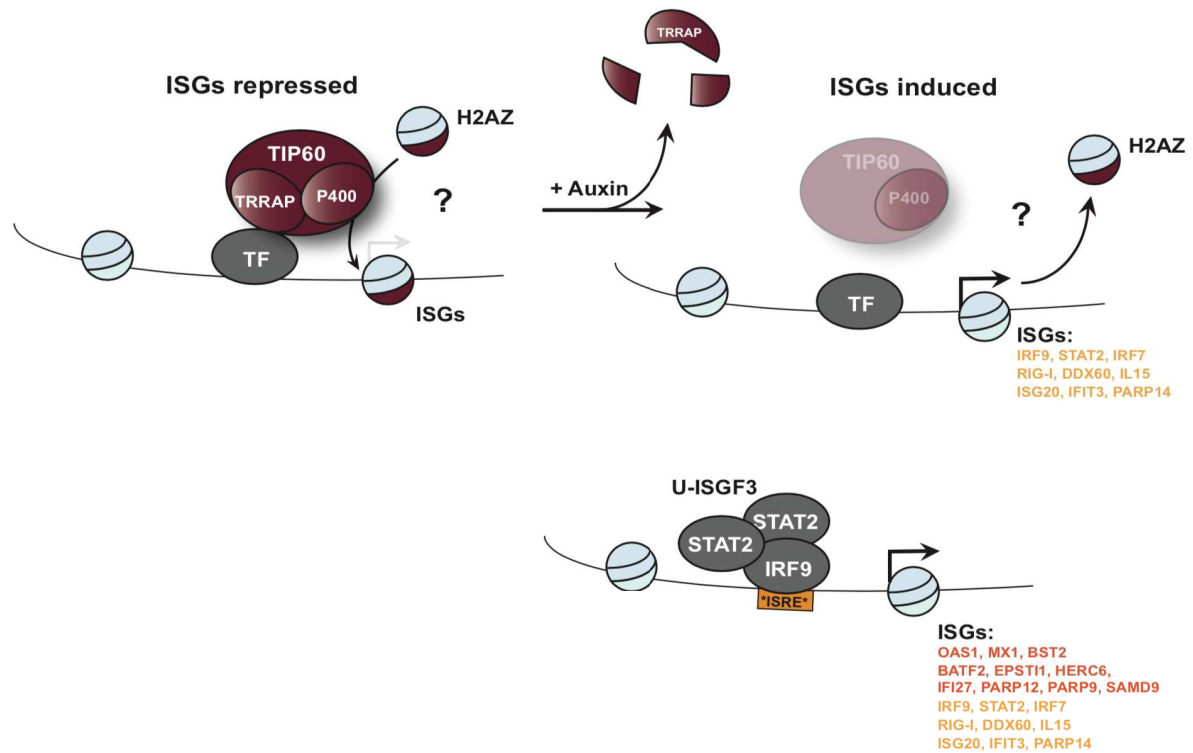


Figure 49: TIP60 complex maintains repressed ISGs. Working model depicting what happens in cells upon TRRAP depletion that could explain the ISG derepression. In the “ISG-repressed” state (left), the TIP60 co-activator, through P400 activity, mediates the deposition of the H2AZ histone variant at ISG promoters, establishing a “repressive” state. In this model, TRRAP is required to interact with unknown transcription factor(s) (TF) allowing the recruitment of TIP60 at chromatin. Then, when TRRAP is degraded by treating cells with auxin (right), TIP60 is not recruited at ISG promoters and H2AZ is no longer incorporated. The repression is relieved, leading to an “active” state and ISG transcription. The subset of ISGs that are subjected to such regulation would be those bound by TRRAP (CUT&RUN data) and include *IRF9* and *STAT2*, which then form U-ISGF3. U-ISGF3 binds to non-canonical ISRE (highlighted with stars) and drives the expression of additional ISGs, including those bound by TRRAP (light orange) as well as a subset of ISGs not bound by TRRAP (dark orange).

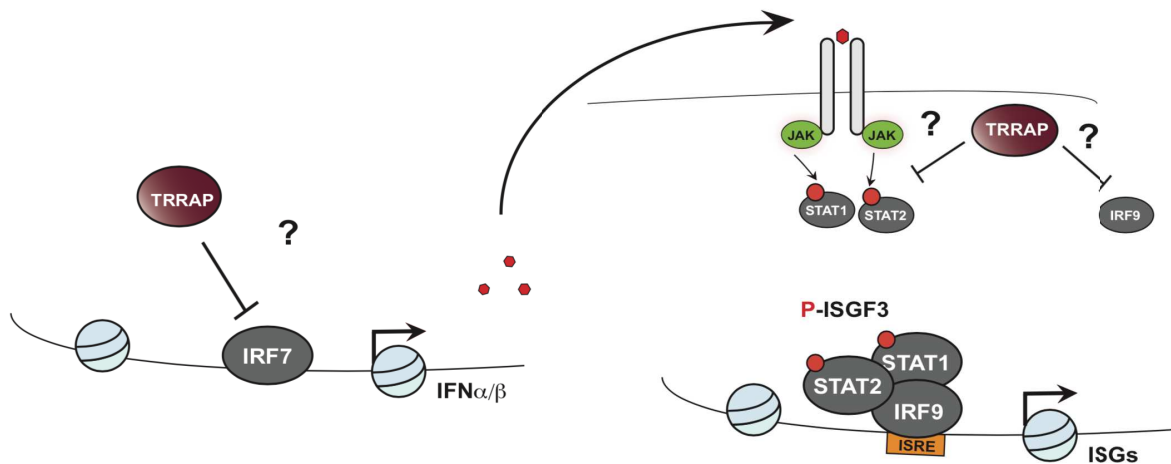


Figure 50: TRRAP inhibits the production of IFN and/or the JAK/STAT pathway. In this second working model, which could complement the first one, TRRAP is acting on the IFN pathway. In presence of TRRAP, IFN alpha and beta genes are repressed indirectly by TRRAP through the repression of IRF7, leading to the activation of JAK/STAT signaling and ISGs transcription by the canonical ISGF3 complex upon TRRAP depletion. TRRAP could also inhibit the JAK/STAT pathway downstream of IRF7 activation and IFN production.

Although, we have not yet determined that TIP60 is responsible for maintaining ISG in a repressed state through the P400-dependent deposition of H2AZ, it would be interesting to assess if this mechanism is only restricted to ISG genes or extended to others direct targets of TRRAP. Importantly, if TIP60 is involved, it raises the question of how the complex is recruited to ISG promoters. Typically, TRRAP-containing complexes are recruited by DNA-bound activators, through direct contact between TRRAP and the trans-activation domain of transcription factors (Murr et al., 2007). However, recent structural analysis of the NuA4 complex from *S. cerevisiae* indicated that Tra1 constitutes a structural core required for the overall assembly of the NuA4 complex (Xuejuan Wang et al., 2018). This observation is in marked contrast with the topology of Tra1 within SAGA, within which it occupies a defined lobe and interacts with the rest of the complex through a limited number of surface contacts (Sharov et al., 2017). These structural data are further supported by functional and phenotypic analyses from our group, which revealed that NuA4 subunit composition is overall affected in *tra2* conditional deletion mutant in fission yeast (Elias-Villalobos A et al., in preparation), whereas SAGA overall composition is not affected by *tra1* deletion (Helmlinger et al., 2011).

4. New insights into the functional cooperation between MYC and TRRAP

Studying the direct targets of TRRAP is relevant in the field of cancer biology because the c-MYC transcription factor requires TRRAP to mediate many of its oncogenic functions. To gain better insight into how MYC and TRRAP cooperate in colorectal cancer cells, we performed CUT&RUN-seq of MYC before and after TRRAP depletion, as well as upon the recovery of TRRAP by washing auxin out from the medium. Venn diagram analysis comparing unique genes bound by TRRAP with unique genes bound by MYC revealed an almost complete overlap for MYC targets. Indeed, 95% of genes bound by MYC are also bound by TRRAP, while TRRAP binds to plenty of genes not bound by c-MYC (Figure 51).

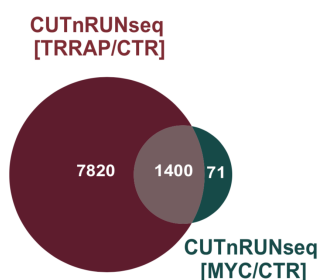


Figure 51: Common target genes bound by TRRAP and MYC. Venn diagram analysis between genes bound by TRRAP (dark red) or by MYC (dark green). Gene lists were obtained from the CUT&RUN-seq analyses.

This observation is consistent with the idea that MYC recruits TRRAP at most of its target genes in colorectal cancer cells, while TRRAP is recruited to promoters by many other transcription factors. For instance, CUT&RUN-seq of MYC revealed that it does not bind ISGs (Figure 52), suggesting that TRRAP is recruited to ISG promoters through another transcription factor or mechanism.

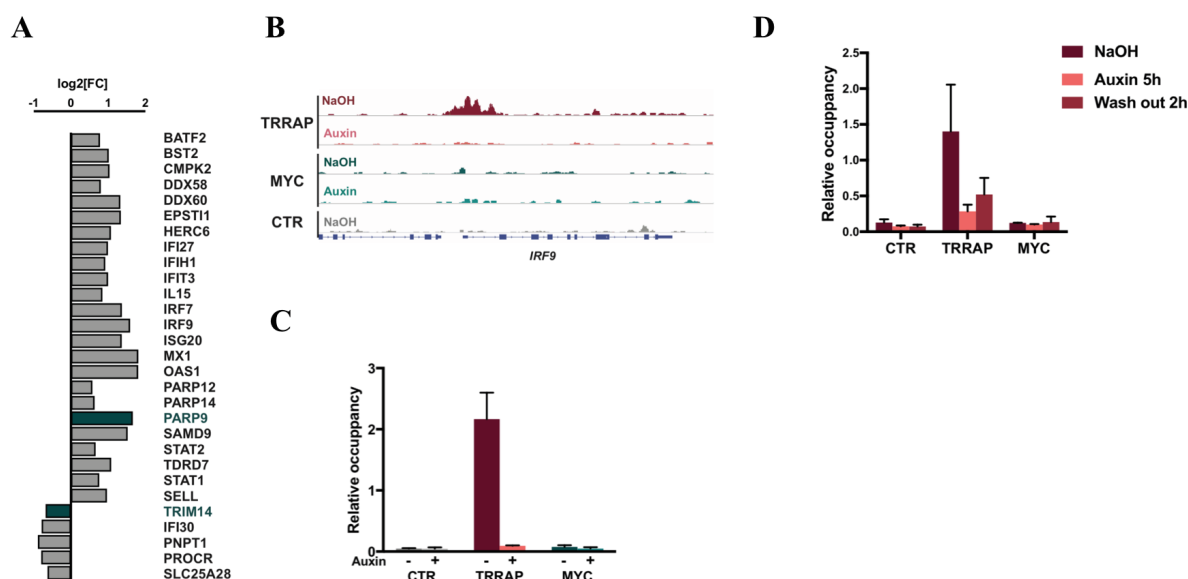


Figure 52: TRRAP binds to ISG promoter in a MYC-independent manner. (A) Bar plot displaying the fold change of selected ISGs from the RNA-seq analysis of TRRAP-dependent transcripts. Column is colored in dark green if MYC binding was detected at the corresponding TSS. (B) IGV snapshot of the CUT&RUN-seq profile of TRRAP and MYC occupancy at the *IRF9* locus in AID-TRRAP cells treated with NaOH or auxin for 12h. (C) CUT&RUN of TRRAP and MYC in AID-TRRAP cells treated with NaOH or auxin for 24h, then quantification of TRRAP and MYC binding at *IRF9* promoter by qPCR. (D) CUT&RUN of TRRAP and MYC in AID-TRRAP cells treated with or without auxin for 5h then washed and incubated without auxin for 2h. *IRF9* relative occupancy was quantified by qPCR.

Additionally, the overlap profile supports a potential role of TRRAP as general co-factor of Pol II transcription, as discussed below. Surprisingly, among these 1400 genes whose promoter is bound by both TRRAP and MYC, our RNA-seq shows that only a quarter are differentially expressed upon TRRAP depletion (Figure 53A). One possible interpretation is that MYC collaborates with TRRAP mostly to modulate the transcription of inducible genes. It is also possible that compensatory mechanisms or factors operate in cells following the prolonged depletion of TRRAP (24 hours), although such time frame remains relatively short. Indeed, by examining genes that are differentially expressed after a shorter period of TRRAP depletion using RNA-seq after 5 hours of auxin treatment, we observed even less genes simultaneously bound by TRRAP and MYC and regulated by TRRAP (Figure 53B). It is also possible that c-MYC recruits a variety of co-factors to regulate the expression of its targets, so that TRRAP depletion would be compensated by others co-activators.

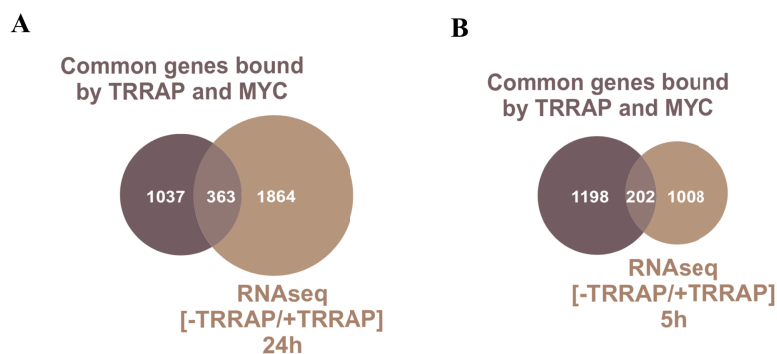


Figure 53: TRRAP and MYC bind to genes mainly not affected after TRRAP depletion. Venn diagrams showing among the common genes bound by TRRAP and MYC, the proportion of genes affected upon TRRAP depletion achieved after 24h (A) or 5h (B) of auxin treatment.

Finally, an important limitation of all our analyses is that RNA-seq measures steady-state mRNA levels, which do not necessarily reflect the transcriptional status of a gene, but, rather, the net balance between RNA synthesis and decay. Therefore, to overcome this bias, we should analyze the nascent transcriptomes, using comparative dynamic transcriptome analysis (cDTA), 4SU, or SLAM-seq to identify the direct transcriptional consequences of TRRAP depletion.

Unexpectedly, this analysis also revealed that, in addition to the well-established model that MYC recruits TRRAP upon DNA binding, the reverse might also happen, because TRRAP contributes to MYC binding at promoters. Indeed, we observed that, upon TRRAP depletion, the genome-wide binding of MYC is affected. For instance, upon TRRAP depletion, MYC binding clearly decreases at the promoter of one of its well-characterized targets, the onco-miR *MIR17HG*, (Figure 54). Moreover, we observed that the expression of *MIR17HG* decreases quickly after the depletion of TRRAP and inversely re-increases rapidly upon TRRAP recovery. Altogether, these observations suggest that TRRAP modulates the recruitment of MYC at *MIR17HG* promoter, and directly regulates the transcription of *MIR17HG*.

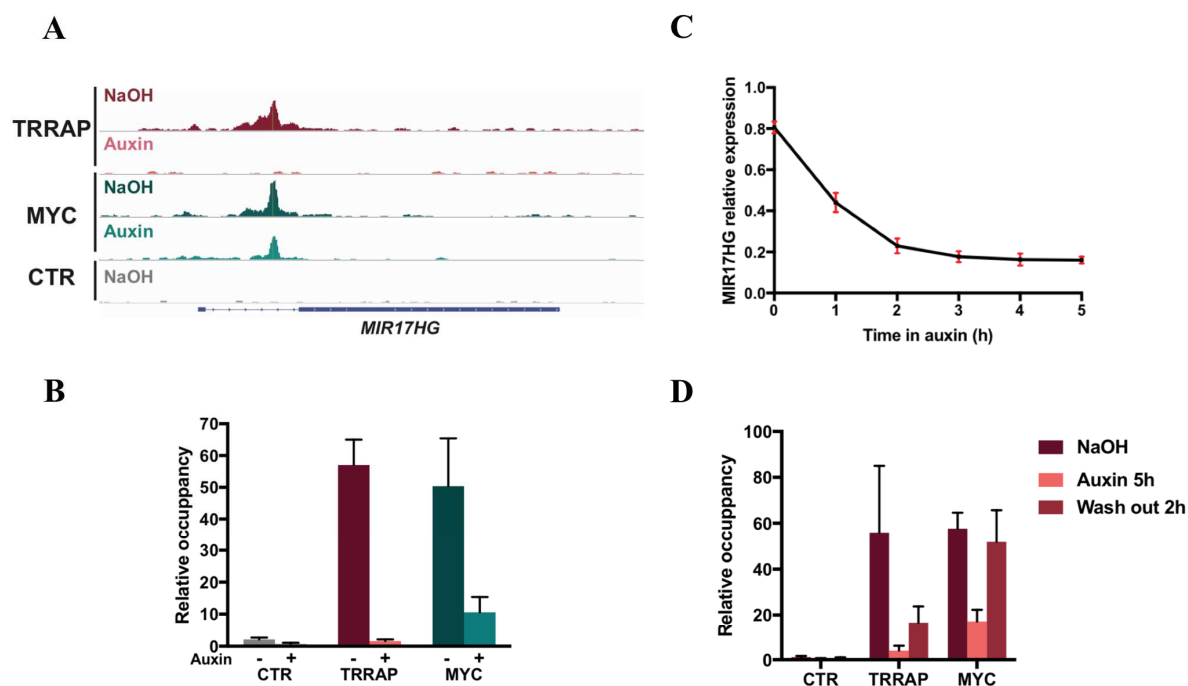


Figure 54: TRRAP depletion affects rapidly the expression of *MIR17HG* and the binding of MYC. (A) Snapshot of TRRAP and MYC CUT&RUN-seq at the *MIR17HG* locus in AID-TRRAP cells treated with auxin or its vehicle (NaOH) for 12h. CTR corresponds to CUT&RUN performed with an IgG control antibody. (B) CUT&RUN-qPCR results of TRRAP and MYC binding at *MIR17HG* promoter in AID-TRRAP cells treated or not with auxin for 24 hours. (C) RT-qPCR analysis of *MIR17HG* expression upon a short time course of TRRAP depletion. (D) CUT&RUN of TRRAP and MYC in AID-TRRAP cells treated with or without auxin for 5h then washed and incubated without auxin for 2h. *MIR17HG* promoter relative occupancy was quantified by qPCR.

Therefore, we hypothesize that TRRAP is required for stabilizing MYC at target gene promoters, or that TRRAP acts as an intermediate for MYC binding to target genes. As already reported, MYC is an unstable protein which turn-over is controlled by the ubiquitin degradation system and plays a critical role in the modulation of its transcriptional activity (Jaenicke et al., 2016). Interestingly, TRRAP interacts with MYC through the MYC box II domain, similarly to E3 ligases. Therefore, we can envisage that, in the absence of TRRAP, the MYC box II domain of MYC is targeted for ubiquitin-dependent proteasomal degradation.

Finally, to address the importance of TRRAP for MYC binding at their targets, we performed CUT&RUN experiments of TRRAP and MYC over a time course of auxin wash out, in other terms over a time course of TRRAP recovery. Analyses are ongoing, and should disclose the dynamic and sequential order of MYC and TRRAP binding at their target genes.

5. TRRAP governs and maintains a tumoral state, characterized by low levels of ISGs

We showed that TRRAP depletion leads to important transcriptional changes. Functional enrichment analyses clearly highlighted what was expected, namely specific MYC and E2F targets signatures. However, the list of genes found differentially expressed after TRRAP depletion is likely incomplete, because we analyzed cells during proliferation, in one specific condition. We can expect that repeating these experiments following distinct stress or stimulation, the list would have been different.

Interestingly, the differential expression of several TRRAP-regulated genes anti-correlates with their differential expression observed when comparing normal colon tissue with a primary tumor (COADREAD cohort). For instance, using the web-based tool UCSC Xena, we observed that *MIR17HG*, which is one of the most downregulated transcript in HCT116 depleted for TRRAP (Figure 55B), is less expressed in normal colon tissues as compared to primary tumors in which it is overexpressed (Figure 55A). The same tendency is observed for other genes, such as *KAT2A* (GCN5) and *KAT2B* (PCAF), already discussed in the introduction for their inherently opposing functions in tumorigenesis (p.35). This analysis suggests that TRRAP is involved in the switch of expression from GCN5 to PCAF and might be responsible for the maintenance of a specific tumoral state.

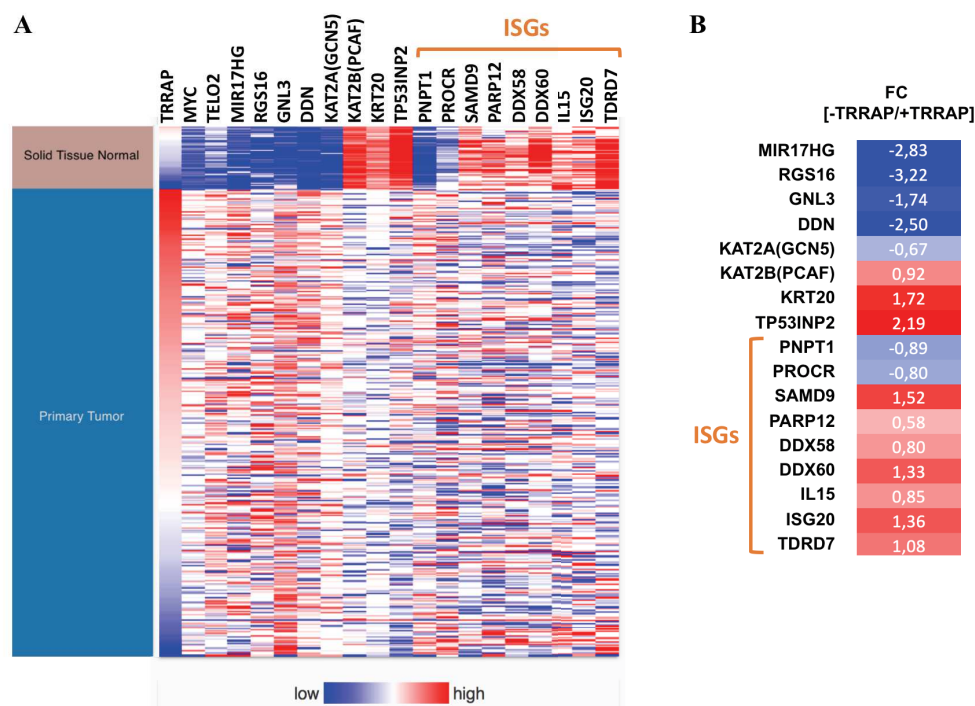


Figure 55: TRRAP governs a specific pro-tumoral transcriptional program. (A) Heat map representation of selected mRNA expression from RNA-seq data obtained in 51 normal tissue samples and 380 primary tumor samples retrieved from The Cancer Genome Atlas (TCGA) COAD-READ project (High expression, in red; low expression, in blue). (B) Heat map display of fold change (FC) of the same selected genes found differentially expressed after TRRAP depletion. FC values are indicated (white), and ISGs are highlighted (orange bracket).

TRRAP is itself overexpressed in tumor as compared to normal tissue, as well as TELO2 (see Figure 55, for example). It is tempting to speculate that, similar to the well-documented addiction of cancer cells to MYC, tumor maintenance relies on a specific transcriptional program regulated by TRRAP and its co-chaperone TTT. Furthermore, a study looking at the specific gene expression signatures of colorectal cancer cells that became resistant to the chemotherapeutic agent irinotecan, identified that 29% of overexpressed genes were ISGs (Gongora et al., 2008). Accordingly, expression levels of a subset of U-ISGF3-dependent ISGs are high in normal colon tissue as compared to primary tumor (Figure 55). Finally, we found that upon TRRAP depletion, ISGs are de-repressed and the rate of cell growth is reduced without obvious change in cell cycle stage distribution, at least in the early stage of TRRAP deletion (not shown).

Altogether, these observations provide evidence that TRRAP might play an important role in tumorigenesis by mediating, among others things, the repression of ISGs.

6. Putative roles of TRRAP over RNA polymerase II transcription.

Preliminary analyses of TRRAP CUT&RUN-seq revealed that TRRAP binds to 9,215 genes, which represent roughly 30% of all transcription start sites (TSS) in the human genome. Interestingly, this value matches the reported median number of active promoters bound by RNA polymerase II in different cell types (de Dieuleveult et al., 2016). Although we have to verify that the promoters bound by TRRAP are associated with active TSS, it is tempting to speculate that TRRAP might play a general role in transcription in humans, similar to yeast SAGA and TFIID (Baptista et al., 2017; Bonnet et al., 2014; Warfield et al., 2017).

In addition, examination of TRRAP binding profile relative to TSS positions revealed that TRRAP binds very close to their TSS, at least in the proximal promoter region. To assess if TRRAP location could overlap with the PIC, the resolution of our bioinformatics analyses needs to be further improved. So far, I think that the observed frequency distribution (Figure 4C, Results section), showing a classical cleavage pattern with two broad peaks extending approximately 300 bp upstream and downstream of the TSS, corresponds to the phased -1 and +1 nucleosomes immediately flanking the nucleosome-depleted region (NDR) where TRRAP binds. Interestingly, the dip observed closer to the TSS may contain high-resolution topological information about TRRAP binding at core promoters in human cells. To accurately determine the binding site of TRRAP, we have to define the exact cleavage pattern of TRRAP-bound MNase, by plotting the end positions of the short fragments (<120 bp) corresponding to the locations where the tethered MNase has cleaved. Such bioinformatics strategy has been successfully employed by the Henikoff laboratory to gain a high resolution view of CTCF binding in human cells, following CU&RUN-seq (Skene and Henikoff, 2017).

Altogether these preliminary data prompted us to assess if, as observed recently in *S. cerevisiae*, SAGA in human cells functions as a general co-factor for RNA Pol II transcription (Baptista et al., 2017). However, we analyzed here the genome-wide distribution of TRRAP, which in human cells is shared between SAGA and TIP60 complexes. Hence, to verify if SAGA has a genome-wide impact on Pol II transcription in human cells, I would perform CUT&RUN-seq of specific subunits of SAGA and TIP60. If we observe a similar broad distribution on active RNA polymerase II-dependent promoters, then, the next fundamental question will be to address how TRRAP recruits SAGA and/or TIP60 to chromatin and stabilizes the PIC constitutively, at nearly all active promoters. As mentioned in the Introduction, one mechanism to recruit SAGA to chromatin is through the TRRAP subunit, which directly interacts with many transcription factors. In *S. pombe*, gene duplication has led to the appearance of two paralogous proteins, Tra1 and Tra2, which have specific and non-redundant roles, such that Tra1 is specific to SAGA and Tra2 to NuA4, the yeast homolog of the TIP60 complex. This unique situation has allowed to tackle the specific role of the Tra1 subunit on SAGA transcriptional activity. Deletion of *tra1* is not lethal contrary to its *tra2* paralog and its TRRAP ortholog in humans, suggesting that TRRAP is essential for viability because of its role within TIP60 complex. Deletion of *tra1* in fission yeast affects the binding of SAGA to promoters only at a subset of genes, suggesting a Tra1-independent recruitment of SAGA, at least at certain promoters (Helmlinger et al., 2011). Thanks to the system which I developed, which enables fast, inducible, and reversible degradation of TRRAP, it would be interesting to analyze whether SAGA relies exclusively on TRRAP to be recruited to chromatin in human cells, and with which dynamic.

CONCLUSION

CONCLUSION

During my PhD, I have addressed the role of the TRRAP co-activator and its chaperone TTT in transcriptional regulation. Using an inducible and reversible system for the degradation of both endogenous proteins, we first showed that TTT is required to incorporate TRRAP within the SAGA complex, likely into the cytoplasm, before its nuclear import. Second, through transcriptomic analyses, we revealed that TTT regulates several TRRAP-dependent genes. These results describe TTT as an important chaperone for the transcriptional activity of TRRAP, the sole pseudokinase of the PIKK family.

Additionally, we discovered that, upon TRRAP depletion, the expression of genes involved in the interferon response from the innate immune system, namely ISGs (Interferon Stimulated Genes), was induced. By analyzing the genome-wide binding of TRRAP *via* CUT&RUN-seq, we identified its direct targets, including the master regulators of the interferon response, the IRF9 and STAT2 transcription factors. Importantly, we carried a functional characterization of the IFN-signaling pathway using a CRISPR/Cas9-based reverse genetics approach and demonstrated that ISG induction following TRRAP depletion is not triggered by the activation of the pathway. Finally, we obtained preliminary evidence that ISG control by TRRAP involves chromatin remodeling activity. The genome-wide chromatin profiling of TRRAP occupancy revealed that TRRAP binds broadly, near to the transcriptional start sites of virtually all active genes. TRRAP binds nearly all MYC-bound promoters but clearly has a potential effect on transcription genome-wide.

Altogether, the results obtained during my thesis allowed to gain novel insights into the transcriptional function of TRRAP, pointing out an unexpected and direct inhibitory role of TRRAP on ISG transcription. Further analyses are needed, however, to decipher the underlying mechanisms and biological relevance of such inhibition in colorectal cancer cells.

REFERENCES

REFERENCES

- Abbott, D.W., Ivanova, V.S., Wang, X., Bonner, W.M., Ausió, J., 2001. Characterization of the stability and folding of H2A.Z chromatin particles: implications for transcriptional activation. *J. Biol. Chem.* 276, 41945–41949. <https://doi.org/10.1074/jbc.M108217200>
- Abraham, R.T., 2004. PI 3-kinase related kinases: ‘big’ players in stress-induced signaling pathways. *DNA Repair* 3, 883–887. <https://doi.org/10.1016/j.dnarep.2004.04.002>
- Acharya, D., Hainer, S.J., Yoon, Y., Wang, F., Bach, I., Rivera-Pérez, J.A., Fazzio, T.G., 2017. KAT-Independent Gene Regulation by Tip60 Promotes ESC Self-Renewal but Not Pluripotency. *Cell Rep.* 19, 671–679. <https://doi.org/10.1016/j.celrep.2017.04.001>
- Adam, M., Robert, F., Larochelle, M., Gaudreau, L., 2001. H2A.Z is required for global chromatin integrity and for recruitment of RNA polymerase II under specific conditions. *Mol. Cell Biol.* 21, 6270–6279.
- Adams, C.C., Workman, J.L., 1995. Binding of disparate transcriptional activators to nucleosomal DNA is inherently cooperative. *Mol. Cell Biol.* 15, 1405–1421.
- Albert, I., Mavrich, T.N., Tomsho, L.P., Qi, J., Zanton, S.J., Schuster, S.C., Pugh, B.F., 2007. Translational and rotational settings of H2A.Z nucleosomes across the *Saccharomyces cerevisiae* genome. *Nature* 446, 572–576. <https://doi.org/10.1038/nature05632>
- Alekseev, S., Nagy, Z., Sandoz, J., Weiss, A., Egly, J.-M., Le May, N., Coin, F., 2017. Transcription without XPB Establishes a Unified Helicase-Independent Mechanism of Promoter Opening in Eukaryotic Gene Expression. *Mol. Cell* 65, 504–514.e4. <https://doi.org/10.1016/j.molcel.2017.01.012>
- Allard, S., Utley, R.T., Savard, J., Clarke, A., Grant, P., Brandl, C.J., Pillus, L., Workman, J.L., Côté, J., 1999. NuA4, an essential transcription adaptor/histone H4 acetyltransferase complex containing Esa1p and the ATM-related cofactor Tra1p. *EMBO J.* 18, 5108–5119. <https://doi.org/10.1093/emboj/18.18.5108>
- Anders, H.-J., Lichtnekert, J., Allam, R., 2010. Interferon- α and - β in kidney inflammation. *Kidney Int.* 77, 848–854. <https://doi.org/10.1038/ki.2010.71>
- Armache, K.-J., Kettenberger, H., Cramer, P., 2003. Architecture of initiation-competent 12-subunit RNA polymerase II. *Proc. Natl. Acad. Sci.* 100, 6964–6968. <https://doi.org/10.1073/pnas.1030608100>
- Atanassov, B.S., Mohan, R.D., Lan, X., Kuang, X., Lu, Y., Lin, K., McIvor, E., Li, W., Zhang, Y., Florens, L., Byrum, S.D., Mackintosh, S.G., Calhoun-Davis, T., Koutelou, E., Wang, L., Tang, D.G., Tackett, A.J., Washburn, M.P., Workman, J.L., Dent, S.Y.R., 2016. ATXN7L3 and ENY2 Coordinate Activity of Multiple H2B Deubiquitinases Important for Cellular Proliferation and Tumor Growth. *Mol. Cell* 62, 558–571. <https://doi.org/10.1016/j.molcel.2016.03.030>
- Aylett, C.H.S., Sauer, E., Imseng, S., Boehringer, D., Hall, M.N., Ban, N., Maier, T., 2016. Architecture of human mTOR complex 1. *Science* 351, 48–52. <https://doi.org/10.1126/science.aaa3870>
- Babenko, V.N., Kosarev, P.S., Vishnevsky, O.V., Levitsky, V.G., Basin, V.V., Frolov, A.S., 1999. Investigating extended regulatory regions of genomic DNA sequences. *Bioinformatics* 15, 644–653. <https://doi.org/10.1093/bioinformatics/15.7.644>
- Babiarz, J.E., Halley, J.E., Rine, J., 2006. Telomeric heterochromatin boundaries require NuA4-dependent acetylation of histone variant H2A.Z in *Saccharomyces cerevisiae*. *Genes Dev.* 20, 700–710. <https://doi.org/10.1101/gad.1386306>

- Bakkenist, C.J., Kastan, M.B., 2004. Initiating Cellular Stress Responses. *Cell* 118, 9–17. <https://doi.org/10.1016/j.cell.2004.06.023>
- Baptista, T., Grünberg, S., Minoungou, N., Koster, M.J.E., Timmers, H.T.M., Hahn, S., Devys, D., Tora, L., 2017. SAGA Is a General Cofactor for RNA Polymerase II Transcription. *Mol. Cell* 68, 130–143.e5. <https://doi.org/10.1016/j.molcel.2017.08.016>
- Baretić, D., Pollard, H.K., Fisher, D.I., Johnson, C.M., Santhanam, B., Truman, C.M., Kouba, T., Fersht, A.R., Phillips, C., Williams, R.L., 2017. Structures of closed and open conformations of dimeric human ATM. *Sci. Adv.* 3, e1700933. <https://doi.org/10.1126/sciadv.1700933>
- Baretić, D., Williams, R.L., 2014. PIKKs — the solenoid nest where partners and kinases meet. *Curr. Opin. Struct. Biol.* 29, 134–142. <https://doi.org/10.1016/j.sbi.2014.11.003>
- Basehoar, A.D., Zanton, S.J., Pugh, B.F., 2004. Identification and Distinct Regulation of Yeast TATA Box-Containing Genes. *Cell* 116, 699–709. [https://doi.org/10.1016/S0092-8674\(04\)00205-3](https://doi.org/10.1016/S0092-8674(04)00205-3)
- Bernecky, C., Herzog, F., Baumeister, W., Plitzko, J.M., Cramer, P., 2016. Structure of transcribing mammalian RNA polymerase II. *Nature* 529, 551–554. <https://doi.org/10.1038/nature16482>
- Bhaumik, S.R., Green, M.R., 2001. SAGA is an essential in vivo target of the yeast acidic activator Gal4p. *Genes Dev.* 15, 1935–1945. <https://doi.org/10.1101/gad.911401>
- Bian, C., Xu, C., Ruan, J., Lee, K.K., Burke, T.L., Tempel, W., Barsyte, D., Li, J., Wu, M., Zhou, B.O., Fleharty, B.E., Paulson, A., Allali-Hassani, A., Zhou, J.-Q., Mer, G., Grant, P.A., Workman, J.L., Zang, J., Min, J., 2011. Sgf29 binds histone H3K4me2/3 and is required for SAGA complex recruitment and histone H3 acetylation. *EMBO J.* 30, 2829–2842. <https://doi.org/10.1038/emboj.2011.193>
- Birck, C., Poch, O., Romier, C., Ruff, M., Mengus, G., Lavigne, A.-C., Davidson, I., Moras, D., 1998. Human TAFII28 and TAFII18 Interact through a Histone Fold Encoded by Atypical Evolutionary Conserved Motifs Also Found in the SPT3 Family. *Cell* 94, 239–249. [https://doi.org/10.1016/S0092-8674\(00\)81423-3](https://doi.org/10.1016/S0092-8674(00)81423-3)
- Bizarro, J., Dodré, M., Huttin, A., Charpentier, B., Schlotter, F., Branlant, C., Verheggen, C., Massenet, S., Bertrand, E., 2015. NUFIP and the HSP90/R2TP chaperone bind the SMN complex and facilitate assembly of U4-specific proteins. *Nucleic Acids Res.* 43, 8973–8989. <https://doi.org/10.1093/nar/gkv809>
- Błaszczyk, K., Olejnik, A., Nowicka, H., Ozgyn, L., Chen, Y.-L., Chmielewski, S., Kostyrko, K., Wesoly, J., Balint, B.L., Lee, C.-K., Bluysen, H.A.R., 2015. STAT2/IRF9 directs a prolonged ISGF3-like transcriptional response and antiviral activity in the absence of STAT1. *Biochem. J.* 466, 511–524. <https://doi.org/10.1042/BJ20140644>
- Bonnet, J., Wang, C.-Y., Baptista, T., Vincent, S.D., Hsiao, W.-C., Stierle, M., Kao, C.-F., Tora, L., Devys, D., 2014. The SAGA coactivator complex acts on the whole transcribed genome and is required for RNA polymerase II transcription. *Genes Dev.* 28, 1999–2012. <https://doi.org/10.1101/gad.250225.114>
- Bonnet, J., Wang, Y.-H., Spedale, G., Atkinson, R.A., Romier, C., Hamiche, A., Pijnappel, W.W.M.P., Timmers, H.T.M., Tora, L., Devys, D., Kieffer, B., 2010. The structural plasticity of SCA7 domains defines their differential nucleosome-binding properties. *EMBO Rep.* 11, 612–618. <https://doi.org/10.1038/emboj.2010.98>
- Boulon, S., Marmier-Gourrier, N., Pradet-Balade, B., Wurth, L., Verheggen, C., Jádý, B.E., Rothé, B., Pescia, C., Robert, M.-C., Kiss, T., Bardoni, B., Krol, A., Branlant, C., Allmang, C., Bertrand, E., Charpentier, B., 2008. The Hsp90 chaperone controls the biogenesis of L7Ae RNPs through conserved machinery. *J. Cell Biol.* 180, 579–595. <https://doi.org/10.1083/jcb.200708110>

- Boulon, S., Pradet-Balade, B., Verheggen, C., Molle, D., Boireau, S., Georgieva, M., Azzag, K., Robert, M.-C., Ahmad, Y., Neel, H., Lamond, A.I., Bertrand, E., 2010. HSP90 and Its R2TP/Prefoldin-like Cochaperone Are Involved in the Cytoplasmic Assembly of RNA Polymerase II. *Mol. Cell* 39, 912–924. <https://doi.org/10.1016/j.molcel.2010.08.023>
- Brady, M.E., Ozanne, D.M., Gaughan, L., Waite, I., Cook, S., Neal, D.E., Robson, C.N., 1999. Tip60 Is a Nuclear Hormone Receptor Coactivator. *J. Biol. Chem.* 274, 17599–17604. <https://doi.org/10.1074/jbc.274.25.17599>
- Brand, M., Yamamoto, K., Staub, A., Tora, L., 1999. Identification of TATA-binding protein-free TAFII-containing complex subunits suggests a role in nucleosome acetylation and signal transduction. *J. Biol. Chem.* 274, 18285–18289.
- Branzei, D., Foiani, M., 2008. Regulation of DNA repair throughout the cell cycle. *Nat. Rev. Mol. Cell Biol.* 9, 297–308. <https://doi.org/10.1038/nrm2351>
- Brasnet, E., Vauray, C., 2005. Insulators are fundamental components of the eukaryotic genomes. *Heredity* 94, 571–576. <https://doi.org/10.1038/sj.hdy.6800669>
- Brown, C.E., Howe, L., Sousa, K., Alley, S.C., Carrozza, M.J., Tan, S., Workman, J.L., 2001. Recruitment of HAT complexes by direct activator interactions with the ATM-related Tra1 subunit. *Science* 292, 2333–2337. <https://doi.org/10.1126/science.1060214>
- Brownell, J.E., Zhou, J., Ranalli, T., Kobayashi, R., Edmondson, D.G., Roth, S.Y., Allis, C.D., 1996. Tetrahymena histone acetyltransferase A: a homolog to yeast Gcn5p linking histone acetylation to gene activation. *Cell* 84, 843–851.
- Brumbaugh, K.M., Otterness, D.M., Geisen, C., Oliveira, V., Brognard, J., Li, X., Lejeune, F., Tibbetts, R.S., Maquat, L.E., Abraham, R.T., 2004. The mRNA surveillance protein hSMG-1 functions in genotoxic stress response pathways in mammalian cells. *Mol. Cell* 14, 585–598. <https://doi.org/10.1016/j.molcel.2004.05.005>
- Bucher, P., 1990. Weight matrix descriptions of four eukaryotic RNA polymerase II promoter elements derived from 502 unrelated promoter sequences. *J. Mol. Biol.* 212, 563–578. [https://doi.org/10.1016/0022-2836\(90\)90223-9](https://doi.org/10.1016/0022-2836(90)90223-9)
- Buratowski, S., Hahn, S., Guarente, L., Sharp, P.A., 1989. Five intermediate complexes in transcription initiation by RNA polymerase II. *Cell* 56, 549–561.
- Burke, T.W., Kadonaga, J.T., 1997. The downstream core promoter element, DPE, is conserved from *Drosophila* to humans and is recognized by TAFII60 of *Drosophila*. *Genes Dev.* 11, 3020–3031.
- Bushnell, D.A., Kornberg, R.D., 2003. Complete, 12-subunit RNA polymerase II at 4.1-Å resolution: Implications for the initiation of transcription. *Proc. Natl. Acad. Sci.* 100, 6969–6973. <https://doi.org/10.1073/pnas.1130601100>
- Butler, J.E.F., Kadonaga, J.T., 2002. The RNA polymerase II core promoter: a key component in the regulation of gene expression. *Genes Dev.* 16, 2583–2592. <https://doi.org/10.1101/gad.1026202>
- Cai, Y., Jin, J., Florens, L., Swanson, S.K., Kusch, T., Li, B., Workman, J.L., Washburn, M.P., Conaway, R.C., Conaway, J.W., 2005. The Mammalian YL1 Protein Is a Shared Subunit of the TRRAP/TIP60 Histone Acetyltransferase and SRCAP Complexes. *J. Biol. Chem.* 280, 13665–13670. <https://doi.org/10.1074/jbc.M500001200>
- Cai, Y., Jin, J., Tomomori-Sato, C., Sato, S., Sorokina, I., Parmely, T.J., Conaway, R.C., Conaway, J.W., 2003. Identification of New Subunits of the Multiprotein Mammalian TRRAP/TIP60-containing Histone Acetyltransferase Complex. *J. Biol. Chem.* 278, 42733–42736. <https://doi.org/10.1074/jbc.C300389200>

- Causier, B., Li, Z., Smet, R.D., Lloyd, J.P.B., Peer, Y.V. de, Davies, B., 2017. Conservation of Nonsense-Mediated mRNA Decay Complex Components Throughout Eukaryotic Evolution. *Sci. Rep.* 7, 16692. <https://doi.org/10.1038/s41598-017-16942-w>
- Chalkley, G.E., Verrijzer, C.P., 1999. DNA binding site selection by RNA polymerase II TAFs: a TAF(II)250-TAF(II)150 complex recognizes the initiator. *EMBO J.* 18, 4835–4845. <https://doi.org/10.1093/emboj/18.17.4835>
- Chan, Y.K., Gack, M.U., 2016. Viral evasion of intracellular DNA and RNA sensing. *Nat. Rev. Microbiol.* 14, 360–373. <https://doi.org/10.1038/nrmicro.2016.45>
- Chen, L., Wei, T., Si, X., Wang, Q., Li, Y., Leng, Y., Deng, A., Chen, J., Wang, G., Zhu, S., Kang, J., 2013. Lysine acetyltransferase GCN5 potentiates the growth of non-small cell lung cancer via promotion of E2F1, cyclin D1, and cyclin E1 expression. *J. Biol. Chem.* 288, 14510–14521. <https://doi.org/10.1074/jbc.M113.458737>
- Chen, X., Liu, M., Tian, Y., Li, J., Qi, Y., Zhao, D., Wu, Z., Huang, M., Wong, C.C.L., Wang, H.-W., Wang, J., Yang, H., Xu, Y., 2018. Cryo-EM structure of human mTOR complex 2. *Cell Res.* 28, 518–528. <https://doi.org/10.1038/s41422-018-0029-3>
- Chen, X.-F., Lehmann, L., Lin, J.J., Vashisht, A., Schmidt, R., Ferrari, R., Huang, C., McKee, R., Mosley, A., Plath, K., Kurdistani, S.K., Wohlschlegel, J., Carey, M., 2012. Mediator and SAGA Have Distinct Roles in Pol II Preinitiation Complex Assembly and Function. *Cell Rep.* 2, 1061–1067. <https://doi.org/10.1016/j.celrep.2012.10.019>
- Cheon, H., Holvey-Bates, E.G., Schoggins, J.W., Forster, S., Hertzog, P., Imanaka, N., Rice, C.M., Jackson, M.W., Junk, D.J., Stark, G.R., 2013. IFN β -dependent increases in STAT1, STAT2, and IRF9 mediate resistance to viruses and DNA damage. *EMBO J.* 32, 2751–2763. <https://doi.org/10.1038/emboj.2013.203>
- Chevillard-Briet, M., Quaranta, M., Grézy, A., Mattera, L., Courilleau, C., Philippe, M., Mercier, P., Corpet, D., Lough, J., Ueda, T., Fukunaga, R., Trouche, D., Escaffit, F., 2014. Interplay between chromatin-modifying enzymes controls colon cancer progression through Wnt signaling. *Hum. Mol. Genet.* 23, 2120–2131. <https://doi.org/10.1093/hmg/ddt604>
- Chittuluru, J.R., Chaban, Y., Monnet-Saksouk, J., Carrozza, M.J., Sapountzi, V., Selleck, W., Huang, J., Utley, R.T., Cramet, M., Allard, S., Cai, G., Workman, J.L., Fried, M.G., Tan, S., Côté, J., Asturias, F.J., 2011. Structure and nucleosome interaction of the yeast NuA4 and Piccolo-NuA4 histone acetyltransferase complexes. *Nat. Struct. Mol. Biol.* 18, 1196–1203. <https://doi.org/10.1038/nsmb.2128>
- Cianfrocco, M.A., Kassavetis, G.A., Grob, P., Fang, J., Juven-Gershon, T., Kadonaga, J.T., Nogales, E., 2013. Human TFIID binds to core promoter DNA in a reorganized structural state. *Cell* 152, 120–131. <https://doi.org/10.1016/j.cell.2012.12.005>
- Clapier, C.R., Iwasa, J., Cairns, B.R., Peterson, C.L., 2017. Mechanisms of action and regulation of ATP-dependent chromatin-remodelling complexes. *Nat. Rev. Mol. Cell Biol.* 18, 407–422. <https://doi.org/10.1038/nrm.2017.26>
- Cloutier, P., Poitras, C., Durand, M., Hekmat, O., Fiola-Masson, É., Bouchard, A., Faubert, D., Chabot, B., Coulombe, B., 2017. R2TP/Prefoldin-like component RUVBL1/RUVBL2 directly interacts with ZNHIT2 to regulate assembly of U5 small nuclear ribonucleoprotein. *Nat. Commun.* 8, 15615. <https://doi.org/10.1038/ncomms15615>
- Cortajarena, A.L., Regan, L., 2006. Ligand binding by TPR domains. *Protein Sci. Publ. Protein Soc.* 15, 1193–1198. <https://doi.org/10.1110/ps.062092506>
- Corujo, D., Buschbeck, M., 2018. Post-Translational Modifications of H2A Histone Variants and Their Role in Cancer. *Cancers* 10. <https://doi.org/10.3390/cancers10030059>

- Cramer, P., Bushnell, D.A., Fu, J., Gnatt, A.L., Maier-Davis, B., Thompson, N.E., Burgess, R.R., Edwards, A.M., David, P.R., Kornberg, R.D., 2000. Architecture of RNA Polymerase II and Implications for the Transcription Mechanism. *Science* 288, 640–649. <https://doi.org/10.1126/science.288.5466.640>
- Cramer, P., Bushnell, D.A., Kornberg, R.D., 2001. Structural Basis of Transcription: RNA Polymerase II at 2.8 Ångstrom Resolution. *Science* 292, 1863–1876. <https://doi.org/10.1126/science.1059493>
- Cunningham, C.N., Southworth, D.R., Krukenberg, K.A., Agard, D.A., 2012. The conserved arginine 380 of Hsp90 is not a catalytic residue, but stabilizes the closed conformation required for ATP hydrolysis. *Protein Sci. Publ. Protein Soc.* 21, 1162–1171. <https://doi.org/10.1002/pro.2103>
- David-Morrison, G., Xu, Z., Rui, Y.-N., Charng, W.-L., Jaiswal, M., Yamamoto, S., Xiong, B., Zhang, K., Sandoval, H., Duraine, L., Zuo, Z., Zhang, S., Bellen, H.J., 2016. WAC regulates mTOR activity by acting as an adaptor for the TTT and Pontin/Reptin complexes. *Dev. Cell* 36, 139. <https://doi.org/10.1016/j.devcel.2015.12.019>
- de Dieuleveult, M., Yen, K., Hmitou, I., Depaux, A., Boussouar, F., Dargham, D.B., Jounier, S., Humbertclaude, H., Ribierre, F., Baulard, C., Farrell, N.P., Park, B., Keime, C., Carrière, L., Berlivet, S., Gut, M., Gut, I., Werner, M., Deleuze, J.-F., Olaso, R., Aude, J.-C., Chantalat, S., Pugh, B.F., Gérard, M., 2016. Genome-wide nucleosome specificity and function of chromatin remodellers in ES cells. *Nature* 530, 113–116. <https://doi.org/10.1038/nature16505>
- Deleu, L., Shellard, S., Alevizopoulos, K., Amati, B., Land, H., 2001. Recruitment of TRRAP required for oncogenic transformation by E1A. *Oncogene* 20, 8270–8275. <https://doi.org/10.1038/sj.onc.1205159>
- Deng, W., Roberts, S.G.E., 2007. TFIIB and the regulation of transcription by RNA polymerase II. *Chromosoma* 116, 417–429. <https://doi.org/10.1007/s00412-007-0113-9>
- Díaz-Santín, L.M., Lukyanova, N., Aciyan, E., Cheung, A.C., 2017. Cryo-EM structure of the SAGA and NuA4 coactivator subunit Tra1 at 3.7 angstrom resolution. *eLife* 6. <https://doi.org/10.7554/eLife.28384>
- Doyon, Y., Côté, J., 2004. The highly conserved and multifunctional NuA4 HAT complex. *Curr. Opin. Genet. Dev.* 14, 147–154. <https://doi.org/10.1016/j.gde.2004.02.009>
- Doyon, Y., Selleck, W., Lane, W.S., Tan, S., Côté, J., 2004. Structural and functional conservation of the NuA4 histone acetyltransferase complex from yeast to humans. *Mol. Cell. Biol.* 24, 1884–1896.
- Dudley, A.M., Rougeulle, C., Winston, F., 1999. The Spt components of SAGA facilitate TBP binding to a promoter at a post-activator-binding step in vivo. *Genes Dev.* 13, 2940–2945.
- Durant, M., Pugh, B.F., 2007. NuA4-directed chromatin transactions throughout the *Saccharomyces cerevisiae* genome. *Mol. Cell. Biol.* 27, 5327–5335. <https://doi.org/10.1128/MCB.00468-07>
- Eisenmann, D.M., Arndt, K.M., Ricupero, S.L., Rooney, J.W., Winston, F., 1992. SPT3 interacts with TFIID to allow normal transcription in *Saccharomyces cerevisiae*. *Genes Dev.* 6, 1319–1331. <https://doi.org/10.1101/gad.6.7.1319>
- Evangelista, F.M., Maglott-Roth, A., Stierle, M., Brino, L., Soutoglou, E., Tora, L., 2018. Transcription and mRNA export machineries SAGA and TREX-2 maintain monoubiquitinated H2B balance required for DNA repair. *J. Cell Biol.* jcb.201803074. <https://doi.org/10.1083/jcb.201803074>
- Farnham, P., 2009. INSIGHTS FROM GENOMIC PROFILING OF TRANSCRIPTION FACTORS. *Nat. Rev. Genet.* 10, 605–616. <https://doi.org/10.1038/nrg2636>

- Feller, C., Forné, I., Imhof, A., Becker, P.B., 2015. Global and Specific Responses of the Histone Acetylome to Systematic Perturbation. *Mol. Cell* 57, 559–571. <https://doi.org/10.1016/j.molcel.2014.12.008>
- Fernández-Sáiz, V., Targosz, B.-S., Lemeer, S., Eichner, R., Langer, C., Bullinger, L., Reiter, C., Slotta-Huspenina, J., Schroeder, S., Knorn, A.-M., Kurutz, J., Peschel, C., Pagano, M., Kuster, B., Bassermann, F., 2013. SCFFbxo9 and CK2 direct the cellular response to growth factor withdrawal via Tel2/Tti1 degradation and promote survival in multiple myeloma. *Nat. Cell Biol.* 15, 72–81. <https://doi.org/10.1038/ncb2651>
- Frank, S.R., Parisi, T., Taubert, S., Fernandez, P., Fuchs, M., Chan, H.-M., Livingston, D.M., Amati, B., 2003. MYC recruits the TIP60 histone acetyltransferase complex to chromatin. *EMBO Rep.* 4, 575–580. <https://doi.org/10.1038/sj.embor.embor861>
- Gaiser, F., Tan, S., Richmond, T.J., 2000. Novel dimerization fold of RAP30/RAP74 in human TFIIF at 1.7 Å resolution 1 Edited by K. Nagai. *J. Mol. Biol.* 302, 1119–1127. <https://doi.org/10.1006/jmbi.2000.4110>
- Gamper, A.M., Kim, J., Roeder, R.G., 2009. The STAGA Subunit ADA2b Is an Important Regulator of Human GCN5 Catalysis. *Mol. Cell. Biol.* 29, 266–280. <https://doi.org/10.1128/MCB.00315-08>
- Gangloff, Y.-G., Romier, C., Thuault, S., Werten, S., Davidson, I., 2001. The histone fold is a key structural motif of transcription factor TFIID. *Trends Biochem. Sci.* 26, 250–257. [https://doi.org/10.1016/S0968-0004\(00\)01741-2](https://doi.org/10.1016/S0968-0004(00)01741-2)
- Gangloff, Y.G., Werten, S., Romier, C., Carré, L., Poch, O., Moras, D., Davidson, I., 2000. The human TFIID components TAF(II)135 and TAF(II)20 and the yeast SAGA components ADA1 and TAF(II)68 heterodimerize to form histone-like pairs. *Mol. Cell. Biol.* 20, 340–351.
- Garraway, L.A., Lander, E.S., 2013. Lessons from the Cancer Genome. *Cell* 153, 17–37. <https://doi.org/10.1016/j.cell.2013.03.002>
- Genereaux, J., Kvas, S., Dobransky, D., Karagiannis, J., Gloor, G.B., Brandl, C.J., 2012. Genetic Evidence Links the ASTRA Protein Chaperone Component Tti2 to the SAGA Transcription Factor Tra1. *Genetics* 191, 765–780. <https://doi.org/10.1534/genetics.112.140459>
- Gershenzon, N.I., Ioshikhes, I.P., 2005. Synergy of human Pol II core promoter elements revealed by statistical sequence analysis. *Bioinformatics* 21, 1295–1300. <https://doi.org/10.1093/bioinformatics/bti172>
- Gévry, N., Chan, H.M., Laflamme, L., Livingston, D.M., Gaudreau, L., 2007. p21 transcription is regulated by differential localization of histone H2A.Z. *Genes Dev.* 21, 1869–1881. <https://doi.org/10.1101/gad.1545707>
- Ghirlando, R., Felsenfeld, G., 2016. CTCF: making the right connections. *Genes Dev.* 30, 881–891. <https://doi.org/10.1101/gad.277863.116>
- Ghobashi, A.H., Kamel, M.A., 2018. Tip60: updates. *J. Appl. Genet.* 59, 161–168. <https://doi.org/10.1007/s13353-018-0432-y>
- Gnatt, A.L., Cramer, P., Fu, J., Bushnell, D.A., Kornberg, R.D., 2001. Structural Basis of Transcription: An RNA Polymerase II Elongation Complex at 3.3 Å Resolution. *Science* 292, 1876–1882. <https://doi.org/10.1126/science.1059495>
- Gongora, C., Candeil, L., Vezzio, N., Copois, V., Denis, V., Breil, C., Molina, F., Fraslon, C., Conseiller, E., Pau, B., Martineau, P., Del Rio, M., 2008. Altered expression of cell proliferation-related and interferon-stimulated genes in colon cancer cells resistant to SN38. *Cancer Biol. Ther.* 7, 822–832.

- Grant, P.A., Duggan, L., Côté, J., Roberts, S.M., Brownell, J.E., Candau, R., Ohba, R., Owen-Hughes, T., Allis, C.D., Winston, F., Berger, S.L., Workman, J.L., 1997. Yeast Gcn5 functions in two multisubunit complexes to acetylate nucleosomal histones: characterization of an Ada complex and the SAGA (Spt/Ada) complex. *Genes Dev.* 11, 1640–1650.
- Grant, P.A., Eberharter, A., John, S., Cook, R.G., Turner, B.M., Workman, J.L., 1999. Expanded Lysine Acetylation Specificity of Gcn5 in Native Complexes. *J. Biol. Chem.* 274, 5895–5900. <https://doi.org/10.1074/jbc.274.9.5895>
- Grant, P.A., Schieltz, D., Pray-Grant, M.G., Yates, J.R., Workman, J.L., 1998. The ATM-related cofactor Tra1 is a component of the purified SAGA complex. *Mol. Cell* 2, 863–867.
- Gray, P.J., Prince, T., Cheng, J., Stevenson, M.A., Calderwood, S.K., 2008. The oncogene Cdc37 is a molecular chaperone: Targeting The Kinome's Favorite Aunt. *Nat. Rev. Cancer* 8, 491–495. <https://doi.org/10.1038/nrc2420>
- Grünberg, S., Hahn, S., 2013. Structural insights into transcription initiation by RNA polymerase II. *Trends Biochem. Sci.* 38, 603–611. <https://doi.org/10.1016/j.tibs.2013.09.002>
- Grünberg, S., Warfield, L., Hahn, S., 2012. Architecture of the RNA polymerase II preinitiation complex and mechanism of ATP-dependent promoter opening. *Nat. Struct. Mol. Biol.* 19, 788–796. <https://doi.org/10.1038/nsmb.2334>
- Guccione, E., Martinato, F., Finocchiaro, G., Luzi, L., Tizzoni, L., Dall'Olio, V., Zardo, G., Nervi, C., Bernard, L., Amati, B., 2006. Myc-binding-site recognition in the human genome is determined by chromatin context. *Nat. Cell Biol.* 8, 764–770. <https://doi.org/10.1038/ncb1434>
- Guillemette, B., Bataille, A.R., Gévry, N., Adam, M., Blanchette, M., Robert, F., Gaudreau, L., 2005. Variant Histone H2A.Z Is Globally Localized to the Promoters of Inactive Yeast Genes and Regulates Nucleosome Positioning. *PLOS Biol.* 3, e384. <https://doi.org/10.1371/journal.pbio.0030384>
- Haberle, V., Stark, A., 2018. Eukaryotic core promoters and the functional basis of transcription initiation. *Nat. Rev. Mol. Cell Biol.* <https://doi.org/10.1038/s41580-018-0028-8>
- Hahn, S., Young, E.T., 2011. Transcriptional Regulation in *Saccharomyces cerevisiae*: Transcription Factor Regulation and Function, Mechanisms of Initiation, and Roles of Activators and Coactivators. *Genetics* 189, 705–736. <https://doi.org/10.1534/genetics.111.127019>
- Hainzl, O., Lapina, M.C., Buchner, J., Richter, K., 2009. The charged linker region is an important regulator of Hsp90 function. *J. Biol. Chem.* 284, 22559–22567. <https://doi.org/10.1074/jbc.M109.031658>
- Hampsey, M., 1998. Molecular Genetics of the RNA Polymerase II General Transcriptional Machinery. *Microbiol. Mol. Biol. Rev.* 62, 465–503.
- Han, Y., Luo, J., Ranish, J., Hahn, S., 2014. Architecture of the *Saccharomyces cerevisiae* SAGA transcription coactivator complex. *EMBO J.* 33, 2534–2546. <https://doi.org/10.15252/embj.201488638>
- Harris, S.F., Shiau, A.K., Agard, D.A., 2004. The Crystal Structure of the Carboxy-Terminal Dimerization Domain of htpG, the *Escherichia coli* Hsp90, Reveals a Potential Substrate Binding Site. *Structure* 12, 1087–1097. <https://doi.org/10.1016/j.str.2004.03.020>
- Haslbeck, V., Eckl, J.M., Drazic, A., Rutz, D.A., Lorenz, O.R., Zimmermann, K., Kriehuber, T., Lindemann, C., Madl, T., Richter, K., 2015. The activity of protein phosphatase 5 towards native clients is modulated by the middle- and C-terminal domains of Hsp90. *Sci. Rep.* 5, 17058. <https://doi.org/10.1038/srep17058>
- Hassan, A.H., Prochasson, P., Neely, K.E., Galasinski, S.C., Chandy, M., Carrozza, M.J., Workman, J.L., 2002. Function and selectivity of bromodomains in anchoring chromatin-modifying

complexes to promoter nucleosomes. *Cell* 111, 369–379.

Hayashi, T., Hatanaka, M., Nagao, K., Nakaseko, Y., Kanoh, J., Kokubu, A., Ebe, M., Yanagida, M., 2007. Rapamycin sensitivity of the *Schizosaccharomyces pombe* tor2 mutant and organization of two highly phosphorylated TOR complexes by specific and common subunits. *Genes Cells* 12, 1357–1370. <https://doi.org/10.1111/j.1365-2443.2007.01141.x>

He, Y., Fang, J., Taatjes, D.J., Nogales, E., 2013. Structural visualization of key steps in human transcription initiation. *Nature* 495, 481–486. <https://doi.org/10.1038/nature11991>

Helmlinger, D., 2012. New insights into the SAGA complex from studies of the Tra1 subunit in budding and fission yeast. *Transcription* 3, 13–18. <https://doi.org/10.4161/trns.3.1.19271>

Helmlinger, D., Marguerat, S., Villén, J., Swaney, D.L., Gygi, S.P., Bähler, J., Winston, F., 2011. Tra1 has specific regulatory roles, rather than global functions, within the SAGA co-activator complex. *EMBO J.* 30, 2843–2852. <https://doi.org/10.1038/emboj.2011.181>

Helmlinger, D., Tora, L., 2017. Sharing the SAGA. *Trends Biochem. Sci.* 42, 850–861. <https://doi.org/10.1016/j.tibs.2017.09.001>

Henri, J., Chagot, M.-E., Bourguet, M., Abel, Y., Terral, G., Maurizy, C., Aigueperse, C., Georgescauld, F., Vandermoere, F., Saint-Fort, R., Behm-Ansmant, I., Charpentier, B., Pradet-Balade, B., Verheggen, C., Bertrand, E., Meyer, P., Cianfèrani, S., Manival, X., Quinternet, M., 2018. Deep Structural Analysis of RPAP3 and PIH1D1, Two Components of the HSP90 Co-chaperone R2TP Complex. *Struct. Lond. Engl.* 1993 26, 1196–1209.e8. <https://doi.org/10.1016/j.str.2018.06.002>

Henry, K.W., 2003. Transcriptional activation via sequential histone H2B ubiquitylation and deubiquitylation, mediated by SAGA-associated Ubp8. *Genes Dev.* 17, 2648–2663. <https://doi.org/10.1101/gad.1144003>

Herceg, Z., Hulla, W., Gell, D., Cuenin, C., Leonart, M., Jackson, S., Wang, Z.Q., 2001. Disruption of Trrap causes early embryonic lethality and defects in cell cycle progression. *Nat. Genet.* 29, 206–211. <https://doi.org/10.1038/ng725>

Hoke, S.M.T., Irina Mutiu, A., Genereaux, J., Kvas, S., Buck, M., Yu, M., Gloor, G.B., Brandl, C.J., 2010. Mutational analysis of the C-terminal FATC domain of *Saccharomyces cerevisiae* Tra1. *Curr. Genet.* 56, 447–465. <https://doi.org/10.1007/s00294-010-0313-3>

Honda, K., Takaoka, A., Taniguchi, T., 2006. Type I Interferon Gene Induction by the Interferon Regulatory Factor Family of Transcription Factors. *Immunity* 25, 349–360. <https://doi.org/10.1016/j.immuni.2006.08.009>

Horejsí, Z., Takai, H., Adelman, C.A., Collis, S.J., Flynn, H., Maslen, S., Skehel, J.M., de Lange, T., Boulton, S.J., 2010. CK2 phospho-dependent binding of R2TP complex to TEL2 is essential for mTOR and SMG1 stability. *Mol. Cell* 39, 839–850. <https://doi.org/10.1016/j.molcel.2010.08.037>

Houry, W.A., Bertrand, E., Coulombe, B., 2018. The PAQosome, an R2TP-Based Chaperone for Quaternary Structure Formation. *Trends Biochem. Sci.* 43, 4–9. <https://doi.org/10.1016/j.tibs.2017.11.001>

Hu, Y., Fisher, J.B., Koprowski, S., McAllister, D., Kim, M.-S., Lough, J., 2009. Homozygous disruption of the Tip60 gene causes early embryonic lethality. *Dev. Dyn. Off. Publ. Am. Assoc. Anat.* 238, 2912–2921. <https://doi.org/10.1002/dvdy.22110>

Huisinga, K.L., Pugh, B.F., 2004. A Genome-Wide Housekeeping Role for TFIID and a Highly Regulated Stress-Related Role for SAGA in *Saccharomyces cerevisiae*. *Mol. Cell* 13, 573–585. [https://doi.org/10.1016/S1097-2765\(04\)00087-5](https://doi.org/10.1016/S1097-2765(04)00087-5)

Hurov, K.E., Cotta-Ramusino, C., Elledge, S.J., 2010. A genetic screen identifies the Triple T

- complex required for DNA damage signaling and ATM and ATR stability. *Genes Dev.* 24, 1939–1950. <https://doi.org/10.1101/gad.1934210>
- Ikura, T., Ogryzko, V.V., Grigoriev, M., Groisman, R., Wang, J., Horikoshi, M., Scully, R., Qin, J., Nakatani, Y., 2000. Involvement of the TIP60 Histone Acetylase Complex in DNA Repair and Apoptosis. *Cell* 102, 463–473. [https://doi.org/10.1016/S0092-8674\(00\)00051-9](https://doi.org/10.1016/S0092-8674(00)00051-9)
- Imseng, S., Aylett, C.H., Maier, T., 2018. Architecture and activation of phosphatidylinositol 3-kinase related kinases. *Curr. Opin. Struct. Biol.* 49, 177–189. <https://doi.org/10.1016/j.sbi.2018.03.010>
- Inoue, H., Sugimoto, S., Takeshita, Y., Takeuchi, M., Hatanaka, M., Nagao, K., Hayashi, T., Kokubu, A., Yanagida, M., Kanoh, J., 2017. CK2 phospho-independent assembly of the Tel2-associated stress-signaling complexes in *Schizosaccharomyces pombe*. *Genes Cells* 22, 59–70. <https://doi.org/10.1111/gtc.12454>
- Izumi, N., Yamashita, A., Hirano, H., Ohno, S., 2011. Heat shock protein 90 regulates phosphatidylinositol 3-kinase-related protein kinase family proteins together with the RUVBL1/2 and Tel2-containing co-factor complex. *Cancer Sci.* 103, 50–57. <https://doi.org/10.1111/j.1349-7006.2011.02112.x>
- Jaenicke, L.A., von Eyss, B., Carstensen, A., Wolf, E., Xu, W., Greifenberg, A.K., Geyer, M., Eilers, M., Popov, N., 2016. Ubiquitin-Dependent Turnover of MYC Antagonizes MYC/PAF1C Complex Accumulation to Drive Transcriptional Elongation. *Mol. Cell* 61, 54–67. <https://doi.org/10.1016/j.molcel.2015.11.007>
- Jiang, X., Sun, Y., Chen, S., Roy, K., Price, B.D., 2006. The FATC Domains of PIKK Proteins Are Functionally Equivalent and Participate in the Tip60-dependent Activation of DNA-PKcs and ATM. *J. Biol. Chem.* 281, 15741–15746. <https://doi.org/10.1074/jbc.M513172200>
- Jin, Q., Yu, L.-R., Wang, L., Zhang, Z., Kasper, L.H., Lee, J.-E., Wang, C., Brindle, P.K., Dent, S.Y.R., Ge, K., 2011. Distinct roles of GCN5/PCAF-mediated H3K9ac and CBP/p300-mediated H3K18/27ac in nuclear receptor transactivation. *EMBO J.* 30, 249–262. <https://doi.org/10.1038/emboj.2010.318>
- Jin, Q., Zhuang, L., Lai, B., Wang, C., Li, W., Dolan, B., Lu, Y., Wang, Z., Zhao, K., Peng, W., Dent, S.Y., Ge, K., 2014. Gcn5 and PCAF negatively regulate interferon- β production through HAT-independent inhibition of TBK1. *EMBO Rep.* 15, 1192–1201. <https://doi.org/10.15252/embr.201438990>
- Kaizuka, T., Hara, T., Oshiro, N., Kikkawa, U., Yonezawa, K., Takehana, K., Iemura, S.-I., Natsume, T., Mizushima, N., 2010. Tti1 and Tel2 are critical factors in mammalian target of rapamycin complex assembly. *J. Biol. Chem.* 285, 20109–20116. <https://doi.org/10.1074/jbc.M110.121699>
- Kakihara, Y., Houry, W.A., 2012. The R2TP complex: Discovery and functions. *Biochim. Biophys. Acta BBA - Mol. Cell Res., AAA ATPases: structure and function* 1823, 101–107. <https://doi.org/10.1016/j.bbamcr.2011.08.016>
- Kamine, J., Elangovan, B., Subramanian, T., Coleman, D., Chinnadurai, G., 1996. Identification of a Cellular Protein That Specifically Interacts with the Essential Cysteine Region of the HIV-1 Tat Transactivator. *Virology* 216, 357–366. <https://doi.org/10.1006/viro.1996.0071>
- Kato, S., Inoue, K., Youn, M.-Y., 2010. Emergence of the osteo-epigenome in bone biology. *IBMS BoneKEy* 7, 314–324. <https://doi.org/10.1138/20100464>
- Kim, S.G., Hoffman, G.R., Poulgiannis, G., Buel, G.R., Jang, Y.J., Lee, K.W., Kim, B.-Y., Erikson, R.L., Cantley, L.C., Choo, A.Y., Blenis, J., 2013. Metabolic stress controls mTORC1 lysosomal localization and dimerization by regulating the TTT-RUVBL1/2 complex. *Mol. Cell* 49, 172–185. <https://doi.org/10.1016/j.molcel.2012.10.003>

- Kim, Y.J., Björklund, S., Li, Y., Sayre, M.H., Kornberg, R.D., 1994. A multiprotein mediator of transcriptional activation and its interaction with the C-terminal repeat domain of RNA polymerase II. *Cell* 77, 599–608.
- Kimura, A., Horikoshi, M., 1998. Tip60 acetylates six lysines of a specific class in core histones in vitro. *Genes Cells Devoted Mol. Cell. Mech.* 3, 789–800.
- Knuesel, M.T., Meyer, K.D., Bernecky, C., Taatjes, D.J., 2009. The human CDK8 subcomplex is a molecular switch that controls Mediator coactivator function. *Genes Dev.* 23, 439–451. <https://doi.org/10.1101/gad.1767009>
- Knutson, B.A., Hahn, S., 2011. Domains of Tra1 Important for Activator Recruitment and Transcription Coactivator Functions of SAGA and NuA4 Complexes. *Mol. Cell. Biol.* 31, 818–831. <https://doi.org/10.1128/MCB.00687-10>
- Kolosenko, I., Fryknäs, M., Forsberg, S., Johnsson, P., Cheon, H., Holvey-Bates, E.G., Edsbäcker, E., Pellegrini, P., Rassoolzadeh, H., Brnjic, S., Larsson, R., Stark, G.R., Grandér, D., Linder, S., Tamm, K.P., Milito, A.D., 2015. Cell crowding induces interferon regulatory factor 9, which confers resistance to chemotherapeutic drugs. *Int. J. Cancer* 136, E51–E61. <https://doi.org/10.1002/ijc.29161>
- Kostek, S.A., Grob, P., De Carlo, S., Lipscomb, J.S., Garczarek, F., Nogales, E., 2006. Molecular Architecture and Conformational Flexibility of Human RNA Polymerase II. *Structure* 14, 1691–1700. <https://doi.org/10.1016/j.str.2006.09.011>
- Kostrewa, D., Zeller, M.E., Armache, K.-J., Seizl, M., Leike, K., Thomm, M., Cramer, P., 2009. RNA polymerase II–TFIIB structure and mechanism of transcription initiation. *Nature* 462, 323–330. <https://doi.org/10.1038/nature08548>
- Koutsogiannouli, E.A., Wagner, N., Hader, C., Pinkerneil, M., Hoffmann, M.J., Schulz, W.A., 2017. Differential Effects of Histone Acetyltransferase GCN5 or PCAF Knockdown on Urothelial Carcinoma Cells. *Int. J. Mol. Sci.* 18. <https://doi.org/10.3390/ijms18071449>
- Kouzarides, T., 2007. Chromatin Modifications and Their Function. *Cell* 128, 693–705. <https://doi.org/10.1016/j.cell.2007.02.005>
- Kraus, T.A., Lau, J.F., Parisien, J.-P., Horvath, C.M., 2003. A Hybrid IRF9-STAT2 Protein Recapitulates Interferon-stimulated Gene Expression and Antiviral Response. *J. Biol. Chem.* 278, 13033–13038. <https://doi.org/10.1074/jbc.M212972200>
- Lagrange, T., Kapanidis, A.N., Tang, H., Reinberg, D., Ebright, R.H., 1998. New core promoter element in RNA polymerase II-dependent transcription: sequence-specific DNA binding by transcription factor IIB. *Genes Dev.* 12, 34–44.
- Lambert, S.A., Jolma, A., Campitelli, L.F., Das, P.K., Yin, Y., Albu, M., Chen, X., Taipale, J., Hughes, T.R., Weirauch, M.T., 2018. The Human Transcription Factors. *Cell* 172, 650–665. <https://doi.org/10.1016/j.cell.2018.01.029>
- Lang, G., Bonnet, J., Umlauf, D., Karmodiya, K., Koffler, J., Stierle, M., Devys, D., Tora, L., 2011. The Tightly Controlled Deubiquitination Activity of the Human SAGA Complex Differentially Modifies Distinct Gene Regulatory Elements. *Mol. Cell. Biol.* 31, 3734–3744. <https://doi.org/10.1128/MCB.05231-11>
- Lang, S.E., Hearing, P., 2003. The adenovirus E1A oncoprotein recruits the cellular TRRAP/GCN5 histone acetyltransferase complex. *Oncogene* 22, 2836–2841. <https://doi.org/10.1038/sj.onc.1206376>
- Larochelle, M., Gaudreau, L., 2003. H2A.Z has a function reminiscent of an activator required for preferential binding to intergenic DNA. *EMBO J.* 22, 4512–4522. <https://doi.org/10.1093/emboj/cdg427>

- Larschan, E., Winston, F., 2001. The *S. cerevisiae* SAGA complex functions in vivo as a coactivator for transcriptional activation by Gal4. *Genes Dev.* 15, 1946–1956. <https://doi.org/10.1101/gad.911501>
- Lau, W.C.Y., Li, Y., Liu, Z., Gao, Y., Zhang, Q., Huen, M.S.Y., 2016. Structure of the human dimeric ATM kinase. *Cell Cycle* 15, 1117–1124. <https://doi.org/10.1080/15384101.2016.1158362>
- Lee, D.-H., Gershenzon, N., Gupta, M., Ioshikhes, I.P., Reinberg, D., Lewis, B.A., 2005. Functional characterization of core promoter elements: the downstream core element is recognized by TAF1. *Mol. Cell. Biol.* 25, 9674–9686. <https://doi.org/10.1128/MCB.25.21.9674-9686.2005>
- Lee, J.-H., Paull, T.T., 2004. Direct activation of the ATM protein kinase by the Mre11/Rad50/Nbs1 complex. *Science* 304, 93–96. <https://doi.org/10.1126/science.1091496>
- Lee, K.K., Sardi, M.E., Swanson, S.K., Gilmore, J.M., Torok, M., Grant, P.A., Florens, L., Workman, J.L., Washburn, M.P., 2011. Combinatorial depletion analysis to assemble the network architecture of the SAGA and ADA chromatin remodeling complexes. *Mol. Syst. Biol.* 7, 503. <https://doi.org/10.1038/msb.2011.40>
- Lempiäinen, H., Halazonetis, T.D., 2009. Emerging common themes in regulation of PIKKs and PI3Ks. *EMBO J.* 28, 3067–3073. <https://doi.org/10.1038/emboj.2009.281>
- Lenhard, B., Sandelin, A., Carninci, P., 2012. Metazoan promoters: emerging characteristics and insights into transcriptional regulation. *Nat. Rev. Genet.* 13, 233–245. <https://doi.org/10.1038/nrg3163>
- Li, B., Carey, M., Workman, J.L., 2007. The Role of Chromatin during Transcription. *Cell* 128, 707–719. <https://doi.org/10.1016/j.cell.2007.01.015>
- Li, B., Pattenden, S.G., Lee, D., Gutiérrez, J., Chen, J., Seidel, C., Gerton, J., Workman, J.L., 2005. Preferential occupancy of histone variant H2AZ at inactive promoters influences local histone modifications and chromatin remodeling. *Proc. Natl. Acad. Sci. U. S. A.* 102, 18385–18390. <https://doi.org/10.1073/pnas.0507975102>
- Li, H., Cuenin, C., Murr, R., Wang, Z.-Q., Herceg, Z., 2004. HAT cofactor Trapp regulates the mitotic checkpoint by modulation of Mad1 and Mad2 expression. *EMBO J.* 23, 4824–4834. <https://doi.org/10.1038/sj.emboj.7600479>
- Li, J., Soroka, J., Buchner, J., 2012. The Hsp90 chaperone machinery: Conformational dynamics and regulation by co-chaperones. *Biochim. Biophys. Acta BBA - Mol. Cell Res.* 1823, 624–635. <https://doi.org/10.1016/j.bbamcr.2011.09.003>
- Li, W., Atanassov, B.S., Lan, X., Mohan, R.D., Swanson, S.K., Farria, A.T., Florens, L., Washburn, M.P., Workman, J.L., Dent, S.Y.R., 2016. Cytoplasmic ATXN7L3B Interferes with Nuclear Functions of the SAGA Deubiquitinase Module. *Mol. Cell. Biol.* 36, 2855–2866. <https://doi.org/10.1128/MCB.00193-16>
- Lim, C.Y., Santoso, B., Boulay, T., Dong, E., Ohler, U., Kadonaga, J.T., 2004. The MTE, a new core promoter element for transcription by RNA polymerase II. *Genes Dev.* 18, 1606–1617. <https://doi.org/10.1101/gad.1193404>
- Lin, L., Chamberlain, L., Zhu, L.J., Green, M.R., 2012. Analysis of Gal4-directed transcription activation using Tra1 mutants selectively defective for interaction with Gal4. *Proc. Natl. Acad. Sci.* 109, 1997–2002. <https://doi.org/10.1073/pnas.1116340109>
- Liu, K., Zhang, Q., Lan, H., Wang, L., Mou, P., Shao, W., Liu, D., Yang, W., Lin, Z., Lin, Q., Ji, T., 2015. GCN5 Potentiates Glioma Proliferation and Invasion via STAT3 and AKT Signaling Pathways. *Int. J. Mol. Sci.* 16, 21897–21910. <https://doi.org/10.3390/ijms160921897>
- Liu, X., Tesfai, J., Evrard, Y.A., Dent, S.Y.R., Martinez, E., 2003. c-Myc transformation

- domain recruits the human STAGA complex and requires TRRAP and GCN5 acetylase activity for transcription activation. *J. Biol. Chem.* 278, 20405–20412. <https://doi.org/10.1074/jbc.M211795200>
- Loizou, J.I., Oser, G., Shukla, V., Sawan, C., Murr, R., Wang, Z.-Q., Trumpp, A., Herceg, Z., 2009. Histone acetyltransferase cofactor Trrap is essential for maintaining the hematopoietic stem/progenitor cell pool. *J. Immunol. Baltim. Md* 1950 183, 6422–6431. <https://doi.org/10.4049/jimmunol.0901969>
- Louder, R.K., He, Y., López-Blanco, J.R., Fang, J., Chacón, P., Nogales, E., 2016. Structure of promoter-bound TFIID and model of human pre-initiation complex assembly. *Nature* 531, 604–609. <https://doi.org/10.1038/nature17394>
- Lu, P.Y.T., Lévesque, N., Michael S. Kobor, 2009. NuA4 and SWR1-C: two chromatin-modifying complexes with overlapping functions and components. *Biochem. Cell Biol.* 87, 799–815. <https://doi.org/10.1139/O09-062>
- Lu, X., Wang, L., Yu, C., Yu, D., Yu, G., 2015. Histone Acetylation Modifiers in the Pathogenesis of Alzheimer's Disease. *Front. Cell. Neurosci.* 9. <https://doi.org/10.3389/fncel.2015.00226>
- Mantovani, R., 1999. The molecular biology of the CCAAT-binding factor NF-Y. *Gene* 239, 15–27.
- Martinez, E., Kundu, T.K., Fu, J., Roeder, R.G., 1998. A Human SPT3-TAFII31-GCN5-L Acetylase Complex Distinct from Transcription Factor IID. *J. Biol. Chem.* 273, 23781–23785. <https://doi.org/10.1074/jbc.273.37.23781>
- Martinez, E., Palhan, V.B., Tjernberg, A., Lyman, E.S., Gamper, A.M., Kundu, T.K., Chait, B.T., Roeder, R.G., 2001. Human STAGA Complex Is a Chromatin-Acetylating Transcription Coactivator That Interacts with Pre-mRNA Splicing and DNA Damage-Binding Factors In Vivo. *Mol. Cell. Biol.* 21, 6782–6795. <https://doi.org/10.1128/MCB.21.20.6782-6795.2001>
- Martino, F., Pal, M., Muñoz-Hernández, H., Rodríguez, C.F., Núñez-Ramírez, R., Gil-Carmona, D., Degliesposti, G., Skehel, J.M., Roe, S.M., Prodromou, C., Pearl, L.H., Llorca, O., 2018. Author Correction: RPAP3 provides a flexible scaffold for coupling HSP90 to the human R2TP co-chaperone complex. *Nat. Commun.* 9, 3063. <https://doi.org/10.1038/s41467-018-05546-1>
- Maston, G.A., Evans, S.K., Green, M.R., 2006. Transcriptional Regulatory Elements in the Human Genome. *Annu. Rev. Genomics Hum. Genet.* 7, 29–59. <https://doi.org/10.1146/annurev.genom.7.080505.115623>
- Maurizy, C., Quinternet, M., Abel, Y., Verheggen, C., Santo, P.E., Bourguet, M., C F Paiva, A., Bragantini, B., Chagot, M.-E., Robert, M.-C., Abeza, C., Fabre, P., Fort, P., Vandermoere, F., M F Sousa, P., Rain, J.-C., Charpentier, B., Cianférani, S., Bandejas, T.M., Pradet-Balade, B., Manival, X., Bertrand, E., 2018. The RPAP3-Cterminal domain identifies R2TP-like quaternary chaperones. *Nat. Commun.* 9, 2093. <https://doi.org/10.1038/s41467-018-04431-1>
- McMahon, Steven B., Buskirk, H.A.V., Dugan, K.A., Copeland, T.D., Cole, M.D., 1998. The Novel ATM-Related Protein TRRAP Is an Essential Cofactor for the c-Myc and E2F Oncoproteins. *Cell* 94, 363–374. [https://doi.org/10.1016/S0092-8674\(00\)81479-8](https://doi.org/10.1016/S0092-8674(00)81479-8)
- McMahon, Steven B., Van Buskirk, H.A., Dugan, K.A., Copeland, T.D., Cole, M.D., 1998. The Novel ATM-Related Protein TRRAP Is an Essential Cofactor for the c-Myc and E2F Oncoproteins. *Cell* 94, 363–374. [https://doi.org/10.1016/S0092-8674\(00\)81479-8](https://doi.org/10.1016/S0092-8674(00)81479-8)
- McMahon, S.B., Wood, M.A., Cole, M.D., 2000. The essential cofactor TRRAP recruits the histone acetyltransferase hGCN5 to c-Myc. *Mol. Cell. Biol.* 20, 556–562.
- Melero, R., Uchiyama, A., Castaño, R., Kataoka, N., Kurosawa, H., Ohno, S., Yamashita, A., Llorca, O., 2014. Structures of SMG1-UPFs Complexes: SMG1 Contributes to Regulate UPF2-

Dependent Activation of UPF1 in NMD. *Structure* 22, 1105–1119.
<https://doi.org/10.1016/j.str.2014.05.015>

Meneghini, M.D., Wu, M., Madhani, H.D., 2003. Conserved histone variant H2A.Z protects euchromatin from the ectopic spread of silent heterochromatin. *Cell* 112, 725–736.

Meyer, K.D., Lin, S.-C., Bernecky, C., Gao, Y., Taatjes, D.J., 2010. p53 activates transcription by directing structural shifts in Mediator. *Nat. Struct. Mol. Biol.* 17, 753–760.
<https://doi.org/10.1038/nsmb.1816>

Meyer, P., Prodromou, C., Hu, B., Vaughan, C., Roe, S.M., Panaretou, B., Piper, P.W., Pearl, L.H., 2003. Structural and functional analysis of the middle segment of hsp90: implications for ATP hydrolysis and client protein and cochaperone interactions. *Mol. Cell* 11, 647–658.

Minsky, N., Shema, E., Field, Y., Schuster, M., Segal, E., Oren, M., 2008. Monoubiquitinated H2B is associated with the transcribed region of highly expressed genes in human cells. *Nat. Cell Biol.* 10, 483–488. <https://doi.org/10.1038/ncb1712>

Mohibullah, N., Hahn, S., 2008. Site-specific cross-linking of TBP in vivo and in vitro reveals a direct functional interaction with the SAGA subunit Spt3. *Genes Dev.* 22, 2994–3006.
<https://doi.org/10.1101/gad.1724408>

Mordes, D.A., Glick, G.G., Zhao, R., Cortez, D., 2008. TopBP1 activates ATR through ATRIP and a PIKK regulatory domain. *Genes Dev.* 22, 1478–1489.
<https://doi.org/10.1101/gad.1666208>

Morita, T., Yamashita, A., Kashima, I., Ogata, K., Ishiura, S., Ohno, S., 2007. Distant N- and C-terminal Domains Are Required for Intrinsic Kinase Activity of SMG-1, a Critical Component of Nonsense-mediated mRNA Decay. *J. Biol. Chem.* 282, 7799–7808.
<https://doi.org/10.1074/jbc.M610159200>

Müller, F., Demény, M.A., Tora, L., 2007. New Problems in RNA Polymerase II Transcription Initiation: Matching the Diversity of Core Promoters with a Variety of Promoter Recognition Factors. *J. Biol. Chem.* 282, 14685–14689. <https://doi.org/10.1074/jbc.R700012200>

Murr, R., Loizou, J.I., Yang, Y.-G., Cuenin, C., Li, H., Wang, Z.-Q., Herceg, Z., 2006. Histone acetylation by Trrap–Tip60 modulates loading of repair proteins and repair of DNA double-strand breaks. *Nat. Cell Biol.* 8, 91–99. <https://doi.org/10.1038/ncb1343>

Murr, R., Vaissière, T., Sawan, C., Shukla, V., Herceg, Z., 2007. Orchestration of chromatin-based processes: mind the TRRAP. *Oncogene* 26, 5358–5372. <https://doi.org/10.1038/sj.onc.1210605>

Mutiu, A.I., Hoke, S.M.T., Genereaux, J., Hannam, C., MacKenzie, K., Jobin-Robitaille, O., Guzzo, J., Côté, J., Andrews, B., Haniford, D.B., Brandl, C.J., 2007. Structure/function analysis of the phosphatidylinositol-3-kinase domain of yeast tra1. *Genetics* 177, 151–166.
<https://doi.org/10.1534/genetics.107.074476>

Myer, V.E., Young, R.A., 1998. RNA Polymerase II Holoenzymes and Subcomplexes. *J. Biol. Chem.* 273, 27757–27760. <https://doi.org/10.1074/jbc.273.43.27757>

Näär, A.M., Taatjes, D.J., Zhai, W., Nogales, E., Tjian, R., 2002. Human CRSP interacts with RNA polymerase II CTD and adopts a specific CTD-bound conformation. *Genes Dev.* 16, 1339–1344.
<https://doi.org/10.1101/gad.987602>

Nagy, Z., Riss, A., Romier, C., le Guezennec, X., Dongre, A.R., Orpinell, M., Han, J., Stunnenberg, H., Tora, L., 2009. The Human SPT20-Containing SAGA Complex Plays a Direct Role in the Regulation of Endoplasmic Reticulum Stress-Induced Genes. *Mol. Cell. Biol.* 29, 1649–1660.
<https://doi.org/10.1128/MCB.01076-08>

Nagy, Z., Tora, L., 2007. Distinct GCN5/PCAF-containing complexes function as co-

activators and are involved in transcription factor and global histone acetylation. *Oncogene* 26, 5341–5357. <https://doi.org/10.1038/sj.onc.1210604>

Nogales, E., Louder, R.K., He, Y., 2017. Structural Insights into the Eukaryotic Transcription Initiation Machinery. *Annu. Rev. Biophys.* 46, 59–83. <https://doi.org/10.1146/annurev-biophys-070816-033751>

Obri, A., Ouararhni, K., Papin, C., Diebold, M.-L., Padmanabhan, K., Marek, M., Stoll, I., Roy, L., Reilly, P.T., Mak, T.W., Dimitrov, S., Romier, C., Hamiche, A., 2014. ANP32E is a histone chaperone that removes H2A.Z from chromatin. *Nature* 505, 648–653. <https://doi.org/10.1038/nature12922>

Ogryzko, V.V., Kotani, T., Zhang, X., Schiltz, R.L., Howard, T., Yang, X.J., Howard, B.H., Qin, J., Nakatani, Y., 1998. Histone-like TAFs within the PCAF histone acetylase complex. *Cell* 94, 35–44.

Orphanides, G., Lagrange, T., Reinberg, D., 1996. The general transcription factors of RNA polymerase II. *Genes Dev.* 10, 2657–2683. <https://doi.org/10.1101/gad.10.21.2657>

Ozsolak, F., Song, J.S., Liu, X.S., Fisher, D.E., 2007. High-throughput mapping of the chromatin structure of human promoters. *Nat. Biotechnol.* 25, 244–248. <https://doi.org/10.1038/nbt1279>

Pancholi, N.J., Price, A.M., Weitzman, M.D., 2017. Take your PIKK: tumour viruses and DNA damage response pathways. *Philos. Trans. R. Soc. B Biol. Sci.* 372, 20160269. <https://doi.org/10.1098/rstb.2016.0269>

Perry, J., Kleckner, N., 2003. The ATRs, ATMs, and TORs are giant HEAT repeat proteins. *Cell* 112, 151–155.

Peterson, C.L., Laniel, M.-A., 2004. Histones and histone modifications. *Curr. Biol.* 14, R546–R551. <https://doi.org/10.1016/j.cub.2004.07.007>

Plaschka, C., Hantsche, M., Dienemann, C., Burzinski, C., Plitzko, J., Cramer, P., 2016. Transcription initiation complex structures elucidate DNA opening. *Nature* 533, 353–358. <https://doi.org/10.1038/nature17990>

Poss, Z.C., Ebmeier, C.C., Taatjes, D.J., 2013. The Mediator complex and transcription regulation. *Crit. Rev. Biochem. Mol. Biol.* 48, 575–608. <https://doi.org/10.3109/10409238.2013.840259>

Pradhan, S.K., Su, T., Yen, L., Jacquet, K., Huang, C., Cote, J., Kurdistani, S.K., Carey, M.F., 2016. EP400 Deposits H3.3 into Promoters and Enhancers During Gene Activation. *Mol. Cell* 61, 27–38. <https://doi.org/10.1016/j.molcel.2015.10.039>

Raisner, R.M., Hartley, P.D., Meneghini, M.D., Bao, M.Z., Liu, C.L., Schreiber, S.L., Rando, O.J., Madhani, H.D., 2005. Histone Variant H2A.Z Marks the 5' Ends of Both Active and Inactive Genes in Euchromatin. *Cell* 123, 233–248. <https://doi.org/10.1016/j.cell.2005.10.002>

Rajagopalan, D., Tirado-Magallanes, R., Bhatia, S.S., Teo, W.S., Sian, S., Hora, S., Lee, K.K., Zhang, Y., Jadhav, S.P., Wu, Y., Gan, Y.-H., Karnani, N., Benoukraf, T., Jha, S., 2018. TIP60 represses activation of endogenous retroviral elements. *Nucleic Acids Res.* <https://doi.org/10.1093/nar/gky659>

Ranish, J.A., Yudkovsky, N., Hahn, S., 1999. Intermediates in formation and activity of the RNA polymerase II preinitiation complex: holoenzyme recruitment and a postrecruitment role for the TATA box and TFIIB. *Genes Dev.* 13, 49–63. <https://doi.org/10.1101/gad.13.1.49>

Rao, Q., Liu, M., Tian, Y., Wu, Z., Hao, Y., Song, L., Qin, Z., Ding, C., Wang, H.-W., Wang, J., Xu, Y., 2018. Cryo-EM structure of human ATR-ATRIP complex. *Cell Res.* 28, 143–156.

<https://doi.org/10.1038/cr.2017.158>

Robert, F., Hardy, S., Nagy, Z., Baldeyron, C., Murr, R., Déry, U., Masson, J.-Y., Papadopoulou, D., Herceg, Z., Tora, L., 2006. The Transcriptional Histone Acetyltransferase Cofactor TRRAP Associates with the MRN Repair Complex and Plays a Role in DNA Double-Strand Break Repair. *Mol. Cell. Biol.* 26, 402–412. <https://doi.org/10.1128/MCB.26.2.402-412.2006>

Rodríguez-Navarro, S., 2009. Insights into SAGA function during gene expression. *EMBO Rep.* 10, 843–850. <https://doi.org/10.1038/embor.2009.168>

Roth, S.Y., Denu, J.M., Allis, C.D., 2001. Histone Acetyltransferases. *Annu. Rev. Biochem.* 70, 81–120. <https://doi.org/10.1146/annurev.biochem.70.1.81>

Ruhl, D.D., Jin, J., Cai, Y., Swanson, S., Florens, L., Washburn, M.P., Conaway, R.C., Conaway, J.W., Chrivia, J.C., 2006. Purification of a human SRCAP complex that remodels chromatin by incorporating the histone variant H2A.Z into nucleosomes. *Biochemistry* 45, 5671–5677. <https://doi.org/10.1021/bi060043d>

Runge, K.W., Zakian, V.A., 1996. TEL2, an essential gene required for telomere length regulation and telomere position effect in *Saccharomyces cerevisiae*. *Mol. Cell. Biol.* 16, 3094–3105.

Sainsbury, S., Bernecky, C., Cramer, P., 2015. Structural basis of transcription initiation by RNA polymerase II. *Nat. Rev. Mol. Cell Biol.* 16, 129–143. <https://doi.org/10.1038/nrm3952>

Saleh, A., Schieltz, D., Ting, N., McMahon, S.B., Litchfield, D.W., Yates, J.R., Lees-Miller, S.P., Cole, M.D., Brandl, C.J., 1998. Tra1p is a component of the yeast Ada.Spt transcriptional regulatory complexes. *J. Biol. Chem.* 273, 26559–26565.

Santisteban, M.S., Kalashnikova, T., Smith, M.M., 2000. Histone H2A.Z Regulates Transcription and Is Partially Redundant with Nucleosome Remodeling Complexes. *Cell* 103, 411–422. [https://doi.org/10.1016/S0092-8674\(00\)00133-1](https://doi.org/10.1016/S0092-8674(00)00133-1)

Sardiu, M.E., Cai, Y., Jin, J., Swanson, S.K., Conaway, R.C., Conaway, J.W., Florens, L., Washburn, M.P., 2008. Probabilistic assembly of human protein interaction networks from label-free quantitative proteomics. *Proc. Natl. Acad. Sci. U. S. A.* 105, 1454–1459. <https://doi.org/10.1073/pnas.0706983105>

Sawan, C., Hernandez-Vargas, H., Murr, R., Lopez, F., Vaissière, T., Ghantous, A.Y., Cuenin, C., Imbert, J., Wang, Z.-Q., Ren, B., Herceg, Z., 2013. Histone acetyltransferase cofactor Trapp maintains self-renewal and restricts differentiation of embryonic stem cells. *Stem Cells Dayt. Ohio* 31, 979–991. <https://doi.org/10.1002/stem.1341>

Saxton, R.A., Sabatini, D.M., 2017. mTOR Signaling in Growth, Metabolism, and Disease. *Cell* 168, 960–976. <https://doi.org/10.1016/j.cell.2017.02.004>

Schoggins, J.W., Rice, C.M., 2011. Interferon-stimulated genes and their antiviral effector functions. *Curr. Opin. Virol.* 1, 519–525. <https://doi.org/10.1016/j.coviro.2011.10.008>

Schopf, F.H., Biebl, M.M., Buchner, J., 2017. The HSP90 chaperone machinery. *Nat. Rev. Mol. Cell Biol.* 18, 345–360. <https://doi.org/10.1038/nrm.2017.20>

Setiaputra, D., Ahmad, S., Dalwadi, U., Steunou, A.-L., Lu, S., Ross, J.D., Dong, M.-Q., Côté, J., Yip, C.K., 2018. Molecular Architecture of the Essential Yeast Histone Acetyltransferase Complex NuA4 Redefines Its Multimodularity. *Mol. Cell. Biol.* 38. <https://doi.org/10.1128/MCB.00570-17>

Shao, H., Revach, M., Moshonov, S., Tzuman, Y., Gazit, K., Albeck, S., Unger, T., Dikstein, R., 2005. Core promoter binding by histone-like TAF complexes. *Mol. Cell. Biol.* 25, 206–219. <https://doi.org/10.1128/MCB.25.1.206-219.2005>

Sharov, G., Voltz, K., Durand, A., Kolesnikova, O., Papai, G., Myasnikov, A.G., Dejaegere, A., Ben Shem, A., Schultz, P., 2017. Structure of the transcription activator target Tra1 within the

- chromatin modifying complex SAGA. *Nat. Commun.* 8. <https://doi.org/10.1038/s41467-017-01564-7>
- Shevchenko, Anna, Roguev, A., Schaft, D., Buchanan, L., Habermann, B., Sakalar, C., Thomas, H., Krogan, N.J., Shevchenko, Andrej, Stewart, A.F., 2008. Chromatin Central: towards the comparative proteome by accurate mapping of the yeast proteomic environment. *Genome Biol.* 9, R167. <https://doi.org/10.1186/gb-2008-9-11-r167>
- Skene, P.J., Henikoff, J.G., Henikoff, S., 2018. Targeted *in situ* genome-wide profiling with high efficiency for low cell numbers. *Nat. Protoc.* 13, 1006–1019. <https://doi.org/10.1038/nprot.2018.015>
- Skene, P.J., Henikoff, S., 2017. An efficient targeted nuclease strategy for high-resolution mapping of DNA binding sites [WWW Document]. *eLife*. <https://doi.org/10.7554/eLife.21856>
- Smale, S.T., Kadonaga, J.T., 2003. The RNA polymerase II core promoter. *Annu. Rev. Biochem.* 72, 449–479. <https://doi.org/10.1146/annurev.biochem.72.121801.161520>
- Smith, E R, Belote, J.M., Schiltz, R.L., Yang, X.J., Moore, P.A., Berger, S.L., Nakatani, Y., Allis, C.D., 1998. Cloning of *Drosophila* GCN5: conserved features among metazoan GCN5 family members. *Nucleic Acids Res.* 26, 2948–2954.
- Smith, E. R., Eisen, A., Gu, W., Sattah, M., Pannuti, A., Zhou, J., Cook, R.G., Lucchesi, J.C., Allis, C.D., 1998. ESA1 is a histone acetyltransferase that is essential for growth in yeast. *Proc. Natl. Acad. Sci. U. S. A.* 95, 3561–3565.
- Sommer, L.A.M., Schaad, M., Dames, S.A., 2013. NMR- and Circular Dichroism-monitored Lipid Binding Studies Suggest a General Role for the FATC Domain as Membrane Anchor of Phosphatidylinositol 3-Kinase-related Kinases (PIKK). *J. Biol. Chem.* 288, 20046–20063. <https://doi.org/10.1074/jbc.M113.467233>
- Stargell, L.A., Bowen, J., Dadd, C.A., Dedon, P.C., Davis, M., Cook, R.G., Allis, C.D., Gorovsky, M.A., 1993. Temporal and spatial association of histone H2A variant hv1 with transcriptionally competent chromatin during nuclear development in *Tetrahymena thermophila*. *Genes Dev.* 7, 2641–2651.
- Stegeman, R., Spreacker, P.J., Swanson, S.K., Stephenson, R., Florens, L., Washburn, M.P., Weake, V.M., 2016. The spliceosomal protein SF3B5 is a novel component of *Drosophila* SAGA that functions in gene expression independent of splicing. *J. Mol. Biol.* 428, 3632–3649. <https://doi.org/10.1016/j.jmb.2016.05.009>
- Stevens, J.L., Cantin, G.T., Wang, G., Shevchenko, Andrej, Shevchenko, Anna, Berk, A.J., 2002. Transcription control by E1A and MAP kinase pathway via Sur2 mediator subunit. *Science* 296, 755–758. <https://doi.org/10.1126/science.1068943>
- Stirling, P.C., Bloom, M.S., Solanki-Patil, T., Smith, S., Sipahimalani, P., Li, Z., Kofoed, M., Ben-Aroya, S., Myung, K., Hieter, P., 2011. The complete spectrum of yeast chromosome instability genes identifies candidate CIN cancer genes and functional roles for ASTRA complex components. *PLoS Genet.* 7, e1002057. <https://doi.org/10.1371/journal.pgen.1002057>
- Sun, Y., Jiang, X., Chen, S., Fernandes, N., Price, B.D., 2005. A role for the Tip60 histone acetyltransferase in the acetylation and activation of ATM. *Proc. Natl. Acad. Sci. U. S. A.* 102, 13182–13187. <https://doi.org/10.1073/pnas.0504211102>
- Sun, Y., Xu, Y., Roy, K., Price, B.D., 2007. DNA Damage-Induced Acetylation of Lysine 3016 of ATM Activates ATM Kinase Activity. *Mol. Cell. Biol.* 27, 8502–8509. <https://doi.org/10.1128/MCB.01382-07>
- Suto, R.K., Clarkson, M.J., Tremethick, D.J., Luger, K., 2000. Crystal structure of a nucleosome core particle containing the variant histone H2A.Z. *Nat. Struct. Biol.* 7, 1121–1124. <https://doi.org/10.1038/81971>

- Suzuki, K., Bose, P., Leong-Quong, R.Y., Fujita, D.J., Riabowol, K., 2010. REAP: A two minute cell fractionation method. *BMC Res. Notes* 3, 294. <https://doi.org/10.1186/1756-0500-3-294>
- Suzuki, Y., Tsunoda, T., Sese, J., Taira, H., Mizushima-Sugano, J., Hata, H., Ota, T., Isogai, T., Tanaka, T., Nakamura, Y., Suyama, A., Sakaki, Y., Morishita, S., Okubo, K., Sugano, S., 2001. Identification and Characterization of the Potential Promoter Regions of 1031 Kinds of Human Genes. *Genome Res.* 11, 677–684. <https://doi.org/10.1101/gr.164001>
- Szutorisz, H., Dillon, N., Tora, L., 2005. The role of enhancers as centres for general transcription factor recruitment. *Trends Biochem. Sci.* 30, 593–599. <https://doi.org/10.1016/j.tibs.2005.08.006>
- Taatjes, D.J., Näär, A.M., Andel, F., Nogales, E., Tjian, R., 2002. Structure, function, and activator-induced conformations of the CRSP coactivator. *Science* 295, 1058–1062. <https://doi.org/10.1126/science.1065249>
- Taipale, M., Jarosz, D.F., Lindquist, S., 2010. HSP90 at the hub of protein homeostasis: emerging mechanistic insights. *Nat. Rev. Mol. Cell Biol.* 11, 515–528. <https://doi.org/10.1038/nrm2918>
- Taipale, M., Krykbaeva, I., Koeva, M., Kayatekin, C., Westover, K.D., Karras, G.I., Lindquist, S., 2012. Quantitative Analysis of Hsp90-Client Interactions Reveals Principles of Substrate Recognition. *Cell* 150, 987–1001. <https://doi.org/10.1016/j.cell.2012.06.047>
- Takahashi, T., Hara, K., Inoue, H., Kawa, Y., Tokunaga, C., Hidayat, S., Yoshino, K., Kuroda, Y., Yonezawa, K., 2000. Carboxyl-terminal region conserved among phosphoinositide-kinase-related kinases is indispensable for mTOR function in vivo and in vitro. *Genes Cells Devoted Mol. Cell. Mech.* 5, 765–775.
- Takai, H., Wang, R.C., Takai, K.K., Yang, H., de Lange, T., 2007. Tel2 Regulates the Stability of PI3K-Related Protein Kinases. *Cell* 131, 1248–1259. <https://doi.org/10.1016/j.cell.2007.10.052>
- Takai, H., Xie, Y., de Lange, T., Pavletich, N.P., 2010. Tel2 structure and function in the Hsp90-dependent maturation of mTOR and ATR complexes. *Genes Dev.* 24, 2019–2030. <https://doi.org/10.1101/gad.1956410>
- Tang, Y., Luo, J., Zhang, W., Gu, W., 2006. Tip60-dependent acetylation of p53 modulates the decision between cell-cycle arrest and apoptosis. *Mol. Cell* 24, 827–839. <https://doi.org/10.1016/j.molcel.2006.11.021>
- Tanimoto, K., Liu, Q., Bungert, J., Engel, J.D., 1999. Effects of altered gene order or orientation of the locus control region on human beta-globin gene expression in mice. *Nature* 398, 344–348. <https://doi.org/10.1038/18698>
- Tapias, A., Zhou, Z.-W., Shi, Y., Chong, Z., Wang, P., Groth, M., Platzer, M., Huttner, W., Herceg, Z., Yang, Y.-G., Wang, Z.-Q., 2014. Trrap-Dependent Histone Acetylation Specifically Regulates Cell-Cycle Gene Transcription to Control Neural Progenitor Fate Decisions. *Cell Stem Cell* 14, 632–643. <https://doi.org/10.1016/j.stem.2014.04.001>
- Taubert, S., Gorrini, C., Frank, S.R., Parisi, T., Fuchs, M., Chan, H.-M., Livingston, D.M., Amati, B., 2004. E2F-Dependent Histone Acetylation and Recruitment of the Tip60 Acetyltransferase Complex to Chromatin in Late G1. *Mol. Cell. Biol.* 24, 4546–4556. <https://doi.org/10.1128/MCB.24.10.4546-4556.2004>
- Tauc, H.M., Tasdogan, A., Meyer, P., Pandur, P., 2017. Nipped-A regulates intestinal stem cell proliferation in *Drosophila*. *Dev. Camb. Engl.* 144, 612–623. <https://doi.org/10.1242/dev.142703>
- Thompson, C.M., Koleske, A.J., Chao, D.M., Young, R.A., 1993. A multisubunit complex associated with the RNA polymerase II CTD and TATA-binding protein in yeast. *Cell* 73, 1361–1375.

- Tsutsumi, S., Mollapour, M., Prodromou, C., Lee, C.-T., Panaretou, B., Yoshida, S., Mayer, M.P., Neckers, L.M., 2012. Charged linker sequence modulates eukaryotic heat shock protein 90 (Hsp90) chaperone activity. *Proc. Natl. Acad. Sci. U. S. A.* 109, 2937–2942. <https://doi.org/10.1073/pnas.1114414109>
- Tyteca, S., Vandromme, M., Legube, G., Chevillard-Briet, M., Trouche, D., 2006. Tip60 and p400 are both required for UV-induced apoptosis but play antagonistic roles in cell cycle progression. *EMBO J.* 25, 1680–1689. <https://doi.org/10.1038/sj.emboj.7601066>
- Umlauf, D., Bonnet, J., Waharte, F., Fournier, M., Stierle, M., Fischer, B., Brino, L., Devys, D., Tora, L., 2013. The human TREX-2 complex is stably associated with the nuclear pore basket. *J Cell Sci* 126, 2656–2667. <https://doi.org/10.1242/jcs.118000>
- Vermeulen, M., Eberl, H.C., Matarese, F., Marks, H., Denissov, S., Butter, F., Lee, K.K., Olsen, J.V., Hyman, A.A., Stunnenberg, H.G., Mann, M., 2010. Quantitative Interaction Proteomics and Genome-wide Profiling of Epigenetic Histone Marks and Their Readers. *Cell* 142, 967–980. <https://doi.org/10.1016/j.cell.2010.08.020>
- Vilar, J.M.G., Saiz, L., 2005. DNA looping in gene regulation: from the assembly of macromolecular complexes to the control of transcriptional noise. *Curr. Opin. Genet. Dev.* 15, 136–144. <https://doi.org/10.1016/j.gde.2005.02.005>
- Wagner, E.J., Carpenter, P.B., 2012. Understanding the language of Lys36 methylation at histone H3. *Nat. Rev. Mol. Cell Biol.* 13, 115–126. <https://doi.org/10.1038/nrm3274>
- Wang, B., Jie, Z., Joo, D., Ordureau, A., Liu, P., Gan, W., Guo, J., Zhang, J., North, B.J., Dai, X., Cheng, X., Bian, X., Zhang, L., Harper, J.W., Sun, S.-C., Wei, W., 2017. TRAF2 and OTUD7B govern a ubiquitin-dependent switch that regulates mTORC2 signalling. *Nature* 545, 365–369. <https://doi.org/10.1038/nature22344>
- Wang, Xuejuan, Ahmad, S., Zhang, Z., Côté, J., Cai, G., 2018. Architecture of the *Saccharomyces cerevisiae* NuA4/TIP60 complex. *Nat. Commun.* 9, 1147. <https://doi.org/10.1038/s41467-018-03504-5>
- Wang, X., Ran, T., Zhang, X., Xin, J., Zhang, Z., Wu, T., Wang, W., Cai, G., 2017. 3.9 Å structure of the yeast Mec1-Ddc2 complex, a homolog of human ATR-ATRIP. *Science* 358, 1206–1209. <https://doi.org/10.1126/science.aan8414>
- Wang, Xiongjun, Zhu, W., Chang, P., Wu, H., Liu, H., Chen, J., 2018. Merge and separation of NuA4 and SWR1 complexes control cell fate plasticity in *Candida albicans*. *Cell Discov.* 4, 45. <https://doi.org/10.1038/s41421-018-0043-0>
- Wang, Z., Plasschaert, L.W., Aryal, S., Renaud, N.A., Yang, Z., Choo-Wing, R., Pessotti, A.D., Kirkpatrick, N.D., Cochran, N.R., Carbone, W., Maher, R., Lindeman, A., Russ, C., Reece-Hoyes, J., McAllister, G., Hoffman, G.R., Roma, G., Jaffe, A.B., 2018. TRRAP is a central regulator of human multiciliated cell formation. *J. Cell Biol.* 217, 1941–1955. <https://doi.org/10.1083/jcb.201706106>
- Warfield, L., Ramachandran, S., Baptista, T., Devys, D., Tora, L., Hahn, S., 2017. Transcription of Nearly All Yeast RNA Polymerase II-Transcribed Genes Is Dependent on Transcription Factor TFIID. *Mol. Cell* 68, 118–129.e5. <https://doi.org/10.1016/j.molcel.2017.08.014>
- Weake, V.M., Workman, J.L., 2012. SAGA function in tissue-specific gene expression. *Trends Cell Biol.* 22, 177–184. <https://doi.org/10.1016/j.tcb.2011.11.005>
- Wurdak, H., Zhu, S., Romero, A., Lorger, M., Watson, J., Chiang, C.-Y., Zhang, J., Natu, V.S., Lairson, L.L., Walker, J.R., Trussell, C.M., Harsh, G.R., Vogel, H., Felding-Habermann, B., Orth, A.P., Miraglia, L.J., Rines, D.R., Skirboll, S.L., Schultz, P.G., 2010. An RNAi screen identifies TRRAP as a regulator of brain tumor-initiating cell differentiation. *Cell Stem Cell* 6, 37–47. <https://doi.org/10.1016/j.stem.2009.11.002>

- Xu, W., Edmondson, D.G., Evrard, Y.A., Wakamiya, M., Behringer, R.R., Roth, S.Y., 2000. Loss of Gcn5l2 leads to increased apoptosis and mesodermal defects during mouse development. *Nat. Genet.* 26, 229–232. <https://doi.org/10.1038/79973>
- Xu, W., Edmondson, D.G., Roth, S.Y., 1998. Mammalian GCN5 and P/CAF Acetyltransferases Have Homologous Amino-Terminal Domains Important for Recognition of Nucleosomal Substrates. *Mol. Cell. Biol.* 18, 5659–5669.
- Yamamoto, T., Horikoshi, M., 1997. Novel Substrate Specificity of the Histone Acetyltransferase Activity of HIV-1-Tat Interactive Protein Tip60. *J. Biol. Chem.* 272, 30595–30598. <https://doi.org/10.1074/jbc.272.49.30595>
- Yamashita, A., Izumi, N., Kashima, I., Ohnishi, T., Saari, B., Katsuhata, Y., Muramatsu, R., Morita, T., Iwamatsu, A., Hachiya, T., Kurata, R., Hirano, H., Anderson, P., Ohno, S., 2009. SMG-8 and SMG-9, two novel subunits of the SMG-1 complex, regulate remodeling of the mRNA surveillance complex during nonsense-mediated mRNA decay. *Genes Dev.* 23, 1091–1105. <https://doi.org/10.1101/gad.1767209>
- Yamauchi, T., Yamauchi, J., Kuwata, T., Tamura, T., Yamashita, T., Bae, N., Westphal, H., Ozato, K., Nakatani, Y., 2000. Distinct but overlapping roles of histone acetylase PCAF and of the closely related PCAF-B/GCN5 in mouse embryogenesis. *Proc. Natl. Acad. Sci. U. S. A.* 97, 11303–11306. <https://doi.org/10.1073/pnas.97.21.11303>
- Yang, A., Zhu, Z., Kapranov, P., McKeon, F., Church, G.M., Gingeras, T.R., Struhl, K., 2006. Relationships between p63 binding, DNA sequence, transcription activity, and biological function in human cells. *Mol. Cell* 24, 593–602. <https://doi.org/10.1016/j.molcel.2006.10.018>
- Yang, C., Bolotin, E., Jiang, T., Sladek, F.M., Martinez, E., 2007. Prevalence of the Initiator over the TATA box in human and yeast genes and identification of DNA motifs enriched in human TATA-less core promoters. *Gene* 389, 52–65. <https://doi.org/10.1016/j.gene.2006.09.029>
- Yang, H., Wang, Jia, Liu, M., Chen, X., Huang, M., Tan, D., Dong, M.-Q., Wong, C.C.L., Wang, Jiawei, Xu, Y., Wang, H.-W., 2016. 4.4 Å Resolution Cryo-EM structure of human mTOR Complex 1. *Protein Cell* 7, 878–887. <https://doi.org/10.1007/s13238-016-0346-6>
- Yang, X.-J., Ogryzko, V.V., Nishikawa, J., Howard, B.H., Nakatani, Y., 1996. A p300/CBP-associated factor that competes with the adenoviral oncoprotein E1A. *Nature* 382, 319–324. <https://doi.org/10.1038/382319a0>
- Yella, V.R., Bansal, M., 2017. DNA structural features of eukaryotic TATA-containing and TATA-less promoters. *FEBS Open Bio* 7, 324–334. <https://doi.org/10.1002/2211-5463.12166>
- Yesudhas, D., Batool, M., Anwar, M., Panneerselvam, S., Choi, S., Yesudhas, D., Batool, M., Anwar, M.A., Panneerselvam, S., Choi, S., 2017. Proteins Recognizing DNA: Structural Uniqueness and Versatility of DNA-Binding Domains in Stem Cell Transcription Factors. *Genes* 8, 192. <https://doi.org/10.3390/genes8080192>
- Yin, X., Liu, M., Tian, Y., Wang, J., Xu, Y., 2017. Cryo-EM structure of human DNA-PK holoenzyme. *Cell Res.* 27, 1341–1350. <https://doi.org/10.1038/cr.2017.110>
- Yin, Y.-W., Jin, H.-J., Zhao, W., Gao, B., Fang, J., Wei, J., Zhang, D.D., Zhang, J., Fang, D., 2015. The Histone Acetyltransferase GCN5 Expression Is Elevated and Regulated by c-Myc and E2F1 Transcription Factors in Human Colon Cancer. *Gene Expr.* 16, 187–196. <https://doi.org/10.3727/105221615X14399878166230>
- Young, J.C., Hoogenraad, N.J., Hartl, F.U., 2003. Molecular chaperones Hsp90 and Hsp70 deliver preproteins to the mitochondrial import receptor Tom70. *Cell* 112, 41–50.
- Zaret, K.S., Carroll, J.S., 2011. Pioneer transcription factors: establishing competence for gene expression. *Genes Dev.* 25, 2227–2241. <https://doi.org/10.1101/gad.176826.111>

- Zhang, H., Roberts, D.N., Cairns, B.R., 2005. Genome-Wide Dynamics of Htz1, a Histone H2A Variant that Poises Repressed/Basal Promoters for Activation through Histone Loss. *Cell* 123, 219–231. <https://doi.org/10.1016/j.cell.2005.08.036>
- Zhao, R., Davey, M., Hsu, Y.-C., Kaplanek, P., Tong, A., Parsons, A.B., Krogan, N., Cagney, G., Mai, D., Greenblatt, J., Boone, C., Emili, A., Houry, W.A., 2005. Navigating the Chaperone Network: An Integrative Map of Physical and Genetic Interactions Mediated by the Hsp90 Chaperone. *Cell* 120, 715–727. <https://doi.org/10.1016/j.cell.2004.12.024>
- Zhao, R., Kakihara, Y., Gribun, A., Huen, J., Yang, G., Khanna, M., Costanzo, M., Brost, R.L., Boone, C., Hughes, T.R., Yip, C.M., Houry, W.A., 2008. Molecular chaperone Hsp90 stabilizes Pih1/Nop17 to maintain R2TP complex activity that regulates snoRNA accumulation. *J. Cell Biol.* 180, 563–578. <https://doi.org/10.1083/jcb.200709061>
- Zhou, T., Chiang, C.M., 2001. The intronless and TATA-less human TAF(II)55 gene contains a functional initiator and a downstream promoter element. *J. Biol. Chem.* 276, 25503–25511. <https://doi.org/10.1074/jbc.M102875200>

ABSTRACT

Gene expression regulation is critical for cells to adapt to external changes and maintain their homeostasis. Transcription is an essential step in gene expression and is controlled by numerous factors and cofactors. One such cofactor is TRRAP, the largest subunit of two distinct chromatin-modifying complexes, SAGA and TIP60. TRRAP interacts with a diverse range of transcription factors including c-MYC and E2Fs, and mediates the recruitment of SAGA and TIP60 to gene promoters. TRRAP is a member of the PIKK family of atypical kinases. Prior studies defined the TTT co-chaperone as an essential regulator of PIKK stability and activity. In contrast to its cognate kinases, TRRAP lacks catalytic residues and is the sole pseudokinase among PIKKs. Although TTT has been shown to stabilize and interact with TRRAP, the role of TTT on TRRAP function remains unknown. Using an inducible degron system that allows the rapid and acute depletion of endogenous proteins, we demonstrated that TTT is required to assemble TRRAP within its functional complexes prior its nuclear import. Additionally, through transcriptomic analyses we determined that TTT regulates a large number of TRRAP-dependent genes in colorectal cancer cells. Profiling of the genome-wide binding of TRRAP *via* CUT&RUN-seq identified the direct targets of TRRAP, of which only a small fraction overlaps with MYC targets. We also uncovered a direct inhibitory role of TRRAP on a subset of the interferon-stimulated genes, which mediate the interferon response in the innate immune system. Altogether, our data suggest that TRRAP and its chaperone TTT are involved in tumorigenesis through the maintenance of a specific transcriptional program.

Keywords: Transcription ♦ Chromatin ♦ TRRAP ♦ Colorectal cancer ♦ Interferon ♦ MYC

RESUME

La régulation de l'expression des gènes est critique pour l'adaptation des cellules à leur environnement et pour leur homéostasie. La transcription, qui représente une étape essentielle de l'expression des gènes, est contrôlée par plusieurs facteurs et cofacteurs. L'un de ces cofacteurs, TRRAP, correspond à la plus grosse sous-unité de deux complexes de remodelage de la chromatine, SAGA et TIP60. TRRAP interagit avec divers facteurs de transcription, tels que c-MYC et E2Fs et permet ainsi le recrutement de SAGA et TIP60 aux promoteurs des gènes. TRRAP est un membre d'une famille de kinases atypiques, les PIKKs. Des études antérieures ont défini la co-chaperonne TTT comme régulateur essentiel de la stabilité et l'activité de ces kinases. Contrairement aux autres PIKKs, TRRAP ne possède pas les résidus requis à son activité catalytique et représente donc la seule pseudo-kinase parmi les PIKKs. Bien que TTT interagisse et stabilise TRRAP, son rôle sur l'activité de ce dernier reste inconnu. En utilisant un système de dégron inducible qui permet la dégradation rapide de protéines endogènes, nous avons démontré que TTT est requis pour l'assemblage de TRRAP dans ses complexes fonctionnels précédant son import nucléaire. De plus, à travers des analyses transcriptomiques, nous avons pu déterminer que TTT régule la transcription de plusieurs gènes TRRAP-dépendants dans des cellules de cancer colorectal. L'analyse du profil de fixation de TRRAP à l'échelle du génome grâce à la technique du CUT&RUN suivie d'un séquençage à haut débit (CUT&RUN-seq), a permis d'identifier les cibles directes de TRRAP, parmi lesquelles seule une fraction restreinte correspond à des cibles directes de MYC. Nous avons également découvert que TRRAP possède un rôle de répresseur direct sur la transcription d'une partie des gènes stimulés par l'interféron qui interviennent dans la réponse à l'interféron du système immunitaire inné. En outre, nos résultats suggèrent que TRRAP et sa co-chaperonne TTT participent à la tumorigenèse notamment en maintenant et régulant un programme transcriptionnel spécifique.

Mots clés : Transcription ♦ Chromatine ♦ TRRAP ♦ Cancer colorectal ♦ Interféron ♦ MYC